

Biomimetic Lipid Bilayers

Anita Catherine Blakeston

Submitted in accordance with the requirements for the degree of
Doctor of Philosophy

The University of Leeds
School of Physics and Astronomy

June 2015

The candidate confirms that the work submitted is her own, except where work which has formed part of jointly-authored publications has been included. The contribution of the candidate and the other authors to this work has been explicitly indicated below. The candidate confirms that appropriate credit has been given within the thesis where reference has been made to the work of others.

This copy has been supplied on the understanding that it is copyright material and that no quotation from the thesis may be published without proper acknowledgement.

The right of Anita Catherine Blakeston to be identified as author of this work has been asserted by her in accordance with the Copyright, Designs and Patents Act 1988.

© 2015 The University of Leeds and Anita Catherine Blakeston

Work that has formed part of jointly-authored publications is indicated below:

Paper 1.

Blakeston, A. C.; Alswieleh, A. M.; Heath, G. R.; Roth, J. S.; Bao, P.; Cheng, N.; Armes, S. P.; Leggett, G. J.; Bushby, R. J.; Evans, S. D., New Poly (amino acid methacrylate) Brush Supports the Formation of Well-Defined Lipid Membranes. *Langmuir* **2015**, *31* (12), 3668-3677.

The contribution of the candidate to this work included performing the experiments to prepare and measure the zeta potentials of the vesicles used to prepare the supported lipid bilayer on the PCysMA brush. The candidate also performed all experiments to ascertain the correct conditions to produce a fluid bilayer and the FRAP experiments to characterise the bilayer. These results are presented in Chapter 5. The candidate also prepared and evaluated the table of interaction potentials. PCysMA brushes were prepared and characterised by A. Alswieleh, with the candidate also contributing to the surface zeta potential measurements of this characterisation process. All AFM scans were performed by G. Heath.

Paper 2.

Bao, P.; Cheetham, M. R.; Roth, J. S.; Blakeston, A. C.; Bushby, R. J.; Evans, S. D., On-Chip Alternating Current Electrophoresis in Supported Lipid Bilayer Membranes. *Analytical chemistry* **2012**, *84* (24), 10702-10707.

The candidate contributed to a series of FRAP experiments to measure the effect of increasing the concentration of Texas Red fluorophore on the fluorescence intensity, diffusion coefficient and mobile fractions of lipid bilayers. This work appears in the supplementary information of the paper and also in this thesis in Chapter 5. The main electrophoresis experiments were performed by P. Bao, M. Cheetham and J. Roth.

Acknowledgements

The work presented in this thesis would not have been possible without the skills of Abdullah Alswieleh in preparing consistently good samples of polymer brushes for testing and providing characterisation data on them. I am very grateful to George Heath and Khizar Sheikh for their AFM expertise in generating good images of my results. Many thanks go to Johannes Roth for his EIS skills and particularly for our many interesting and extensive scientific discussions. I am also indebted to Mengui Li and Michael Carton for sharing their knowledge of protein reconstitutions.

From a very young age I wanted to be a scientist, but life had other plans for me. I, therefore, owe a special thanks to Prof. Steve Evans for taking a big risk by investing valuable resources in a chartered accountant/chemistry graduate, to help me fulfil my ambition. I am also grateful for his support during the writing of my publication and thesis. Thank you also to Prof. Richard Bushby for his valuable discussions and support throughout my research.

Last, but not least, thank you to my family and friends, who had no idea why I needed to go on this journey, but supported me anyway.

Abstract

The aims of the collaboration project, of which this project plays a key part, are to establish a new field of “low-dimensional chemistry” in order to synthesize manipulate and characterise the components of the photosynthetic system of *Rhodobacter Sphaeroides*. At a fundamental level, the physical processes involved in membrane biochemistry are to be investigated. Specifically, the environment in which the light harvesting components are found, their structure and function, including proton gradient formation, diffusion mechanisms, electron transport and the molecular association between them were to be studied.

“The ultimate goal of the collaboration project was the reconstruction, on a chip in a synthetic low-dimensional system, of the complete photosynthetic pathway of the bacterium Rhodobacter Sphaeroides.”

The creation of a homogeneous, fluid, polymer supported lipid bilayer to contain and maintain the integrity of these proteins, whilst under investigation, was a key part of the project.

To create this successful system many polymer brush supports were examined, which were anionic, cationic and zwitterionic polyelectrolytes. Some were pH responsive and some were fully charged and did not change with pH. The properties of a range of lipid vesicles were studied using DLS, so that the zeta potential of the liposomes could be measured and then tuned specifically to be attracted to the oppositely charged polymer brush surfaces. It was found that at very low charge (a zwitterionic lipid vesicle or surface) no vesicles were attracted. At very high charge (a highly cationic or anionic polymer or lipid vesicle) vesicles were attracted to the surface, but remained intact and did not fuse to form a bilayer. These highly charged combinations of surfaces and vesicles created an intriguing “de-quenching halo” effect, which is worthy of further investigation. At a specific point of low to mid-charge interaction a fluid bilayer was formed on a brush which had a surface of low charge and was interacting with a charged vesicle. The successful polymer brush support was created using a short novel amino acid polycysteine methacrylate brush, which is pH responsive and can be micro-patterned. The vesicles used were composed of 25 mol % DOTAP, a cationic lipid, in combination with a zwitterionic POPC lipid. The diffusion coefficient of the bilayer deposited on the brush was measured using FRAP and found to match the rates measured for lipid bilayers on glass, which is considered to be the “standard” for comparison. The mobile fractions also compared very well to this standard.

AFM scans showed a homogeneous surface and break-through force measurement confirmed a bilayer of 5 nm in thickness, as expected for a single bilayer.

Attempts were subsequently made to incorporate proteins into this system by a number of methods, including creating proteoliposomes containing light harvesting components from the *Rhodobacter Sphaeroides*. The most promising of these was the development of a “one-step detergent depletion method” for creating a solubilised bilayer, adding protein and rinsing away the detergent in a single experiment. The characterisation of the system by TIRF, dark field and AFM microscopy was indicating success and paves the way for future work.

In testing the polymer brushes as candidates for supporting a lipid bilayer, one with the potential to be used to create compartments in a corral for segregating the individual protein components of a light harvesting bacterium was also confirmed. This protein and lipid resistant Poly(2-(methacryloyloxy)ethyl phosphorylcholine), will facilitate the study of their function, by micro-patterning. In conjunction with the PCysMA this system has the potential be used to create corrals between these compartments which allow the free movement of ions between the proteins. The long term goal is to generate energy following light absorption by the proteins.

The project is truly multidisciplinary and has presented the opportunity for collaboration between researchers in the disciplines of physics, chemistry and biology. The work presented here combines knowledge of membrane biophysics with polymer chemistry, and protein biochemistry.

Contents

1. Introduction	1
1.1. The Low-Dimensional Chemistry collaboration project.....	1
1.2. Rhodobacter Sphaeroides and the study of light harvesting	1
1.3. The cell membrane	4
1.4. Cell membranes on planar solid supports	4
1.5. Cell membranes on ‘non-solid’ supports	5
1.6. Thesis orientation	6
1.7. References.....	8
2. Background	10
2.1. Introduction	10
2.2. Lipids and self-assembly	10
2.3. Bilayers on solid supports	20
2.4. Polymer supported lipid bilayers	34
2.5. Summary of background and aim of the thesis	58
2.6. References	60
3. Experimental theory	69
3.1. Polymer brushes	69
3.2. Lipid vesicles.....	73
3.3. Detergents, solubilisation and reconstitution of proteins.....	74
3.4. Contact angle	79
3.5. Flow cells.....	81
3.6. Fluorescence recovery after photobleaching (FRAP).....	82
3.7. Dynamic Light Scattering (DLS)	90
3.8. Other analysis tools.....	97
3.9. References.....	107

4. Experimental methods.....	111
4.1. Bilayer formation and characterisation	111
4.2. Polymer brushes	118
4.3. References	123
5. Testing bilayer formation on zwitterionic and anionic brushes	124
5.1. Introduction	124
5.2. Lipids and incubation methods.....	125
5.3. Surface initiation	133
5.4. PCysMA brushes.....	136
5.5. PMPC polymer brushes.....	154
5.6. PMAA polymer brushes	156
5.7. PKSPMA polymer brushes.....	159
5.8. The use of charged probes and charged lipids with charged polymers for FRAP. 161	
5.9. Discussion and conclusions for zwitterionic and anionic brushes	168
5.10. References	174
6. Transmembrane protein incorporation into a polymer supported lipid bilayer	179
6.1. Introduction	179
6.2. Attempted reconstitution of proteorhodopsin into cationic lipid vesicles	180
6.3. Attempted reconstitution of cytb03 into cationic vesicles.....	183
6.4. The use of short chain lipids or detergent depletion for direct reconstitution of proteins into a bilayer	187
6.5. Summary, conclusions and further work.....	200
6.6. References	202
7. Testing of bilayer formation on cationic brushes	202
7.1. Introduction	202
7.2. Lipids used for incubation	205
7.3. Bilayer formation on cationic polymer brushes.....	207
7.5. Summary and discussion of work on cationic brushes	224
7.6. Table 1 summary of results.....	228
7.7. References	229
8. Summary, conclusions and future work.....	232
8.1 Summary.....	232
8.2 Future work.....	234

Appendix 1. The importance of lipid bilayers to the project	237
Appendix 2. Polymers tested but not reported	238
Appendix 3. FRAP protocol detail	238
Appendix 4. Correct dilution for DLS experiments	239
Appendix 5. DLS at 25°C and 50°C	240

List of Figures

Figure 1.1: Schematic of the <i>Rh. Sphaeroides</i> with light harvesting complexes distributed around it in a lipid bilayer membrane. LH2 complexes are shown as green rings. The LH1-RC are seen as dimers (red circles of LH1) with blue reaction centres within them. Cyt bc1 and ATP synthase are also visible beneath the main structure.....	3
Figure 1.2: Simplified schematic of the energy absorption and proton transfer processes in the <i>Rh. Sphaeroides</i> which leads to the production of stored energy as ATP. LH2 and LH1 absorb photons and the excitation energy passes to the reaction centre where charge separation follows. The excited bacteriochlorophyll dimer in the RC, transfers an electron to a secondary acceptor, Q_B . The Q_B picks up two protons from the cytoplasmic space to create the reduced quinol, QH_2 . Quinol is oxidised by cytochrome c2, and the cytochrome bc1 complex. Two protons are then released into the periplasmic space. The blue arrows show electron transfer and the purple arrows show proton transfer. The redox cycle is completed when the oxidised bacteriochlorophyll is reduced. Finally ATP synthase utilises the protons of this transmembrane proton gradient to convert ADP to ATP, by reacting with a phosphate group.	3
Figure 1.3: A simple plan for the outcomes of the project. This scheme is based on the creation of the corrals, using polymer brushes, which will contains the light harvesting proteins and house the surrounding medium in which the components ubiquinone, protons and electrons can diffuse between the proteins.....	4
Figure 1.4: Schematic of the polymer brush supported lipid bilayer, as part of the system shown in Figure 1.3. This shows an incorporated transmembrane protein, Cyt bc1, with the corral boundary walls provided by a lipid resistant brush.....	7
Figure 2.1: Schematic model of the cell membrane showing a cell and highlighting the composition of the membrane and details of the lipid bilayer.	13
Figure 2.2: Examples of the structures of lipids found in a cell membrane showing the hydrophilic headgroups and hydrophobic chains.....	14
Figure 2.3: The structures of the commonly used lipids, POPC, DOPG, DOTAP and DMPC..	16
Figure 2.4: The structure of the liposome, micelle and planar bilayer and the packing parameter pf the single and long chain lipids.	17
Figure 2.5: Diagram indicating the geometrical space occupied by lipid molecules with different acyl chain lengths and the structures created by aggregation of lipids and detergent molecules. (a) highly disordered, kinked chains, (b) straighter chains, forming bilayers and (c) detergent molecules which form micelles.	19

Figure 2.6: Shows the phases of a lipid bilayer. S is the order parameter of the acyl chain D is the diffusion coefficient. The liquid ordered phase has the order of a solid, but is very fluid. a) L_d diffusion is >1 but low chain order b) the gel phase, has diffusion is >1 with high chain order c) The gel phase is highly ordered with low diffusion <0.001	20
Figure 2.7: Cholesterol.....	22
Figure 2.8: Four possible outcomes following the incubation of lipid vesicles on a solid surface.	25
Figure 2.9: Mechanisms of vesicle rupture: (A) an isolated adsorbed vesicle ruptures spontaneously, driven by its support-induced deformation; (B) neighbouring adsorbed vesicles fuse and eventually rupture; (C) the active edge of a supported bilayer patch induces the rupture of a neighbouring vesicle; (D) the cooperative action of several neighbouring vesicles leads to the rupture of a first vesicle (at the critical vesicular coverage). The active edge thereby exposed triggers the rupture of adjacent vesicles.	25
Figure 2.10: A “trapped” vesicle. The surface-bound vesicle is located sufficiently far away to remain unaffected by the bilayer edges though close enough to prevent the edge-induced rupture of other vesicles from solution. Such an arrangement inhibits the further propagation of bilayer growth, leaving trapped vesicles as defects.	26
Figure 2.11: Illustration of the 2D model of an adsorbed vesicle. The different bead types are initially randomly distributed within the vesicle, and then rearrange upon adsorption according to energy minimization (corresponding to electrostatic interaction with the surface and lateral diffusion of lipids within the outer leaflet of the lipid bilayer in real vesicles). ⁶⁷	28
Figure 2.12: Changes in the deformation of vesicles as the surface interaction is increased. ⁴⁹	30
Figure 2.13: The phase diagram for the influence of ionic strength and pH for A) similarly charged surface and vesicles B) oppositely charged vesicles and surface.	31
Figure 2.14: Schematic illustration of the influence of large buffer counterions in solution.	32
Figure 2.15: Zeta potential of oxide nanoparticles measured in 1 g/L NaCl solution, indicating that titanium oxide (triangles) has an overall lower zeta potential than silicon oxide (squares). Titanium oxide has a lower isoelectric point of \sim pH 5 compared to that of silicon oxide at \sim pH 7.5.	34
Figure 2.16: Basic glycolipid structure.	37
Figure 2.17: Chemical structure of the synthetic membrane mimic used in early work by Buschl.	38
Figure 2.18: Methacrylic terpolymer used by Spinke.	38
Figure 2.19: Coupling of dextran to epoxy silane on silicon surface.	40
Figure 2.20: Schematic of influenza virus deposited onto dextran polymer cushion.	41

Figure 2.21: A schematic of the PEG polymer system and below it the structure of the PEG-silane-lipid used.	42
Figure 2.22: Schematic and structures of glycoacrylate polymer with surface coupling.	43
Figure 2.23: Schematic of the process for PEG-SLB self-assembly. Liposomes incorporating a low percentage of lipids with PEG chains attached to their headgroup self-assembled on the SiO ₂ surface and fuse into a PEG-SLB. The final structure features PEG chains on both sides of the lipid bilayer. The chemical structure of a PEG(5)-PE lipid is also shown.....	44
Figure 2.24: The cartoons depict the interpretation of the observed differences in the staining with different lipid-phase markers (green stars, DiD; red stars, AF647CTX). (c) Relative distributions of different lipid-phase markers between the apparent <i>I_d</i> and <i>I_o</i> phases observed for (red) PA and (green) OA-tethered membranes.	45
Figure 2.25: Structures of mercaptoethanol SAM and the cholesterol tether molecule cholesterolpolyethyleneoxy thiol (CPEO3) used to form a tethered bilayer membrane using eggPC lipid vesicles.	46
Figure 2.26: Schematic depiction of the structure of the PEG-supported lipid bilayer with incorporated protein.....	47
Figure 2.27: Schematic of tethered membrane domains with light harvesting complexes LH1-RC and LH2 in the same membrane patches.....	48
Figure 2.28: Structure of Polyacrylamide.	49
Figure 2.29: poly(2-(N-3-sulfopropyl-N,N-dimethyl ammonium)ethyl methacrylate).....	50
Figure 2.30: Schematic view of the covalently immobilized maleic acid copolymer layers; <i>R</i> varies with the type of co-monomer unit (octadecene, propene, or ethylene).....	51
Figure 2.31: poly(acrylic acid) as the anhydride, formed by PAA when spin coated. Hydrating at pH 8-10 converts it back to an acid.....	52
Figure 2.32: Schematic of poly(acrylic acid) brush with an inserted ion channel. ¹¹⁴	53
Figure 2.33: Structure of polydopamine.....	54
Figure 2.34: Schematic showing the pH and temperature response of Carboxylate polymers under pH conditions.	55
Figure 2.35: The structures of the DMAEMA and MMA monomers.	56
Figure 2.36: Structure of the polymer PDDA.	57
Figure 2.37: Deposition of vesicles on a hydrated cationic PDDA, grown on gold, as a function of phospholipid composition and sodium chloride concentration.	57
Figure 2.38: A diagram of the PEM produced from layers of PDDA and PSS attached to a gold surface by using a thiol SAM.	58
Figure 2.39: The chemical structures of (a) PAH, (b) PSS and (c) PDADMAC and (d) POPC and (e) POPS lipids.	59
Figure 3.1: Three conformations of polymer attached to solid surface.....	72

Figure 3.2: Matyjaszewski's simplified mechanism for ATRP.....	73
Figure 3.3: Formation of unilamellar vesicles from dried lipid, via a multilamellar stage. ..	75
Figure 3.4: Cartoon of a transmembrane protein embedded in a lipid bilayer.	76
Figure 3.5: Examples of non-ionic detergents such as OG and β DDM.....	78
Figure 3.6: Methods available for reconstituting proteins. a) Transferring a single protein into a patch of membrane. b) Incorporating the protein into a proteoliposome and then rupturing this in a solid surface. c) As for b), but using a chemically modified surface to tether the bilayer to the surface. d) A proteoliposome can be fused into a pore-spanning lipid bilayer. e) A GUV containing the protein is ruptured to span a mechanical pore. f) The protein is tethered to a surface and a bilayer reconstituted around it.....	79
Figure 3.7: Three phases, which can be plotted graphically between the axes of lipid concentration (x axis) and detergent concentration (y axis), show micelles and vesicles, which a phase between where both can exist.	80
Figure 3.8: Young's equation to determine contact angle and surface energy.	82
Figure 3.9: Example of goniometer showing droplet dispensing and recording camera (FTA, First Ten Angstroms).	82
Figure 3.10: (a) flow cell for incubating glass and polymer samples with lipid for FRAP and (b) modified flow cell for TIRF and dark field microscope.	84
Figure 3.11: Commonly used fluorophores structures, FITC, Texas Red (centre) and Atto 590.	85
Figure 3.12: Jablonski energy levels diagrams. (top) Matching of absorption and emission spectra to energy level changes. (below) Possible energy absorption and emission pathways.....	86
Figure 3.13: Diagram of fluorescence microscope showing incident white light from arc lamp and absorbed and emitted light directed onto the sample or to the eyepiece/CCD by the filter cube. ²	87
Figure 3.14: Change in fluorescence intensity with time.	89
Figure 3.15: Full width half maximum Gaussian distribution (x_2-x_1).	90
Figure 3.16: Experimental measurements (Gaussian profile) of time (x axis) and intensity readings (y axis).	90
Figure 3.17: Variance (square of standard deviation of Gaussian) at time intervals, slope = diffusion coefficient.	91
Figure 3.18: The accumulation of charged layers around a spherical particle in a dielectric medium, showing the extent of the electrical double layer and its components, the Stern layer and diffuse layers.	94
Figure 3.19: The relative effects of electro-osmotic and electro-phoretic motion of particles in a tracer solution at distances from a solid surface of interest. These are measured to determine the surface zeta potential.	96

Figure 3.20: Graphical representation of the measurements at positions above (Figure 3.2), showing the how the surface zeta potential is calculated.....	97
Figure 3.21: (a) Phase plot, indicating fast field reversal with time and (b) distribution plots, which determine the distribution of result values and both should be as close to these ideals of good data is to be obtained.	98
Figure 3.22: Example of good quality size measurement of SUVs using a Zetasizer nano....	99
Figure 3.23: (a) Example of UV vis spectrum, indicating peaks of absorbance and the colour of the light at that wavelength. (b) Example of a UV vis absorbance v wavelength plot....	100
Figure 3.24: AFM force curve to measure a bilayer thickness for POPC on glass.	102
Figure 3.25: AFM surface scans of POPC bilayer (a) height scan and (b) phase image in tapping mode.....	103
Figure 3.26: Contact mode image of surface which appears to be covered in vesicles.....	104
Figure 3.28: (a) Equivalent circuit for one time constant and (b) the equivalent Nyquist plot, showing low frequencies on the right, moving to higher frequencies to the left. ²⁴ (c) actual data plot during the stages of bilayer formation.....	106
Figure 3.29: Diagram of the TIRF cell, showing the angles of incidence and reflection of the light beam to be greater than the critical angle, producing an evanescent wave at the sample surface.	107
Figure 3.30: Path of light through dark field microscope, showing how the main beam is diverted away from the sample. Light diffracted by the sample itself is collected to create the image.	108
Figure 5.1: Chemical structures of the PMPC, PMAA, PKSPMA and PCysMA brushes.....	128
Figure 5.2: Zeta potentials of DOTAP:POPC (25:75) lipid vesicles measured over a range of pH values.....	130
Figure 5.3: Zeta potentials of vesicles with increasing ratios of DOTAP:POPC in 10 mM phosphate buffer at pH 7 without NaCl (black squares) and with 140 mM NaCl (red circles).	131
Figure 5.4: A comparison of the headgroups of DOPC and DOTAP. The angle of orientation of the PC headgroup was suggested to change as a result of changing the ionic strength of the surrounding solution.	132
Figure 5.5: Adjacent vesicles of 25% DOTAP:POPC on an oppositely charged surface, such as glass (top) and polymer brush (below) will lead either to a layer of adsorbed intact vesicles or a fluid bilayer. Rearrangement of the charged lipids within the vesicle may reduce vesicle-vesicle repulsion and support fusion.	134
Figure 5.6: Surface zeta potentials of a clean glass surface measured over a range of pH.	137
Figure 5.7: Schematic represents the formation of initiators including the formation of 3-aminopropyltriethoxysilane (APTES), and subsequent reaction with bromoisobutryl bromide (BIBB).....	137

- Figure 5.8:** The surface zeta potential of the APTES and BIBB-APTES functionalized glass substrates immersed in aqueous solution as a function of solution pH. (■) APTES film. (●) BIBB-APTES film. 138
- Figure 5.9:** Schematic showing the production of PCysMA polymer brushes using ATRP on a silicon (glass) surface. Full details are given in Chapter 4 and reference 27. 139
- Figure 5.10:** Height images using AFM of PCysMA brush grown by ATRP on silicon. Images are $2 \mu\text{m}^2$ and the lighter areas in the dry image show a higher height profile (higher rms roughness) of up to 5 nm when compared to the hydrated image on the right..... 140
- Figure 5.11:** (a) Ellipsometric measurement of pH response of PCysMA in buffer showing wet thickness. (b) Shows how the chemical structure changes with pH. 141
- Figure 5.12:** Surface zeta potential plot of PCysMA (dry length 7 nm) over the pH range from 2 to 11 it can be seen that at low pH below 3 the surface zeta is positive, from pH 3 to 8 it is ~ -10 mV and above this it become increasingly negative..... 142
- Figure 5.13:** ^1H NMR spectra recorded in D_2O for PCysMA at pH 7 (lower) at room temperature an(upper) held at 50°C for 2 hours. Note no signs of degradation in the heated sample. Inset is the structure of PCysMA showing the positions of the protons of interest..... 143
- Figure 5.14:** (a) Effect of heating PCysMA sample on the advancing contact angle. Sample was heated from room temperature and cooled again. (b) PMEDSAH results by Azzaroni *et al.* after heating and cooling. 145
- Figure 5.15:** Configurations of zwitterionic chains under different solution conditions.²⁹ . 145
- Figure 5.16:** FRAP image following the incubation of POPC lipid vesicles on PCysMA brush after incubation for 3 days..... 146
- Figure 5.17:** FRAP image following the incubation of 10% DOTAP:POPC lipid vesicles on PCysMA brush after incubation for 4 days. 147
- Figure 5.18:** Graph showing the diffusion characteristics of a bilayer with images immediately after bleaching and after 5 minutes of FRAP recovery. The bilayer was formed on a PCysMA brush using vesicles composed of 25 % DOTAP:POPC and 0.5 mol % Texas Red in 10 mM phosphate buffer at pH 7. Two aliquots of lipid were injected, with heating to 50°C after the second. An extended incubation of 48 h then took place. The brushes had a dry thickness of ~ 7 nm..... 148
- Figure 5.19:** Fluorescence recovery after photobleaching graphs and images at bleaching and after 5 min. A double bilayer adsorbed on a PCysMA brush (top graph) following incubation at room temperature and then at 50°C for 1 hour, with a second aliquot of lipid. A single bilayer (graph below) formed following a further 48 h room temperature incubation of the same sample. In all cases the vesicles contained 25 % DOTAP:POPC and 0.5 mol % Texas Red in 10 mM phosphate buffer at pH 7. The brushes had a dry thickness of ~ 7 nm. Images were taken immediately at bleaching (left) and after 5 min recovery time (right). (Both sets of images are enlarged below the graphs.) 150

- Figure 5.20:** FRAP graph of a bilayer on a PCysMA brush formed after incubation at 50 °C for 1 h and a further 48 h. Vesicles contained 50 % DOTAP:POPC and 0.5 mol % Texas Red in 10 mM phosphate buffer at pH 7 were used. The brushes had a dry thickness of 7 nm and images were taken immediately at bleaching (left) and after 5 min recovery time (right). 151
- Figure 5.21:** AFM images following bilayer formation on a PCysMA brush (a) height image, (b) height profile also showing single adsorbed vesicle, (c) breakthrough force curve indicating a 5 nm bilayer thickness, (d) 2 μm^2 “scratched” region surrounded by lipid bilayer on PCysMA brush, (e) image at base of the 2 μm^2 scratched area, (f) height profile across the bilayer /polymer scratch edge (position indicated by red dashed lines), (g) height profile of the surface at base of the scratched area..... 153
- Figure 5.22:** Impedance measurements (a) plot and model circuit (inset) for a lipid bilayer on PCysMA grown from a gold substrate. (b) Plot of gold (black circles) PCysMA on gold (red squares) and lipid bilayer (orange triangles)..... 154
- Figure 5.23:** Spin-coating of 25% DOTAP lipids from isopropanol onto dried PCysMA, length 7 nm.(a) Images at bleaching point (left) and after 10 min (right) (b) Diffusion graph..... 156
- Figure 5.24:** Variation of surface zeta potential of PMPC with pH, measured in 1 mM KCl. 157
- Figure 5.25:** Example of the results when testing a PMPC brush, after incubating with a range of cationic, anionic and zwitterionic lipid compositions. Images show evidence of a very small amount of lipid adsorption. 158
- Figure 5.26:** Example from the literature of the pH response of PMAA brush, showing the pKa to be 6.5 and that it is fully dissociated and extended at pH 7.5. 159
- Figure 5.27:** FRAP images at bleaching (top) and after 5 min (below). (a) Images of 10% DOTAP incubated on PMAA. (b) After incubating with 25% DOTAP. Both (a) and (b) used a concentration of 0.5 mg/mL in 10 mM phosphate buffer at pH 7. 160
- Figure 5.28:** Graphs comparing the diffusion rates of glass (red plot) (25% DOTAP vesicles) with PCysMA black plot (25% DOTAP vesicles) with PMAA (25 % DOTAP vesicles) blue plot. 161
- Figure 5.29:** Graphs comparing the detail of the first 25 sec of the diffusion slopes shown in Figure 5. 26., of glass (red plot) (25% DOTAP vesicles) with PCysMA black plot (25% DOTAP vesicles) with PMAA (25 % DOTAP vesicles) blue plot..... 162
- Figure 5.30:** FRAP images at bleaching (top) and after 5 min (below).(a)Images of 10% DOTAP incubated on PKSPMA. (b) PKSPMA incubated with 25% DOTAP. Some very slow diffusion is seen on the left, but an immobile layer of lipid only on the right image. Both (a) and (b) used a concentration of 0.5 mg/mL in 10 mM phosphate buffer at pH 7. 163
- Figure 5.32:** Images at bleaching (left) and after 5 min (right) for the Texas Red concentrations, in mol %, shown in white on the images. The images show the deterioration in the quality of the bilayer as the Teas Red concentration is increased. It also shows an increasing immobile fraction as the Texas Red concentration increases, as evidenced by the incomplete recovery of the bleached spot. 166

- Figure 5.33:** Graphical presentation of the relative intensity of fluorescence measured from the images in Figure 5.32 (before FRAP bleaching) using concentrations of 0.5, 1.0, 2.0, 3.0, 4.5, 6.0 mol % Texas Red in a POPC bilayer on glass. (a) Plot of the expected intensity level, which should increase linearly (red circles) with concentration of Texas Red. The actual result (black squares) shows that the intensity reduces with increased Texas Red concentration. (b) Theoretical result with no self-quenching (black squares) and theoretical result with self-quenching of Texas Red (black circles) with actual results superimposed (red circles). 167
- Figure 5.34:** Recovery profile of a lipid bilayer formed from a zwitterionic POPC lipid and a charged Texas Red probe at 0.5 mol % (also anionic) using a glass substrate (highly anionic), (left) image of bleached spot immediately after bleaching and (right) intensity profile across the beached spot. 168
- Figure 5.35:** Bleached spot (left) and intensity profile (right) of lipid layer formed from POPC (zwitterionic lipid) and 6% Texas Red (anionic probe) on (highly anionic) glass, showing a lighter halo around the bleached spot and peaks on the intensity profile. 168
- Figure 5.36:** Bleached spot and intensity profile of lipid layer formed from 25% DOTAP:POPC (cationic lipid) and 0.5 % Texas Red (probe) on PKSPMA (highly anionic brush), showing a bright area around the bleached spot. 168
- Figure 5.37:** Bleached spot and intensity profile of lipid layer formed from 25% DOPG:POPC (anionic lipid) and 0.5 mol% Texas Red probe, on quaternary amine PMETAC, (highly cationic brush), again showing a bright halo around the bleached spot. 169
- Figure 5.38:** A summary of the structures, contact angles and surface zeta potentials of the four brushes, PMPC, PMAA, PKSPMA and PCysMA. Below there are two images, the top one at bleaching and below it after 5 minutes recovery. 172
- Figure 5.39:** Surface zeta of the brushes and zeta potentials of the lipids showing the result of the incubations for each combination of these (top). Below are the combined zeta potentials of the surface and vesicles. 173
- Figure 6.1:** Schematic of the vesicles and the PRh direction of insertion (left). Inset (right) is the PDB schematic of the PRh protein structure. 180
- Figure 6.2:** Calibration graph for 5(6) Carboxyfluorescein (CF), plotting pH against the emission ratio at 530 nm after irradiating with light at 490 and 460 nm. (The inset grid indicates the run number). 181
- Figure 6.3:** Photograph of the vials of liposomes after encapsulating CF, inserting PRh and removing the detergent with Biobeads. The yellow colour indicates that CF is present and the pink indicates that PR is present. The results indicate that the protein is present in the POPC:POPG sample, but not in the DOPC:DOTAP sample. 182
- Figure 6.4:** Emission ratio readings for DOPG vesicles after incorporating PRh, before and after illuminating for 10 min. 182
- Figure 6.5:** Plot of absorbance against wavelength showing back ground (black), absorbance of cytb3 in *E.coli* (blue) and cytb3 in 25% DOTAP:POPC vesicles. In *E.coli*

~37% of the protein was incorporated; in 25% DOTAP this measure was lower at 17%. The line shows the 408 absorbance line, characteristic of cytbo3.....	184
Figure 6.6: Fluorescence recovery plot of a 25% DOTAP:POPC lipid bilayer incorporating cytbo3 incubated on glass coverslip. Images are inset which were taken at bleaching and after 5 min of fluorescence recovery.....	185
Figure 6.7: Top left (a) is the AFM height scan of the cytbo3, with (b) the PDB structure of it. Below in (c) is the surface scan height measurement and (d) a schematic of the top of the protein in the bilayer.	186
Figure 6.8: FRAP recovery curve of 25% DOTAP:POPC lipid vesicles containing Cyt b03 incubated on a short ((7nm) PCysMA brush.....	187
Figure 6.9: Shows the structure of POPC and DHPC-C6 with a schematic of the expected structure of the bicelle leading to bilayer formation on glass.....	188
Figure 6.10: 50:50 mixture of long (DOTAP:POPC) and short chain (DHPC-C6) lipids incubated on a 7 nm PCysMA brush. Inset, are the images at bleaching and after 5 min. (a) has a 25:75 ratio of DOTAP:POPC and (b) 50:50 ratio of DOTAP:POPC.....	190
Figure 6.11: Plot of change in diameter of 25% DOTAP:POPC MLVs when solubilised with increasing amounts of β DDM. On the right is a diagram, depicting the characteristics of the MLV as it is solubilised with detergent, published by Seddon <i>et al.</i>	192
Figure 6.12: (a) Diffusion coefficient of 3:1 β DDM:lipid bilayer incubated with C10H vesicles on glass showing images at bleaching and after 5 min. (b) the same sample viewed using TIRF.	195
Figure 6.13: (a) Dark field image of a DDM solubilised bilayer (b) DDM solubilised bilayer containing C10H vesicles, in which the cytbc1 was tagged with gold nanoparticles.	196
Figure 6.1: FRAP images of bilayer on PCysMA using β DDM/MLVs and C10H vesicles, (top) after 1 h, (mid) after 24 h and (lower) after 5 days.	
Figure 6.15: Bilayer on PCysMA using β DDM/MLVs and C10H vesicles. Diffusion graph and FRAP images, (after 5 days incubation). All images are shown at bleaching and after 5 min FRAP recovery.	197
Figure 6.16: AFM scans of the bilayer on the sample seen in Figure 6.13. (a) yellow line marks the scan, which is seen in profile in (b) height profile indicates a height of 20 nm. (c) Shows a breakthrough force curve, which does not indicate a bilayer breakthrough characteristic.....	198
Figure 6.17: Further AFM images of the potential C10H vesicle on PCysMA. Image (a) shows an elevated feature which is shown also in false colour in (c). The image (b) is a published image of the crystallised C10H vesicle.....	199
Figure 7.1: DLS study on a range of DOPG:POPC tip sonicated lipid vesicles, in MilliQ. Plots show size (black plot) and zeta potential (blue plot) changes with increasing mol % of DOPG.....	207

- Figure 7.2:** (a) PTBAEMA crosslinking in THF and hexane. (b) Ellipsometric thickness of the PTBAEMA brush. (■)= linear brush (◆)= surface x linked, (●)= x-linked throughout. (Courtesy of Abdullah Alswieleh) 208
- Figure 7.3:** PTBAEMA (a■) linear brush, (b●) x-linked throughout and (c◆) surface x linked. Provided by Abdullah Alswieleh. 210
- Figure 7.4:** PTBAEMA, fully cross-linked incubated with (a) & (b) POPC and (c) & (d) 50% DOPG vesicles. Images at bleaching (a) & (c) showing a well-defined bleached spot and (b) & (d) after 10 minutes FRAP recovery. In the case of (d), with 50% DOPG, a very slow recovery of the bleached spot can be seen (a fluid lipid bilayer on glass would have fully recovered in less than 10 min). The diffusion graph is presented below in Figure 7.5..... 211
- Figure 7.5:** Diffusion coefficient graph for the result of incubating 50% DOPG on the PTBAEMA (fully cross-linked) brush in MilliQ. 212
- Figure 7.6:** (a) Variation of surface zeta potential of PDMAEMA with pH. 213
- Figure 7.7:** PDMAEMA incubated with 50% DOPG:POPC at pH 5. Image at bleaching (left) and after 10 min FRAP recovery (right). 215
- Figure 7.8:** FRAP diffusion coefficient for PDMAEMA incubated with 50% DOPG:POPC.... 215
- Figure 7.9:** Zeta potential of PMETAC showing its surface zeta potential of +30 mV (without NaCl added to the buffer) and its response in buffer solutions with increasing concentrations of NaCl (black circles) from 10 mM to 200 mM. (The published narrative records these concentrations as 0.2 M etc., though the graph legend records 0.2 mM)... 216
- Figure 7.10:** Quaternisation of PDMAEMA brushes, with (a) C1, (b) C12 and (c) C18 chains. 217
- Figure 7.11:** Five samples of PMETAC-C1 (fully quaternised) incubated as indicated on the image with 0, 25%, 50%, 75% and 90% DOPG:POPC vesicles. The image in the left was taken immediately after bleaching and on the right after 10 minutes recovery. 219
- Figure 7.12:** FRAP images at bleaching at after 10 min on PMETAC (C1 quaternised throughout the chain). Comparative diffusion curves for bilayers on glass ($D = 1.4 \mu\text{m}^2 \text{s}^{-1}$) with POPC (●) and for the PMETAC surface (■) using 50% DOPG lipids in PBS buffer at pH 7 ($D = 0.13 \mu\text{m}^2 \text{s}^{-1}$ and a mobile fraction of 59%)..... 220
- Figure 7.13:** Lipid deposited on the quaternised PMETAC-C1 surface, indicating that intact vesicles are present..... 222
- Figure 7.14:** Measurements of the lipid/vesicle layer on a PMETAC (C1 quaternised) brush indicating the area size of the scan (a) and its height profile and (b) the force curve showing multiple breakthrough points (white arrows). 223

Abbreviations

2D	two dimensional layer
ADP	adenosine diphosphate
AFM	Atomic Force Microscopy
APTES	3-aminopropyltriethoxysilane
ATO	adenosine triphosphate
ATRP	Atom Transfer Radical Polymerization
BIBB	2-bromoisobutryl bromide
CaCl ₂	Calcium chloride
CF	5,6 carboxyfluorescein
CMC	critical micelle concentration
CPE03	cholesterolphosphatidylethanolamine thiol
Cyt bc1 / bo3	Cytochrome bc1 /bo3
Cyt c2	cytochrome c2
DLS	Dynamic Light Scattering
DMPC	1,2-dimyristoyl- <i>sn</i> -glycero-3-phosphocholine
DOPC	1,2-dioleoyl- <i>sn</i> -glycero-3-phosphocholine
DOTAP	1,2-dioleoyl-3-trimethylammonium-propane
egg-PC	egg-phosphatidylcholine
EIS	Electrical Impedance Spectroscopy
FCS	Fluorescence Correlation Spectroscopy
FRAP	Fluorescence Recovery After Photobleaching
FTIR	Fourier Transform Infrared
FWHM	Full Width Half Maximum
GH24000	DODA-poly(D-glucose-2-propenoate), telechelic lipopolymer
LB	Langmuir Blodgett deposition
LB/LS	Langmuir Blodgett/Langmuir Schaeffer
LH1	Light-harvesting complex 1
LH2	Light-harvesting complex 2
MLV	Large multilamellar vesicles
MUA	11-mercaptopundecanoic acid
NaCl	Sodium Chloride
ND	neutral density filter
NHS-EDC	<i>N</i> -Hydroxysuccinimide and (1-ethyl-3-(3-dimethylaminopropyl)carbodiimide hydrochloride)
NMR	Nuclear Magnetic Resonance
OG	<i>n</i> -octyl- β -D-glucopyranoside
PA	palmitic acid
PAA	poly(acrylic acid)
PAH	poly(allylamine hydrochloride)
PAM	polyacrylamide
PCysMA	poly (cysteine methacrylate)
PDADMAC/	poly(diallyldimethylammonium chloride)
PDDA	
PDMAEMA	poly (N,N- dimethylamino ethylmethacrylate)
PDMAEMS- PMMA	poly[2-(dimethylamino)ethyl methacrylate- <i>block</i> -methyl methacrylate]

PDMS	Poly(dimethylsiloxane)
PE	phosphoethanolamine
PEG	Poly(ethylene glycol)
PEL	polyelectrolyte monolayer brushes
PEM	polyelectrolyte multilayers
PEMA	poly(ethene-alt-maleic anhydride)
PKSPMA	poly(3-sulfopropylmethacrylate potassium salt)
PMAA	poly(methacrylic acid)
PMETAC	poly(2-(Methacryloyloxy)ethyl trimethylammonium chloride)
PMPC	Poly(2-(methacryloyloxy)ethyl phosphorylcholine)
PNIPAAm	poly(N-isopropylacrylamide-co-carboxyacrylamide)
POMA	poly(octadecene-alt-maleic anhydride)
POPC	1-palmitoyl-2-oleoyl- <i>sn</i> -glycero-3-phosphocholine
PPMA	poly(propenealt-maleic anhydride)
PS	phospho-L-serine
PSBMA	poly(2-(N-3-sulfopropyl-N,N-dimethyl ammonium)ethyl methacrylate)
PSS	poly(styrene sulfonate)
PTBAEMA	poly(2-(tert-butylamino)ethylmethacrylate)
QCM-D	quartz crystal microbalance with dissipation
RC	Reaction centre
SAM	Self-assembled monolayer
Si-ATRP	Surface Initiated Atom Transfer Radical Polymerisation
SLB	planar-supported lipid bilayers
SPR	Surface Plasmon Resonance
SUV	Small unilamellar vesicles
TIRF	Total Internal Reflection Microscopy
TMP	Transmembrane proteins
UV vis	Ultraviolet/visible spectrometer
β DDM	<i>n</i> -dodecyl- β -d-maltoside

1. Introduction

1.1. The Low-Dimensional Chemistry collaboration project

This thesis reports on research which contributes to a collaboration project between the University of Sheffield and the University of Leeds. The project brings together scientists with a range of skills, with the aim of re-creating photosynthesis in a laboratory by manipulating natural and man-made components on a nanoscale. The biologists will disassemble the light harvesting bacterium *Rhodobacter Sphaeroides* (*Rh. Sphaeroides*) into its component parts and then make genetic modifications to improve its light harvesting efficiency. Chemists will create artificial low-dimensional polymer based environments in which to reassemble these components to study their structure. Finally, physicists will create an artificial membrane to encapsulate the components, measure their functionality and create images of the structures using atomic force microscopy (AFM), fluorescence correlation spectroscopy (FCS) and other tools.

The aims of the collaboration project, which is ongoing, are to establish a new field of “low-dimensional chemistry” in order to synthesize manipulate and characterise the components of the photosynthetic system. Further, the hypothesis that these low-dimensional molecular structures will exhibit very different properties and behaviour from bulk molecular phases may yield new insights into fundamental processes.⁵ At a fundamental level, the physical processes that are involved in membrane biochemistry will be explored. The group will specifically look at proton gradient formation, diffusion mechanisms, electron transport, and the molecular association between the light harvesting components.

“The ultimate goal of the project will be the reconstruction, on a chip in a synthetic low-dimensional system, of the complete photosynthetic pathway of the bacterium Rhodobacter Sphaeroides.”⁵

1.2. Rhodobacter Sphaeroides and the study of light harvesting

The structure of the bacterium *Rh. Sphaeroides* is shown in Figure 1.1¹, indicating the approximate construction and location of the key light harvesting protein components, light-harvesting 2 (LH2), light-harvesting 1 (LH1), reaction centre (RC), Cytochrome bc1 (Cyt bc1) and adenosine triphosphate (ATP) synthase, which are embedded within the cell membrane, a lipid bilayer. The functions of the components are described below in Figure 1.2.

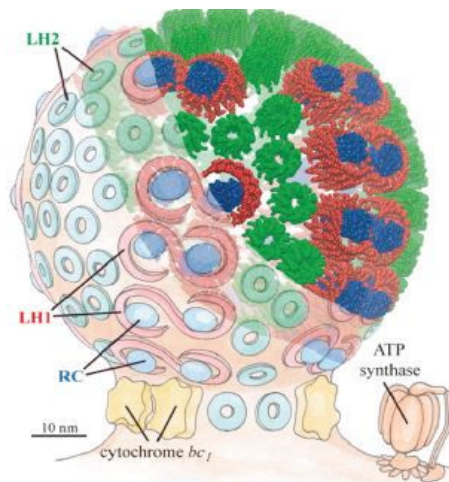


Figure 1.1: Schematic of the *Rh. Sphaeroides* with light harvesting complexes distributed around it in a lipid bilayer membrane. LH2 complexes are shown as green rings. The LH1-RCs are seen as dimers (red circles of LH1) with blue reaction centres within them. Cyt *bc1* and ATP synthase are visible beneath the main structure.¹

The simplified schematic, in Figure 1.2., taken from work by Cogdell *et al.*,² shows the energy pathway in a purple photosynthetic bacterium, such as the *Rh. Sphaeroides* from light absorption to its storage in adenosine triphosphate (ATP). (The structures do not represent the actual organisation of the components). Two light harvesting complexes, LH2 and LH1 absorb photons and the excitation energy passes to the reaction centre (RC) where charge separation follows. The excited bacteriochlorophyll dimer in the RC, transfers an electron to a secondary acceptor, Q_B . The Q_B picks up two protons from the cytoplasmic space to create the reduced quinol, QH_2 . Quinol is oxidised by cytochrome *c2*, and the cytochrome *bc1* complex. Two protons are then released into the periplasmic space. As protons are pumped across the membrane, a substantial transmembrane proton gradient is created. The redox cycle is completed when the oxidised bacteriochlorophyll is reduced. Finally ATP synthase rotates to accumulate sufficient protons to convert adenosine diphosphate (ADP) into adenosine triphosphate ATP, by adding a third phosphate group. To release the stored energy the phosphate group is removed by hydrolysis of ATP back to ADP.³

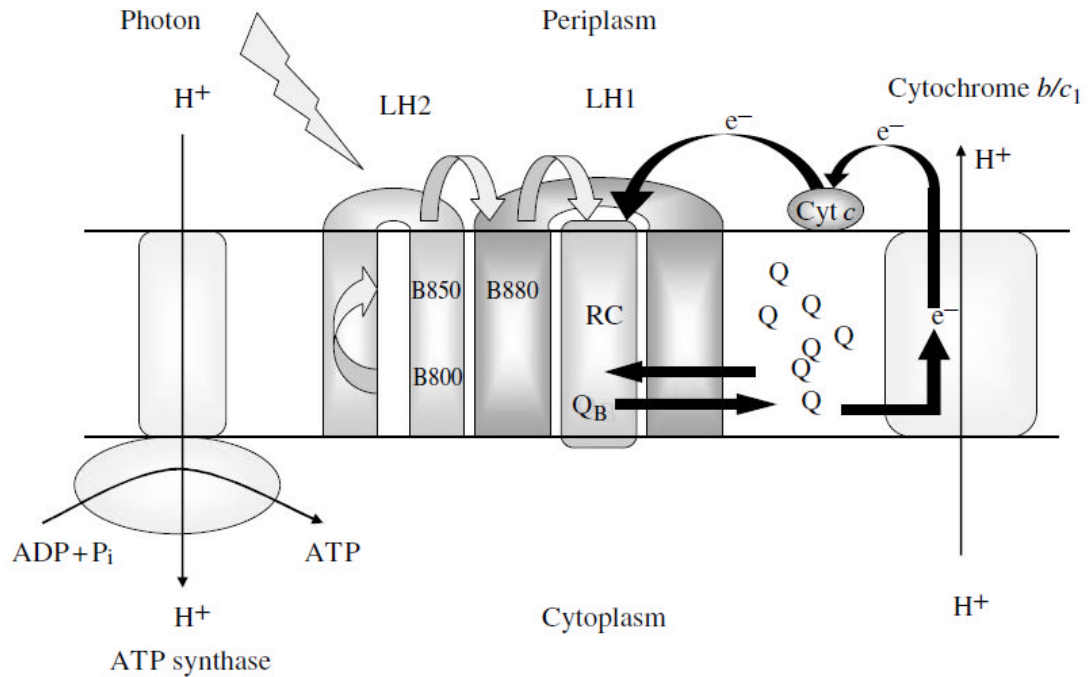


Figure 1.2: Simplified schematic of the energy absorption and proton transfer processes in a purple photosynthetic bacterium, such as the *Rh. Sphaeroides*, which leads to the production of stored energy as ATP. The light harvesting complexes, LH2 and LH1, absorb photons and the excitation energy passes to the reaction centre where charge separation follows. The cycle follows a redox reaction involving quinol, whereby protons are released into the periplasmic space. Finally ATP synthase utilises the protons of this transmembrane proton gradient to convert ADP to ATP. ²

In order to investigate and mimic this process, the project researchers will create a low-dimensional, nanoscale, construction similar to that shown in Figure 1.3. The boxes in Figure 1.3., represent a schematic version of the planned reproduction of the natural process shown in Figure 1.2.

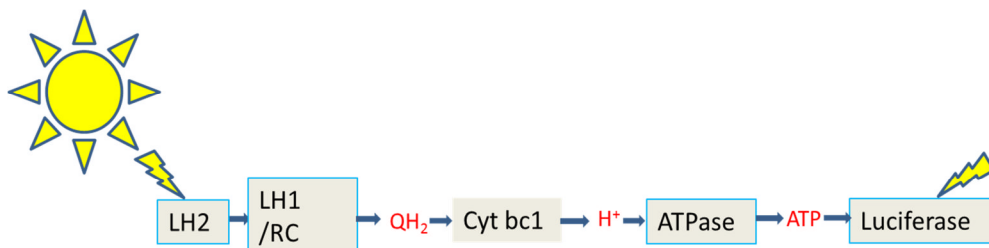


Figure 1.3: A simple plan for the outcomes of the project. This scheme is based on the creation of the corrals, using polymer brushes, which will contain the light harvesting proteins and house the surrounding bilayer medium in which the components ubiquinone, protons and electrons can diffuse between the proteins.

The components of the light harvesting system are shown contained in the grey boxes which will form a series of 'corrals' fabricated from polymer brushes. The corrals are joined

by narrow channels (indicated by the arrows), also created by polymer brushes. The channels, allow diffusion of the transport molecules such as ubiquinone, protons and ATP (shown in red). The scale of this construction will be measured in nanometres and the manipulation of proteins will also take place at low-dimensions, even at single protein level. These size restrictions set a huge challenge for project.

In order to maintain the integrity of the proteins, lipid bilayers (which are discussed in more detail in Chapter 2) will be incorporated into the 'corrals' at all stages. This will be done either by: 1) using the polymer brushes, which are resistant to lipids, as the boundary walls of the container or 2) depositing the lipid bilayer directly onto the brush or 3) surrounding a protein tethered to nanoposts within the corral. The light harvesting membrane proteins of LH2, LH1-RC, Cyt bc1 and ATP synthase will be incorporated into the bilayers within these corrals. The diffusion of quinones and protons between them, via the channels, will then be measured. Ultimately the production of ATP will generate the energy output, measured by the activation of Luciferase.⁴

It can be seen from this that lipid bilayers are vital components in this construction in order to maintain the integrity of the proteins being investigated. The creation of homogeneous, fluid polymer-supported lipid bilayers is thus an integral part of all of the work packages making up this project and is the essence of the work presented in this thesis.⁵

1.3. The cell membrane

The lipid bilayer, making up a natural cell membrane, has been described as one of the basic building blocks of life, the humble container for the important molecules of life as exemplified by the *Rh. Sphaeroides* in Figure 1.1. More significantly, a greater role of the membrane lipids has now been recognised as an integral part of cellular function.^{6 7 8}

Embedded within the cell membrane are many proteins, ion channels and pumps. Together these allow the membrane to transport small molecules, passively transport others and provide a barrier to unwanted molecules.

The study of membrane proteins has been a very important research area since 1964, when Singer and Nicholson⁹ proposed the fluid mosaic model for the cell membrane structure and began work on studying the proteins associated with it.

1.4. Cell membranes on planar solid supports

McConnell and co-workers¹⁰ were responsible for the ground-breaking work in trying to create a model system wherein a bilayer membrane would self-assemble on a planar surface. This would allow proteins to be incorporated into the bilayer and studied using a comprehensive array of microscopic and surface analysis techniques. From their inception, planar-supported lipid bilayers (SLBs) have provided useful model systems for studying: the role of membrane composition, the function of membrane proteins in 2D systems and in the development of ion channel-based sensors.^{11 12 13 14} Taking the phospholipids and proteins from a natural membrane and assembling them on a glass substrate creates a practical model system for delving into the natural world of protein function. From a simple starting point work began to expand its capacity, to produce lipid bilayers on other surfaces which might allow the re-assembly of the membrane with its proteins into something that more closely mimics nature.

1.5. Cell membranes on 'non-solid' supports

When a model lipid cell membrane is formed on a planar solid surface, it is typically separated from the surface by a thin water layer of 0.5 to 1.0 nm thickness.¹⁵ However, many membrane proteins have large extra-cellular domains that protrude above and below the bilayer, making it likely that these extra-membranous domains may interact adversely with the underlying solid support.^{16 17} A number of approaches have been explored to provide an appropriate spacer between the underlying solid support and the lipid membrane over the past three decades. So far no single strategy has provided a model system which would support a fluid bilayer and allow the incorporation of functional proteins.

Maintaining the natural cell's structure is the cytoskeleton¹⁸, which is bound by the lipid membrane, keeping the organelles in place. It is composed of microfilaments of monomeric actin and microtubules of dimeric tubulin, which have many of the properties of a dynamic biopolymer.¹⁹ In their natural state the cells also maintain a separation of between 10 and 100 nm via an extra cellular matrix and a cell-surface glycocalix.²⁰ In principle, hydrophilic polymer brushes could play a similar role to the cytoskeleton or glycocalyx and provide a potential support system for a lipid bilayer. As will be shown in Chapter 2, some of the early lipid membrane supports followed this model.

The properties required of a polymer brush would be to present a hydrated support that would interact minimally with any incorporated transmembrane proteins (TMPs), whilst

providing a robust support for a mobile bilayer. The underlying hydrated polymer brush would also provide a suitable 'reservoir' to allow the diffusion of ions and small molecules, which could transfer only via the incorporated TMPs. In an ideal system the interaction mechanisms by which the bilayer formed on these polymers would be understood and could be applied to other support systems.

Shown in Figure 1.4, is a detailed depiction of the corral containing Cyt bc1 shown in Figure 1.3. This construction approach would offer opportunities to incorporate all the light-harvesting proteins in the design of a biomimetic energy capture system as described above. It would also act as a platform for studying protein function, protein interactions with small molecules or as sensors in clinical diagnostics.

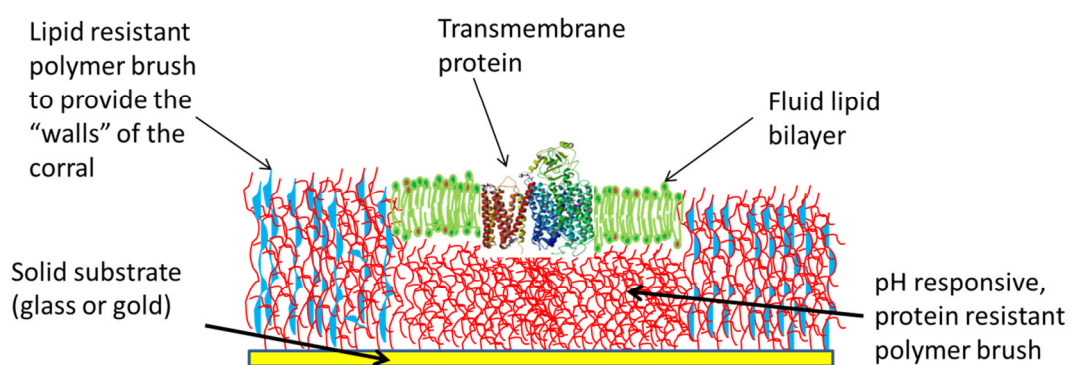


Figure 1.4: Schematic of the polymer brush supported lipid bilayer, as part of the system shown in Figure 1.3. This shows an incorporated transmembrane protein, Cyt bc1, with the corral boundary walls provided by a lipid resistant brush.

1.6. Thesis orientation

In order to provide the supported lipid bilayers on the protein resistant polymer brush, the results of incubating different lipid vesicles on a range of anionic, zwitterionic and cationic polymer supports are presented. The possible interactions taking place between the polymer brush and lipid vesicles/bilayer are also discussed. This has resulted in the publication of work to produce a successful novel polymer brush supported lipid bilayer. The system was then developed further in attempts to find an efficient method to incorporate light harvesting proteins into the system, as depicted in Figure 1.4. Presented in Chapter 2 is the background to the mechanics of the self-assembly process on planar substrates. This includes a discussion of the lipid-surface interactions which will support the discussions in the results sections. There follows a literature search of previous work on lipid bilayers deposited on polymer supports.

Chapter 3 explains the theoretical aspects of the key analysis methods used to characterise the lipids, the polymer brushes and the results of the deposition of lipid vesicles onto the polymer brushes. It covers polymer theory, as well as the methods, such as dynamic light scattering (DLS) used to characterise the lipid vesicles and polymer surfaces. Also covered is fluorescence recovery after photobleaching (FRAP), which is vital to characterising the interactions between lipids and the polymer brushes.

In Chapter 4 the experimental details are recorded for creating lipid vesicles, and incubating these on polymer supports. The methods for the attempts to incorporate light harvesting proteins are covered here also.

The first results Chapter (5) shows the detailed experimental results and discussions for the work on zwitterionic and anionic polymer brush surfaces. This covers the testing of the zeta potentials of the lipid vesicles and the characterisation of the polymer brush candidates tested for supported bilayer formation. This chapter concludes with the results of testing the incubation of lipid vesicles on polymer brushes in order to create fluid lipid bilayers.

Following this, in Chapter 6, attempts to introduce proteins into this new polymer supported bilayer system can be found, following a number reconstitution routes.

Chapter 7 reports on characterising the lipid vesicles and the experimental work done in attempting to form bilayers on cationic polymers, in a similar way to the work in Chapter 5.

Finally, in Chapter 8 the work is summarised and future work is suggested.

1.7. References

¹ Şener, M. K.; Olsen, J. D.; Hunter, C. N.; Schulten, K., Atomic-level structural and functional model of a bacterial photosynthetic membrane vesicle. *Proceedings of the National Academy of Sciences* **2007**, *104* (40), 15723-15728.

² Cogdell, R. J.; Gall, A.; Köhler, J., The architecture and function of the light-harvesting apparatus of purple bacteria: from single molecules to in vivo membranes. *Quarterly reviews of biophysics* **2006**, *39* (03), 227-324.

³ *Nature*, **2014**, Scitable definitions ATP-318.

⁴ Fraga H, Fernandes D, Novotny J, Fontes R, Esteves da Silva JC, "Firefly luciferase produces hydrogen peroxide as a coproduct in dehydroluciferyl adenylate formation". *Chembiochem* **2006** *7* (6): 929–35

Light is emitted because the reaction between ATP and luciferase forms oxyluciferin in an electronically excited state. The reaction releases a photon of light as oxyluciferin returns to the ground state.

⁵ The information about the project was collected from the grant application information, available only to members of the collaboration, found at :

<http://www ldc.group.shef.ac.uk/Members/LDC%20Case.pdf>

⁶ Lagarde, M., Geloën, A., Record, M., Vance, D. & Spener, F. Lipidomics is emerging. *Biochimica et biophysica acta* **2003**, 1634, 61.

⁷ Zhu, C., Hu, P., Liang, Q.-L., Wang, Y.-M. & Luo, G.-A., Recent Advances in Lipidomics. *Chinese Journal of Analytical Chemistry* **2009**, *37*, 1390-1396.

⁸ Tanaka, M.; Sackmann, E., Polymer-supported membranes as models of the cell surface. *Nature* **2005**, *437* (7059), 656-663.

⁹ Singer, S. J.; Nicolson, G. L., The Fluid Mosaic Model of the Structure of Cell Membranes. *Science* **1972**, *175* (4023), 720-731.

¹⁰ Brian, A. A.; McConnell, H. M., Allogeneic stimulation of cytotoxic T cells by supported planar membranes. *Proceedings of the National Academy of Sciences* **1984**, *81*, 6159-6163.

¹¹ McConnell, H.; Watts, T.; Weis, R.; Brian, A., Supported planar membranes in studies of cell-cell recognition in the immune system. *Biochimica et Biophysica Acta (BBA)-Reviews on Biomembranes* **1986**, 864, 95-106.

-
- ¹² Tamm, L. K.; McConnell, H. M., Supported phospholipid bilayers. *Biophysical journal* **1985**, *47*, 105-113.
- ¹³ Grieshaber, D.; MacKenzie, R.; Vörös, J.; Reimhult, E., Electrochemical biosensors-Sensor principles and architectures. *Sensors* **2008**, *8*, 1400-1458.
- ¹⁴ Naumann, R.; Jonczyk, A.; Hampel, C.; Ringsdorf, H.; Knoll, W.; Bunjes, N.; Gräber, P., Coupling of proton translocation through ATPase incorporated into supported lipid bilayers to an electrochemical process. *Bioelectrochemistry and Bioenergetics* **1997**, *42*, 241-247.
- ¹⁵ White, R. J.; Zhang, B.; Daniel, S.; Tang, J. M.; Ervin, E. N.; Cremer, P. S.; White, H. S., Ionic conductivity of the aqueous layer separating a lipid bilayer membrane and a glass support. *Langmuir* **2006**, *22*, 10777-10783.
- ¹⁶ Sumino, A.; Dewa, T.; Takeuchi, T.; Sugiura, R.; Sasaki, N.; Misawa, N.; Tero, R.; Urisu, T.; Gardiner, A. T.; Cogdell, R. J.; Hashimoto, H.; Nango, M., Construction and structural analysis of tethered lipid bilayer containing photosynthetic antenna proteins for functional analysis. *Biomacromolecules* **2011**, *12*, 2850-2858.
- ¹⁷ Giess, F.; Friedrich, M. G.; Heberle, J.; Naumann, R. L.; Knoll, W., The protein-tethered lipid bilayer: a novel mimic of the biological membrane. *Biophysical journal* **2004**, *87* (5), 3213-3220.
- ¹⁸ The intracellular matrix
- ¹⁹ Morris, J. R.; Lasek, R. J., Monomer-polymer equilibria in the axon: direct measurement of tubulin and actin as polymer and monomer in axoplasm. *The Journal of cell biology* **1984**, *98* (6), 2064-2076.
- ²⁰ Rehfeldt, F.; Steitz, R.; Armes, S. P.; von Klitzing, R.; Gast, A. P.; Tanaka, M., Reversible Activation of Diblock Copolymer Monolayers at the Interface by pH Modulation, 2: Membrane Interactions at the Solid/Liquid Interface. *The Journal of Physical Chemistry B* **2006**, *110* (18), 9177-9182.

2. Background

2.1. Introduction

This background information chapter is divided into three sections. In the first of these (2.2) the basics of the cell membrane will be introduced along with the lipids which form a major role in the cell membrane structure through their ability to self-assemble into a number of useful containment structures. Following this, the second section (2.3) will delve into the world of the self-assembly of lipid bilayers onto solid substrates which provides a very important introduction to the behaviours of lipids, vesicles and bilayers on planar supporting surfaces, underpinning the work in this thesis. The value of this work has been vital to many areas of fabrication science that find applications in diverse research from medicine to artificial energy creating systems.¹ Expanding on this, in the third section (2.4) systems will be discussed which are specifically relevant to the research being done here and are examples of other polymer-supported lipid bilayer systems.

2.2. Lipids and self-assembly

2.2.1. Cells and lipids

2.2.1.1. Introduction

The lipid membrane plays a key role in this fabrication project and creating the appropriate membrane environment to support functioning proteins is critical to its success. The schematic in Figure 2.1 shows the plasma membrane of a representative cell. The cell membrane is a lipid bilayer composed of a large number of different lipids, which are amphiphilic, having an ionic headgroup with hydrophobic chains attached.² They provide the environment for incorporated membrane proteins. The membrane is bound on one side by the glycocalyx and on the other (intracellular) side by the cytoskeleton. A natural membrane, in addition to lipids and proteins, contains cholesterol in a ratio of between 20 to 50%.³

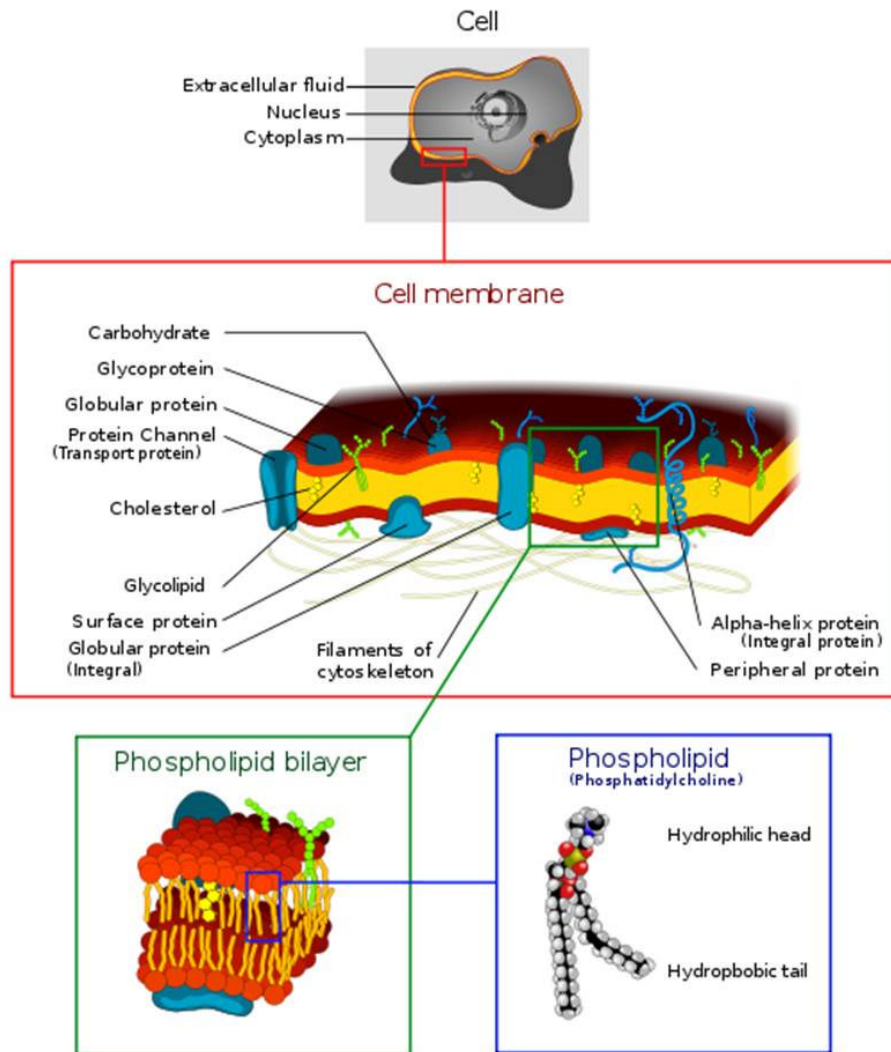


Figure 2.1: Schematic model of the cell membrane showing a cell and highlighting the composition of the membrane and details of the lipid bilayer. Image copied from ref. 4.

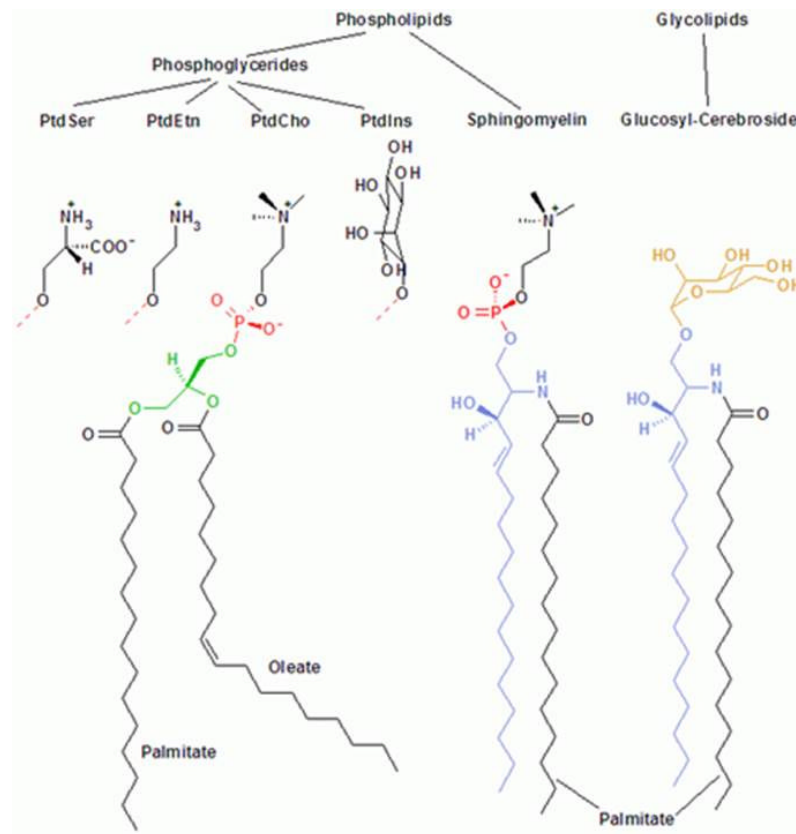


Figure 2.2: Examples of the structures of lipids found in a cell membrane showing the hydrophilic headgroups and hydrophobic chains. Image copied from ref. 5.

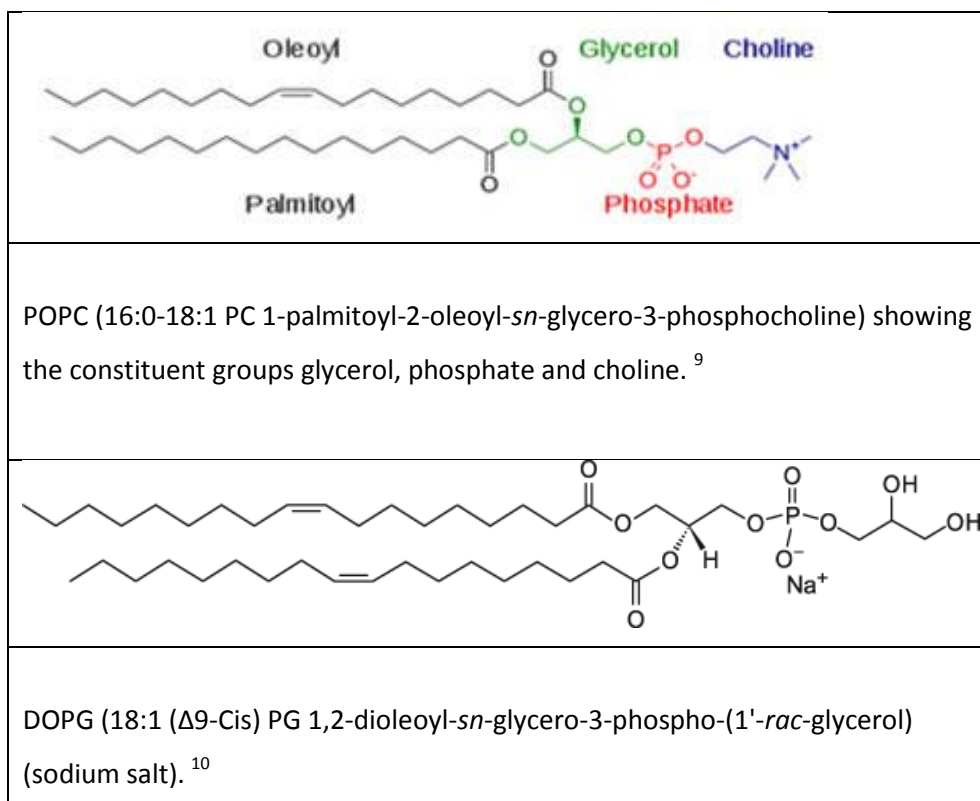
2.2.1.2. Lipid acyl chains

The phospholipid molecule is based on glycerol (see Figure 2.3) which has undergone esterification to attach two fatty acids (long chain hydrocarbons) to the first and second carbons.⁶ The fatty acid chains form the hydrophobic part of the molecule. There are many variables for the composition and length of the carbon chains and the nomenclature applied includes a reference to the chain length of the carbon backbone, position and conformation of any double bonds. These are generally *cis* (and not *trans*) in nature (see oleate in Figure 2.2). This creates a kink in the chain, affecting the packing of lipids, their fluidity in the membrane and lowering the transition temperature. Chain lengths for the fatty acids vary between two and thirty six, usually with an even number of carbons and with the most common having between sixteen and eighteen.⁷ In experimental work using lipids it is important to select those in the appropriate phase. To form fluid bilayers at room temperature, the lipid will need to be in the fluid phase, so lipids like 1-palmitoyl-2-oleoyl-*sn*-glycero-3-phosphocholine (POPC) or 1,2-dioleoyl-*sn*-glycero-3-phosphocholine (DOPC), which have acyl chain lengths of 18 carbons and one (in POPC) or two (in DOPC) unsaturated bonds, are preferred. Lipids such as 1,2-dimyristoyl-*sn*-glycero-3-

phosphocholine (DMPC), shown in Figure 2.3, have been extensively used in the literature, but have a melting temperature higher than room temperature and typically will have acyl groups of chain length of 14 carbons with no unsaturated bonds.

2.2.1.3. Lipid headgroups

To complete the basic structure of the phospholipid the phosphate (from phosphoric acid) attaches to the third (hydroxyl) oxygen of the glycerol. Other groups can be added to the head group to complete its ionic characteristics. The head groups of phosphocholine (PC) and phosphoethanolamine (PE) lipids are zwitterionic which means that they have both a positively charged quaternary amine group (choline) and a negatively charged phosphate group (see Figure 2.3). The headgroups phospho-(1'-*rac*-glycerol) (PG), and phospho-L-serine (PS) are negatively charged. These charged lipids have negatively charged phosphate (PO_4^-) or both a phosphate and an acid group (COO^-) in the headgroup respectively, and no amine functionality. There are no positively charged membrane lipids occurring in nature,⁸ however, the cationic lipid 1,2-dioleoyl-3-trimethylammonium-propane (DOTAP) is commonly used in experimental work which has been synthesized to include a quaternary amine group.



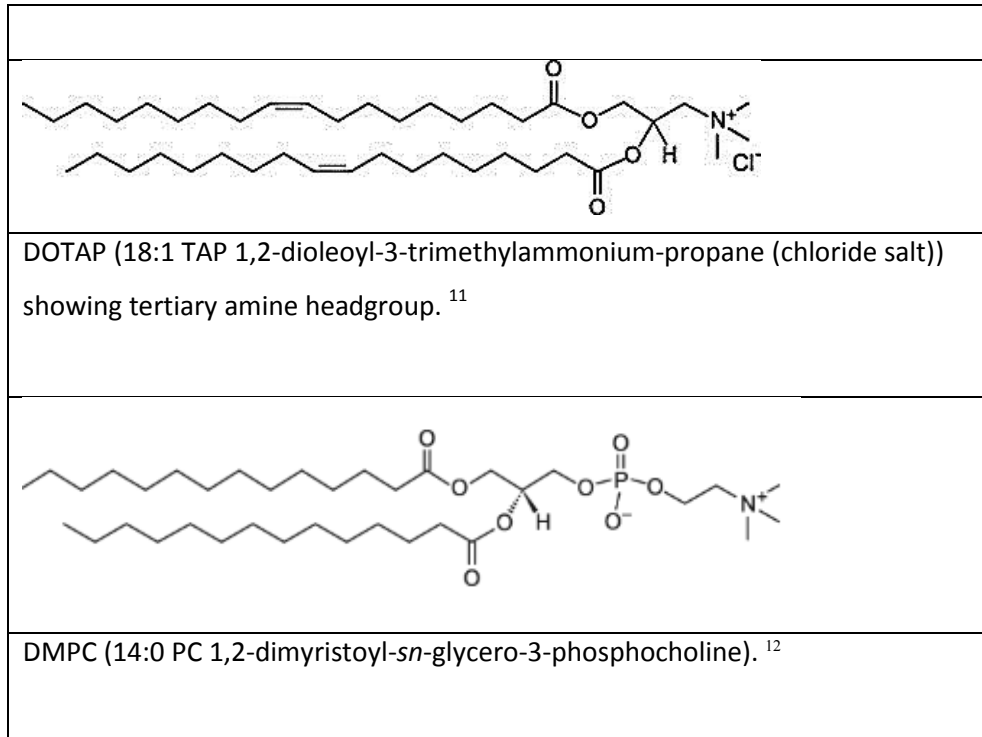


Figure 2.3: The structures of the commonly used lipids, POPC, DOPG, DOTAP and DMPC. Images taken from Avanti lipids online.

Shown above, in Figure 2.3, are the chemical structures of three lipids used in these studies, POPC, DOPG, DOTAP, with DMPC shown for completeness. The formula for POPC shows the three building blocks, a glycerol, two fatty acids chains and an ionic headgroup.

2.2.1.4. Micelles and vesicles

The useful activity, structure and fluidity of lipids in a bilayer, in vesicle or planar form, are seen only when it is fully hydrated. However, the hydrophobic tails of the lipid molecule, held together by van der Waals interactions, cannot readily insert into the quasi-ordered hydrogen bonding network¹³ of the water, without disrupting the hydrogen bonds. Any consideration of the mechanisms of self-assembly must consider the interaction free-energies and geometry of the molecules along with the thermodynamics of the whole system.^{Error! Bookmark not defined.} Critical to the self-assembly process is the behaviour of lipids interacting with water.

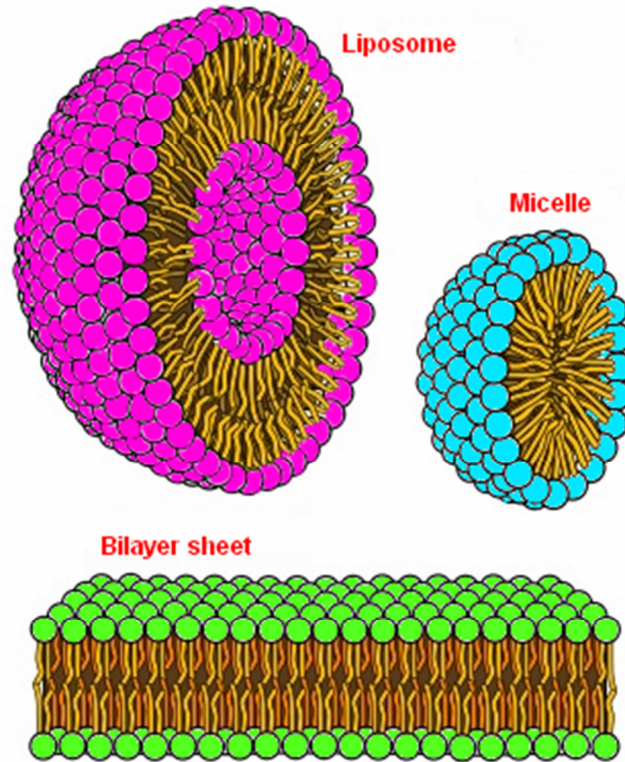


Figure 2.4: The structure of the liposome, micelle and planar bilayer and the packing parameter of the single and long chain lipids. Image from ref. 14.

The hydrophobic effect is the observed tendency of non-polar substances like these lipids to aggregate in aqueous solution and excluded water molecules.¹⁵ Water molecules naturally form a three dimensional network of hydrogen bonds between the protons and oxygen atoms of adjacent molecules. The introduction of a non-polar substance which, cannot form hydrogen bonds, will disrupt this network. To minimize this disruption, the water molecules will reorganize around the non-polar solute. The rearrangement creates an ordered layer of water molecules, which are more constrained. This leads to a loss of translation and rotational entropy of the water molecules, making the process unfavorable.¹⁶ By aggregating together the “hydrophobic” molecules reduce the surface area exposed to water and thereby the entropic cost of introducing the hydrophobic component into the aqueous phase. The free energy of such a transfer has both enthalpic and entropic components, given by the Gibbs free energy equation:

$$\Delta G = \Delta H - T\Delta S \quad (2.1)$$

Thus amphiphilic lipid molecules when added to water will organise themselves to minimise the contact between the hydrophobic chains with the water, whilst maximising the contact of the ionic headgroups with it. They will do this most effectively by forming into a spherical ‘micelles’ or ‘vesicles’. In the latter The external water facing layer is

composed of the ionic headgroups and the interior contains the hydrophobic chains. The water restructures itself to form a solvation shell around the outside of the vesicle.^{16 17 18 19} This *hydrophobic effect* is one of the most important non-specific interactions in biology for folding and creating proteins and lipid bilayers in water.^{20 21} A full discussion of this topic is not possible here but the reader is referred to recent texts e.g. Israelachvili 3rd edition. p151-7.²⁴

As a result of the above effects amphiphiles in water will form structures which are governed by the acyl chains attached to the polar headgroups. The packing parameter, which directly relates to this the shape, is calculated from the surface area of the lipid, a , the volume occupied by the hydrophobic chain v and the critical length of the acyl chain l . There are a number of shapes which could satisfy this parameter.²² For the assembly of micelles, which contain only one layer of lipid molecules, the surface area must be large, satisfied by the molecules having a large headgroup area and one small hydrocarbon tail volume.

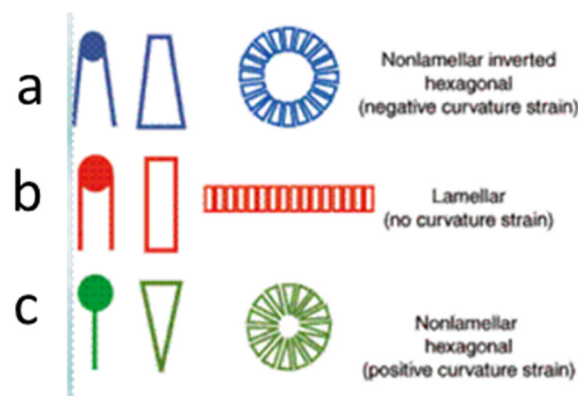


Figure 2.5: Diagram indicating the geometrical space occupied by lipid molecules with different acyl chain lengths and the structures created by aggregation of lipids and detergent molecules. (a) Highly disordered, kinked chains, (b) Straighter chains, forming bilayers and (c) Detergent molecules which form micelles. Image copied from ref. 23.

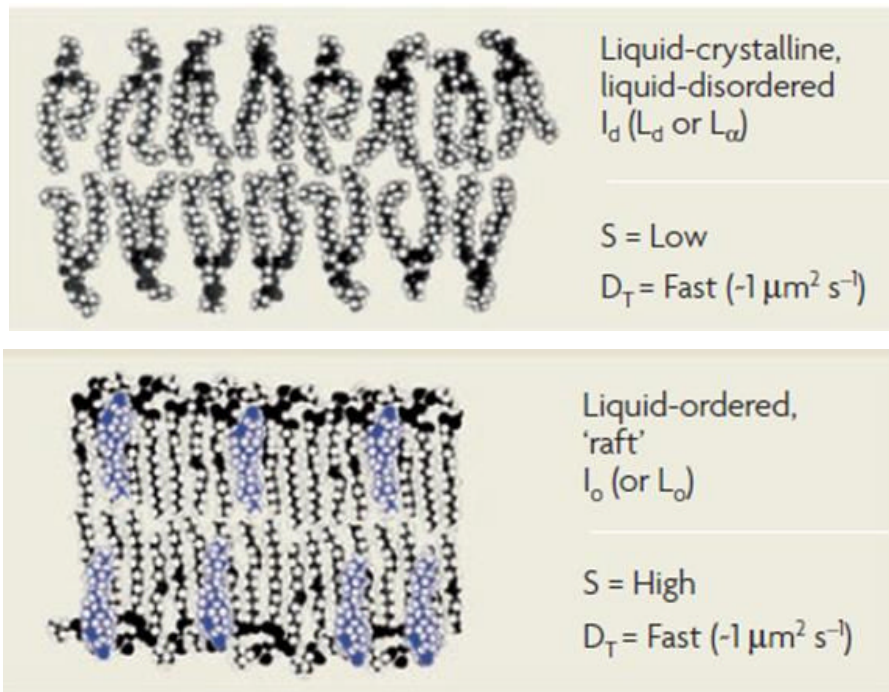
A pyramid shaped space will be occupied by this structure (Figure 2.5 (c)).²⁴ If lipid amphiphiles have relatively small headgroups and two bulky hydrophobic chains they cannot pack into micelles and will prefer to form bilayer vesicles/membranes.²⁵ These have two layers of lipids with adjacent hydrophobic chains. In this case v/al is close to 1, the chain length occupies an area twice that of the amphiphiles and is more cylindrical (Figure 2.5(b)).²⁴ The concentration of amphiphile molecules required in solution to cause a transition into micelles or vesicles is the CMC, critical micelle concentration. This decreases with increasing hydrophobicity of the molecule. Thus the CMC for micelle formation is

higher than that for forming vesicles.²⁴ The doubling of chains increases the hydrophobicity which lowers the CMC. It also increases the 'residence time' of molecules within the aggregate, which means that micelle constituent molecules will exchange with free molecules in solution more frequently than those of the lipids which form a 'bilayer' vesicle.^{Error! Bookmark not defined.}

2.2.1.5. Lipid bilayers

Lipid bilayers, the lamellar version of the lipid vesicle, are one of the most useful biomimetic systems and can be fabricated using many compositions of lipids, both natural and artificial. In addition to the factors which affect self-assembly, discussed above, there are some specific considerations to be taken into account when selecting lipids for experimental work.

The phase behaviour of a lipid bilayer, which is determined by its acyl chain structure, is of great significance in biology and consequently of research into lipid membranes.²⁵ The bilayer (lamellar) states can be liquid ordered, liquid disordered and gel phase with a characteristic phase transition temperature i.e. the point at which it changes from the gel (solid) to the fluid (liquid) phases, shown in Figure 2.6.²⁶



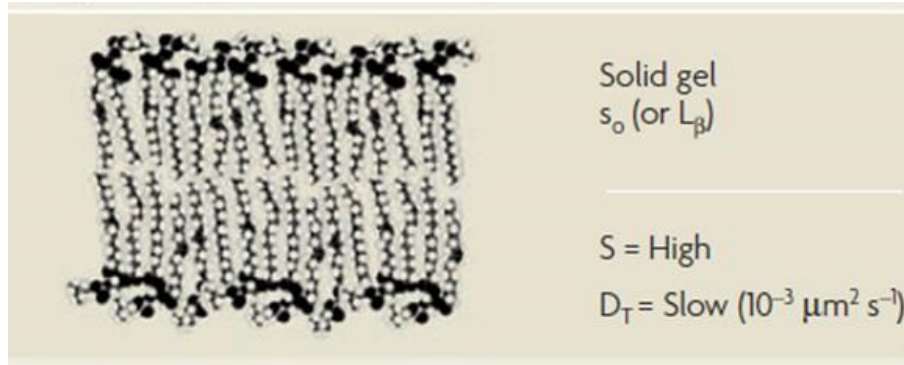


Figure 2.6: Shows the phases of a lipid bilayer. S is the order parameter of the acyl chain D is the diffusion coefficient. The liquid ordered phase has the order of a solid, but is very fluid. a) L_d diffusion is >1 but low chain order b) the gel phase, has diffusion is >1 with high chain order c) The gel phase is highly ordered with low diffusion <0.001 . Image taken from ref. 26.

The lipid molecules of the bilayer in the two liquid phases are restricted to movement in two dimensions in both cases, but have a 'random walk' diffusional degree of freedom around the bilayer.²⁷ Emphasis is placed on the fluid states to achieve the goal of this work on polymer supported lipid bilayers. One of the important and fundamental properties of this fluidity is that small defects in the bilayer will be re-sealed by the motion and rearrangement of the lipids. The significance of this for the natural cell membranes, containing proteins, is in the ability of the cell membrane to create a '*giga seal*' i.e. $>G\Omega$ and a large capacitance $\sim 2 \mu\text{F}/\text{cm}^2$.²⁸ This is vital to ensuring that the transfer of ions takes place only via the medium of the inserted proteins. This gives absolute control to the cell membrane (and its components) over the chemical composition of the cells' internal and external environments. There is a third motional freedom for the lipid molecules within the membrane whereby they will 'flip-flop', exchanging places between leaflets of the bilayer. This is a limited activity when compared to the diffusion in the flat plane because the ionic headgroup will need to traverse the hydrophobic core of the lipid bilayer, an activity which is energetically unfavourable.²⁹ This flip-flop activity, though limited, has been found to have a significant effect in charged systems, such as when a charged lipid is used to form a bilayer on an oppositely charged support, where an electrostatic driving force is at work.

The non-bilayer states, such as the hexagonal or cubic phases relate to membrane events such as pore formation, cell fission and fusion, which are transient states and will not be expanded on here.³⁰

Van der Waals forces are the main interactive force between the acyl chains of the lipid molecules in the bilayer and this interaction strength is what governs the phase behaviour.

^{31 32} The longer chains have a greater interaction area and hence a greater interaction

strength, which will restrict the movement of the individual lipids. As a rule of thumb a shorter chained lipid will have fewer points of interaction with its neighbours and will have more freedom of movement. The degree of saturation of the chain also has an effect in that an unsaturated *cis* bond will create a kink in the chain creating a disturbance in the packing of the lipids in the bilayer (see Figure 2.2). This will reduce the proximity of the next lipid, weaken the van der Waals attraction and make the bilayer more fluid.²⁵ As examples, the transition temperature (T_m) for a chain length of 18 carbons with no double bonds will be 80 °C. For a chain length of 18 with 1 double bond it will be 1 °C.²⁵

Natural membranes are composed of more than one type of lipid with different phase behaviours. This allows lipids of different types, those in the liquid phase and those in the gel phase, to accumulate as areas of separate phases.³³ One consequence of this is that certain proteins will partition into a specific phase, allowing concentration of that protein in one area of the natural membrane.³³ A discussion of the lipid membrane would not be complete without mentioning cholesterol. As shown in **Error! Reference source not found.**, it has an area of fused rings attached to a short acyl chain, which gives it a rigid structure, significantly disrupting the local lipid packing.

This section described the character and properties of lipids and their self-assembly into micelles, vesicles and bilayers. A more detailed study of the self-assembly of bilayers on solid substrates now follows.

2.3. Bilayers on solid supports

2.3.1. Introduction

In an ideal case, the spreading of vesicles (composed of the appropriate lipids, like POPC) onto a hydrated solid support is followed by adsorption of the vesicles onto the surface, rupture and spreading to form a defect free, fluid bilayer (Figure 2.4, lower image) . This process creates a flat bilayer 'sheet', two molecules thick, in which the individual lipids maintain a structure where the ionic head-groups face to the water side, the *proximal* leaflet facing the substrate and the *distal* leaflet facing into the liquid) with the hydrophobic lipid tails to the interior. Provided the sample is maintained in a hydrated environment the individual lipids will freely diffuse in 2D around the membrane area which will be defect free and stable. This simple and reproducible method potentially provides a suitable platform for the incorporation and study of membrane proteins.

Model cell membranes can be prepared on solid supports which are usually silicon oxides or gold depending on the characterization method or end use to be employed. The characterisation methods available for studying planar bilayers on solid supports are: nuclear magnetic resonance (NMR),³⁴ Fourier transform infrared (FTIR),³⁵ surface plasmon resonance (SPR),³⁶ neutron scattering,³⁷ quartz crystal microbalance with dissipation QCM-D,³⁸ AFM,³⁹ and FRAP⁴⁰

Presented in this section are some examples of work done to establish how good bilayers can be formed and insights into the mechanisms behind their formation on solid supports (SLBs), which may inform the deposition of lipid bilayers on polymer supports, presented later.

2.3.2. Bilayer formation

2.3.2.1. Introduction

Since the pioneering work on planar supported lipid bilayers by McConnell,^{41 42 43} extensive research has been done to develop this useful model system for studying the role of membrane composition and the function of membrane proteins.^{44 45 46 47} A vesicle interacts with a planar surface by a combination of long-range attraction and short-range repulsion forces which include electrostatic interactions, van der Waals, hydration and steric forces.²⁴ At the boundary edge of the adsorbed vesicles there is a balance in play between the adhesive and bending stresses.⁴⁸ Boxer's group⁴⁹ made important early contributions to the experimental work by finding that the process of bilayer formation is affected by the surface charge, chemical composition and roughness of the surface, taking into account the vesicle composition, charge and size. Two other groups have made significant contributions, headed by Brisson and Kasemo having studied the bilayer formation process in depth both experimentally and using simulations. Finally, the composition of the surrounding solution (ions, pH and ionic strength, temperature) plays an important role.^{50 51 52 53 54}

Despite many years of research the process is still not fully understood to a point where the bilayer deposition on solid supports can be translated directly across to the production of bilayers on 'non-solid' supports like polymers. The discussion which follows begins with an overview of the bilayer formation process, followed by work done in understanding the mechanisms and conditions involved.

2.3.2.2. The bilayer pathway

Early theoretical work on the possible interactions between vesicles and surfaces was presented by Seifert⁵⁵ in the 1990s, later confirmed by Reviakine⁵⁶ and also developed mathematically by Blount.⁵⁷ Seifert and Lipowsky presented theoretical data and described the vesicle shapes possible for a range of different bending and adhesive stresses.⁵⁸ This work suggested that vesicles interacting strongly with the surface would spread out to maximize the interaction area, creating a highly unfavourable bending energy and facilitating vesicle rupture.⁵⁹ Seifert also suggested that the propensity of vesicles to rupture depended on their size, so that below a critical size they would not rupture. Reviakine⁵⁶ used AFM to study bilayer formation on mica from zwitterionic vesicles. They also found that the outcome depended on vesicle size and concentration and that small isolated vesicles (<25 nm) remained intact, but larger vesicles ruptured to form a bilayer when higher concentrations of vesicles were present. They proposed that different bending moduli were applicable to the different sized vesicles. Keller⁶⁰ and Zhdanov⁶⁷ combined QCM-D and SPR with computer simulations to establish that surface bound vesicles, during the bilayer formation process, required 'critical vesicle coverage' and that the stress of deformation of vesicles in close proximity would induce rupture. This early work was followed by Brisson's group^{61 62} who studied the adsorption process of vesicles on a mica surface using QCM-D and AFM and proposed four 'qualitatively different' pathways for bilayer formation after the application of lipid vesicles to a planar surface. In the first case, with a low surface coverage, a complete bilayer is produced, as shown in Figure 2.7 (A). A fluid bilayer would also be formed by vesicle fusion but required a higher surface coverage, as seen in (B). The third variant is that a vesicular layer is adsorbed but does not fuse into a bilayer (C). The final pathway is that no vesicles adsorb onto surface (D).

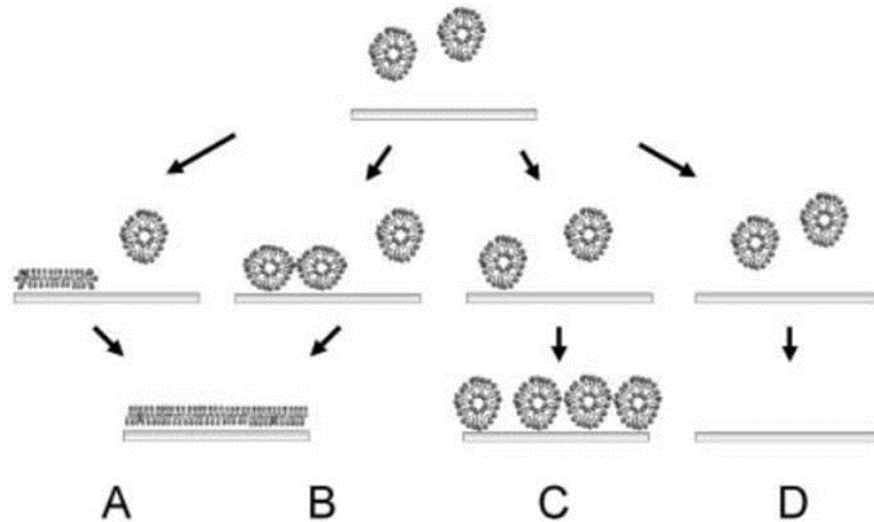


Figure 2.7: Four possible outcomes following the incubation of lipid vesicles on a solid surface. Image copied from ref. 61.

Following through the successful bilayer formation pathways A and B (in Figure 2.7) further work by Brisson's group suggested four possible mechanisms for bilayer formation driven by the interactions between lipid vesicles and the support, those between adsorbed vesicles and also the molecular interactions within adsorbed vesicles.

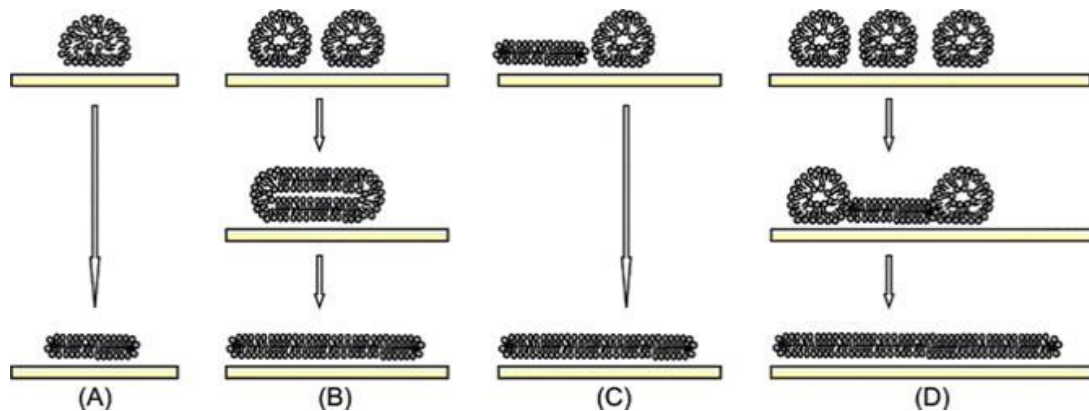


Figure 2.8: Mechanisms of vesicle rupture: (A) an isolated adsorbed vesicle ruptures spontaneously, driven by its support-induced deformation; (B) neighbouring adsorbed vesicles fuse and eventually rupture; (C) the active edge of a supported bilayer patch induces the rupture of a neighbouring vesicle; (D) the cooperative action of several neighbouring vesicles leads to the rupture of a first vesicle (at the critical vesicular coverage). The active edge thereby exposed triggers the rupture of adjacent vesicles. Image copied from ref. 63.^{61 62}

According to Brisson,⁵⁶ the critical steps begin with the attraction between the vesicle and the surface, (Figure 2.8) which requires a balance between the adhesion energy and the cost in curvature energy when the vesicle flattens onto it. When a 'critical coverage' of

vesicles is reached on the surface, the interaction between them is short ranged as they will be confined together in a limited space. The deformation induced stress between the vesicle and support, enhanced by the proximity of other vesicles, induces rupture. Growth of the bilayer takes place by fusion of the unfolded vesicles, as the edge, which is exposed by each vesicle after rupture, is thermodynamically unfavorable. Gozen *et al.*⁶³ found that for a circular patch of bilayer the edge energy is

$$E_{Edge} = 2\pi r\gamma \quad (2.2)$$

R is the radius of the patch and γ is the edge tension.⁶⁴

The formula for the bending energy is given below.

$$E_{bend} = 4\pi(2\kappa + \bar{\kappa}) \quad (2.3)$$

Here κ is the bending modulus and $\bar{\kappa}$ is the Gaussian modulus.⁶⁵ If the bending energy cost is greater than the edge energy, then a bilayer will form. If the bending energy is lower, a vesicle will be the most stable option.⁶⁶

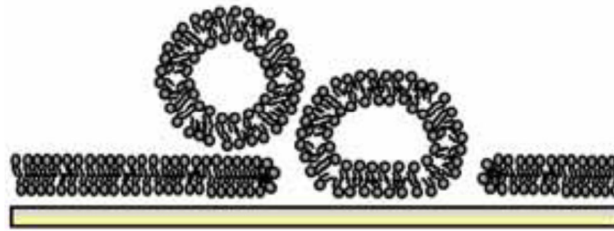


Figure 2.9: A “trapped” vesicle. The surface-bound vesicle is located sufficiently far away to remain unaffected by the bilayer edges though close enough to prevent the edge-induced rupture of other vesicles from solution. Such an arrangement inhibits the further propagation of bilayer growth, leaving trapped vesicles as defects. Image copied from ref. 62.

This fusion process can be prompted by the proximity of other bilayer patches or nearby vesicles where the proximity effect appears to be twofold: a) to ensure a sufficient concentration to cause rupture and b), to ensure a supply of new vesicles in the area to ensure that there are no gaps between bilayer edges which may inhibit full bilayer formation. Richter⁶¹ proposed that a trapped vesicle could remain separated from the bilayer edge and prevent rupture in that region (Figure 2.9), causing a defect. Zhdanov *et al.*⁶⁷ suggested that when a 'critical coverage' of vesicles is reached on the surface many vesicles will be closely confined. If the vesicles are not able to move across the surface there will be extra stress induced, which ruptures the vesicle. If vesicles can roll across the surface some of the stress will be released so it becomes important that a critical coverage

is achieved.⁶⁷ As vesicles rupture, the active edge of the bilayer patch will slide across the surface and will catalyse the rupture of more vesicles in the vicinity.⁶⁸ However, Richter argued that the lateral movement of the vesicles and bilayer were required to ensure the interaction of the edges of patches, reducing the line tension and facilitating full bilayer formation. Weirich *et al.* followed the formation of bilayers from DMPC.⁶⁹ The results suggested that vesicles rearranged on the surface, moving around in thermal motion as more vesicles adsorb before they rupture and fuse. They further suggested that vesicles can desorb as fusion takes place as they are not as readily attracted to the forming bilayer surface as they are to glass.

2.3.2.3. The effect of vesicle charge

The experimental work presented later in this thesis focusses on the use of charged vesicles interacting with charged and uncharged polymer surfaces. It was therefore necessary to research in some detail the work presented in the literature on charged lipid vesicles interacting with charged solid surfaces.

Richter, working in Brisson's group,^{61 70} studied the effect of adsorbing negative (DOPS), neutral (DOPC) and positively charged (DOTAP) onto an anionic (quartz) surface using QCM-D. Positively charged DOTAP vesicles appeared to rupture when in isolation on the negatively charged support and formed a bilayer at concentrations lower than for the neutral or negative vesicles (Figure 2.8, path A). This was suggested to be the result of the vesicles electrostatic attraction with the surface combined with the reduced stability of the isolated vesicles. The bilayer formation and spreading appeared to follow slowly, which they attributed to vesicle-vesicle repulsion. Vesicles with neutral (DOPC) or 25% charge (DOTAP:DOPC or DOPS:DOPC) required a greater coverage of vesicles before rupture would occur (Figure 2.8, B). Vesicles of 50% DOPS did adsorb onto the surface but remained as a vesicular layer. When incubating vesicles of high negative charge (65% DOPS) there was no adsorption at all, with electrostatic repulsion between the vesicles playing a dominant role.

The effects of the vesicle charge on vesicle deformation were investigated by Kasemo's group using simulations.⁷¹ They investigated the result of vesicles interacting with an anionic silica surface and varied the vesicle charge progressively from negative to positive. They found that the adsorption kinetics and bilayer formation changed from a) no adsorption to b) a layer of adsorbed vesicles c) a bilayer produced from a critical coverage of vesicles to d) spontaneous rupture of vesicles without full coverage, as defined earlier by

Brisson's group. Dimitrievski⁷¹ found that when a vesicle approached the (anionic) silica surface that the positively charged lipids were attracted and negative ones repelled, as expected (shown in Figure 2.10). Dipolar (zwitterionic) PC lipids, however, were weakly attracted as there was a dipole in operation within the lipid arising from the cationic amine group being closest to the surface. This, they suggested, allowed some measure of electrostatic interaction to take place with the surface. When the vesicle approached the surface there was an energy cost and the deformation took place at the expense of elastic energy. There was clearly a balance to be reached when the interactions between surface and vesicle were moderately attractive.

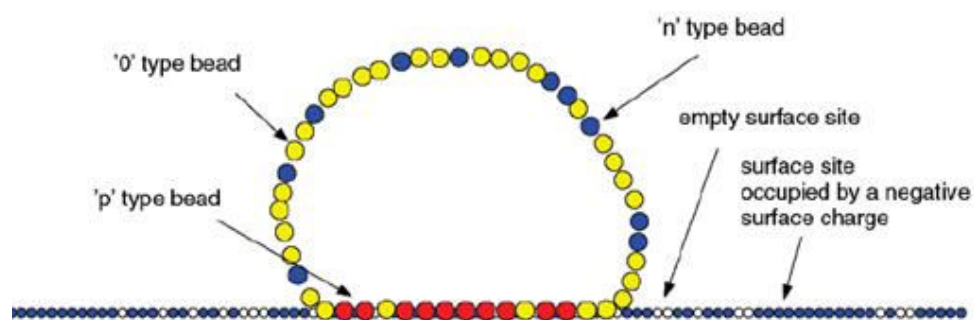


Figure 2.10: Illustration of the 2D model of an adsorbed vesicle. The different bead types are initially randomly distributed within the vesicle, and then rearrange upon adsorption according to energy minimization (corresponding to electrostatic interaction with the surface and lateral diffusion of lipids within the outer leaflet of the lipid bilayer in real vesicles). Image taken from ref. 71.

When a vesicle is oppositely charged to the surface it could rupture spontaneously without requiring a critical coverage.⁶² However, if strongly attracted to the surface the patches may not be mobile, which appeared to be an important requirement to create a mobile bilayer. For >40% p-type there was evidence of spontaneous rupture. In the latter instance the group suggested two possible unfolding scenarios. The first was where the vesicle ruptured at one end, leaving it attached to a bilayer patch and the second where it ruptured at both ends. In the second case it may leave a bilayer patch with another one floating above it, which may be adsorbed onto the first patch.

Looking further into the interactions of the lipid headgroups with solid surfaces, Fortunelli⁷² performed a detailed simulation to elucidate the effects of three types of lipid: DOPC, DOPS, DMTAP interacting with titanium oxide surfaces. They found that the DOPC lipid has a zwitterionic headgroup with no net charge but has a dipole moment, containing four reactive oxygen atoms which allow the lipid to form coordinated and H-bonded complexes

with the surface and water. The DOPS headgroup has an acidic group and a total of 6 reactive oxygen atoms allowing a stronger involvement in H-bonding to water and surface -OH groups. DOPS headgroups are also able to form inter-lipid H-bonds via -NH_3^+ and -C=O or, less commonly, -P=O . The carbonyl oxygen atoms form mono or bi-dentate coordination with the surface titanium atoms and the -NH_3^+ groups can bridge to the oxygen atoms on the surface using hydrogen bonding. They further found that the most stable attachments appeared to be where the lipid carboxyl oxygen atoms are rigidly pinned to the surface and -NH_3^+ groups interact with the surface hydroxyls. The DMTAP headgroup has a positive charge with 2 reactive oxygen atoms, but its interaction is dominated by the bulky $\text{-N(CH}_3)_3$ group, which causes steric hindrance, so this moiety stays near the surface. These molecules have only two active carbonyl oxygen atoms and the binding is ruled by long-range electrostatic interactions between the amine and the surface.⁷²

Jackman *et al.*,⁷³ following on from work done by Tero,⁷⁴ were curious to understand the reasons why the interaction between titanium and vesicles was stronger than that between glass and similar vesicles. They considered that on hydrophilic substrates silica and mica, vesicles adsorbed and ruptured to form a bilayer, whereas on titanium oxide and gold, vesicles will adsorb and remain intact. On hydrophobic substrates like self-assembled monolayers lipids will form a monolayer. They looked at the charge interactions between vesicles and titanium oxide surfaces. Jackman concluded that electrostatic attraction was insufficient to cause vesicle rupture. The group considered a combination of DLVO forces and a repulsive hydration force. Further, they found that the hydration force accounted for short-range repulsion at $< 2\text{ nm}$ separation, with an equilibrium being observed at 1.8 nm .⁷⁵ At separations below 3 nm the interaction would be strongly attractive van der Waals with weak hydration repulsion. They suggested that the processing technique may attenuate the hydration force because a lower density of surface hydroxyls would be less capable of forming a hydrogen bonded water layer.⁷³

Proposing three options for vesicles spreading on the surface, Wu *et al.*⁴⁸ worked on simulating the shapes of vesicles adsorbing onto the surface and their interactions with charged surfaces. They suggested that stages began with intact vesicles, followed by partial disintegration of vesicles and, finally, full SLB formation. Wu compared the shapes achieved

for three interaction energies with the surface: 5, 10 and 16 $k_B T$, looking at the extremes of the angles between the vesicle edge and the surface as shown in Figure 2.11.

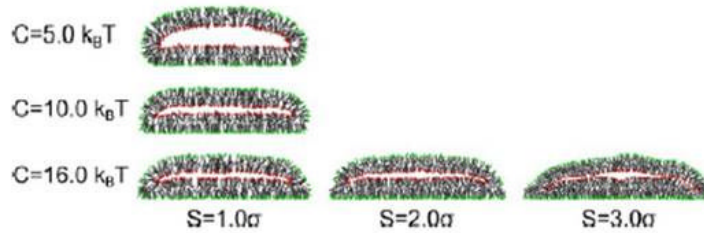


Figure 2.11: Changes in the deformation of vesicles as the surface interaction is increased. Image copied from ref. 48.

Vesicles were seen to deform more at high (surface) potential interaction strengths which increased the contact area with the surface. They found that the vesicles adsorbed, flattened, then a pore formed at the lower edge near to the flattened area where the deformation is greatest where there is, what they described as 'packing frustration'. Following this the vesicle top shrank and the pore size increased and the bilayer formed. Although the group were working with a planar solid surface this is an interesting concept and may translate to the interactions between charged vesicles and charged polymer surfaces.

2.3.2.4. The effect of buffer ions, osmotic pressure and pH on bilayer formation

Presenting a view of the bilayer formation process on planar surfaces, Boxer's group⁴⁹ and also Johnson and co-workers⁷⁶ created a phase diagram (Figure 2.12) which demonstrated how successful vesicle fusion was influenced by the ionic strength and pH of the buffer. The egg-PC vesicles were slightly anionic (by using a charged fluorophore) and the surface was also anionic (glass). Fusion occurred at low pH or high ionic strength if vesicles are slightly negative and the surface was glass (also negatively charged). Adsorption was inhibited at higher pH and lower ionic strength.

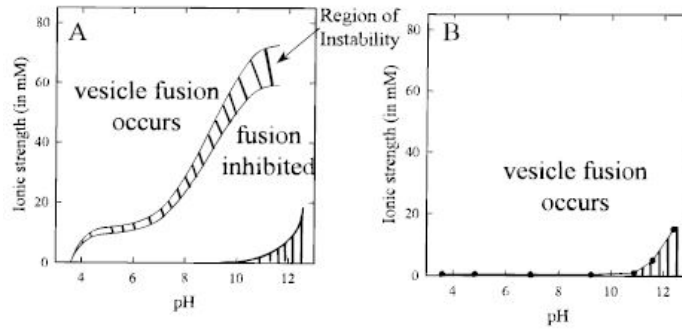


Figure 2.12: The phase diagram for the influence of ionic strength and pH for A) similarly charged surface and vesicles B) oppositely charged vesicles and surface. Image copied from ref. 49.

The solution conditions did not affect the vesicle fusion when the vesicles and surface were oppositely charged and at all ionic strengths and pH the fusion is successful. The role of the buffer in the attraction of vesicles to the surface was further considered by Cha *et al.*⁷⁷ who demonstrate that even for zwitterionic lipids the electrostatic interaction is critical in controlling the adsorption and fusion of lipid vesicles and that the outcome was strongly influenced by the buffer composition (Figure 2.13). On both positive and negative SAM layers with a high surface charge density (>80%), neutral lipids would form bilayers. However, they found that when using uncharged lipids on a less charged surface that a 'large' buffer ion (e.g. Tris, $C_3H_5(OH)_3-NH_3^+$) having an opposite charge to the surface, prevented bilayer formation. They suggested that the electrical double layer repulsion created by the large counterions was the cause. If the lipids used were oppositely charged to the surface, this critical dependence was not observed. Using a positively charged lipid with a negative surface, a fluid bilayer was formed with either buffer. It was possible to aid the adsorption of negatively charged vesicles to the similarly charged surface by adding Ca^{2+} ions which act as a fusogen between the carboxylate or phosphate groups of the lipids and the surface.⁵⁶ The completion of the bilayer in this case required excess vesicles to be available from the surrounding suspension.⁶⁷

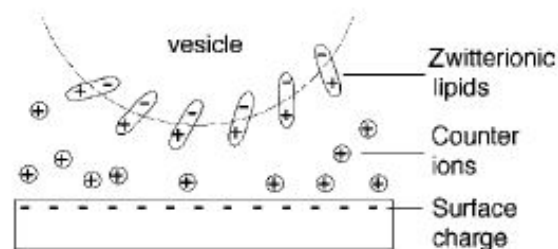


Figure 2.13: Schematic illustration of the influence of large buffer counterions in solution. Image copied from ref. 77

Cha also added salt (NaCl and CaCl₂) to the buffer to evaluate how that modified the result, an effect also studied by Seantier and co-workers,⁷⁸ who specifically related the dependence of bilayer formation on monovalent and divalent ions. They found that the divalent ions are effective in much lower concentrations than mono-valent ones. They found that critical vesicle coverage varied depending on the ions which affect the vesicle-surface, and vesicle-vesicle interactions, by screening or bridging the charge effects. The literature indicates that a stabilising effect is important when binding of the ions to the POPC lipids takes place as the ionic strength is increased. This promotes bilayer formation by enhancing vesicle-surface and vesicle-vesicle interactions. The divalent ions form a bridge between the surface and the lipid headgroups, and it was also suggested^{79 80} that the presence of calcium may decrease the thickness of the water layer, increasing the adhesion between the vesicle and the surface.

Three groups looked in detail at the osmotic effects and whether excess pressure inside or outside of the vesicle would influence the rupture mechanism. Hain and co-workers⁸¹ used the principle that hyperosmotic stress within the vesicle will induce water to enter from outside, whereas hypo-osmotic levels within the vesicles cause the water to be expelled. They found that high osmotic pressure outside the vesicle did affect the deformation of the vesicle but the pathway of vesicle rupture was not affected by these osmotic pressure changes. The effect of changing the internal osmotic pressure of vesicles was also studied by Zhu *et al.*⁸² who observed that the change in osmotic condition did not affect the vesicle height. Zhu concluded that the deformation by close contact with other vesicles was more important in causing rupture. The change in osmotic pressure was concluded to have little effect *per se* on the vesicles fusion process, which confirmed work done by Boxer. However, the change in vesicle shape caused by the change in osmotic pressure may aid the fusion process. Jackman *et al.*⁵³ demonstrated that they could influence the rupture pathway by changing the osmotic pressure outside the vesicle. They found that zero salt outside the vesicle would produce a vesicular layer, whilst 1M salt outside the vesicle would induce rupturing without the requirement for critical vesicle coverage, a result which was suggested earlier by Reimhult.⁸³

The effect of changing pH was studied further by Frank's group⁸⁴ who looked at the differences in adsorption and rupture of POPC vesicles onto silica and titanium substrates, following the kinetics by QCM-D. They reported that under acidic pH the vesicles and the

solid surfaces were near neutral, suggesting that adsorption was not electrostatically driven. However, electrostatics influenced fusion and bilayer propagation, more so with titanium than silica surfaces in order to form a bilayer. At higher pH intact vesicles were adsorbed, at lower pH a bilayer is formed, but the pH needed to be more acidic (pH3) for titanium than for silica. The kinetics of adsorption on silica changed to one step kinetics (i.e. immediate rupture) at low pH 4 with a difference in action being observed depending on the vesicle size. It was suggested that van der Waals, hydration and steric forces are at play with silica, but that there is some additional electrostatic requirement with titanium.

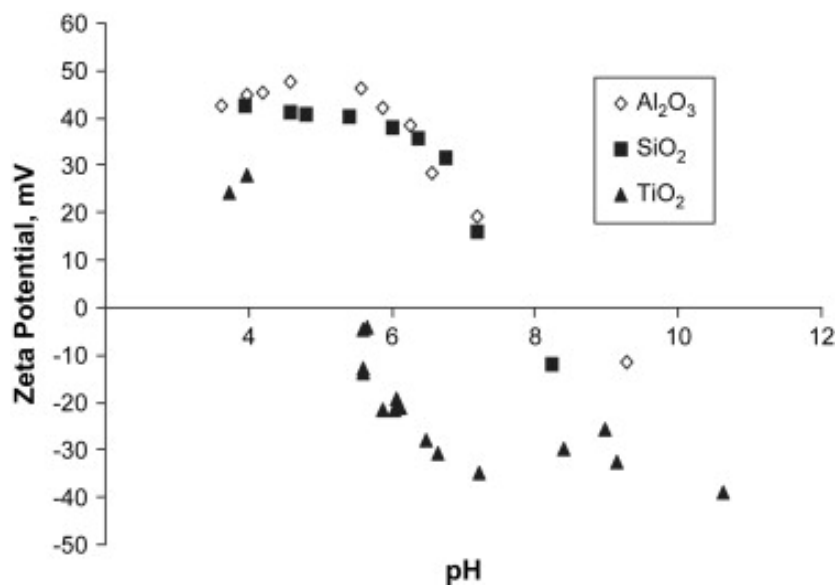


Figure 2.14: Zeta potential of oxide nanoparticles measured in 1 g/L NaCl solution, indicating that titanium oxide (triangles) has an overall lower zeta potential than silicon oxide (squares). Titanium oxide has a lower isoelectric point of ~ pH 5 compared to that of silicon oxide at ~ pH 7.5. Image copied from ref. 85.

At alkaline pH vesicles were adsorbed onto both surfaces, without fusion. The vesicles on titanium were more easily removed than those on the silica under these conditions. The zeta potential measurements⁸⁵ indicated that titanium oxide had a lower zeta potential than silicon oxide, as shown in Figure 2.14.

In summary, a significant volume of work has been done which studied the effect of osmotic pressure and pH on the rupture process. There is no agreement within the literature as to whether the change in NaCl concentrations affects the rupture process. The research perhaps favours the view that it may influence the rupture/bilayer formation pathway, once vesicles have adsorbed, by changing their shape, rather than creating the initial conditions for adsorption. The effect of pH has been demonstrated by considering the effect on the electrostatic interactions between the vesicles and the surface. The buffer

pH was further suggested to determine whether vesicles on the surface would fuse or remain intact.

2.3.2.5. The effect of temperature

During the process of testing the polymer brush systems, shown later in Chapter 5, it became evident that increasing the temperature during bilayer formation contributed to the success of at least one system. An investigation of the literature revealed a number of studies looking at the effect of increased temperature on lipids, vesicles and on bilayer formation.

Kasemo's group^{83 86 87} investigated the effect of temperature on bilayer formation over a temperature range of 278 to 313 K. Using QCM-D they found that the minimum frequency and maximum dissipation shifts decreased with increasing temperature, suggesting that a lower concentration of vesicles was needed on the surface for fusion to take place when the temperature was elevated. They specifically showed that the adsorption kinetics were temperature dependent and that a higher surface concentration of vesicles was required at lower temperature for vesicle fusion to take place. They measured the vesicle to bilayer activation energy to be 5 kcal/mol.

QCM-D was also used by Reviakine and other groups^{88 89 90} to study the effect of temperature on the deformation of DPPC and DMPC vesicles. They found that there was greater deformation of the vesicle at higher temperatures and that this deformation would aid rupture. To counter this argument, Cho and coworkers⁹¹ considered that there was a disadvantage with using QCM-D is that the amount of trapped water measured by this method would vary with temperature, making accurate readings difficult. Cho used SPR and found that an elevated temperature of 50 °C would cause some deformation in the DOPC. Adsorbed vesicles undergo shape changes by interacting with the surface and with nearby vesicles,

$$Q = \frac{Wr^2}{\kappa_1} \quad (2.4)$$

Where W is the contact energy per unit area, r is the 'un-deformed' radius of the vesicle and κ_1 is the membrane bending rigidity. If Q is large the vesicles will be easily deformed and more likely to rupture.^{92 93}

The lipids used in this study have high transition temperatures (T_m) and would pass through the transition point in the temperature range studied, causing a phase change

from gel to fluid. The lower T_m lipids, such as POPC and DOTAP would not pass through this phase change during that temperature range. Pan *et al.*,⁹⁴ studied DOPC vesicles and bilayers using X-Ray scattering in the temperature range 15 °C to 45 °C and they found that the area per lipid increased from (70 to 75 Å²) and the bilayer became thinner as the temperature increased.

To summarise the work done on the effect of temperature there is some disagreement as to the accuracy of the measurements made using QCM-D. The majority of the work has been done using higher T_m lipids and it is difficult to translate this work to all lipids, such as those with lower T_m . This is because it follows the effect in increasing the temperature (from room temperature to 50 °C) on bilayer formation through a change in phase from gel to fluid. One relevant argument may have been made by Pan, however, who suggested that there a greater volume is occupied by the individual lipids causing the vesicles' deformation to increase when they are heated.

2.4. Polymer supported lipid bilayers

2.4.1. Introduction

A brief and initially unremarkable looking paper on the incorporation of polymeric analogues into lipid vesicles was presented in 1984 by Helmut Ringsdorf's group, subtitled "*How to bridge the gap between Polymer Science and Membrane Science*". At that point he was making the rather radical suggestion that chemists may be encroaching on the "*foreign grounds*" of bio-membranes. It is common practice today for science projects to be funded which encourage an alliance between the sciences, medicine, mathematics, engineering and more. Collaborations are such an obvious common sense idea that his 'radical' idea sounds anachronous, made as it was 30 years ago at the dawn of the polymer supported bilayer era.

More interesting is the fact that the ideas and results presented in this and associated papers are forward thinking (as discussed below) and begs the question why research in the field has not yet achieved its full potential. So far no model surface of a membrane spacer, with all the properties required to mimic the natural cell and to support the incorporation of proteins for functional testing, has yet been published.

Within this section of the thesis the background to the fields of polymer-supported lipid membranes will be described. Studies on the use of natural macromolecules similar to those found in the extra- and intra-cellular matrices will be introduced first. The second body of work to be considered is the extensive use of polyethylene glycol (PEG) and its

derivatives. This leads logically from the work on natural systems and develops the idea that lipopolymers can create hydrophobic tethers into the bilayer membrane in a similar way to the natural cholesterol and glycolipids. Thirdly, the body of work on polyelectrolyte monolayer brushes (PELs) is covered, into which group the experimental work presented in this thesis fits. This body of literature is explained in some detail, as the findings from this are not only relevant to the preparation but also to the discussion of the results (both positive and negative) of the interactions between the polymers and lipids. Finally, this group of PELs is extended to include polyelectrolyte multilayer brushes (PEMs) where polymer films have been prepared using charged polymers in alternating layers, to aid the control of the polymer support properties and electrical charge. Some of these examples link back to the first group of 'natural' membrane supports. Again, the aim of highlighting these systems is to inform the understanding of the results presented in this thesis.

2.4.2. Natural polymer systems

This review begins by presenting a number of systems where the researchers have modelled their polymer supports on aspects of the cell glycocalyx, which has amongst its components the glycolipid, as shown in Figure 2.15. In its simplest form this membrane support structure includes a lipid fatty acid chain, which inserts into the lipid membrane and a sugar group which extends into the aqueous environment outside the cell. The systems presented below are based on naturally occurring polymers and the work shows how the understanding of the requirements for a successful polymer supported bilayer system has developed.

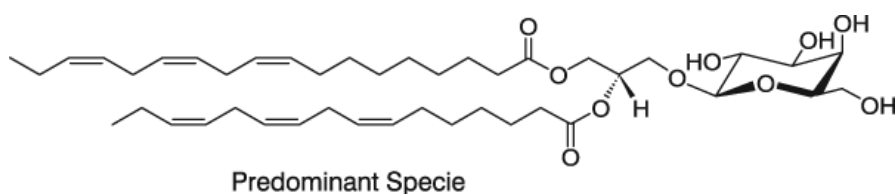


Figure 2.15: Basic glycolipid structure of the cell's glycocalyx. Image copied from ref. 95.

The work of Buschl *et al.*⁹⁶ referred to the need to combine the properties of natural cells with the durability of polymer membranes. Planar lipid bilayers at the air-water interface are less stable than the natural systems they mimic. In order to increase the stability they created liposomes from lipid-diene-lecithin (Figure 2.16), the diene component being polymerised by UV, which created stability within the vesicles.

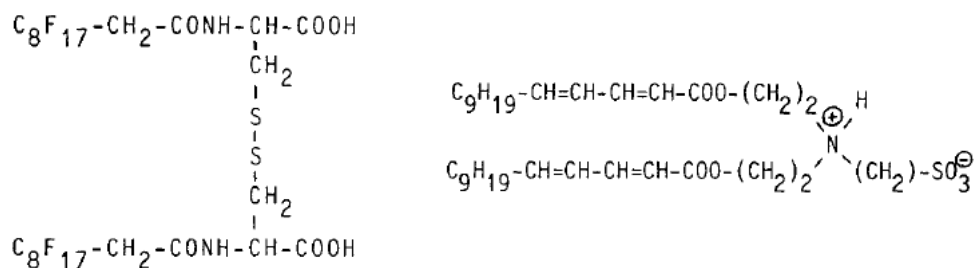


Figure 2.16: Chemical structure of the synthetic membrane mimic used in early work by Buschl. Image taken from ref. 96.

The discussion concluded by demonstrating the incorporation of ATP-synthase which was found to be fully functional in the more stable polymeric form of the liposomes.⁹⁷ Following from this observation, Spinke *et al.*⁹⁸ attempted to solve a series of practical problems which were evident from this earlier work. The first was that the system needed to be prepared on a planar support, rather than as a liposome, in order to take advantage of new characterisation methods being developed. They also considered that the method of preparing bilayers, by Langmuir Blodgett deposition (LB)⁹⁹ was a problem as protein incorporation into the bilayer was not possible using this process. To add to this, the solid substrate was considered too rough for the deposition of a fluid bilayer. They proposed that these issues could be solved by preparing bilayers which were bound to, but decoupled from a solid surface by inserting a flexible polymer layer between the glass substrate and the lipid. To this end they prepared co- monomers with various functionalities which covalently linked to the solid surface (Figure 2.17). This methacrylic terpolymer with a hydrophilic side chain and disulfide group acted as a functionalised self-assembled monolayer (SAM), chemically attaching to the substrate and providing tethers into the initial lipid monolayer. A bilayer was subsequently completed by fusing lipid vesicles of DMPC at $T > T_m$. The DMPC vesicles were doped with biotinyl - PE and binding experiments with streptavidin were performed to confirm that a bilayer had formed.

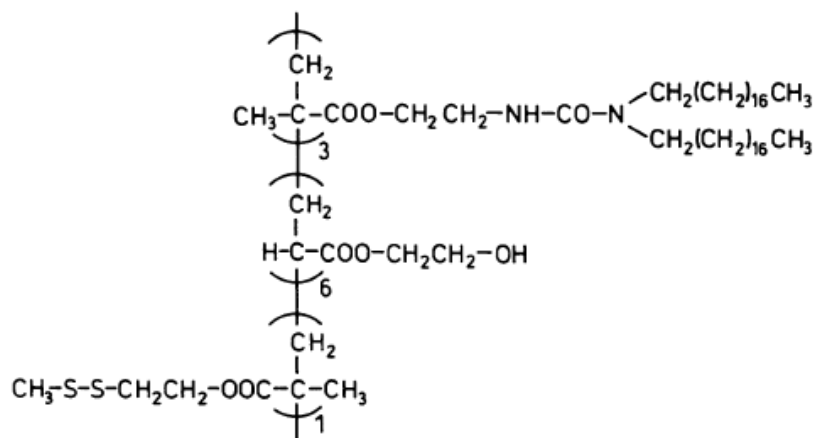


Figure 2.17: Methacrylic terpolymer used by Spinke. Image taken from ref. 98.

Following this work Baumgart *et al.*¹⁰⁰ were the first to attempt to form bilayers on chitosan, a naturally occurring linear polysaccharide. They used the Langmuir Blodgett/Langmuir Schaeffer (LB/LS)¹⁰¹ method to deposit lipid bilayer membranes on agarose (as a control) and chitosan using lipids containing DMPC, egg-PC and cholesterol. Thin chitosan films were prepared by spin coating onto silicon wafers and measured, by ellipsometry, about 140 nm dry length. Small unilamellar vesicles SUVs were prepared by tip sonication and the lipids were allowed to incubate on the polymer surfaces 'for several hours'. The group discovered that a fluid, stable bilayer could be formed on chitosan, but not on agarose. They suggested that the chitosan, with a positive zeta potential generated by the glucosamine segments, interacted with the choline headgroup of the lipid.¹⁰² They cited ease of preparation and control of thickness as advantages of this system, but did not incorporate any protein into it.

In similar work, done by Goennenwein,¹⁰³ cellulose, also a natural long chain polysaccharide, was prepared by LB deposition into glass. Vesicles of 1:1 DMPC:DMPG containing blood platelet integrin receptors, were fused directly onto the surfaces of both a glass control and the cellulose coated glass. This method of preparing the bilayer overcomes the above mentioned disadvantage of using LB deposition for lipids, which does not support the incorporation of proteins. A homogenous lipid bilayer was formed on the cellulose substrate with a diffusion constant for the integrins of $0.6 \mu\text{m}^2 \text{s}^{-1}$ and a mobile fraction of 25%. The diffusion rate for the lipids was $3.3 \mu\text{m}^2 \text{s}^{-1}$, with 77% recovery. This was 10 times faster than was observed for a similar system directly on glass where the integrins in the bilayer were virtually immobile. A protein was successfully incorporated in this system and it was mobile, however, the cellulose was not covalently linked to a support and had limited stability.

The next stage of development for the above work using natural polymers was to ensure that there was control over the length of the polymer cushion and that it was covalently linked to the surface to add stability. Dextran, a naturally occurring branched polysaccharide, was covalently attached to glass via an epoxy link by Elender *et al.*¹⁰⁴ They prepared silanised glass using an epoxysilane (4-aminobutyl-dimethylmono-methoxysilane (ABDMS),) (annealed at 75°C). This was then reacted with a photochemical *N*-Hydroxysuccinimide and (1-ethyl-3-(3-dimethylaminopropyl)carbodiimide hydrochloride) (NHS-EDC) linker, followed by soaking in a 30% Dextran solution. This produced a 0.8 nm dry film, measured by ellipsometry. They suggested that some control of the dextran thickness would be afforded by including a passivation step by soaking in water to deactivate some of the silane -OH groups with which the dextran reacts.

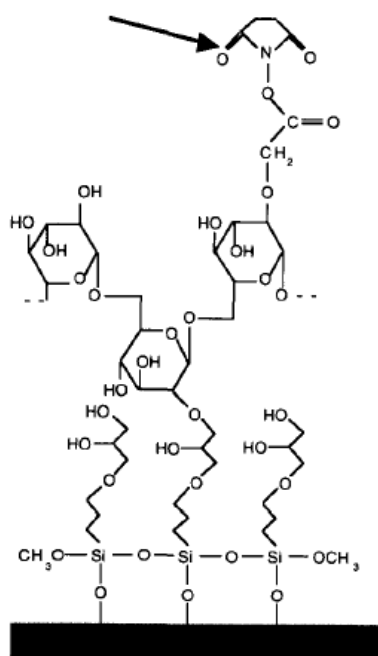


Figure 2.18: Coupling of dextran to epoxy silane on silicon surface. Image copied from ref. 104.

The final mean film thickness was about 3 nm, which increased to ~60 nm in water. The dextran became smooth when swollen and suitable for supporting a lipid bilayer which they created using 20% cholesterol-DMPC by LB/LS. The cholesterol created a higher bending modulus than pure DMPC, (when poor quality bilayers formed,) which they proposed would suppress the repulsive undulation forces. The diffusion rate of $2.8 \mu\text{m}^2 \text{s}^{-1}$ compared well to the rate of free bilayers of this cholesterol-DMPC mixture on glass alone. This method was developed further by Floyd and co-workers,¹⁰⁵ who used vesicle fusion to prepare a bilayer.

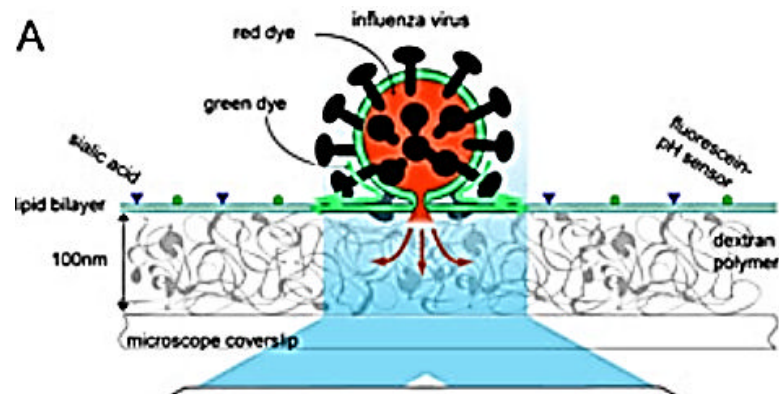


Figure 2.19: Schematic of influenza virus deposited onto dextran polymer cushion, taken from ref. 105.

They incorporated an influenza virus onto a 100 nm Dextran cushion and studied its fusion with the bilayer as shown in Figure 2.19.

In summary, the use of naturally occurring polymers has overcome some of the challenges of creating a polymer supported bilayer system and may have characteristics in common with the environment of the cell membrane in nature. There is evidence that a suitable length of cushion, covalently coupled to the substrate has been produced. Mobile bilayers, prepared by vesicle fusion have been formed and a protein incorporated, however these characteristics are not all present in any one system. Furthermore, the brush length, chain chemistry and environmental response to pH and temperature have not been demonstrated to be controllable in these systems.

2.4.3. Polyethylene glycol (PEG) and tethered systems

The systems presented in this section are polymers, chemically attached to a solid surface and incorporating a lipid-like molecule. The lipid anchor molecule provides a link between the polymer and the lipid bilayer by inserting into the hydrophobic core of the bilayer. A number of these are based on PEG which has been used extensively to create protein resistant surfaces on medical devices.¹⁰⁶ It does not interact with the planar glass substrates used as supports for the polymer supported bilayer systems¹⁰⁷ and water is a good (θ) solvent for the polymer.¹⁰⁸ Because there is no interaction between the PEG and the substrate, a method of tethering the two by attaching lipid anchors to the PEG

molecule (a phospholipid-PEG conjugate) was required. This can be achieved by covalent attachment it to the silica substrate using an ethoxysilane monolayer (SAM).

Wagner and co-workers¹⁰⁸ presented a PEG based tethered polymer supported planar bilayer system onto which they reconstituted laterally mobile proteins of cytochrome b_5 and Annexin V. PEG2000-DMPE-triethoxysilane(DPS)monolayers, shown in Figure 2.20, were spread onto a glass surface, using the Langmuir Blodgett method. This created a covalent link to the silica surface on deposition. The concentration of polymer used was consistent with producing a collapsed polymer regime at low chain grafting density.

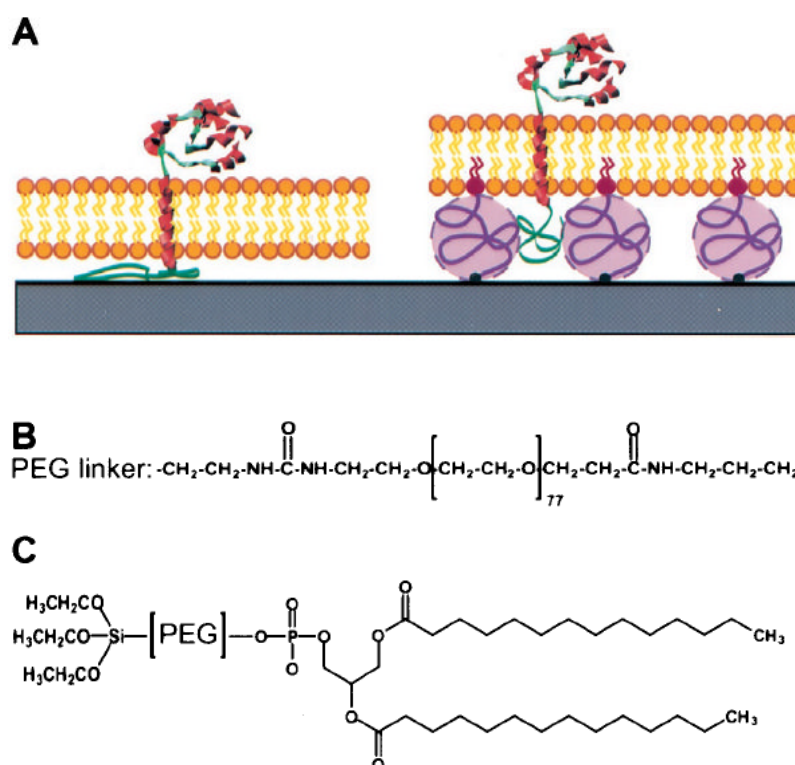


Figure 2.20: A schematic of the PEG polymer system and below it the structure of the PEG-silane-lipid used to insert into the lipid bilayer, taken from ref. 108.

(The polymer characteristics are explained fully in Chapter 3.1). Proteoliposome vesicles of a 9:1 mixture of POPC:POPG lipids and protein were extruded and fused onto the dried polymer layer. The FRAP data showed diffusion rates for the lipids of 0.8 to $1.0 \mu\text{m}^2 \text{s}^{-1}$, and similar rates for the proteins, but only 25% of the proteins were mobile. They concluded that the lipids had coupled to the polymer.

In a development of this system Hwang *et al.*¹⁰⁹ studied a glycoacrylate polymer, shown in Figure 2.21, which has properties similar to the natural glycocalyx.

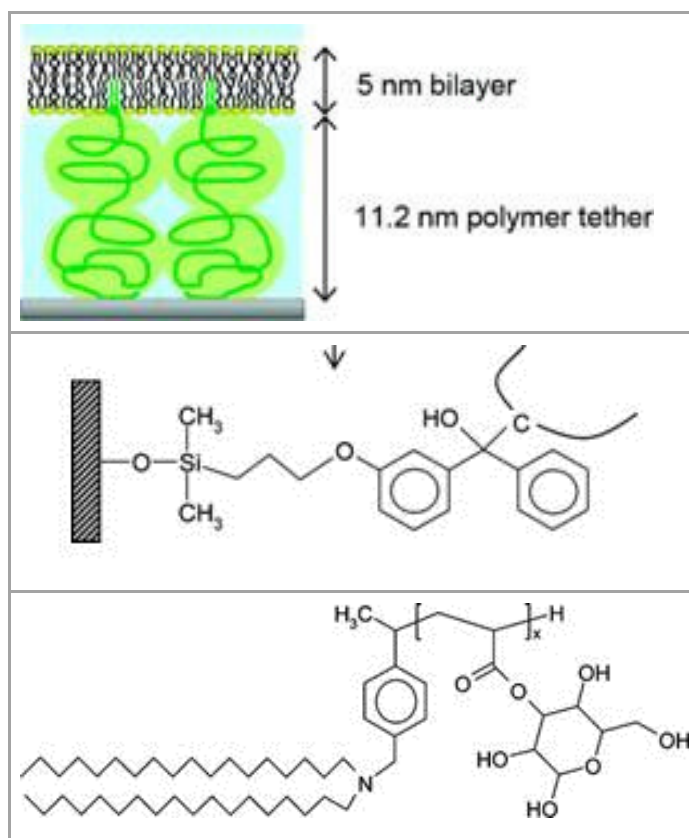


Figure 2.21: Schematic of a benzophenone functionalized silicon surface to which is attached a glycoacrylate polymer, supporting a lipid bilayer. The structures of the SAM and polymer are shown beneath. Images are taken from ref. 109.

A lipopolymer monolayer was formed by LB transfer of the DODA-poly(D-glucose-2-propenoate), telechelic lipopolymer (GH24000), which was linked by a photochemical reaction to the benzophenone functionalized surface. A range of polymer concentrations (mixed with egg-PC lipid) was tested. This created a spacer of ~ 11 nm which had attached to it a double acyl chain lipid moiety which would insert into the proximal leaflet of the bilayer. Finally the distal leaflet was created by the fusion of egg-PC vesicles prepared in a 10 mM Tris buffer at pH 8 with 100 mM NaCl. Following a series of FRAP experiments, it was seen that the lateral fluidity and mobile fractions of bilayers decreased when the percentage of GH24000 tether within the lipid was increases in a linear fashion. A control on glass whereby the same lipids were deposited in glass produced a diffusion coefficient of $5 \mu\text{m}^2 \text{s}^{-1}$. However, when using the polymer system with 5% GH24000 combined with egg-PC this rate had fallen to less than $2 \mu\text{m}^2 \text{s}^{-1}$.

Kaufmann *et al.*¹¹⁰ also investigated the formation of supported lipid bilayers on a PEG tether. They stated that whilst vesicle fusion on PEG in the mushroom regime has been successful (as demonstrated by Wagner above), in the brush state it is less so and they wished to address this.

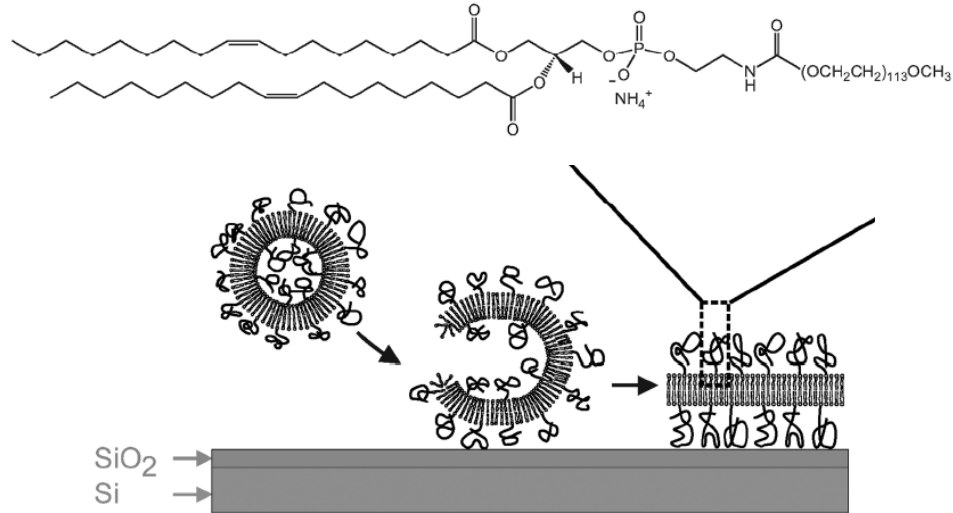


Figure 2.22: Schematic of the process for PEG-SLB self-assembly. Liposomes incorporating a low percentage of lipids with PEG chains attached to their headgroup self-assembled on the SiO₂ surface and fuse into a PEG-SLB. The final structure features PEG chains on both sides of the lipid bilayer. The chemical structure of a PEG(5)-PE lipid is also shown. Image taken from ref. 110.

Kaufmann used vesicles of POPC, prepared by extrusion, containing a range of mol ratios (from 0.25 to 3 mol%) of PEG-PE. The group found that 0.5 mol% PEG(5000)-PE gave the best diffusion rate, of $2.6 \text{ um}^2 \text{ s}^{-1}$. QCMD showed that PEG-PE lipids alone do not rupture to form a bilayer and that increasing the PEG-PE acts as a barrier to rupture, as demonstrated in Figure 2.22. They concluded that PEG-SLB formation works at low concentrations of PEG-PE lipids, in which the PEG takes on a collapsed configuration, which does not create as much space as the extended brush configuration. The compromise the group reached was to use a low concentration of PEG 5000 which gave an adequate spacer layer with reasonable lipid mobility.

In an alternative application of a PEG polymer brush, Roder *et al.*¹¹¹ formed a membrane by fusing vesicles of DOPC, sphingomyelin and cholesterol on a PEG polymer brush. The vesicles were incubated on the PEG brush, which was attached to a glass substrate which had been functionalised with palmitic acid (PA). Initially there was no diffusion of the lipids detected by fluorescence recovery, only surface bound vesicles. The addition of a PEG solution to this result did induce fusion and resulted in phase separated lipid domains. Roder then separated the lipids into liquid ordered and liquid disordered domains within

the bilayer. Their premise was that the density of the tethering groups (a result of the density of the polymer chains on the surface as shown in Figure 2.23), determined the phase separation of the bilayer which in turn influenced the diffusion rate of the lipids.

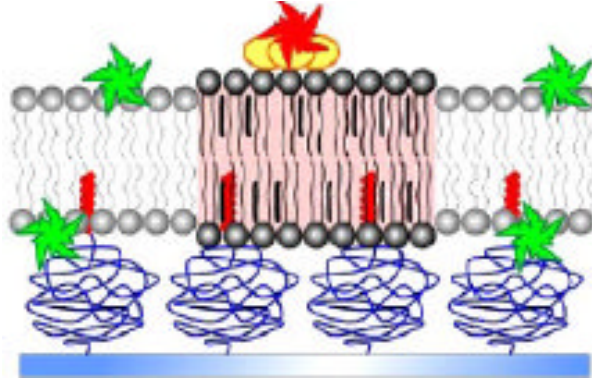


Figure 2.23: The cartoon, taken from ref. 107, depicts the interpretation of the observed differences in the staining with different lipid-phase markers (green stars, DiD; red stars, AF647CTX). (c) Relative distributions of different lipid-phase markers between the apparent I_d and I_o phases observed for (red) PA and (green) OA-tethered membranes. ¹¹¹

Diffusion in the lipid disordered domains was $\sim 3.1 \mu\text{m}^2/\text{s}$, while for the ordered domains it was $\sim 0.4 \mu\text{m}^2/\text{s}$. They incorporated a transmembrane helix (IFNAR1) (Figure 2.23) which diffused well in the liquid disordered domains, however an immobile fraction of the protein was observed. The protein was not found in the liquid ordered phase.

Following up on the use of cholesterol, it was found that this had been used in earlier work by Jenkins *et al.* ¹¹² who developed microcontact printed ($20 \times 20 \mu\text{m}$) “wells” on a gold electrode. These were formed by “inking” a polydimethylsiloxane (PDMS) stamp with cholesterolpolyethyleneoxy thiol (CPEO3) molecules. The wells were then backfilled with a mercaptoethanol SAM layer. Subsequent incubation with extruded egg-PC lipid vesicles (of 90 nm diameter in BaCl_2) created a bilayer into which the cholesterol molecules inserted and acted as a tether, as shown in Figure 2.24.

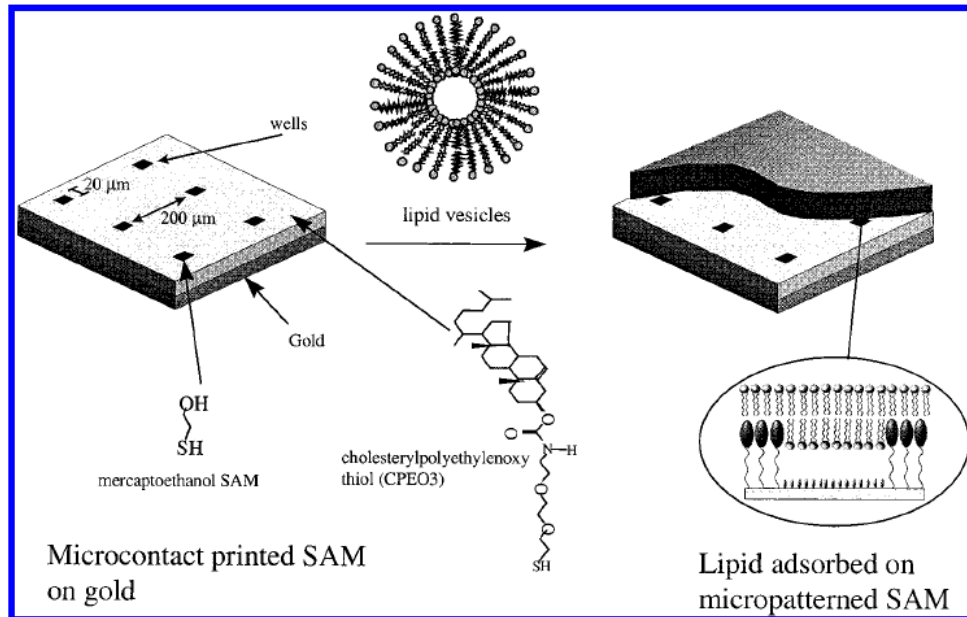


Figure 2.24: Structures of mercaptoethanol SAM and the cholesterol tether molecule cholesteryl polyethyleneoxy thiol (CPEO3) used to form a tethered bilayer membrane using eggPC lipid vesicles. Image taken from ref. 112.

The combination of the SAM and bilayer created a layer which supported the incorporation of a channel forming peptide (gramicidin) and an ion transporter (valinomycin), which were both found to be functioning after incorporation.

The final example of a PEG supported system Oijen *et al.*¹¹³ produced mobile bilayers by incorporating cholesterol into the lipid formulation. The results showed good lipid diffusion rates for the lipid bilayer and the transmembrane proteins incorporated in it. They prepared the system by coating glass coverslips with an APTES SAM and coating them with the lipid-PEG conjugate PE-PEG/mPEG at an optimum 5:95 ratio. Increasing the ratio showed a tendency to produce stacked bilayers. The lipids DOPC:cholesterol in an 80:20 ratio, were spin-coated directly from isopropanol, onto the lipid-functionalised PEG brush. A HEPES buffer was used to rehydrate the lipid. Following this polymer preparation step, proteoliposomes (DOPC,DOPE and DOPG) with glycophorin A incorporated into them were deposited onto the spin coated lipid layer (Figure 2.25). This process was aided by using high molecular weight PEG and EDTA as fusogens. FRAP and single molecule tracking was used to confirm good lipid and protein mobility.

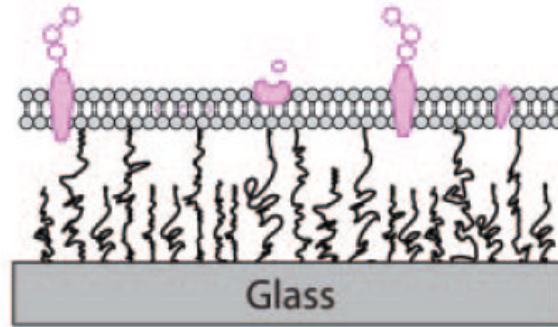


Figure 2.25: Schematic depiction of the structure of the PEG-supported lipid bilayer with incorporated protein produced by Oijen. Image taken from ref. 113.

Finally, a tethered system has been produced by Sumino *et al.*¹¹⁴ who reconstructed the LH2 and LH1-RC light harvesting systems of *Rh. Sphaeroides* into bilayers on solid supports and observed light transfer between the two. They created domains by incorporating each LHC component into a different lipid formulation and allowing the bi-layer /LH complex to self-assemble in different areas of the solid support. The LH2 was incorporated into a cationic vesicle and fused into an anionic membrane, containing LH1-RC. The spacing mechanism was 5 nm high, created by immobilising avidin on the glass substrate and creating a biotin linkage into the bilayer (Figure 2.26).

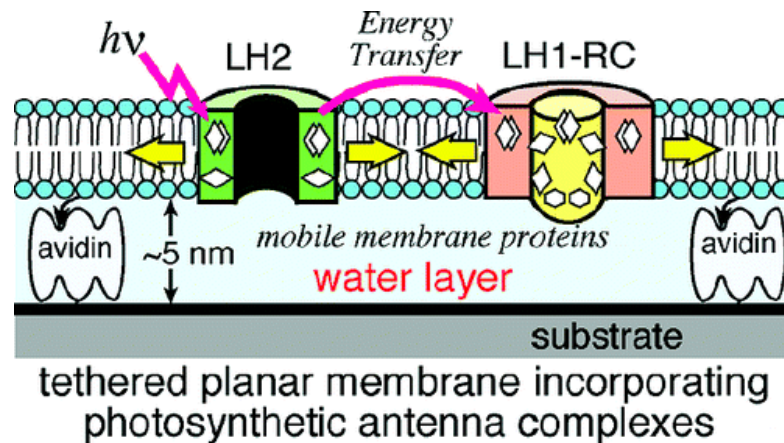


Figure 2.26: Schematic, taken from ref. 110, of tethered membrane domains with light harvesting complexes LH1-RC and LH2 in the same membrane patches.¹¹⁴

LH1-RC and LH2 absorption bands were observed, suggesting the complexes were still functioning in the bilayer, but the diffusion coefficient for LH2 was very low at $0.01 \mu\text{m}^2 \text{s}^{-1}$ and diffusion for LH1-RC was not observed at all. The lack of mobility makes this system

less than ideal, as it suggests that the proteins are tethered in some way to the surface, which may reduce their functionality.

In summary, there is a large body of work that incorporates PEG or similar molecules as a polymer spacer. These polymer systems are coupled to the solid support via a SAM, which makes them stable and the lipid-like anchors insert into the bilayer. However, they have drawbacks in that they provided a limited chain length to create the space between the substrate and the bilayer containing proteins. In addition, the lipid bilayer formation methods used in some cases were suitable for directly incorporating proteins into the bilayer. The system by Oijen *et al.* shows the most promise, but still requires a number of steps to prepare a stable and mobile system.

2.4.4. Polyelectrolytes

Polyelectrolyte polymer brushes can change conformation and charge as a result of changing the pH, ionic strength or temperature of the surrounding environment as discussed in chapter 3. The charged state of the chains can be varied by selecting specific monomers to create a homo-polymer or using two or three monomers with different properties as a di- or tri-block system. They can be prepared by a method which allows control over the reaction kinetics (reaction time) so that brushes of specific thickness (length) can be produced. These properties facilitate 'tuning' of the surface by changing the hydrophilicity i.e. the charged state or the degree of extension of the brush. This process offers options for the successful incubation of lipid vesicles on the polymer to form a fluid bilayer. The polymer systems presented here vary in thickness, in a range between 5 to 100 nm dry lengths, as measured by ellipsometry. Most of the systems are chemically attached to a solid support via a self-assembled intermediate SAM and grown using atom transfer radical polymerization ATRP (discussed in chapter 3).

The types of lipids employed vary from zwitterionic to charged headgroups with some having high transition temperatures, such as DMPC and some with transition temperatures near to zero (DOPC, POPC, DOTAP, DOPG). The bilayers were formed using different methods which include LB/LS deposition, vesicles fusion and spin-coating (these methods are presented in chapter 4). Some of these examples show the diffusion rates for the lipid bilayers without proteins and some show that proteins can be incorporated into the bilayer and give evidence for the function and mobility.

The list is not exhaustive, but examples have been selected which are linked by the use of common conditions or deposition methods, so are not chosen at random. They demonstrate the principles and options available when choosing how to create a good polymer supported lipid membrane.

In the first example Smith *et al.*¹¹⁵ demonstrated that zwitterionic POPC lipid bilayers could be formed, via the standard fusion of tip sonicated vesicles, onto a polyacrylamide (PAM) brush (Figure 2.27). This is a neutral (uncharged) polymer brush grown by ATRP to thicknesses of 2.5 nm, 5 nm and 10 nm.

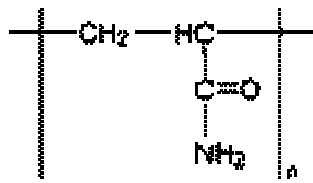


Figure 2.27: The structure of polyacrylamide, from ref. 115.

It was found by incubating POPC vesicles (at pH 8 in a phosphate buffer at 28°C) for 30 min, that a fluid bilayer was formed which had a lipid diffusion coefficients (D) of $\sim 2 \mu\text{m}^2 \text{s}^{-1}$, similar to the diffusion rate for bilayers on glass. They also found a similar result with the short polymer brush, of length 2.5nm, but considered that at this brush did not provide a large enough space for the extra-membranous domain of any incorporated protein to function correctly. The diffusion rate on the polymer of 5 nm length was better than that for 10 nm, when it slowed significantly. They suggested the reason for this was that the 10 nm brush offered a rougher surface than the 5nms. Interestingly, they also attributed the ability to form bilayers on these surfaces as due to the smoothness (rms roughness <0.5 nm) produced by ATRP, whilst the spin coated counterparts of the polymer (rms roughness ~ 3 nm) would not support bilayer formation. They discussed an optimum thickness which would be a trade-off between the appropriate decoupling of the membrane from the solid support and an increasing roughness presented by using a longer brush. They confirmed that this brush was a suitable candidate by incorporating a protein, (hDOR), and successfully binding a ligand to it, to confirm its functionality.

The similarities between the above system and the next one are that both groups used zwitterionic vesicles and varied the chain length of the polymer to good effect. Santonicola *et al.*¹¹⁶ grew zwitterionic 'charge balanced', pH responsive, sulfobetaine polymer brushes

poly(2-(N-3-sulfopropyl-N,N-dimethyl ammonium)ethyl methacrylate) (PSBMA, Figure 2.28) via ATRP on a SAM coated glass.

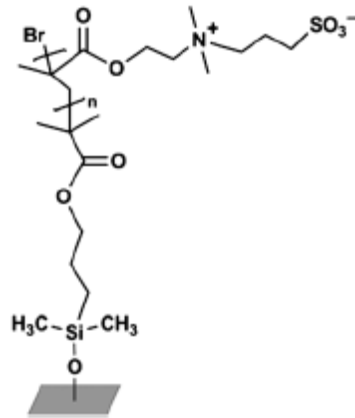


Figure 2.28: poly(2-(N-3-sulfopropyl-N,N-dimethyl ammonium)ethyl methacrylate), attached to glass via a SAM. Image taken from ref. 116.

They found, when using extruded DOPC vesicles, that bilayer adsorption could be tuned by controlling the grafting density and hence the polymer brush thickness. No bilayer formation was obtained for polymers with a swollen thickness > 35 nm (contact angle of $\sim 20^\circ$). However, for brushes of thickness ~ 16 nm (CA of $\sim 31^\circ$) bilayers with lipid diffusion coefficients of the order of $1 \mu\text{m}^2 \text{s}^{-1}$ could be observed. They used a similar phosphate buffer at pH 7.4 to Smith (above), but added 150 mM KCl, in order to tune the electrostatic interactions. They found that the polymers needed to be equilibrated in buffer before incubating for 16 h with lipid in order to generate this result.

In common with the previous system, the work by Renner and co-workers,¹¹⁷ compares bilayer formation on three different brush lengths, but in this case the chain lengths were varied not by increasing the brush reaction time, but by using polymer chains of different lengths. A series of spin-coated maleic anhydride-based, pH-responsive brushes, were shown to support bilayer formation.

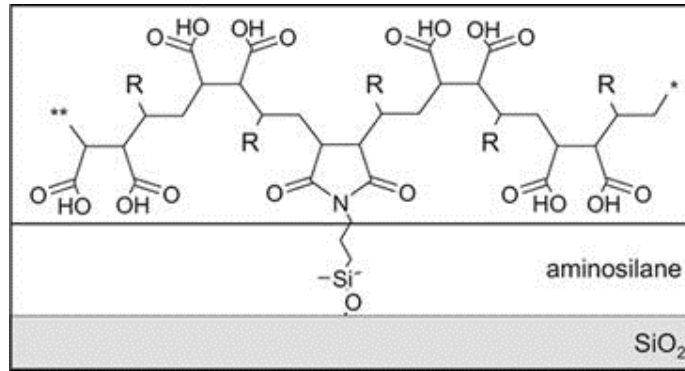


Figure 2.29: Schematic view of the covalently immobilized maleic acid copolymer layers; *R* varies with the type of co-monomer unit (octadecene, propene, or ethylene). Image from taken from ref. 117.

Renner's group used lipids which were close to the natural membrane composition; a mixture of egg-PC (neutral), PS, PE (both negative) and cholesterol in the ratio 5:2:1:2:0.1. They tested three variants of the maleic anhydride based brushes (poly(octadecene-*alt*-maleic anhydride) (POMA) poly(propene-*alt*-maleic anhydride) (PPMA) and poly(ethene-*alt*-maleic anhydride) (PEMA)), of dry thickness 4 nm, 25 nm and 60 nm respectively. The brush lengths were varied by changing the side chain *R* (see Figure 2.29). The results of vesicle incubation led to lipid diffusion coefficients of $0.26 \mu\text{m}^2 \text{s}^{-1}$, 0.6 and $1.24 \mu\text{m}^2 \text{s}^{-1}$, respectively. They found it necessary to reduce electrostatic repulsion, created by the carboxylic acid groups on the maleic anhydride, by lowering the pH to 4. At this pH the brush collapsed and the best diffusion rates were observed. These were still slower than the diffusion rates they measured for the same lipids on glass. The group successfully incorporated a functioning protein, by solubilizing a preformed bilayer and adding BACE protein. The mobile fraction of lipids in the bilayer was reduced to 60-80 % when the protein was added but they found that the activity of the protein was enhanced when incorporated into this system.

The next example El-khouri et al.¹¹⁸ produced a pH responsive hydrophilic cushion of poly(acrylic acid) (PAA), of up to 50nm as shown in Figure 2.30. In common with the above work spin coating was used, in this case to deposit the PAA onto an APTES SAM.

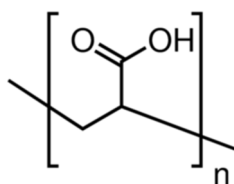


Figure 2.30: poly(acrylic acid) as the anhydride, formed by PAA when spin coated. Hydrating at pH 8-10 converts it back to an acid. Image taken from ref. 118.

Changing the concentration of the PAA solution allowed variations in brush thickness to be achieved. Under acidic conditions, at $\text{pH} < 5$, the polymer layer is collapsed, but under alkaline conditions the layer can swell to three times its coating thickness. LB/LS deposition was used to prepare neutral bilayers of DMPC, (above the transition, T_m) on the surfaces. FRAP experiments showed that the bilayers were fluid, with a diffusion coefficient of $2.56 \mu\text{m}^2/\text{s}$ at $\text{pH} 9.2$, and compared well to the rates they obtained on glass. The diffusion coefficient at $\text{pH} 4$ was reduced and showed little fluorescence recovery after bleaching. The group suggested this was because the polymer topology was modified by the pH change and the membrane may have coupled to the polymer.

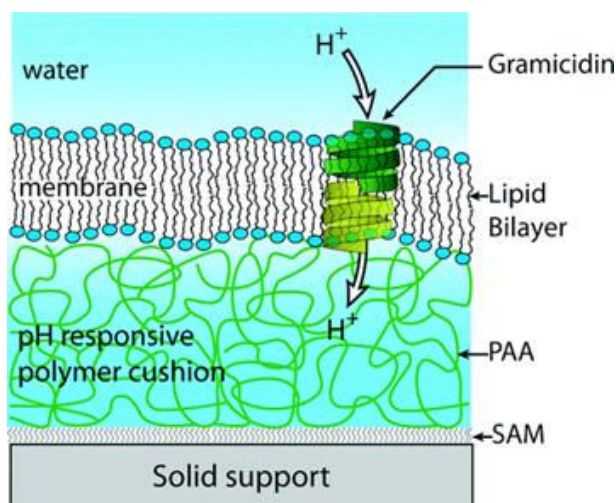


Figure 2.31: Schematic of poly(acrylic acid) brush with an inserted ion channel from ref. 118.

After incorporating gramicidin into the bilayer they observed changes in the thickness of the PAA brush. These, they suggested, resulted from changes in the pH of the buffer surrounding the brush, proving that the gramicidin was functioning as a proton pump (see schematic in Figure 2.31).

It is interesting that when Renner (presented earlier) used a carboxylic acid brush the pH required for bilayer formation was pH 4. For El Khouri, also using a carboxylic acid brush, the successful incubation took place at pH 9.2.

The system introduced by Nirasay¹¹⁹ and coworkers also utilises an anionic polymer system and zwitterionic DMPC lipids. This group formed a 20 nm (dry length) polydopamine film (Figure 2.32), with a surface roughness of 2 nm, from a solution of dopamine. (A surface roughness of 0.5 nm is considered to be acceptable). Polydopamine contains amine, catechol and quinone and becomes negatively charged by the loss of a proton from the -OH groups. Nirasay used tip sonicated and extruded DMPC and DOPC vesicles, rehydrated in a 10 mM sodium phosphate buffer. They successfully deposited fluid lipid bilayers by incubating the vesicles onto the dry film, and heating the sample above the T_m for DMPC, (23°C).

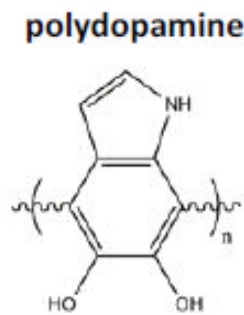


Figure 2.32: Structure of polydopamine from ref. 119.

Diffusion constants of 5.9 and $7.2 \mu\text{m}^2 \text{s}^{-1}$ were measured. These compared well to their measured diffusion rates on glass of $7.8 \mu\text{m}^2 \text{s}^{-1}$. They suggested that the negatively charged polymer surface formed an interaction with the choline (+ve) of the PC lipid headgroup. As they used a buffer of low ionic strength they considered that the sodium ions from it would not shield the electrostatic interaction between the approaching lipid vesicles and the charged polymer. This is the first example, in this review, where the electrostatic interaction between the vesicle head group and the polymer has been specifically considered.

The next piece of research examines an anionic polymer, in common with the work of Nirasay, but Kaufmann *et al.*¹²⁰ in this work used charged cationic lipids rather than zwitterionic ones and chose a novel method of creating the bilayer, which suggested that

they wished to take advantage of the electrostatic attractions between the polymer brush and the lipids.

poly(N-isopropylacrylamide-co-carboxyacrylamide (PNIPAAm) (Figure 2.33) is a temperature responsive polymer and its combination with a carboxy acrylamide confers pH responsiveness for use as a support for lipid bilayers. The carboxylic acid groups on the copolymer exhibit a net negative charge.

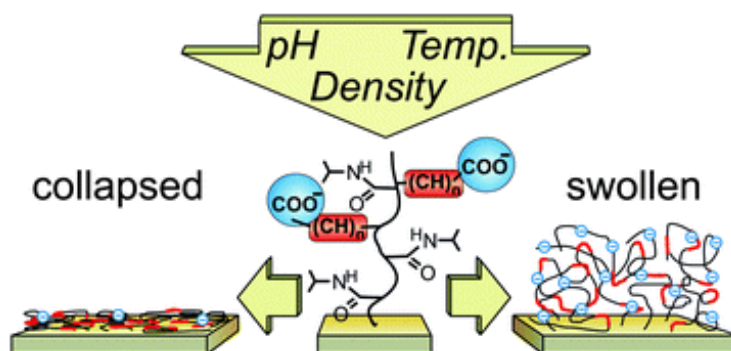


Figure 2.33: Schematic showing the pH and temperature response of Carboxylate polymers under pH conditions from ref. 120 above

A mixture of DOTAP:POPC vesicles, with a lipid ratio of 1:9, was incubated on the polymer. Insufficient lipids adsorbed by this method and no bilayer was formed, so vesicles prepared in water, were left to dry on the polymer and then re-hydrated slowly overnight.

Depending on the pH there was weak electrostatic coupling between the bilayer and the polymer which was not affected greatly when the pH and temperature were subsequently changed, to allow the polymer to hydrate and swell. FRAP experiments measured a diffusion coefficient of $5.7 \mu\text{m}^2/\text{s}$ in water with an increase to $7 \mu\text{m}^2/\text{s}$ in buffer across all pH values at 25°C and up to $9 \mu\text{m}^2/\text{s}$ at 40°C at pH 8. All results were higher than their equivalent measurements on glass.

In contrast to the above systems, most of which featured anionic polymers, there follows examples of work where anionic lipids have been deposited on cationic polymer brushes.

A pH responsive poly[2-(dimethylamino)ethyl methacrylate-*block*-methyl methacrylate] PDMAEMA-PMMA diblock copolymer was prepared by Rehfeldt *et al.*¹²¹ on which to deposit a lipid bilayer. The block copolymer has a hydrophilic PDMAEMA block which is a weak polyelectrolyte base and is terminated with a hydrophobic block PMMA (Figure 2.34).

The pH response of the PDMAEMA block responds to pH by changing conformation and hydration properties.¹²¹

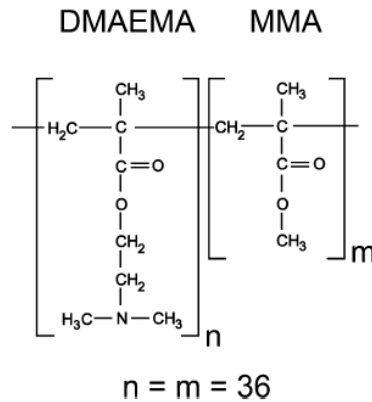


Figure 2.34: The structures of the DMAEMA and MMA monomers from ref. 121.

Extruded vesicles were prepared from 50:50 SOPC:SOPG lipids (negatively charge, with a pKa of 3.6, chosen to mimic the sialic acid residues in natural membranes). They were rehydrated in a PBS buffer (10mM sodium phosphate and 100mM NaCl). The group studied the effect of pH on the adsorption of lipids and found that at all pHs a homogeneous bilayer formed on the polymer. The thickness of the films at pH 5.5, when the PDMAEMA block tertiary amines are protonated (85% positively charged), is lower than that at pH 8.5, where it is only 12% protonated. The reason for the difference in thickness of the polymer, they suggested, was due to water reservoir between the polymer and bilayer being greater at the higher pH of 8.5 when the polymer is uncharged. Unfortunately there is no FRAP data to confirm the diffusion of the lipids. There is only one fluorescence image, which they suggest indicates a homogenous bilayer.

The next study, by Tang et al.¹²², followed the kinetics of bilayer deposition on poly(diallyldimethylammonium chloride) PDDA, also a cationic polymer (Figure 2.35). They followed the effect of lipid composition and buffer on the bilayer formation on the polymer. A SAM formed from 11-mercaptoundecanoic acid (MUA) was tethered to a gold substrate via a thiol link. PDDA was then deposited from solution on top to create a polymer of a 2-3 nm dry length. Vesicles, prepared from a mixture of zwitterionic and negatively charged lipids (60:40 DOPG:POPC) were deposited on the polymer, resulting in the formation of a smooth bilayer when the vesicles fused.

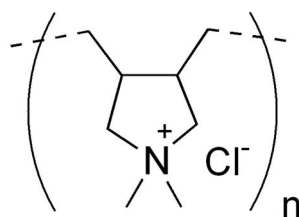


Figure 2.35: Structure of the polymer PDDA from ref. 122.

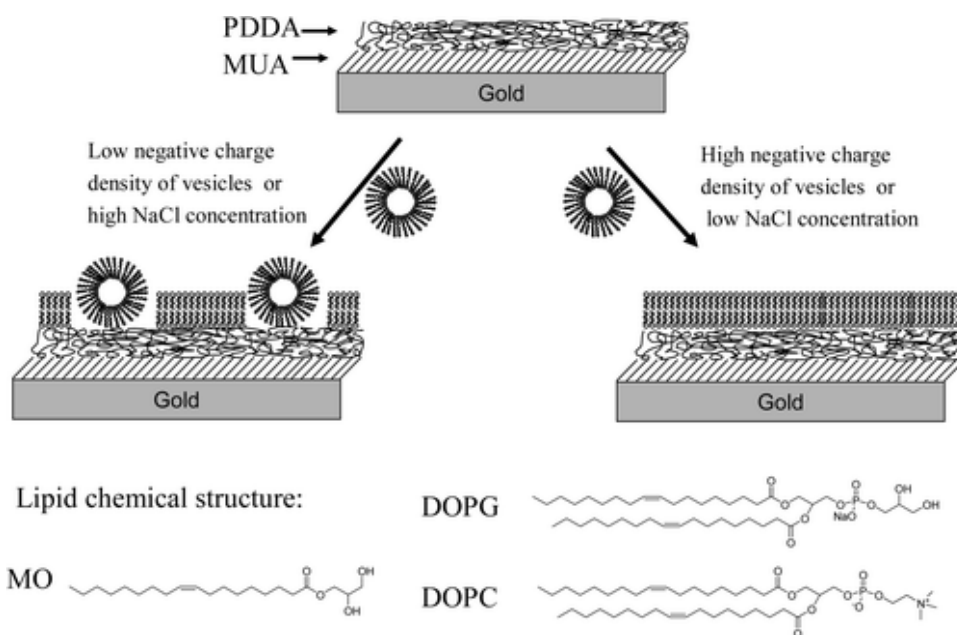


Figure 2.36: Deposition of vesicles on a hydrated cationic PDDA, grown on gold, as a function of phospholipid composition and sodium chloride concentration. Image copied from ref. 122.

Higher or lower concentrations of DOPG did not produce a bilayer. At low or zero ionic strength of NaCl vesicles ruptured and formed bilayers. When increasing the salt concentration in the buffer intact vesicles were adsorbed on the polymer and bilayer formation did not take place. Tang suggested that the added ions screened the electrostatic forces and weakened the vesicle interactions to the polymer.

In the final examples of this group of polyelectrolyte supports, the PELs have been formulated into multilayers (PEMs). These are layered polymers where each layer has different charge (electrical) properties. It is helpful to note that these are different from di- and tri-block copolymers in which the individual polymer chain is built up from segments of different monomers. These PEL multilayers are considered by some to be a more flexible version of the polymer supports presented above as they provide the option to not only

vary the thickness of the layers, but to control the charge by alternately layering cationic and anionic polymers.

In the previous example, work was presented on a PEL system by Tang who successfully formed bilayers on a single PDDA polymer layer. In a development of that work Ma *et al.*¹²³ created polymer multilayers using PDDA and also incorporated a protein. They created a PEM cushion composed of a thiol SAM monolayer on a gold layer by alternating PDDA (+) and poly(styrene sulfonate) (PSS) (-). The deposition took place layer by layer using electrostatic interactions to create a PDDA/PSS/PDDA system (Figure 2.37). Ma found that when incubating the PEM surface with vesicles containing SOPS (a negatively charged lipid) and POPC in a salt free buffer, they could form a bilayer when using vesicle fusion at any ratio of the lipids. If they used pure SOPS the diffusion coefficient was $1.2 \times 10^{-9} \text{ cm}^2/\text{s}$ and with 25% POPC it increased to $2.1 \times 10^{-9} \text{ cm}^2/\text{s}$, still much slower than they measured for POPC vesicles incubated on bare glass.

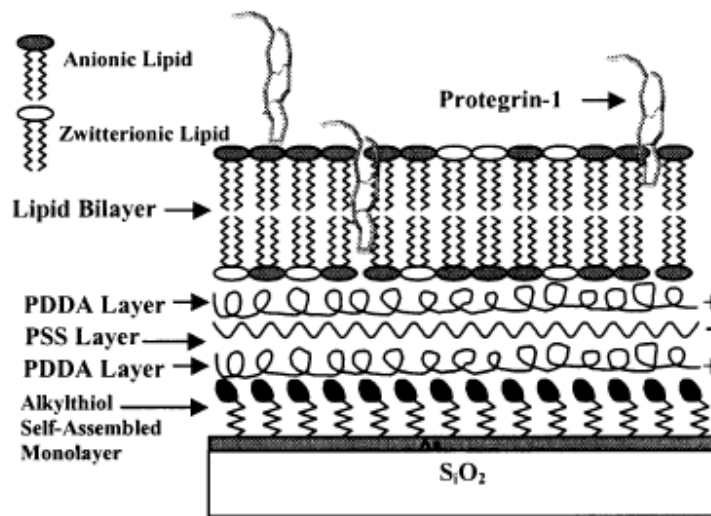


Figure 2.37: A diagram of the PEM produced from layers of PDDA and PSS attached to a gold surface by using a thiol SAM. Image copied from ref. 123.

An ion channel forming peptide, protegrin-1, was possibly incorporated into the bilayer and suggested to have inserted by SPR, though the authors agree that SPR alone is inconclusive. This is not a transmembrane protein and does not extend beneath the bilayer. For this reason it does not prove the efficacy of the PEM cushion in keeping the protein separated from the solid substrate.

In the next example, Fischlechner *et al.*¹²⁴ also used PSS, a strong polyanion, as the lower layer of the PEM. They added either a top layer of poly(allylamine hydrochloride) (PAH) or poly(diallyldimethylammonium chloride) (PDADMAC) which are weak and strong polycations, respectively (Figure 2.38).

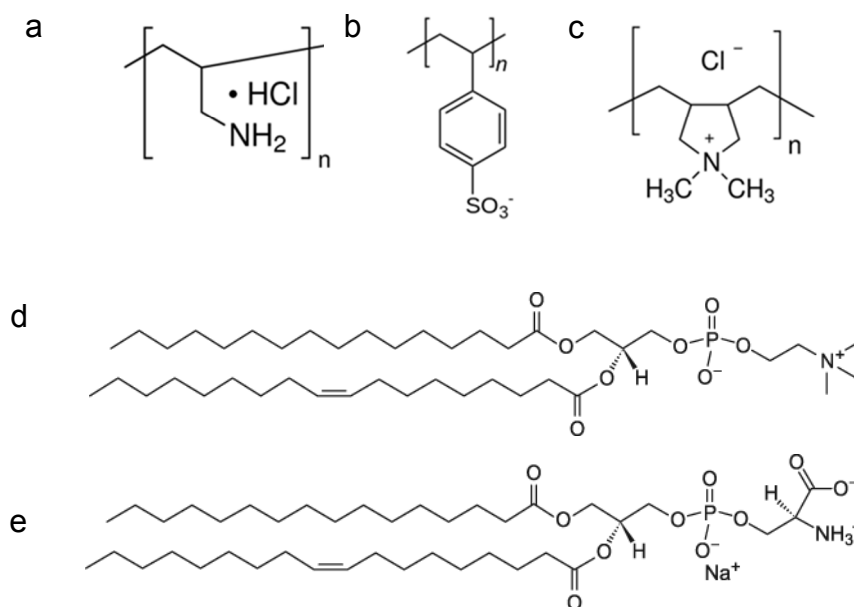


Figure 2.38: The chemical structures of (a) PAH, (b) PSS (c) PDADMAC (d) POPC and (e) POPS lipids. Images taken from Avanti lipids ref. 124.

They investigated the interaction of various vesicles composed of a range of ratios of POPC:POPS. They incubated these onto combinations of PAH and PDADMAC on PSS, in PBS or a buffer containing 0.1M NaCl. Fischlechner found that all lipids adsorbed to some degree, but vesicles with a mixture of 1:1 POPC:POPS lipids ruptured and spread immediately when PAH was the top layer with PSS below. In this case there was an electrostatic interaction between the anionic vesicles (generated by the POPS) and the cationic PAH layer. With 100% POPS only there was slower adsorption, followed by partial rupture of vesicles, but no bilayer was formed, despite there being a much stronger electrostatic interaction. With PDADMAC (quaternary amine) as the top layer a large amount of POPS:POPC vesicles were adsorbed, but they did not fuse into a bilayer, possibly suggesting binding of the lipid into the polymer. This group also found that more POPS lipids adsorbed in NaCl than in phosphate buffer and concluded that the phosphate ion interfered with the binding of the PDADMAC amine with the carboxylic acid on the POPS lipid headgroup.

2.5. Summary of background and aim of the thesis

In this chapter the nature of lipids have been discussed, explaining how and why lipid vesicles are formed and the role they play in creating cell membranes in nature. The use of biomimetic lipid membranes, formed on solid substrates, such as glass, have been presented along with a study of the effects on bilayer formation of varying the conditions such as pH, ionic strength and temperature. Both experimental work and simulation theory has been discussed for these systems on solid surfaces. Whilst these systems provide very useful study examples, the incorporation of proteins, particularly transmembrane proteins, demand a more sophisticated substrate system.

As illustrations of these, a range of polymer supported lipid bilayers beginning with the earliest works, have been presented. They include uncharged and charged polymer systems, on which a variety of methods have been used to attempt bilayer formation. For most of these systems there has been some control over the brush growth and thickness. There has also been control over the charge associated with the polymer, either by selecting charged monomers and controlling the pH of the surrounding buffer, or creating alternating layers of charged polymers. Lipids of varying formulations have been used and deposited by vesicle fusion or Langmuir (LB/LS) or spin-coating methods. There has been some success in incorporating proteins into the systems and these examples have added insight into what constitutes a successful system. The indications are that by using a protein resistant polymer brush of a specific length as a spacer mechanism, the TMP will not interact chemically or electrostatically with either the solid support or the spacer itself. In order to create this system a polymer brush must be chemically attached to a solid support forming a layer of specific length in a uniform manner with a low (rms) surface roughness. The method of forming the polymer brush must allow control of reaction conditions these can be correlated to growing brushes of a specified length and grafting density. It is not possible to prescribe an ideal length for the brush though this should exceed the size of the extra-membrane portion of the TMP being studied or the protein may be denatured. A number of research groups have suggested that lengths between 5nm and 30nms should be used, based purely on focussing effort on successfully preparing lipid bilayers on these polymer surfaces. These groups have not necessarily incorporated and studied a range of TMPs into the bilayers to definitively correlate polymer length with the successful functioning of the proteins. It is clear that the polymer should be hydrophilic as its function is to provide a hydrated cushion on which to form the lipid bilayer. A measure of this is that the water contact angle should fall below 90°. The hydrated

polymer, which must not interact with the protein, will also form a reservoir through which chemical or electrical gradients can be measured. For this purpose the bilayer supported on it, containing the TMP must provide an electrical seal which will allow only the exchange of protons via the mechanism of the TMP.

The literature has presented some clear pointers for producing a successful polymer supported bilayer system and the work presented here focuses in on these by employing brushes which are grown by ATRP, are hydrophilic, responsive to the environmental conditions and which are protein resistant. The brushes are as short as possible, whilst allowing room for a 5 to 10 nm transmembrane protein to be incorporated.

A number of suitable polymer brush candidates are presented in this thesis, which potentially satisfy these criteria, and the following study demonstrates the steps taken to try to create a successful polymer – supported bilayer system containing a light-harvesting TMP.

2.6. References

-
- ¹ Mashaghi, S.; Jadidi, T.; Koenderink, G.; Mashaghi, A., Lipid nanotechnology. *International journal of molecular sciences* **2013**, *14* (2), 4242-4282.
- ² R. B. Gennis. Biomembranes - Molecular Structure and Function. Springer-Verlag, 1989 New York.
- ³ Vist, M. R. & Davis, J. H. Phase equilibria of cholesterol/dipalmitoylphosphatidylcholine mixtures: deuterium nuclear magnetic resonance and differential scanning calorimetry. *Biochemistry* **1990** *29*, 451-464.
- ⁴ http://en.wikipedia.org/wiki/File:Cell_membrane_detailed_diagram_4.svg
- ⁵ http://en.wikipedia.org/wiki/Membrane_lipids Image of membrane lipids.
- ⁶ Burgos, C. E.; Ayer, D. E.; Johnson, R. A., A new, asymmetric synthesis of lipids and phospholipids. *The Journal of Organic Chemistry* **1987**, *52* (22), 4973-4977.(references and citations)
- ⁷ Berg, J.M., Tymoczko, J.L., Stryer, L.,. *Biochemistry*. **2002** Fifth edition. New York: W Freeman
- ⁸ Garcia-Celma, J. J.; Hatahet, L.; Kunz, W.; Fendler, K., Specific anion and cation binding to lipid membranes investigated on a solid supported membrane. *Langmuir* **2007**, *23* (20), 10074-10080.
- ⁹<http://www.avantilipids.com/POPC> Structure of POPC
- ¹⁰ <http://www.avantilipids.com/DOPG> Structure of DOPG
- ¹¹<http://www.avantilipids.com/DOTAP> Structure of DOTAP
- ¹²<http://www.avantilipids.com/DMPC> Structure of DMPC
- ¹³ Fayer, M. D. (2011). Dynamics of Water Interacting with Interfaces, Molecules, and Ions. *Accounts of Chemical Research* **45**, 3-14.
- ¹⁴ <http://chemistry.tutorvista.com/biochemistry/phospholipids.html> Image of lipid. (accessed 15 Jan 15)
- ¹⁵ Chandler D (2005). "Interfaces and the driving force of hydrophobic assembly". *Nature* **437** (7059): 640–7. doi:10.1038/nature04162. PMID 16193038.
- ¹⁶ Tanford C (1973). The hydrophobic effect: formation of micelles and biological membranes. New York: Wiley. ISBN 978-0-471-84460-0
- ¹⁷ Hammer, M. U.; Anderson, T. H.; Chaimovich, A.; Shell, M. S.; Israelachvili, J., The search for the hydrophobic force law. *Faraday discussions* **2010**, *146*, 299-308.

-
- ¹⁸ Israelachvili, J. N.; Mitchell, D. J.; Ninham, B. W., Theory of self-assembly of lipid bilayers and vesicles. *Biochimica et Biophysica Acta (BBA)-Biomembranes* **1977**, *470* (2), 185-201.
- ¹⁹ Czolkos, I.; Jesorka, A.; Orwar, O., Molecular phospholipid films on solid supports. *Soft Matter* **2011**, *7* (10), 4562-4576.
- ²⁰ Damodaran, S., Beyond the hydrophobic effect: Critical function of water at biological phase boundaries—A hypothesis. *Advances in colloid and interface science* **2015**.
- ²¹ Garde, S.; Patel, A. J., Unraveling the hydrophobic effect, one molecule at a time. *Proceedings of the National Academy of Sciences* **2011**, *108* (40), 16491-16492.
- ²² Nagarajan, R., Molecular packing parameter and surfactant self-assembly: the neglected role of the surfactant tail. *Langmuir* **2002**, *18* (1), 31-38.
- ²³ <http://www.uib.cat/depart/dba/cellbiology/lipid.html> Image of cell (accessed 7 April 2015)
- ²⁴ Israelachvili, J. N., *Intermolecular and Surface Forces*. Elsevier Science: **2010**.
- ²⁵ W. Rawicz, K. C. Olbrich, T. McIntosh, D. Needham and E. Evans."Effect of chain length and unsaturation on elasticity of lipid bilayers." *Biophysical Journal*. **2000** *79*. 328-39.
- ²⁶ Van Meer, G.; Voelker, D. R.; Feigenson, G. W., Membrane lipids: where they are and how they behave. *Nature reviews molecular cell biology* **2008**, *9* (2), 112-124
- ²⁷ Saxton, M.; Jacobson, K., Single-particle tracking: applications to membrane dynamics. *Annual review of biophysics and biomolecular structure* **1997**, *26*, 373.
- ²⁸ Mach, T.; Chimere, C.; Fritz, J.; Fertig, N.; Winterhalter, M.; Fütterer, C., Miniaturized planar lipid bilayer: increased stability, low electric noise and fast fluid perfusion. *Analytical and bioanalytical chemistry* **2008**, *390* (3), 841-846.
- ²⁹ Bergelson, L.; Barsukov, L., Topological asymmetry of phospholipids in membranes. *Science* **1977**, *197* (4300), 224-230.
- ³⁰ Tate, M.; Eikenberry, E.; Turner, D.; Shyamsunder, E.; Gruner, S., Nonbilayer phases of membrane lipids. *Chemistry and physics of lipids* **1991**, *57* (2), 147-164.
- ³¹ Nagle, J. F.; Tristram-Nagle, S., Structure of lipid bilayers. *Biochimica et Biophysica Acta (BBA)-Reviews on Biomembranes* **2000**, *1469* (3), 159-195.
- ³² Rand, R.; Parsegian, V., Hydration forces between phospholipid bilayers. *Biochimica et Biophysica Acta (BBA)-Reviews on Biomembranes* **1989**, *988* (3), 351-376.
- ³³ S. Munro."Lipid rafts: elusive or illusive?" *Cell*. **2003** *115*. () 377-388.

³⁴ Bayerl, T. M. & Bloom, M. Physical-properties of single phospholipid-bilayers adsorbed to micro glass-beads — a new vesicular model system studied by H-2-nuclear magnetic resonance. *Biophys. J.* **1990**, 58, 357–362.

³⁵ Tatulian, S. A., Hinterdorfer, P., Baber, G. & Tamm, L. K. Influenza hemagglutinin assumes a tilted conformation during membrane-fusion as determined by attenuated total-reflection FTIR spectroscopy. *EMBO J.* **1995**, 14, 5514–5523.

³⁶ Terrettaz, S., Stora, T., Duschl, C. & Vogel, H. Protein-binding to supported lipid-membranes Investigation of the cholera-toxin ganglioside interaction by simultaneous impedance spectroscopy and surface-plasmon resonance. *Langmuir* **1993**, 9, 1361–1369 ().

³⁷ Johnson, S. J. et al. Structure of an adsorbed dimyristoylphosphatidylcholine bilayer measured with specular reflection of neutrons. *Biophys. J.* **1991** 59, 289–294.

³⁸ Richter, R.; Mukhopadhyay, A.; Brisson, A., Pathways of lipid vesicle deposition on solid surfaces: a combined QCM-D and AFM study. *Biophysical Journal* **2003**, 85, 3035-3047.

³⁹ Schonherr, H.; Johnson, J. M.; Lenz, P.; Frank, C. W.; Boxer, S.G. Vesicle Adsorption and Lipid Bilayer Formation on Glass Studied by Atomic Force Microscopy. *Langmuir* **2004**, 20, 11600–11606.

⁴⁰ Dopico, A.M., Methods in membrane lipids, *Methods in Molecular Biology*. **2007**. New Jersey: Humana Press.

⁴¹ Brian, A. A.; McConnell, H. M., Allogeneic stimulation of cytotoxic T cells by supported planar membranes. *Proceedings of the National Academy of Sciences* **1984**, 81, 6159-6163

⁴² Tamm, L. K.; McConnell, H. M., Supported phospholipid bilayers. *Biophysical Journal* **1985**, 47, 105-113.

⁴³ McConnell, H.; Watts, T.; Weis, R.; Brian, A., Supported planar membranes in studies of cell-cell recognition in the immune system. *Biochimica et Biophysica Acta (BBA)-Reviews on Biomembranes* **1986**, 864, 95-106.

⁴⁴ McIntosh, T. J.; Simon, S. A., Roles of bilayer material properties in function and distribution of membrane proteins. *Annu. Rev. Biophys. Biomol. Struct.* **2006**, 35, 177-198.

⁴⁵ de Planque, M. R.; Killian, J. A., Protein-lipid interactions studied with designed transmembrane peptides: role of hydrophobic matching and interfacial anchoring. *Molecular Membrane Biology* **2003**, 20, 271-284.

-
- ⁴⁶ Van Meer, G.; Voelker, D. R.; Feigenson, G. W., Membrane lipids: where they are and how they behave. *Nature Reviews Molecular Cell Biology* **2008**, *9*, 112-124.
- ⁴⁷ Phillips, R.; Ursell, T.; Wiggins, P.; Sens, P., Emerging roles for lipids in shaping membrane-protein function. *Nature* **2009**, *459*, 379-385.
- ⁴⁸ Wu, H. L.; Chen, P. Y.; Chi, C. L.; Tsao, H. K.; Sheng, Y. J. Vesicle deposition on hydrophilic solid surfaces. *Soft Matter* **2013**, *9*, 1908-1919.
- ⁴⁹ Cremer, P. S.; Boxer, S. G., Formation and Spreading of Lipid Bilayers on Planar Glass Supports. *The Journal of Physical Chemistry B* **1999**, *103* (13), 2554-2559.
- ⁵⁰ Richter, R. P.; Brisson, A. R., Following the formation of supported lipid bilayers on mica: a study combining AFM, QCM-D, and ellipsometry. *Biophysical journal* **2005**, *88* (5), 3422-3433.
- ⁵¹ Cho, N.-J., Contribution of Temperature to Deformation of Adsorbed Vesicles Studied by Nanoplasmonic Biosensing. *Langmuir* **2014**.
- ⁵² Cho, N.-J.; Frank, C. W., Fabrication of a planar zwitterionic lipid bilayer on titanium oxide. *Langmuir* **2010**, *26* (20), 15706-15710.
- ⁵³ Jackman, J. A.; Choi, J.-H.; Zhdanov, V. P.; Cho, N.-J., Influence of osmotic pressure on adhesion of lipid vesicles to solid supports. *Langmuir* **2013**, *29* (36), 11375-11384.
- ⁵⁴ Lind, T. K.; Cárdenas, M.; Wacklin, H. P., Formation of supported lipid bilayers by vesicle fusion: Effect of deposition temperature. *Langmuir* **2014**, *30* (25), 7259-7263.
- ⁵⁵ Seifert, U.; Lipowsky, R., Adhesion of vesicles. *Physical Review A* **1990**, *42* (8), 4768.
- ⁵⁶ Reviakine, I.; Brisson, A., Formation of supported phospholipid bilayers from unilamellar vesicles investigated by atomic force microscopy. *Langmuir* **2000**, *16* (4), 1806-1815.
- ⁵⁷ Blount, M. J.; Miksis, M. J.; Davis, S. H., The equilibria of vesicles adhered to substrates by short-ranged potentials. *Proceedings of the Royal Society A: Mathematical, Physical and Engineering Science* **2013**, *469*, 20120729.
- ⁵⁸ Seifert, U.; Berndl, K.; Lipowsky, R., Shape transformations of vesicles: Phase diagram for spontaneous-curvature and bilayer-coupling models. *Physical Review A* **1991**, *44*, 1182.
- ⁵⁹ Smith, A. M.; Vinchurkar, M.; Gronbeck-Jensen, N.; Parikh, A. N., Order at the edge of the bilayer: Membrane remodeling at the edge of a planar supported bilayer is accompanied by a localized phase change. *Journal of the American Chemical Society* **2010**, *132*, 9320-9327.

-
- ⁶⁰ Keller, C. A.; Kasemo, B., Surface Specific Kinetics of Lipid Vesicle Adsorption Measured with a Quartz Crystal Microbalance. *Biophysical journal* **1998**, *75* (3), 1397-1402.
- ⁶¹ Richter, R. P.; Mukhopadhyay, A.; Brisson, A. *Biophys. J.* **2003**, *85*, 3035-3047
- ⁶² Richter, R. P.; Bérat, R.; Brisson, A. R., Formation of solid-supported lipid bilayers: an integrated view. *Langmuir* **2006**, *22* (8), 3497-3505.
- ⁶³ Gozen, I.; Dommersnes, P., Pore dynamics in lipid membranes. *The European Physical Journal Special Topics* **2014**, *223* (9), 1813-1829.
- ⁶⁴ Antonietti, M.; Förster, S., Vesicles and liposomes: a self-assembly principle beyond lipids. *Advanced Materials* **2003**, *15* (16), 1323-1333.
- ⁶⁵ Hu, M.; Briguglio, J. J.; Deserno, M., Determining the Gaussian curvature modulus of lipid membranes in simulations. *Biophysical journal* **2012**, *102* (6), 1403-1410.
- ⁶⁶ Marrink, S. J.; Mark, A. E., Molecular dynamics simulation of the formation, structure, and dynamics of small phospholipid vesicles. *Journal of the American Chemical Society* **2003**, *125* (49), 15233-15242.
- ⁶⁷ Zhdanov, V. P.; Kasemo, B., Comments on Rupture of Adsorbed Vesicles. *Langmuir* **2001**, *17* (12), 3518-3521.
- ⁶⁸ Rädler, J.; Strey, H.; Sackmann, E., Phenomenology and kinetics of lipid bilayer spreading on hydrophilic surfaces. *Langmuir* **1995**, *11*, 4539-4548.
- ⁶⁹ Weirich, K. L.; Israelachvili, J. N.; Fygenson, D. K., Bilayer edges catalyze supported lipid bilayer formation. *Biophysical journal* **2010**, *98* (1), 85-92.
- ⁷⁰ Richter, R. P.; Brisson, A. R., Following the formation of supported lipid bilayers on mica: a study combining AFM, QCM-D, and ellipsometry. *Biophysical journal* **2005**, *88* (5), 3422-3433.
- ⁷¹ Dimitrievski, K.; Kasemo, B., Simulations of lipid vesicle adsorption for different lipid mixtures. *Langmuir* **2008**, *24* (8), 4077-4091.
- ⁷² Fortunelli, A.; Monti, S., Simulations of lipid adsorption on TiO₂ surfaces in solution. *Langmuir* **2008**, *24* (18), 10145-10154.
- ⁷³ Jackman, J. A.; Zan, G. H.; Zhao, Z.; Cho, N.-J., Contribution of the hydration force to vesicle adhesion on titanium oxide. *Langmuir* **2014**, *30* (19), 5368-5372.
- ⁷⁴ Tero, R.; Ujihara, T.; Urisu, T. Lipid bilayer membrane with atomic step structure: Supported bilayer on a step-and-terrace TiO₂ surface. *Langmuir* **2008**, *24* (20), 11567-11576.

-
- ⁷⁵ Nabika, H.; Fukasawa, A.; Murakoshi, K. Tuning the dynamics and molecular distribution of the self-spreading lipid bilayer. *Phys.Chem. Chem. Phys.* **2008**, *10* (16), 2243–2248.
- ⁷⁶ Johnson, J. M.; Ha, T.; Chu, S.; Boxer, S. G., Early steps of supported bilayer formation probed by single vesicle fluorescence assays. *Biophysical Journal* **2002**, *83*, 3371-3379.
- ⁷⁷ Cha, T.; Guo, A.; Zhu, X.-Y., Formation of supported phospholipid bilayers on molecular surfaces: role of surface charge density and electrostatic interaction. *Biophysical journal* **2006**, *90* (4), 1270-1274.
- ⁷⁸ Seantier, B.; Kasemo, B. Influence of mono- and divalent ions on the formation of supported phospholipid bilayers via vesicle adsorption. *Langmuir* **2009**, *25* (10), 5767–5772.
- ⁷⁹ Berquand, A.; Levy, D.; Gubellini, F.; Le Grimellec, C.; Milhiet, P. E. *Ultramicroscopy* **2007**, *107*, 928–933.
- ⁸⁰ Garcia-Manyes, S.; Oncins, G.; Sanz, F. *Electrochim. Acta* **2006**, *51*, 5029–5036.
- ⁸¹ Hain, N.; Gallego, M.; Reviakine, I., Unraveling supported lipid bilayer formation kinetics: osmotic effects. *Langmuir* **2013**, *29* (7), 2282-2288.
- ⁸² Zhu, T.; Jiang, Z.; Nurlybaeva, E. M. R.; Sheng, J.; Ma, Y., Effect of osmotic stress on membrane fusion on solid substrate. *Langmuir* **2013**, *29* (21), 6377-6385.
- ⁸³ Reimhult, E.; Höök, F.; Kasemo, B., Intact vesicle adsorption and supported biomembrane formation from vesicles in solution: influence of surface chemistry, vesicle size, temperature, and osmotic pressure. *Langmuir* **2002**, *19*, (5), 1681- 1691
- ⁸⁴ Cho, N.-J.; Jackman, J. A.; Liu, M.; Frank, C. W., pH-Driven assembly of various supported lipid platforms: A comparative study on silicon oxide and titanium oxide. *Langmuir* **2011**, *27* (7), 3739-3748.
- ⁸⁵ Jiang, W.; Mashayekhi, H.; Xing, B., Bacterial toxicity comparison between nano- and micro-scaled oxide particles. *Environmental Pollution* **2009**, *157* (5), 1619-1625.
- ⁸⁶ Dimitrievski, K.; Reimhult, E.; Kasemo, B.; Zhdanov, V. P. Simulations of temperature dependence of the formation of a supported lipid bilayer via vesicle adsorption. *Colloids Surf., B* **2004**, *39* (1), 77–86.
- ⁸⁷ Jing, Y.; Trefna, H.; Persson, M.; Kasemo, B.; Svedhem, S. Formation of supported lipid bilayers on silica: relation to lipid phase transition temperature and liposome size. *Soft Matter* **2014**, *10* (1), 187–195.

-
- ⁸⁸ Reviakine, I.; Gallego, M.; Johannsmann, D.; Tellechea, E., Adsorbed liposome deformation studied with quartz crystal microbalance. *The Journal of chemical physics* **2012**, *136* (8), 084702.
- ⁸⁹ Lind, T. K.; Cárdenas, M.; Wacklin, H. P., Formation of supported lipid bilayers by vesicle fusion: Effect of deposition temperature. *Langmuir* **2014**, *30* (25), 7259-7263.
- ⁹⁰ Jing, Y.; Trefna, H.; Persson, M.; Kasemo, B.; Svedhem, S., Formation of supported lipid bilayers on silica: relation to lipid phase transition temperature and liposome size. *Soft Matter* **2014**, *10* (1), 187-195.
- ⁹¹ Cho, N.-J., Contribution of Temperature to Deformation of Adsorbed Vesicles Studied by Nanoplasmonic Biosensing. *Langmuir* **2014**.
- ⁹² Seifert, U.; Lipowsky, R. Adhesion of vesicles. *Phys. Rev. A* **1990**, *42* (8), 4768.
- ⁹³ Seifert, U. Configurations of fluid membranes and vesicles. *Adv. Phys.* **1997**, *46* (1), 13-137.
- ⁹⁴ Pan, J.; Tristram-Nagle, S.; Kučerka, N.; Nagle, J. F., Temperature dependence of structure, bending rigidity, and bilayer interactions of dioleoylphosphatidylcholine bilayers. *Biophysical journal* **2008**, *94* (1), 117-124.
- ⁹⁵ <http://www.avantilipids.com> Image of glycolipid.
- ⁹⁶ Büschl, R.; Folda, T.; Ringsdorf, H., Polymeric monolayers and liposomes as models for biomembranes. How to bridge the gap between polymer science and membrane biology? *Die Makromolekulare Chemie* **1984**, *6* (S19841), 245-258.
- ⁹⁷ Wagner, N.; Dose, K.; Koch, H.; Ringsdorf, H., Incorporation of ATP synthetase into long-term stable liposomes of a polymerizable synthetic sulfolipid. *FEBS letters* **1981**, *132* (2), 313-318.
- ⁹⁸ Spinke, J.; Yang, J.; Wolf, H.; Liley, M.; Ringsdorf, H.; Knoll, W., Polymer-supported bilayer on a solid substrate. *Biophysical journal* **1992**, *63* (6), 1667.
- ⁹⁹ Langmuir, I.; Schaefer, V.; Sobotka, H., Multilayers of Sterols and the Adsorption of Digitonin by Deposited Monolayers. *Journal of the American Chemical Society* **1937**, *59* (9), 1751-1759. Langmuir Blodgett is a mechanical deposition process by which a monolayer of lipids is created by immersing the solid substrate in the lipid suspension. The monolayer is formed at the air-water interface as the surface is lifted out of the suspension. A second monolayer can be subsequently deposited in a similar manner.
- ¹⁰⁰ Baumgart, T.; Offenhäusser, A., Polysaccharide-supported planar bilayer lipid model membranes. *Langmuir* **2003**, *19* (5), 1730-1737.
- ¹⁰¹ I.R. Peterson, "Langmuir Blodgett Films ", *J. Phys. D* **1990** *23*, 4, () 379-95

A monolayer of lipids or other material is formed on the solid surface at the air-water interface.

¹⁰² Marrink, S.-J.; Tieleman, D. P.; van Bueren, A. R.; Berendsen, H. J. C. *Faraday Discuss.* **1996**, 103, 191-201

¹⁰³ Goennenwein, S.; Tanaka, M.; Hu, B.; Moroder, L.; Sackmann, E., Functional incorporation of integrins into solid supported membranes on ultrathin films of cellulose: impact on adhesion. *Biophysical journal* **2003**, 85 (1), 646-655.

¹⁰⁴ Elender, G.; Kühner, M.; Sackmann, E., Functionalisation of Si/SiO₂ and glass surfaces with ultrathin dextran films and deposition of lipid bilayers. *Biosensors and Bioelectronics* **1996**, 11 (6), 565-577.

¹⁰⁵ Floyd, D. L.; Harrison, S. C.; van Oijen, A. M., Method for measurement of viral fusion kinetics at the single particle level. *Journal of visualized experiments: JoVE* **2009**, (31).

¹⁰⁶ Prime, K. L., and G. M. Whitesides. Self-assembled organic monolayers: model systems for studying adsorption of proteins at surfaces. *Science*. **1991**. 252:1164 – 1167.)

¹⁰⁷ Ariga, K., J. S. Shin, and T. Kunitake. Interaction of lipid monolayers with aqueous neutral polymers and consequent monolayer stabilization and improved Langmuir Blodgett transfer. *J. Colloid Interface Sci.* **1995**.170:440–448.

¹⁰⁸ Wagner, M. L.; Tamm, L. K., Tethered polymer-supported planar lipid bilayers for reconstitution of integral membrane proteins: silane-polyethyleneglycol-lipid as a cushion and covalent linker. *Biophysical journal* **2000**, 79 (3), 1400-1414.

¹⁰⁹ Hwang, L. Y.; Götz, H.; Hawker, C. J.; Frank, C. W., Glyco-acrylate copolymers for bilayer tethering on benzophenone-modified substrates. *Colloids and Surfaces B: Biointerfaces* **2007**, 54 (2), 127-135.

¹¹⁰ Kaufmann, S.; Papastavrou, G.; Kumar, K.; Textor, M.; Reimhult, E., A detailed investigation of the formation kinetics and layer structure of poly (ethylene glycol) tether supported lipid bilayers. *Soft Matter* **2009**, 5 (14), 2804-2814.

¹¹¹ Roder, F.; Birkholz, O.; Beutel, O.; Paterok, D.; Piehler, J., Spatial Organization of Lipid Phases in Micropatterned Polymer-Supported Membranes. *Journal of the American Chemical Society* **2013**, 135 (4), 1189-1192.

¹¹² Jenkins, A. T. A.; Boden, N.; Bushby, R. J.; Evans, S. D.; Knowles, P. F.; Miles, R. E.; Ogier, S. D.; Schönherr, H.; Vancso, G. J., Microcontact printing of lipophilic self-

assembled monolayers for the attachment of biomimetic lipid bilayers to surfaces.

Journal of the American Chemical Society **1999**, *121* (22), 5274-5280.

¹¹³ Mashaghi, S.; van Oijen, A. M., A versatile approach to the generation of fluid supported lipid bilayers and its applications. *Biotechnology and bioengineering* **2014**, *111* (10), 2076-2081.

¹¹⁴ Sumino, A., Dewa, T., Takeuchi, T., Sugiura, R., Sasaki, N., Misawa, N., Tero, R., Urisu, T., Gardiner, A. T., Cogdell, R. J., Hashimoto, H. & Nango, M., Construction and Structural Analysis of Tethered Lipid Bilayer Containing Photosynthetic Antenna Proteins for Functional Analysis. *Biomacromolecules* **2011**, *12*, 2850-2858.

¹¹⁵ Smith, E. A.; Coym, J. W.; Cowell, S. M.; Tokimoto, T.; Hruby, V. J.; Yamamura, H. I.; Wirth, M. J., Lipid Bilayers on Polyacrylamide Brushes for Inclusion of Membrane Proteins. *Langmuir* **2005**, *21* (21), 9644-9650.

¹¹⁶ Santonicola, M. G.; Memesa, M.; Meszynska, A.; Ma, Y.; Vancso, G. J., Surface-grafted zwitterionic polymers as platforms for functional supported phospholipid membranes. *Soft Matter* **2012**, *8* (5), 1556-1562.

¹¹⁷ Renner, L.; Osaki, T.; Chiantia, S.; Schwille, P.; Pompe, T.; Werner, C., Supported Lipid Bilayers on Spacious and pH-Responsive Polymer Cushions with Varied Hydrophilicity. *The Journal of Physical Chemistry B* **2008**, *112* (20), 6373-6378.

¹¹⁸ El-khoury, R. J.; Bricarello, D. A.; Watkins, E. B.; Kim, C. Y.; Miller, C. E.; Patten, T. E.; Parikh, A. N.; Kuhl, T. L., pH Responsive Polymer Cushions for Probing Membrane Environment Interactions. *Nano Letters* **2011**, *11* (5), 2169-2172.

¹¹⁹ Nirasay, S.; Badia, A.; Leclair, G.; Claverie, J. P.; Marcotte, I., Polydopamine-supported lipid bilayers. *Materials* **2012**, *5* (12), 2621-2636.

¹²⁰ Kaufmann, M.; Jia, Y.; Werner, C.; Pompe, T., Weakly coupled lipid bilayer membranes on multistimuli-responsive poly (N-isopropylacrylamide) copolymer cushions. *Langmuir* **2010**, *27* (2), 513-516.

¹²¹ Rehfeldt, F.; Steitz, R.; Armes, S. P.; von Klitzing, R.; Gast, A. P.; Tanaka, M., Reversible Activation of Diblock Copolymer Monolayers at the Interface by pH Modulation, 2: Membrane Interactions at the Solid/Liquid Interface. *The Journal of Physical Chemistry B* **2006**, *110* (18), 9177-9182.

¹²² Tang, Y.; Wang, Z.; Xiao, J.; Yang, S.; Wang, Y. J.; Tong, P., Studies of phospholipid vesicle deposition/transformation on a polymer surface by dissipative quartz crystal microbalance and atomic force microscopy. *The Journal of Physical Chemistry B* **2009**, *113* (45), 14925-14933.

¹²³ Ma, C.; Srinivasan, M. P.; Waring, A. J.; Lehrer, R. I.; Longo, M. L.; Stroeve, P., Supported lipid bilayers lifted from the substrate by layer-by-layer polyion cushions on self-assembled monolayers. *Colloids and Surfaces B: Biointerfaces* **2003**, *28* (4), 319-329.

¹²⁴ Fischlechner, M.; Zaulig, M.; Meyer, S.; Estrela-Lopis, I.; Cuéllar, L.; Irigoyen, J.; Pescador, P.; Brumen, M.; Messner, P.; Moya, S., Lipid layers on polyelectrolyte multilayer supports. *Soft Matter* **2008**, *4* (11), 2245-2258.

3. Experimental theory

3.1. Polymer brushes

3.1.1. Introduction

The surfaces of interest on which the lipid bilayers were deposited were formed from polymer brushes, grown from a solid substrate. In order to explain the experimental results it is essential to understand some basic principles of their production, characterisation and properties. The work in this thesis focuses specifically on charged *homopolymer* brushes, formed by first attaching anchor groups to a planar surface with a high grafting density (the *initiator*) and then reacting them with one type of monomer.¹ There is the flexibility, within the method, to include other monomers to form *diblock* or *triblock* polymer brushes with different response characteristics but these are not the focus of the work presented in this thesis. Following the chemical reaction of the monomers with this initiator layer, the brushes can be grown with sufficient density to create interactions and repulsion between the chains, which causes extension of the chains. These chains exhibit very different properties from freely diffusing polymer chains in solution and have resulted in many novel and useful properties.² Polymer brushes are defined as "*dense layers of chains confined to a surface where the distance between the grafts is much less than the unperturbed dimensions*".³ Alexander and de Gennes, who were pioneers of this work, defined the grafting density as the inverse distance of two surface attached polymer chains. If the distance is larger than the chains they will collapse onto the surface in a 'pancake' regime. Where the grafting density is low, but the chains do not interact with the surface, the chains will coil into a 'mushroom' regime.

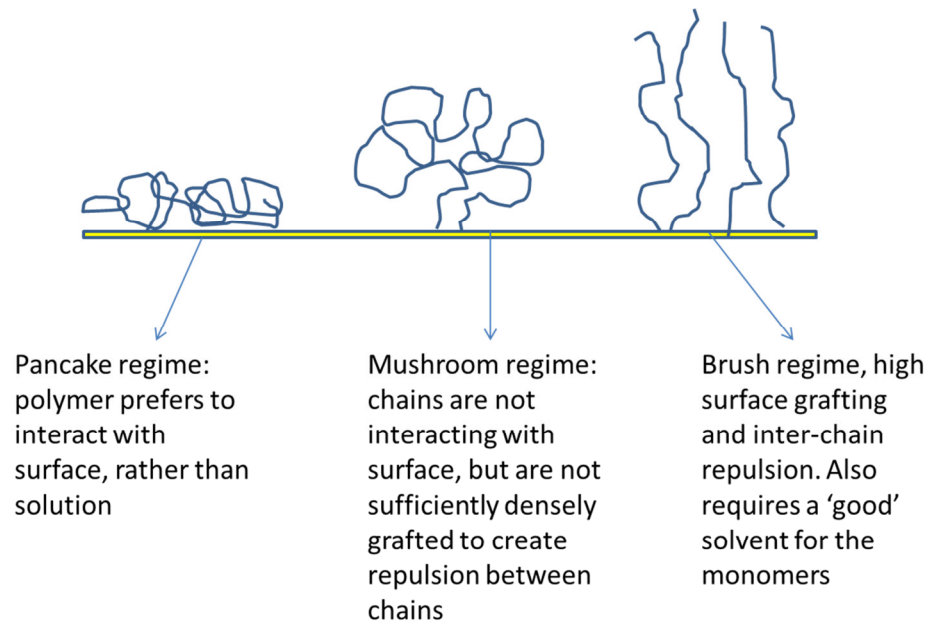


Figure 3.1: Three conformations of polymer attached to solid surface.

In the third case, when there is a high grafting density, the chains stretch away, in a direction normal to the surface, in a brush formation. (Figure 3.1) This third case is the conformation which provides suitable surfaces for the work presented here.^{4 5}

The high steric crowding, resulting from the brush regime, forces chains to extend outwards from the surface in an entropically unfavourable conformation.⁶ This stretching leads to a loss of conformational entropy (compared to free chains) and creates interaction energy between the tethered chains. This counterbalances the elastic free energy of the chains which tend to force them to collapse back towards the surface from which they are grown.⁷ The chains in this configuration maintain an *excluded volume*, between them. This is defined as a volume which is inaccessible to other molecules because of the presence of the first chain and is slightly greater than the theoretical volume occupied by a single polymer chain.¹⁰

3.1.2. Surface initiated atom transfer polymerisation (Si-ATRP)

The process of producing the polymers, by surface initiated atom transfer radical polymerisation allows brushes of controlled thickness (length) and grafting density to be produced. ATRP also allows polymers to be tailor-made and composed of a variety of monomers giving the polymer specific properties, which can vary with solution and other environmental conditions.⁸ In general terms the first stage involves the deposition onto a cleaned surface, such as piranha cleaned glass, of a silane APTES self-assembled monolayer (SAM) which terminates in a reactive amine group. This reacts with 2-bromoisobutryl

bromide (BIBB) and provides the bromide required for the next stage of the reaction with the monomer. The next stage for the generic reaction of this initiated surface is shown in Figure 3.2. Briefly, the surface groups form radicals by transferring bromine to a metal catalyst (in this case a copper catalyst). The exposed radical then reacts with a monomer, which continues in a cycle until the reaction is stopped. The reaction time will thus determine the final polymer chain length. The reaction is summarised by Matyjaszewski, a pioneer of the process: “ATRP is the reversible homolytic transfer of a radically transferable atom, or group, typically a halogen atom, from a monomeric, polymeric or surface tethered alkyl (pseudo) halide, to a transition metal complex initially in a lower oxidation state, forming an active organic radical and a transition metal complex in a higher oxidation state followed by donation of the transferred atom/group back to the growing radical reforming a dormant oligo/polymeric species and the lower oxidation state transition metal complex.”⁹

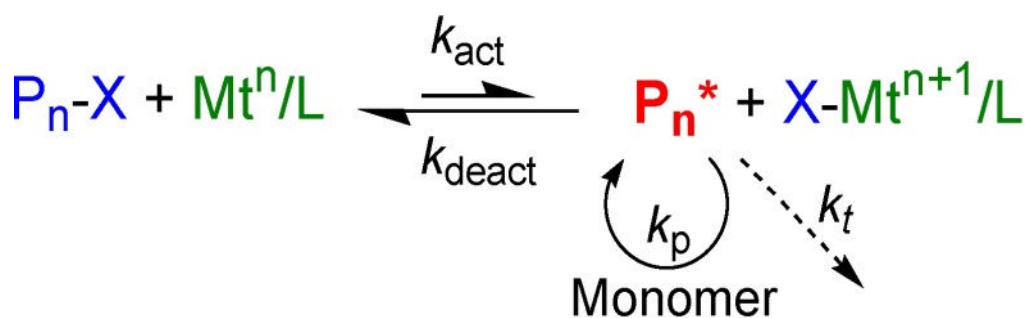


Figure 3.2: Matyjaszewski's simplified mechanism for ATRP. Image from ref 8, 9

The resulting polymer brushes can be neutral, strong electrolytes or weak polyelectrolytes, depending on the monomer chemistry chosen. Neutral polymers have no charged groups along the chain whereas strong polyelectrolytes have fixed charges along the chain, which are not pH responsive. In order to have practical application, weak polyelectrolytes, with monomers which respond to environmental conditions in a controlled manner, are selected. This is most flexibly achieved by using monomers which are weakly basic or weakly acidic where the charged groups are capable of gaining or losing protons depending on the solution pH.^{10 7} The two charged variants are discussed in more detail below.

3.1.3. Strong PELs

These brushes have charged groups along the chains and the conformation they adopt will be governed by electrostatic interactions and the osmotic pressure of the counterions in solution rather than the osmotic pressure of the macromolecular segments.³ The number

and location of the charges along the chain is fixed and the solution pH ion will not affect them. The structure of strong polyelectrolyte brushes is influenced by the grafting density, degree of dissociation and the ionic strength of the solution. In strongly charged brushes where the grafting density and charges are high, all counterions will be trapped within the brush.⁷ In this case the brush height bears a linear relationship to the degree of polymerisation (number of monomers in the chain), but not to the grafting density. In this 'osmotic regime' the brush height is a function of balance between the osmotic pressure of the trapped counterions and the restoring elastic force of the chains.¹⁴ If salt is added at low concentrations screening takes place at only the outer edge of the brush and height is not affected. If the solution ion concentration reaches that of the counterion concentration within the brush the osmotic pressure and entropic elasticity are balanced. As more salt is added the osmotic pressure within the brush is reduced and the height decreases.³

3.1.4. Weak PELs

The weakly charged PELs exist in equilibrium between neutral, associated and dissociated charged entities, which is influenced by solution pH and not the location of charges on the polymer. The charges on the polymer can change location because of this equilibrium.³ In weak polyacids (e.g. carboxylate) at low pH, an abundance of protons will reduce the charge density by protonation of the charged moieties, collapsing the brush. Increasing the pH will generate more charges, by deprotonating the acid groups and will increase electrostatic repulsion and extend the chains. Conversely in weak polybases (e.g. amine) at low pH the groups will be protonated, increasing the charge and extending the chains.⁶ At high pH the chains will collapse as the protons are removed and the groups are neutralised.^{11 6} Polyzwitterions are also of interest, which have both positive and negatively charged groups on the chains, so they exhibit characteristics similar to the polyacid or polybase as described above depending on the pH, but over a range of neutral pH will exhibit a charge neutral regime.^{12 13}

The effect of low salt concentration provides a counterintuitive result. With the addition of small amounts of monovalent ions some of the cations can be exchanged for protons, while maintaining overall neutrality of the polymer chain.¹ However, the binding constant is lower than that for the acid/base (protons) so an increase in charge will result, causing an increase in osmotic pressure and chain extension. If the salt concentration surrounding the brush is increased significantly a weak PEL brush in solution will shrink, as the osmotic

pressure difference is balanced between the interior of the brush (lower osmotic pressure) and the surrounding solution (higher pressure).¹⁴

The practical aspects of this can be seen in chapter 5 and 6 where the brushes pH response is shown.

3.2. Lipid vesicles

A brief description of how the small unilamellar vesicles are formed is presented below.

Detail on the production of these is included in chapter 4 and the physics of the bilayer and vesicle formation process are described in chapter 2.2. A dried lipid film when hydrated in a chosen buffer and then vortex mixed until cloudy, forms into large multilamellar vesicles (MLV). The vesicles can be tip sonicated until the solution became clear, which indicated that the MLVs had become unilamellar vesicles with a diameter of approximately 25 nm. These stages are demonstrated in Figure 3.3.

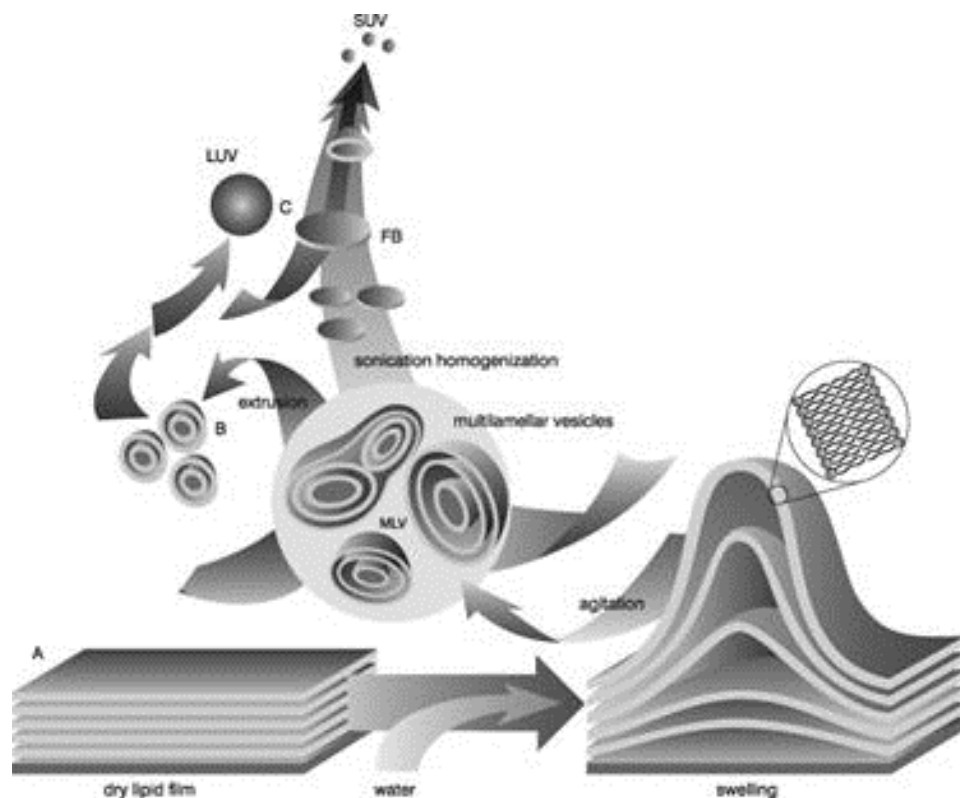


Figure 3.3: Formation of unilamellar vesicles from dried lipid, via a multilamellar stage. Image from ref 15.

Vesicle extrusion through a membrane can be used as an alternative method which replaces the tip sonication stage and physically removes the multilayers to create mono-disperse unilamellar vesicles, by forcing them through a membrane of a suitable pore size.

Tip sonication is easy to use and produces reproducible samples of small vesicles. Extrusion is preferred when proteins are to be incorporated into vesicles or larger vesicles are required as tip sonication will denature the protein.

3.3. Detergents, solubilisation and reconstitution of proteins

3.3.1. Introduction

Many important cell membrane proteins are located within and on the surface of the lipid bilayer. They provide communication between the inside and outside of the cell and interact with molecules in the surrounding extracellular space and cytoplasm to create the functions which support life. With the exception of bacteriorhodopsin in the *Halobacteria Salinara*, individual proteins are present in small quantities in the cell.^{16 17} To obtain a purified sample of the protein in sufficient quantity for study, it must be isolated from its membrane and then over-expressed or genetically modified. The aim is to form a sufficiently concentrated sample so that the protein can be crystallised to study its structure. For functional studies the protein will be reconstituted into a fluid bilayer environment.

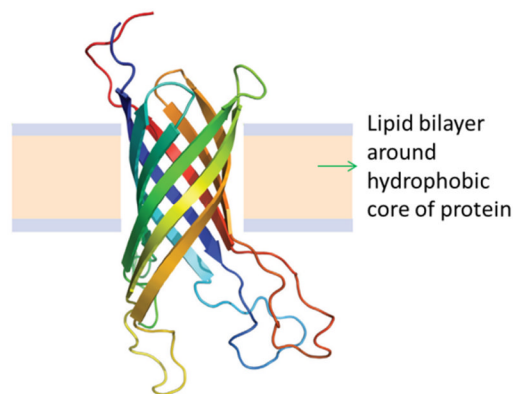


Figure 3.4: Cartoon of a transmembrane protein embedded in a lipid bilayer. Image from ref 18.

There are a limited number of water soluble proteins and a transmembrane protein has three regions: the extracellular area (cis), the hydrophobic transmembrane portion, bound by the lipid bilayer and an intracellular (trans) section.¹⁹ The transmembrane portion will maintain its structure and function in its natural lipid membrane environment as shown in Figure 3.4.

3.3.2. Solubilising and reconstituting proteins

To study proteins out of their natural environment requires them to be reconstituted into a biomimetic lipid membrane. The process is aided by using detergent molecules to act as an

intermediary, that bind around, and maintain the integrity of, the hydrophobic core. After the protein has been transferred into the lipid bilayer, the detergent, being more water soluble than the lipids, can be rinsed away.²⁰ Heerklotz *et al.* defined these processes.

*“Solubilization is the dissolution of a bilayer membrane by increasing the relative amount of detergent in the solution. Reconstitution is the opposite process by which bilayer membrane morphology is recovered by lowering the relative amount of detergent.”*²¹

Detergents contain one hydrophobic chain (whereas lipids have two) and a polar headgroup and, as can be seen in chapter 2, Figure 2.5. The general shape is conical so that when exposed to water or buffer they will form micellar structures (where the hydrophobic tails are hidden from the water and the larger polar headgroups are exposed to it, Figure 2.5).²² There is a critical detergent concentration (CMC) below which individual detergent molecules remain in solution and above which the molecules will form micelles. This CMC is dependent on pH and temperature, as well as the presence of other ions or proteins.²⁵ An excess of detergent, above the CMC is required to solubilise the protein. The CMC is determined by a combination of the repulsive forces of the head group and the hydrophobic interactions of the tail groups.^{23 26}

3.3.3. Types of detergent

Two main types of detergent are compared here. Ionic detergents have a charged headgroup, with hydrophobic tail region. They are effective in solubilising proteins, but are usually denaturing, however, some proteins can be re-natured when reconstituted back into a lipid bilayer.¹⁹

Non-Ionic Detergents

R = glucose, x = 7, n-octyl- β -D-glucopyranoside

R = maltose, x = 9, decyl- β -D-maltoside

x = 11, dodecyl- β -D-maltoside

$RO(CH_2)_x-CH_3$

x = 9, Triton[®] X-100

x = 7-8, Triton[®] X-114

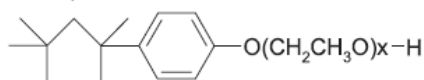


Figure 3.5: Examples of non-ionic detergents such as OG and β DDM. Taken from ref 19.

Non-ionic detergents (Figure 3.5) have a uncharged head group, such as n-octyl- β -d-glucopyranoside (OG) and n-dodecyl- β -d-maltoside (β DDM). These are milder to use for

reconstitutions and work by breaking the lipid-lipid interactions and lipid-protein interactions rather than protein-protein interactions. This allows the protein to be isolated in its biologically active form surrounded by detergent molecules which have replaced the lipid molecules of the natural membrane.²⁴

3.3.4. Reconstitution methods

In Figure 3.6 the methods currently available for reconstitution are summarised:¹⁹ a) Transferring a single protein into a patch of membrane. b) Incorporating the protein into a proteoliposome and then rupturing this on a solid surface. c) As for b), but using a chemically modified surface to tether the bilayer to the surface. d) A proteoliposome can be fused into a pore-spanning lipid bilayer. e) A GUV containing the protein is ruptured to span a mechanical pore. f) The protein is tethered to a surface and a bilayer reconstituted around it.

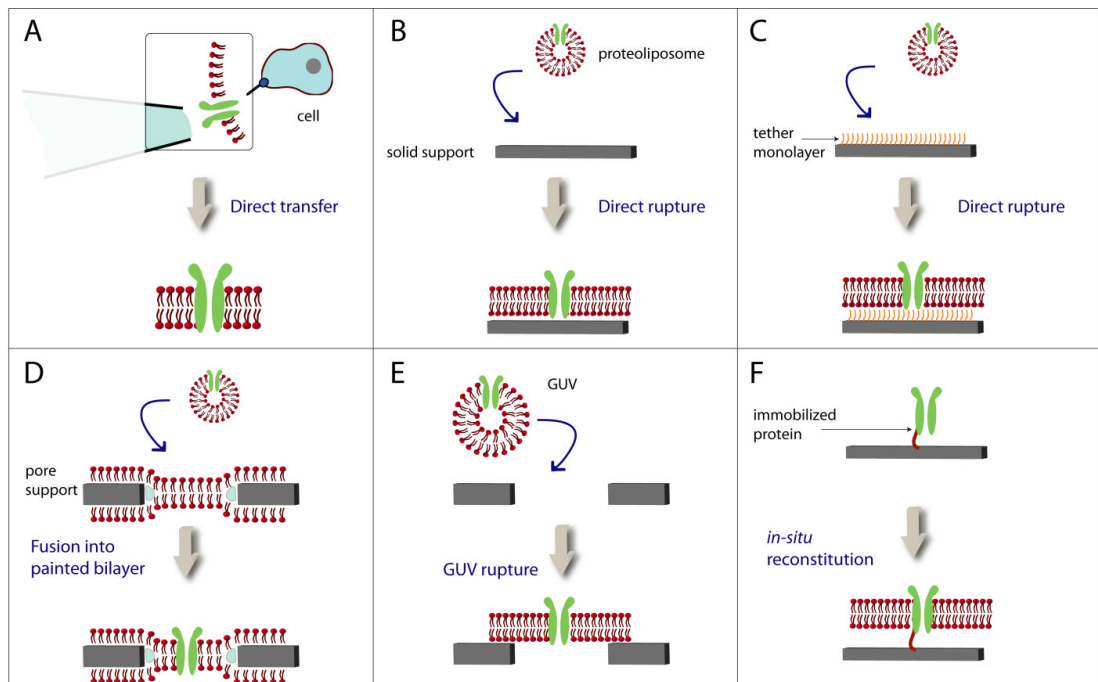


Figure 3.6: Methods available for reconstituting proteins. a) Transferring a single protein into a patch of membrane. b) Incorporating the protein into a proteoliposome and then rupturing this in a solid surface. c) As for b), but using a chemically modified surface to tether the bilayer to the surface. d) A proteoliposome can be fused into a pore-spanning lipid bilayer. e) A GUV containing the protein is ruptured to span a mechanical pore. f) The protein is tethered to a surface and a bilayer reconstituted around it. Image from ref 20.

In order to achieve the above reconstitutions, Rigaud *et al.*²⁵ suggested a number of practical issues to consider by which the protein can be reconstitution into a vesicle or bilayer. The first uses a dilution approach so that as the detergent encapsulated protein is

added to a liposome solution this will dilute the detergent concentration to below its CMC, the micelles become unstable and the protein transfers from the detergent micelles into the liposome. In the second method he suggests that a detergent is added to a liposome suspension. The liposomes become saturated with detergent, making them permeable to the protein. The detergent is then removed by dilution dialysis or by adsorption onto Biobeads.²⁵

Heerklotz *et al.*²¹ defined three phases, which can be plotted graphically between the axes of lipid concentration (x axis) and detergent concentration (y axis), as shown in Figure 3.7. The area defined as 'micelles' contains detergent monomers and some mixed detergent-lipid mixed micelles. The area 'vesicles' contains bilayers as vesicles or bilayer sheets and between them is an area which contains detergent monomers, mixed vesicles and mixed micelles. The suitability of a detergent depends on its lipid-detergent-protein phase range.

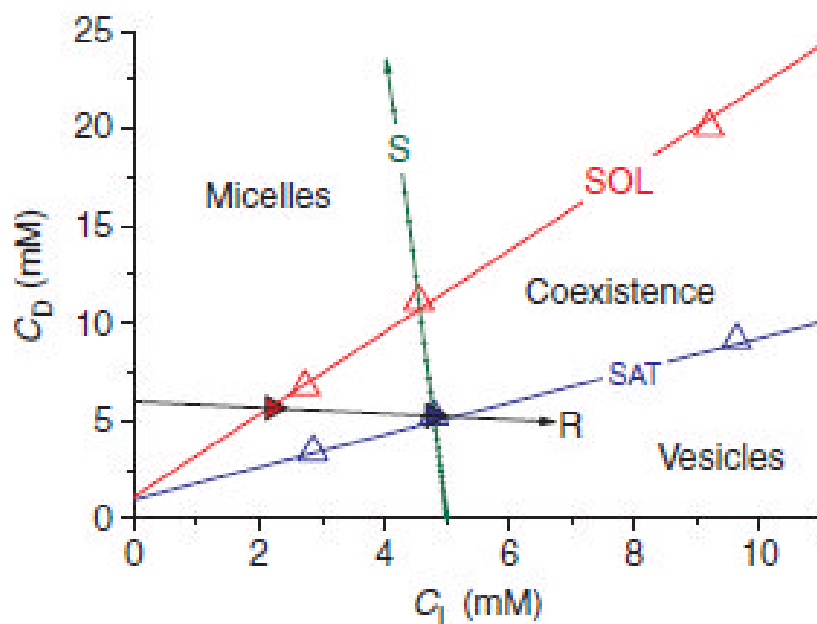


Figure 3.7: Three phases, which can be plotted graphically between the axes of lipid concentration (x axis) and detergent concentration (y axis), show micelles and vesicles, which a phase between where both can exist. Graph from ref 21.

The detergent OG is able to trigger protein reconstitution when vesicles are present, without disrupting the bilayer, whereas Triton requires reconstitution to begin at the phase where mixed vesicles and mixed micelles are present. The phases can be tested before reconstitution using dynamic light scattering as demonstrated in chapter 6. The molar

concentrations of micelles in solution can be calculated from the aggregation number (which is the number of detergent molecules per micelle) and the molecular weight of the detergent monomer.^{26 27}

3.3.5. Detergent methods for preparing lipid bilayers

One method for preparing lipid bilayers by Vacklin,²⁸ and also by Tiberg,²⁹ requires the co-adsorbing of lipids and surfactants from a mixed –micelle solution, on to a silica surface. The detergent lipid mixture was composed of DOPC lipid and β DDM detergent. The detergent did not adsorb onto the silica surface, so could be easily removed by very slow rinsing after the adsorption step. This is the method adopted in chapter 6 for incorporating light harvesting proteins into a bilayer on a polymer brush.

In a further study on this method, Lee *et al.*³⁰ investigated the packing conformation of the lipid bilayer formed from a β DDM detergent -DPPC lipid mixture. They confirmed that the packing conformation did not differ from that formed from lipid only and that there was no residual detergent left on the surface. This suggested that the lipids were correctly organised in a configuration normal to the silica solid (quartz) surface. The lipid density at the surface was gradually increased as the detergent was removed during rinsing. A different use of detergent was reported by Kataoka-Hamai³¹ for bilayer formation. Their process consisted of a number of steps. First a lipid-PEG was grafted to glass using a silane linker. This was incubated with lipid-detergent micelles consisting of DOPC lipid and OG detergent, prepared from dried lipid solubilised with buffer containing the detergent. A method of using detergent to produce asymmetrical bilayers was reported by Visco *et al.*³² They applied a concentrated methyl- β -cyclodextrin solution containing the lipid of interest, in this case sphingomyelin. A mediated lipid exchanged took place into a bilayer previously formed with DOPC by vesicle fusion, which then enriched the upper layer with sphingomyelin.

These detergent depletion methods and elements of the detergent characteristics above will be applied in chapter 6 where protein reconstitution attempts are presented.

3.4. Contact angle

3.4.1. Background

The method is a way of determining how hydrophobic or hydrophilic the polymer brushes are, before testing bilayer formation on them. The interaction of a water droplet was

observed as it is dispensed onto the dry brush surface. The shape and the angle it formed between the air and brush surface was measured, as seen in Figure 3.8. An angle of $<90^\circ$ was considered to indicate that the surface is hydrophilic and if $>90^\circ$ it tends towards being hydrophobic. Low contact angles ($<20^\circ$) indicated a strong attraction between two hydrophilic surfaces (the water and the sample) which was observed as the rapid spreading of the water droplet across the surface. Higher contact angles resulted from lower attraction between the surface and the water i.e. a greater surface tension within the water itself and a lower surface energy of the sample.

Contact angle measurements were made at the air/liquid/solid (three phase) interface as shown in Figure 3.8 (a). The measurement of the shape of the droplet was determined by the Young's equation where the contact angle played the role of a boundary condition.

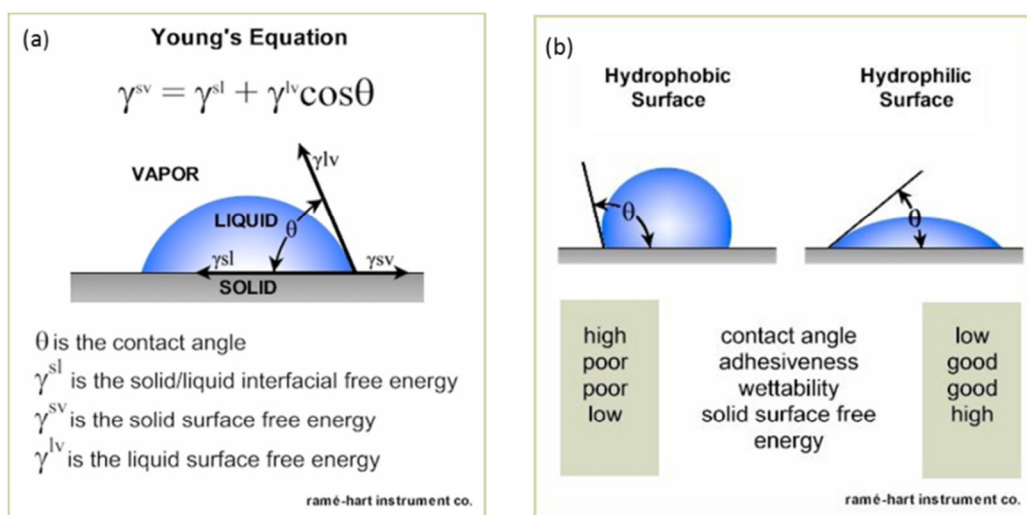


Figure 3.8: Young's equation to determine contact angle and surface energy. Image from ref 33.

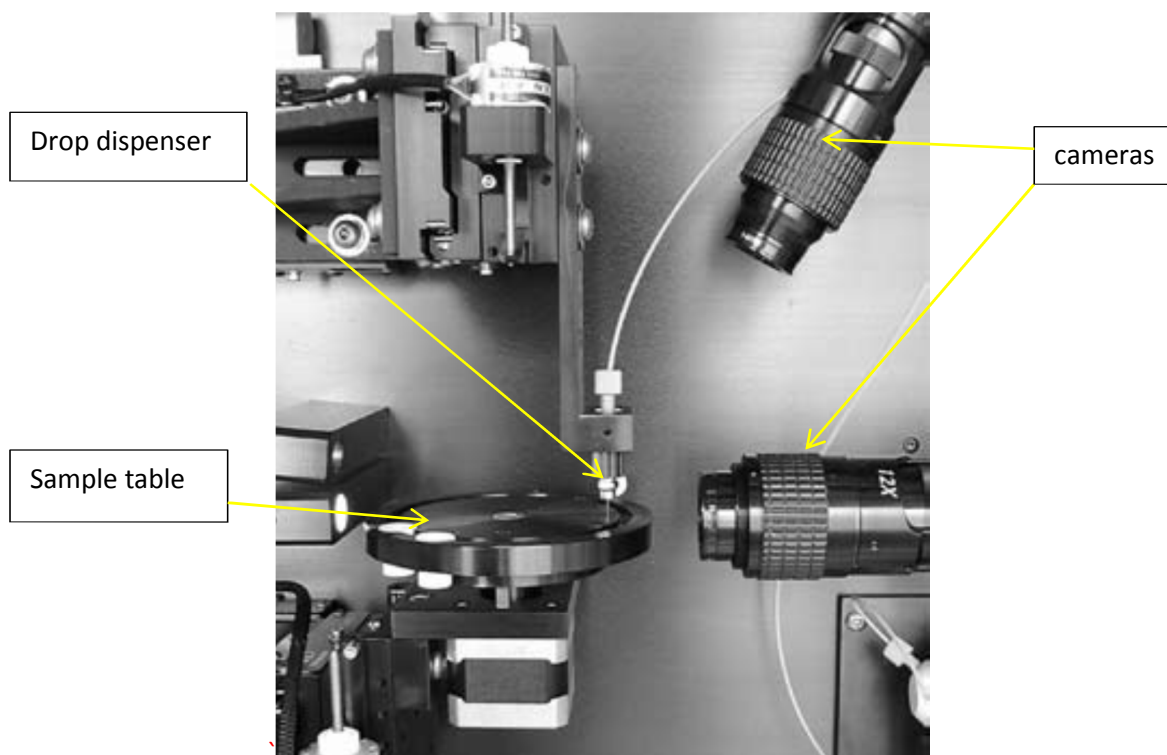


Figure 3.9: Example of goniometer showing droplet dispensing and recording camera (from FTA, First Ten Angstroms)³⁴.

An advancing (water flowed towards the surface) and receding angle (drop was retracted) were measured, the hysteresis between the two gave an indication of surface roughness. A number of measurements were taken across the samples to determine an average reading. The variance between these provided an indication of the homogeneity across the sample surface. This method was easy to use and generated reproducible results, providing the surfaces and the droplets were kept contaminant free. It was proposed that a low contact angle may correlate with the ability of the polymer brush to support lipid bilayers and this was tested throughout the experimental work.

3.4.2. Practical aspects and errors

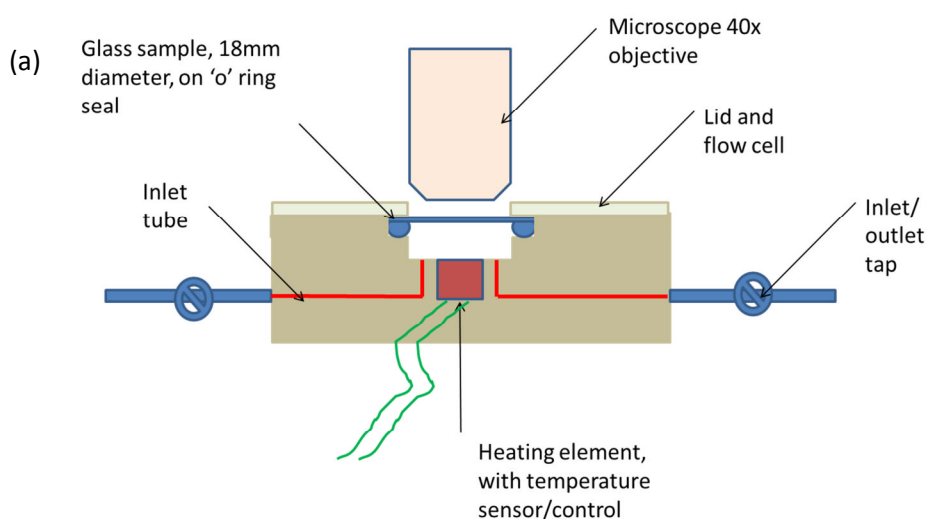
The system must be completely flushed with ultrapure (MilliQ) water, be free from air bubbles and kept free from dust and organic contaminants, especially on the tip. The readings must be taken when the surface being tested was flat (i.e. parallel to the equipment stage). As the readings were taken during the pumping of water onto the surface ("ramp positive") the readings shown on the graph, taken in a time series, should follow a stable pattern and create a linear graph. The readings were be repeated if this was not the case.

3.5. Flow cells

3.5.1. Cells and use

In order to provide a controlled environment for testing bilayer formation and to control the flow of rinsing medium, home-made flow cells were used. Two types were required depending on the type of microscopy being used. The one shown in Figure 3.10 (a) was used for most incubations for FRAP experiments. It has a deep base with a reservoir of 0.7 μ L and a heating Peltier heating element fixed in the base. The sample was sealed in the location described (Figure 3.10 (a)) and the inlet and outlet valves were used to inject lipid and rinsing water into the cell in a controlled manner, whilst excluding air from the system, which would dehydrate the bilayer. The camera objective was located at the top.

The lower cell (Figure 3.10 (b)) was a thinner cell, used for TIRF and dark field microscopy as the regular cell above was too deep for the microscope working distance. This cell was made by gluing a round 18 mm sample coverslip to a 3D printed 'O' ring on one side and to a flat slide on the other. The needles and taps were inserted through this 'O' ring for injecting the sample and rinsing solution.



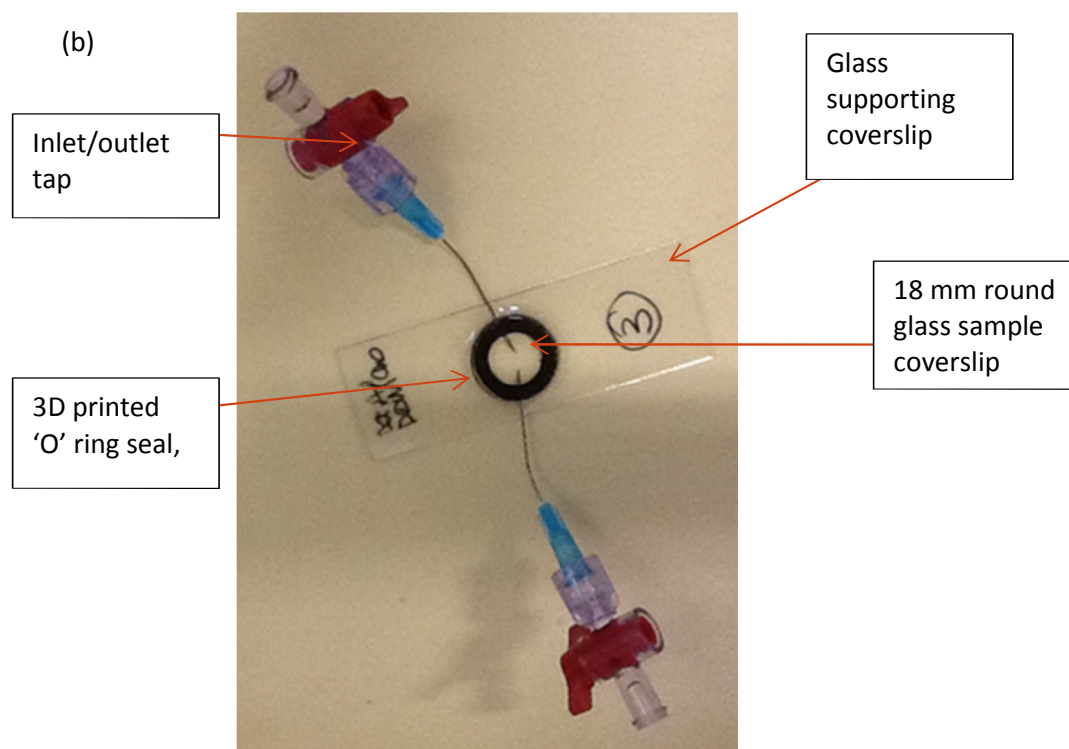


Figure 3.10: (a) flow cell for incubating glass and polymer samples with lipid for FRAP and (b) modified flow cell for TIRF and dark field microscope.

3.5.2. Errors

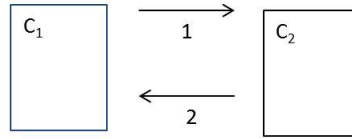
The exclusion of air was essential when creating lipid bilayers and the ability to reproduce the incubation conditions across a range of samples was important, which this system allowed. It also allows the rinsing protocol to be exactly reproduced. The cell must be cleaned and rinsed thoroughly between samples to ensure there were no contaminants to interfere with the bilayer formation.

3.6. Fluorescence recovery after photobleaching (FRAP)

3.6.1. Diffusion

Mobile particles, such as individual lipids which form a hydrated lipid bilayer, move in a random manner under thermal (Brownian) motion. Simple diffusion is the movement of particles from a region of high concentration to a region of lower concentration. The net rate of particles moving through an area, by diffusion is referred to as the flux. This flux is related to the change in pressure of the particles and the diffusion rate. Factors which affect the diffusion rate will be the distance of travel, the molecule size (Graham's law states that smaller particles will move faster) the pressure (i.e. quantity or concentration) of particles in the area and the size of the area they are diffusing within.³⁵

This provides a basic equation relating the rate at which the particles move to the change in pressure of the particles, the surface area and the rate of diffusion (diffusion constant). In a simple 2D case, where c is the concentration of particles diffusing between 2 locations:



Where (1) is the flux in one direction:

$$\frac{c_1 D}{\Delta x} \quad (3.1)$$

And (2) is the flux in the other:

$$\frac{c_2 D}{\Delta x} \quad (3.2)$$

The net flux is:

$$(c_1 - c_2) \frac{D}{\Delta x} \text{ where } (c_1 - c_2) = dc \quad (3.3)$$

From this the combined flux, J can be derived for 2 dimensional diffusion:

$$J = -D \frac{dc(x)}{dx} \quad (3.4)$$

In a 2D area the particles will diffuse not only in a left right motion, but in any direction and a diffusion constant of the square of length of walk with time, is required.

Fick's first law applies to a system in steady state where the concentration of particles is constant. For a case where concentration changes over time a further iteration is required:

$$J = -D \frac{\partial c(x)}{\partial x} \text{ where} \quad (3.5)$$

$$\frac{\partial c(x, t)}{\partial t} = - \frac{\partial J}{\partial x} = D \cdot \frac{\partial^2 c}{\partial x^2} \quad (3.6)$$

In 3D space this can be written as:

$$\frac{\partial c}{\partial t} = D \cdot \Delta^2 c, \text{ where } \Delta^2 \text{ is the Laplace operator.} \quad (3.7)$$

Applying this in practical terms to the formation of a lipid bilayer on a solid or polymer brush surface, it is possible to measure the quality of the bilayer formed by considering the

rate of diffusion of individual lipid molecules within it. To enable this process to be measured and analysed fully a fluorescent probe is attached to a small percentage of the lipids. Examples of probes are shown in Figure 3.11.

3.6.2. Fluorescence Recovery after Photobleaching theory

This method of fluorescence microscopy utilized the absorption and emission of light by an appropriate probe within the lipid bilayer and its choice was influenced by considering any natural fluorescence of the sample. The probe, which was assumed to diffuse in the same manner as the bilayer lipids, was chosen to absorb light at a given wavelength and emit at another longer, lower energy wavelength. This difference is referred to as the Stokes shift. The microscope contains filters that filter out the exciting light and allow the emitted light through to the detector, usually to be collected by a CCD³⁶ camera.

FRAP is a simple to use method of following 'large scale' diffusion of the order of microns, rather than the diffusion of individual lipids, when fluorescence correlation spectroscopy may be used.

3.6.2.1. Energy absorption and emission

The probe will usually be a conjugated molecule with greater than 8 conjugated double bonds and for measuring the diffusion in a lipid bilayer, will be attached to a lipid-like molecule. In these molecules there is a relatively small (1.5 to 3 eV) energy difference between the ground state and excited state meaning that low energy photons, within the visible spectrum, can excite the electrons out of the ground state.³⁷

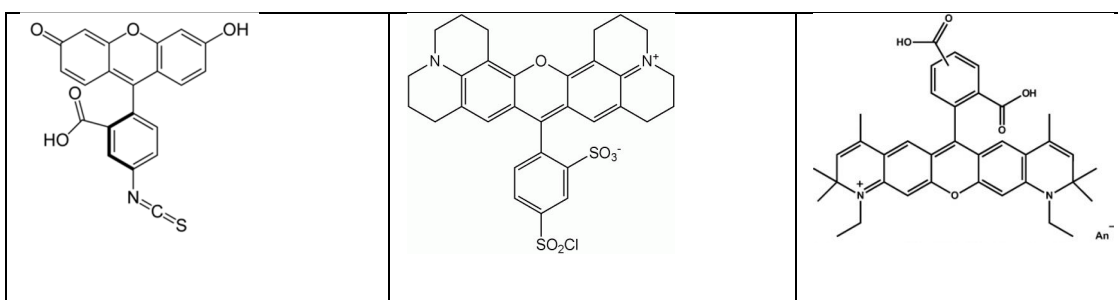


Figure 3.11: Commonly used fluorophores structures, FITC, Texas Red (centre) and Atto 590. Structures from ref 38.

The FITC fluorophore absorbs at 485nm (blue/green) and emit at 517nm (Texas Red 589/615nm).

Initially the fluorescent molecules occupy the ground state, s_0 obeying the Boltzmann distribution law and after irradiation there is a transition to an excited state s_1 . Excited state fluorophores can react with other molecules or free oxygen leading to a non-fluorescent product, which has been permanently (chemically) modified.³⁹

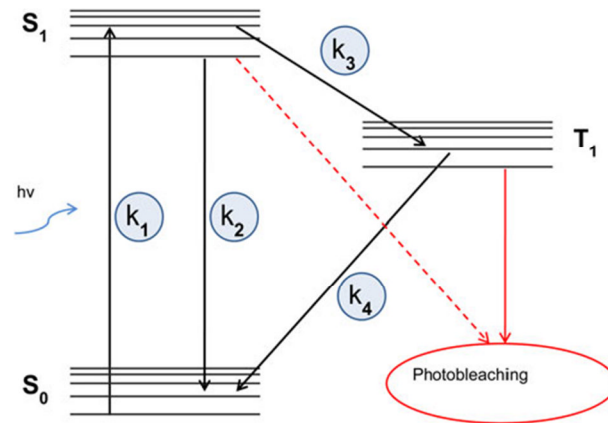


Figure 3.12: Jablonski energy levels diagram showing the possible energy absorption and emission pathways, taken from reference 39.

There is a set of rate equations for the different transitions possible within the system.³⁹

$$\frac{\partial}{\partial t} [S_0] = -k_1[S_0] + k_2[S_1] + k_4[T_1] \quad (3.8)$$

$$\frac{\partial}{\partial t} [S_1] = k_1[S_0] - (k_2 + k_3)[S_1] \quad (3.9)$$

$$\frac{\partial}{\partial t} [T_1] = -k_3[S_1] - k_4[T_1] \quad (3.10)$$

$k_1 k_2 k_3 k_4$ are the rate constants for the transitions, shown in Figure 3.1, with k_1 representing the initial illumination.

The rate of absorption of the incident light ($H \text{ Wm}^{-2}$) can be shown as:

$$k_1 = \sigma_a \left(H \frac{\lambda}{hc} \right) \quad (3.11)$$

Where the fluorophore absorption cross section is $\sigma_a \text{ m}^2$ per molecule, λ is the wavelength of the incident light h is Planck's constant and c is the speed of light. The steady state condition is reached and shown as a function of irradiation by:

$$T_1(t) = \frac{k_1 k_3}{k_1(k_3 + k_4) + (k_2 + k_3)} \quad (3.12)$$

This approaches a constant:

$$\frac{k_3}{(k_3 + k_4)} \quad (3.13)$$

at high irradiation levels. As the intensity of incident light increases the triplet state population increases and saturates. The photobleaching is assumed to be a first order reaction.^{39 40}

The fluorescence intensity reduces by radiative and non-radiative processes. The excited state can emit a photon and revert to the ground state in a radiative process whereby the rate is k_f



It can also lose energy as heat whereby the conversion reverts back to the ground state or by intersystem crossing whereby the rate is k_{nr} .

The quantum yield for fluorescence

$$\Phi = \frac{k_f}{k_f + k_{nr}} \quad (3.15)$$

In the presence of a quenching process the reaction will become a second order equation (due to the presence of a second species, such as oxygen, causing the quenching) k_q . Φ then becomes:

$$\Phi = \frac{k_f}{k_f + k_{nr} + k_q} \quad (3.16)$$

The relative quantum yield can now be calculated, yielding the Stern-Volmer expression:⁴¹

$$\Phi^0 / \Phi = 1 + \frac{k_q}{k_f + k_{nr}} \quad (3.17)$$

3.6.2.2. Fluorescence microscope

Figure 3.13 shows the path of the incident light (green), exciting the fluorophore and the emitted light (red) on a simple fluorescence set up. The camera filter block contains two band-pass filters and a dichroic mirror which direct light of the appropriate wavelength to the sample and after interacting with the fluorophores, up to the camera. For the FRAP experiments the fluorophores are bleached in a small spot ($\sim 28 \mu\text{m}$ diameter) with intense white light (from a mercury arc lamp) and photo images taken at intervals afterwards. After bleaching, non-bleached fluorophores from the surrounding area exchange with the bleached fluorophores and the intensity in the area of the bleached spot increases and “recovery” takes place.

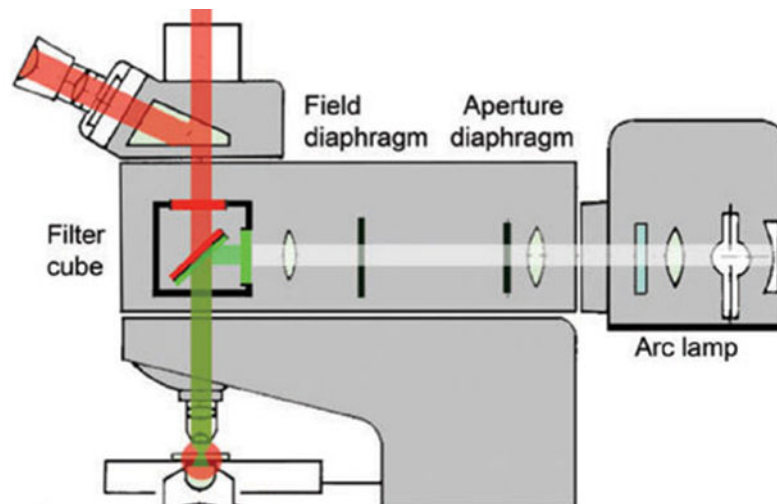


Figure 3.13: Diagram of fluorescence microscope showing incident white light from arc lamp and absorbed and emitted light directed onto the sample or to the eyepiece/CCD by the filter cube. From ref 37.

The speed of this process is an indicator of bilayer quality and the mobility of the lipids. The completeness of this recovery back to the original intensity measures the fraction of lipids which are fully mobile.

3.6.3. Fluorescence spectroscopy practical aspects

3.6.3.1. Camera set up and measurements

The sample was placed under the objective, generally a 40x, to allow sufficient concentration of the bleaching beam intensity during bleaching. After carefully focusing onto the sample an initial image was taken with the shutter open and then with it ‘closed’. This ‘closed’ position is set to allow an aperture of $28 \mu\text{m}$ in diameter for light to pass. With the shutter closed, the sample was bleached using full beam intensity for 30 seconds (or a

time appropriate for the fluorophore to be fully bleached). The shutter was opened immediately after this and a series of images are taken. The image interval was usually 5 seconds and images were collected until the sample had fully recovered. This recovery was confirmed by observing a dynamic intensity profile across the sample using the imaging software of the microscope. To adjust the image intensity, neutral density (ND) filters were used and binning can be selected on the camera to achieve maximum signal to noise ratio. A 2x2 binning was preferred to give a good signal to noise ratio. The settings for these were recorded for each measurement as this can be used to give an indication of relative fluorescence intensities between samples.

3.6.3.2. Data analysis for diffusion constant and mobile fraction measurement

Two of the more frequently used methods of determining diffusion coefficients will be discussed here. Figure 3.17. (top) shows the bleaching and recovery of the area of interest and its effect (in cartoon form) on the fluorophores in the bilayer.

The first method measures the change in the Gaussian profile of the bleached spot over time.

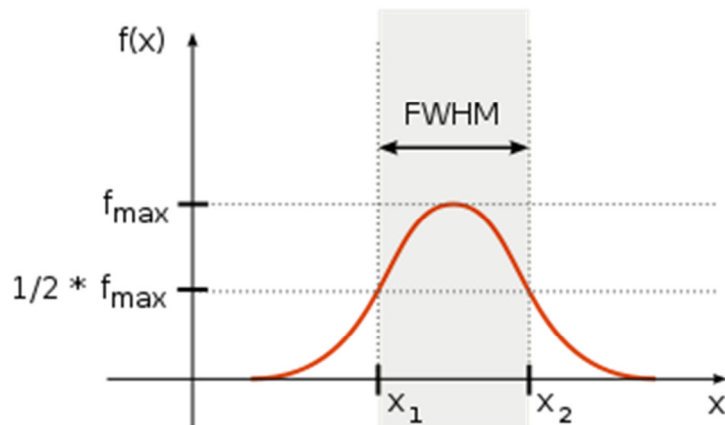


Figure 3.14: Full width half maximum Gaussian distribution (x_2-x_1). From ref 42.

The profile shows the intensity (y axis) versus location in pixels or microns along a predetermined line across the image (x axis) at different times. The distance x_1 to x_2 will increase with time and reduce in intensity.

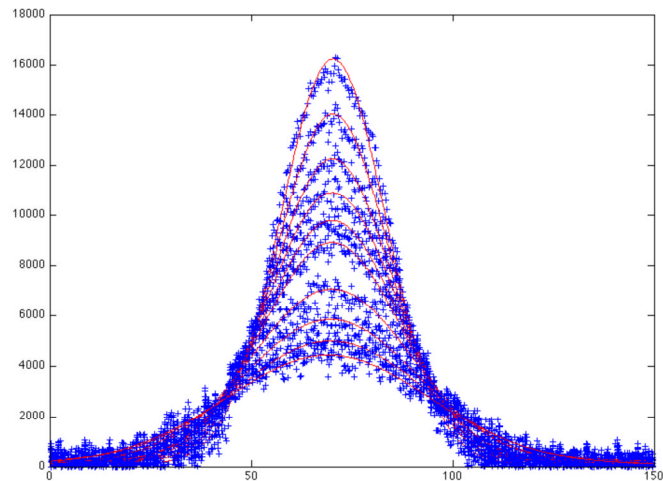


Figure 3.15: Experimental measurements (Gaussian profile) of time (x axis) and intensity readings (y axis).

Using Fick's Law:

$$\partial_t c(r,t) = \nabla(D(r,t)\nabla c(r,t)) \quad (3.18)$$

The differential equation can be solved to give:

$$\sigma^2(t) = \sigma_0^2 + 2Dt \quad (3.19)$$

Here σ^2 is the variance of the full width half maximum of the Gaussian profile. This is plotted against time and the slope provides the diffusion coefficient. The profile of the measurements taken, which can be programmed into fitting software, is shown below in Figure 3.16.

Plotting this full width half maximum (FWHM) formula for a series of time-interval measurements gave a graph where the slope = D, the diffusion coefficient, in this case $\sim 1.4\mu\text{m}^2/\text{s}$, as shown in Figure 3.16.

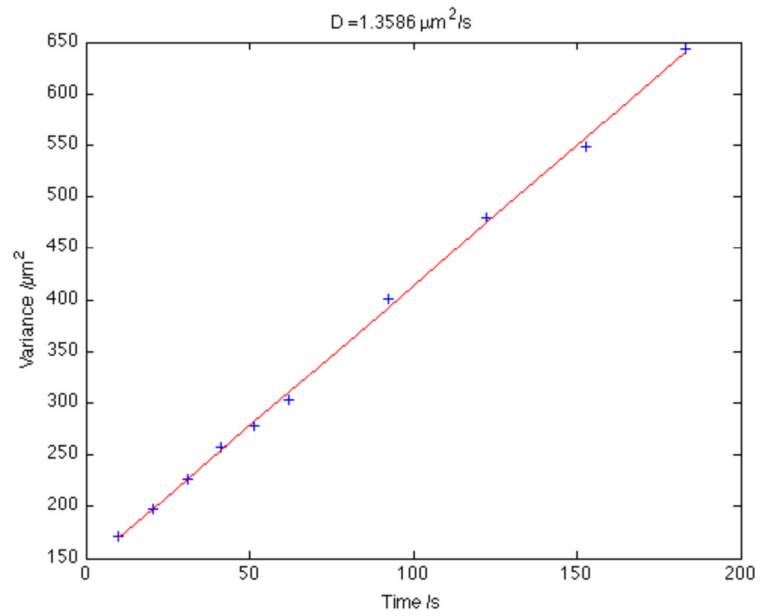


Figure 3.16: Variance (square of standard deviation of Gaussian) at location intervals, slope = diffusion coefficient.

The second method presented initially by Axelrod ⁴⁴ measures the average intensity of the photobleached region over time.

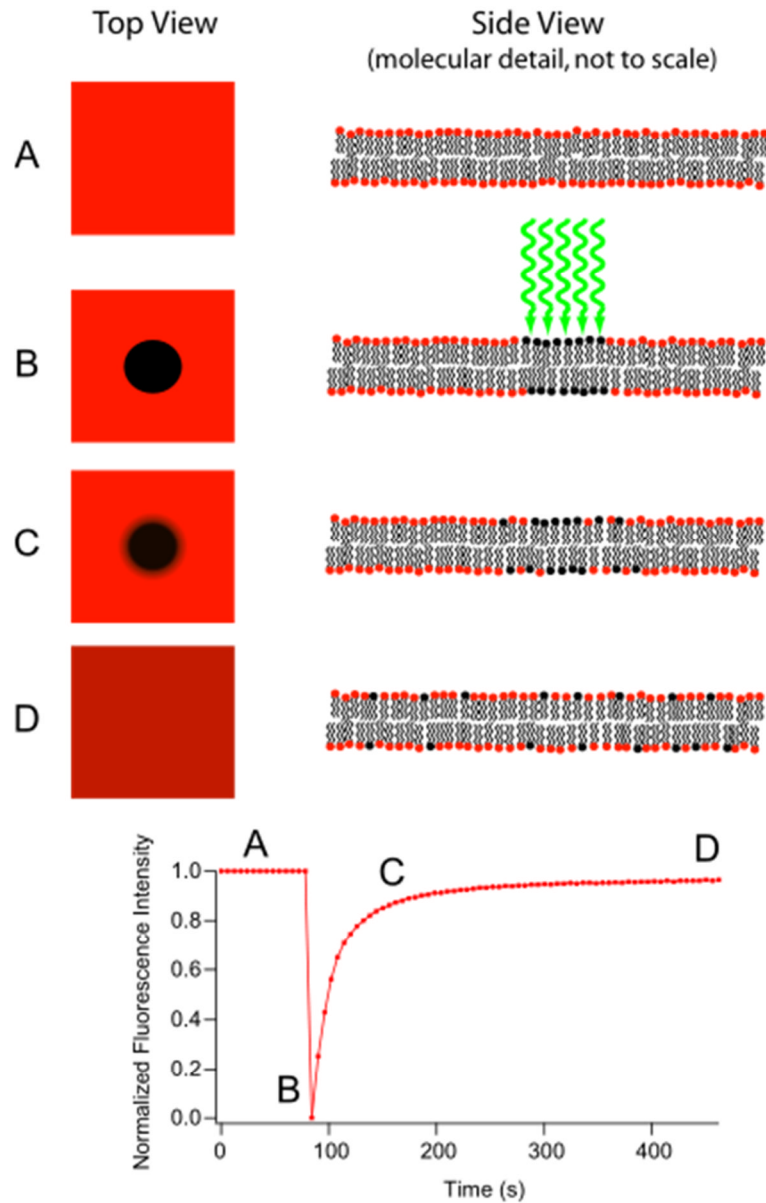


Figure 3.17: Change in fluorescence intensity with time. Top: showing the effect on the fluorophores of the bilayer. Below: this recovery intensity is represented graphically. Graph from ref 43.

The initial reading at A, as shown in Figure 3.14, is normalised to 1.0 and shows the fully open aperture recording the full intensity of the fluorophore image before bleaching. This initial intensity is subtracted from each time interval reading. The second reading, Figure 3.17 B, is of the bleached spot which is determined to be zero intensity. The following points (shown on graph as C and D) are of the intensity of the bleached spot, up to full recovery of intensity, if fully mobile. If the bilayer is not fully mobile the final intensity reading will not return to 1.0. In practice, for a good quality bilayer, this will be ~95%. The mobile fraction can then be calculated directly from the graph at the Y intercept.⁴⁴

Presented is our own departmental protocol, the initially the intensity of the open-aperture field before bleaching is measured and then the intensity with the aperture “closed”. The aperture does not close fully but leaves a small circular region open through which the intense bleaching light passes onto the sample. There is also partial bleaching of the field during the collection of the images as the FRAP recovery takes place and this must be corrected for in the image analysis. To do this a reference area the size of the bleached spot is measured away from the bleached spot. The reduction in intensity of this reference field is measured and compared to the first image to generate a correction factor.

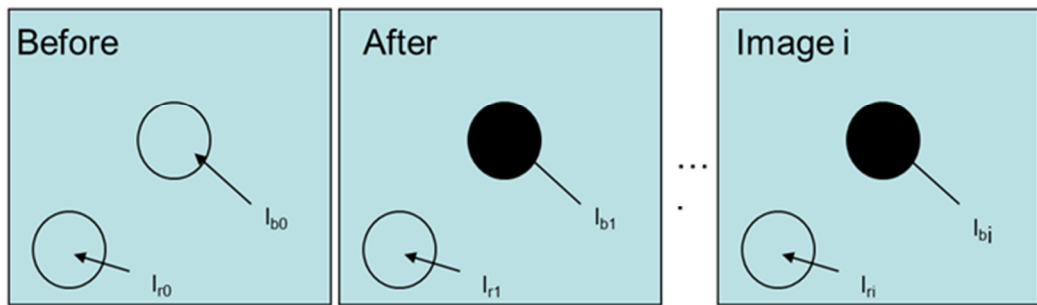


Figure 3.18 Three images showing the FRAP field of view and the circular measurements taken. Images from the physics department protocol.

The intensities are measured at the locations and times specified above- before bleaching, immediately after bleaching and the third box represents the measures taken during recovery. Using the formula repeated for all images:

$$I_{b2}^* = I_{b2} + (I_{r1} - I_{r2}) \quad (3.20)$$

The normalised corrected intensity is found by:

$$f(t) = \frac{I_{bi}^* - I_{b1}}{I_{b0}^* - I_{b1}} \quad (3.21)$$

Plotting the normalised intensity versus time and fitting the curve using ImageJ and the Box-Lucas equation:

$$y(t) = A(1 - e^{-t/\tau}) \quad (3.22)$$

The half-time recovery becomes:

$$t_{half} = \frac{\ln 0.5}{-\tau} \quad (3.23)$$

The diffusion coefficient D is calculated:

$$D = 0.22r^2 / t_{half} \quad (3.24)$$

The mobile fraction can be found by:

$$M = \frac{I_{b-final}^* - I_{b1}}{I_{r0} - I_{b1}} \quad \text{where} \quad I_{b-final}^* \quad (3.25)$$

is the corrected intensity of the final image.

The first method follows the changes in profile of the Gaussian of the bleached spot and provides an accurate measure of the diffusion coefficient. The accuracy of the result obtained by this method is not affected by either the diffusion during bleaching time or photobleaching during imaging. The second method provides a good result for both the diffusion coefficient and the mobile fraction, but allowance has to be made in the calculation for photobleaching during imaging.

3.6.3.3. Errors

A number of assumptions are made during this FRAP measurement and calculation process, which do not fully apply in practice:

- The beam is of a uniform circular disc
- The fluorophores are irreversibly bleached in a *first order* reaction
- The diffusion is two dimensional
- The beam has a uniform Gaussian profile
- No diffusion takes place during photobleaching
- There is an infinite reservoir of unbleached fluorophores to diffuse into the bleached spot

It is important that the conditions and measurements are as accurate as possible in all experiments where comparisons of FRAP data are made. If this is observed then good reproducible data can be obtained.

3.7. Dynamic Light Scattering (DLS)

3.7.1. Introduction

The DLS measurement of the size and charge on small particles in solution has applications in many areas, being used extensively in the colloid and polymer industries. The size (and charge) of particles between <1 nm and > 1µm can be made using dynamic light scattering in a Malvern Instruments Zetasizer nano. The advantage of this instrument is that it is widely used and Malvern Instruments is one of the leading suppliers of these devices, providing good advice and support. The downside is that the system measurements rely on statistical distributions of particle sizes and charge. The mean, median and mode of each population are measured and the measurements are thus sensitive to the presence of large particulates, formed by aggregation of smaller ones or particulate contaminants. The

number weighted distribution, where all particles have equal weighting or the volume weighted distribution of particles sizes can be used. When measuring the volume weighted distribution the built in software will plot the frequency against size to provide the measurement result without further calculation and the sample must be subjected to careful dilution. The software does give a clear indication when the measurement is within acceptable limits, so attention must be paid to any error messages (see later section).

Alternative instruments could be used and include the Coulter Counter; where the volume or size of each individual particle is measured (seen as a change in electrical resistance as particles in liquid pass through a micro-channel). This process is widely used in medicine, specifically for measuring cell sizes, and is also used in manufacturing. It can be used for small cells of $<1\mu\text{m}$. An alternative method is to use imaging microscopy. Each individual particle is imaged and the method can be used on concentrated samples, however, the lower imaging size limit is of the order of microns, whereas the particles requiring measurement here are on the nm scale.

Neither of these latter methods can be used for both the size and charge measurements, so the DLS principle was preferred as it facilitates both of these to be measured on the same sample.

3.7.2. DLVO theory

The work presented in this thesis is an examination of the interaction of lipid vesicles with polymer brush surfaces both of which incorporate a range of charged and zwitterionic groups. These interactions take place in media of high dielectric constant, i.e. water or buffer. For these types of system the balance of interactions can be better understood by referring to DLVO theory. This theory is particularly pertinent where DLS is introduced in this chapter to examine the surface charges on the vesicles and the polymer brushes. The properties of the suspended particles are influenced, not only by the charged groups on their surfaces, but also by the nature of the medium, its pH, ionic strength and temperature. The following references have been consulted for this background section: 23, 45, 46, 47 and 48.

3.7.2.1. Van der Waals interactions

Van der Waals interactions are one element of the total interactions between particles in suspension. They are generated by fluctuations in the electron cloud around one atomic nucleus, which induce dipoles in a second nearby atom. The induced dipoles can change

sign, but are usually attractive. The temperature, pH and the ionic strength of the surrounding medium only minimally affect them. Three types of Van der Waals interactions have been identified: London/dispersion, generated by induced dipoles, which are usually attractive; Keesom, generated between two permanent dipoles and the Debye, between permanent and induced dipoles.

Van der Waals interaction energies (W) between two atoms or small molecules (at a distance D apart) can be calculated as follows:

$$W_{vdW}(D) = -\frac{C}{R^6} \quad (3.26)$$

The sum of the interaction energies in a system composed of more than two atoms or molecules is described by the Hamaker constant A :

$$A = \pi^2 C \rho_1 \rho_2 \quad (3.27)$$

Where ρ is the number of atoms, per unit volume, of each of the two different particles and C is the coefficient of the atom-pair potential. The Hamaker constant is of the order of 10^{-19} J.

This can now be extended to measure the van der Waals interaction energy between two macromolecular spheres of radius R_1 and R_2 :

$$W(D) = \frac{-A}{6D} \left(\frac{R_1 R_2}{R_1 + R_2} \right) \quad (3.28)$$

For a macromolecule, radius R , near a flat surface, this becomes:

$$W(D) = \frac{-AR}{6D} \quad (3.29)$$

For macromolecular particles, such as lipid vesicles, all the pair potentials between the molecules can be summed, so that the net interaction energy depends on the size (radius) of the vesicles. The net interaction energy decays more slowly, with interaction distance, than for the case of two small molecules.

3.7.2.2. The electrical double layer

Systems where van der Waals interactions are the only ones present are very few and so they do not provide the full explanation of the possible interactions between charged particles or surfaces at distances of a few molecule diameters (nm or μm). In addition to the van der Waals interactions there will be electrostatic repulsion between particles which have a surface charge. This electrostatic repulsion is significant here for two reasons.

Firstly, to measure the vesicles zeta potential, using DLS, requires that the particles remain separated in suspension. Secondly, the charged vesicles, when incubated near a polymer surface, will experience an electrostatic interaction (attractive or repulsive) dependent on their respective zeta potentials. This will affect their ability to fuse into a bilayer membrane.

Surface charges on particles have a number of origins. The particles can contain chemically charged groups, such as acid -COOH , which becomes charged by removal of a proton. In electrolytes ions, such as Ca^{2+} can be adsorbed from solution onto a negatively charged surface. The result of this will be the formation of a charged surface of co-ions, which is balanced by a layer of counterions, known as the Stern layer, electrostatically attracted to the surface. In conjunction with this Stern layer there is a layer of more diffuse counterions, which exchange rapidly by thermal agitation. Together these form the Gouy-Chapman electrical double layer, as shown in Figure 3.20. The distribution of counterions near to a surface can be determined using the Nernst equation²³.

In natural systems, ions present in solution, including Na^+ and Ca^{2+} , will change the distribution and the electrical potential of charged surfaces. The Grahame equation²³ can be used to relate the surface charge density to the surface potential. It can be shown that, at constant surface charge density, the surface potential falls as the electrolyte concentration increases. Divalent ions have a more pronounced effect on lowering the surface potential than monovalent ions. As an example, the size of this diffuse double layer, measured as the Debye length, in pure water at pH 7 measured 1 μm , in 1M NaCl it reduced to 0.3 nm.

3.7.2.3. Combining van der Waals and double-layer theory - DLVO

In practise, one must consider the combination of electrostatic and van der Waals interactions and it is helpful to consider the combination of these using a graphical representation, as demonstrated here between two particles. Figure 3.19, below, shows the interaction energy at distances up to 30 nm. The van der Waals is purely attractive at all distances and its decay characteristic, reducing as a function of distance, is shown by the red plot. It is also almost insensitive to solution pH and ionic strength. The double-layer repulsion, however, shows an fall in energy with distance from the surface, as shown by the blue plot.

As an illustration, in dilute electrolyte solution, where the Debye length is long, the combination of the electrostatic repulsion and the van der Waals attraction (green plot). In a solution of higher ionic strength the Debye length is shorter, resulting in a shift in the peak to shorter distances. For surfaces of low charge density there will be a lower repulsion and as the surface charge approaches zero the van der Waals attraction will dominate. The green plot shows the combined effect, showing an energy barrier and an energy minimum to close approach.

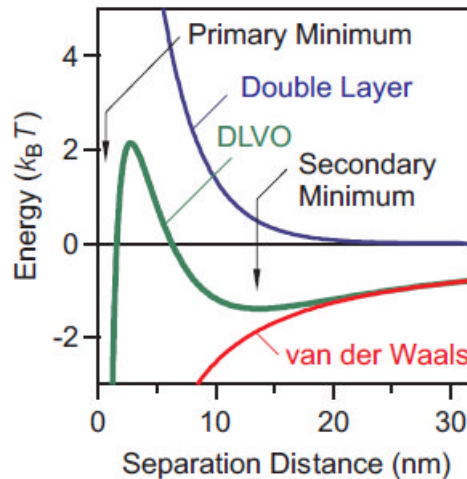


Figure 19 Graph showing the interaction energy for electrostatic and van der Waals interactions for two particles. Taken from reference 49

To summarise, the interaction energies between particles or surfaces have van der Waals and double layer contributions. The former are short ranged and usually attractive, whilst the latter are usually repulsive. In the case of double layer repulsion this is affected by the composition of the buffer, its pH and temperature.

3.7.3. Particle size

Dynamic light scattering techniques utilise the Brownian motion of small particles (<1 μ m in size) in suspension and the fact that larger particles move more slowly than smaller ones. Laser light is incident on the solution and the effects of the particles in scattering the light are utilised to measure the particle size. The correlation of reflected intensity, which reduces over time, can be used to calculate the diffusion coefficient which is applied to the Stokes-Einstein equation for computing the hydrodynamic radius:

$$D = \frac{kT}{6\pi\eta R} \quad (3.30)$$

D is proportional to the decaying correlation curve.

k is the Boltzmann constant

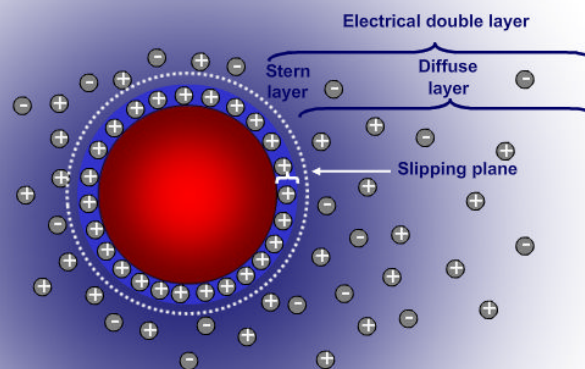
η is the medium viscosity

R_H is the hydrodynamic radius (some calculations use the diameter in which case the factor 3 is required, not 6. Size measurements are performed at 173° (or “back scattered”) or 7° from the incident beam).

3.7.4. Particle zeta and electrophoresis

If an electric field is applied to a suspension of charged particles, this light scattering effect, measured as a Doppler shift, can be used to measure the particles' electrophoretic motion. After taking into account the effect of the electroosmotic motion of the dispersion, the zeta potential can be calculated. The zeta potential is assumed to be the overall charge a particle acquires in a medium which depends on the surface chemistry of the particle and the properties of the dispersant. The zeta potential of the particle is related to the surface charge, however, as it is measured at the slipping plane, where the Stern layer of attached counterions moves past the bulk solution it is more correctly describing its charge interaction potential.⁵⁰ Small changes in pH or ionic strength can have a marked effect on zeta potential. The higher the particle zeta potential (>30 mV) the more stable and less likely to aggregate the particle will be.

Zeta Potential



Zeta Potential = Electrical potential at the slipping plane
(Charge a particle acquires in a particular medium)

Figure 3.20: The accumulation of charged layers around a spherical particle in a dielectric medium, showing the extent of the electrical double layer and its components, the Stern layer and diffuse layers. Image from ref 51.

A charged particle in solution attracts counterions to its surface (Stern layer) and next to this a further diffuse layer of mostly counterions and a few co-ions. Electrophoretic mobility is the velocity of a charged particle relative to the liquid it is suspended in, under the influence of an electric field.

It will move towards the electrode of opposite charge at a velocity which is proportional to its zeta potential. There is a dependence on the dielectric constant, viscosity of the medium and temperature.

For measurement purposes the incident beam is first split into a reference beam and an active beam. The phase shift is measured, which is the rate of change of frequency with time (Doppler shift). This is applied to the following equation to calculate the particle mobility:

$$\Delta f = \frac{2v \sin(\theta / 2)}{\lambda} \quad (3.31)$$

Where λ is the wavelength of the incident laser light

v is the velocity of the particle

θ is the scattering angle

Using Henry's equation, the zeta potential is calculated using the applied field strength, dielectric constant of the medium and its viscosity:-

$$U_E = \frac{2\epsilon z f (ka)}{3\eta} \quad (3.32)$$

where U_E is the electrophoretic mobility,

ϵ , is the dielectric constant of the medium

η is the viscosity of the medium

The Henry function is $f(ka)$. $1/ka$ is the Debye length, (where a is the particle radius) and is expressed as the Smoluchowski approximation of 1.5 for applications in polar media when the particle radius > double layer length.

Measurements are made using forward scatter and a detection angle of 13°.

3.7.4. Surface zeta potential

The above method is applied to small particles in suspension and has recently been modified to measure the surface zeta potential of planar surfaces, using a similar

methodology. The measurement is made by placing the small flat sample in a modified dip-cell using the same effect felt at the surface of a particle at the slipping plane. A polystyrene tracer particle dispersed in a buffer of 1% KCl is the mobile particle used to make the measurements. To effect the measurements for the surface potential the electrophoretic mobility of the tracer particle is measured and also the electroosmotic effect in order to separate out the electrophoretic mobility component. This is explained in the diagram below.

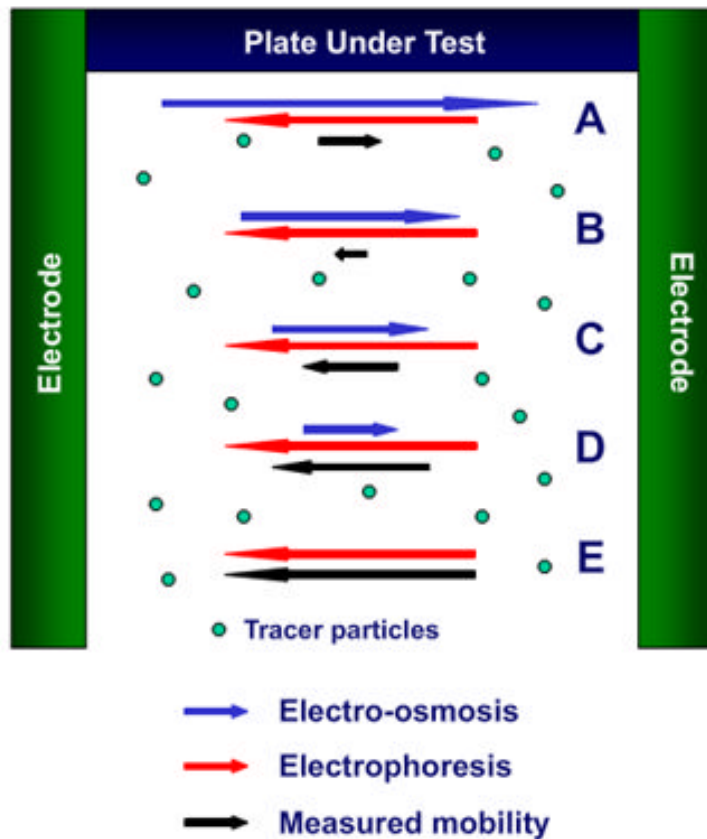


Figure 3.21: The relative effects of electro-osmotic and electro-phoretic motion of particles in a tracer solution at distances from a solid surface of interest. These are measured to determine the surface zeta potential. Diagram from ref 52.

The process depends on taking measurements at positions A to D (125 μ m, 250 μ m, 375 μ m, 500 μ m) from the surface of interest. The red vectors indicate electrophoretic motion, which is constant at the range of distances. The blue vectors indicate the electroosmotic component which reduces with distance from the surface, to point E (at 1000 μ m) where the component is electrophoretic only. The terminal velocity of particles in an electric field

is reached faster (μs) than for electroosmotic flow. A combination of fast- and slow-field reversal measurements separates these two flow rates.

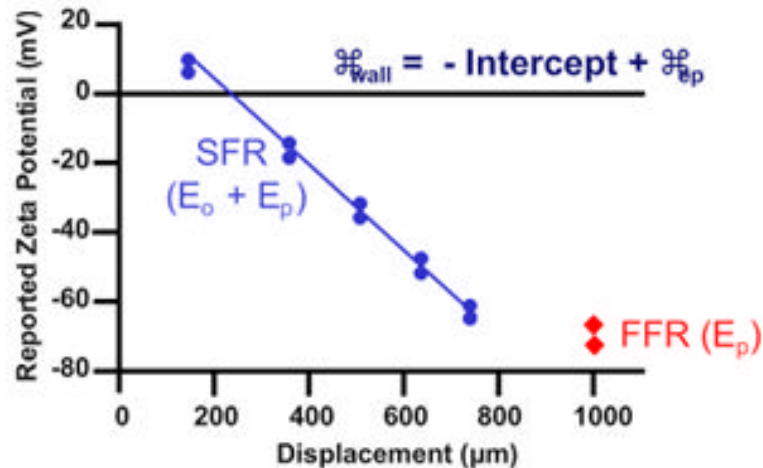


Figure 3.22: Graphical representation of the measurements at positions above (Figure 3.21), showing the how the surface zeta potential is calculated. Graph from ref 52.

The Y intercept (of the displacement from surface (X) against apparent zeta potential (Y)) and the tracer potential at the point of 1000 μm from the surface are both applied to the following equation:

$$\zeta_{wall} = - \text{intercept} + \zeta_{tracer} \quad (3.33)$$

to provide the surface zeta potential of the surface of interest, using a non-interactive tracer in a specified buffer at a specific pH and temperature.

Two other methods of measuring surface potential include streaming potential,⁵³ which requires specialist equipment, and capillary flow⁵⁴. Both methods also require careful preparation and sealing of the samples. The adapted dip cell method used here to measure surface zeta potential is preferred as it allows a small sample to be quickly installed in an open dip-cell, with no sealing required. The measurements follow a simple protocol very similar to that used for regular zeta potential measurements.

3.7.6. Errors

The accuracy of the measurements of size and zeta from this system depends on the concentration of the suspensions. Sizing can be done in 4 mg/mL solutions but for the zeta they need to be diluted to 1/10 of this. Both measurements can be made satisfactorily at 0.4 mg/mL.

There are many error messages which can be recorded by the system during reading. They include: too high or low sample concentration, or that bubbles are present in the sample, which can be corrected easily.

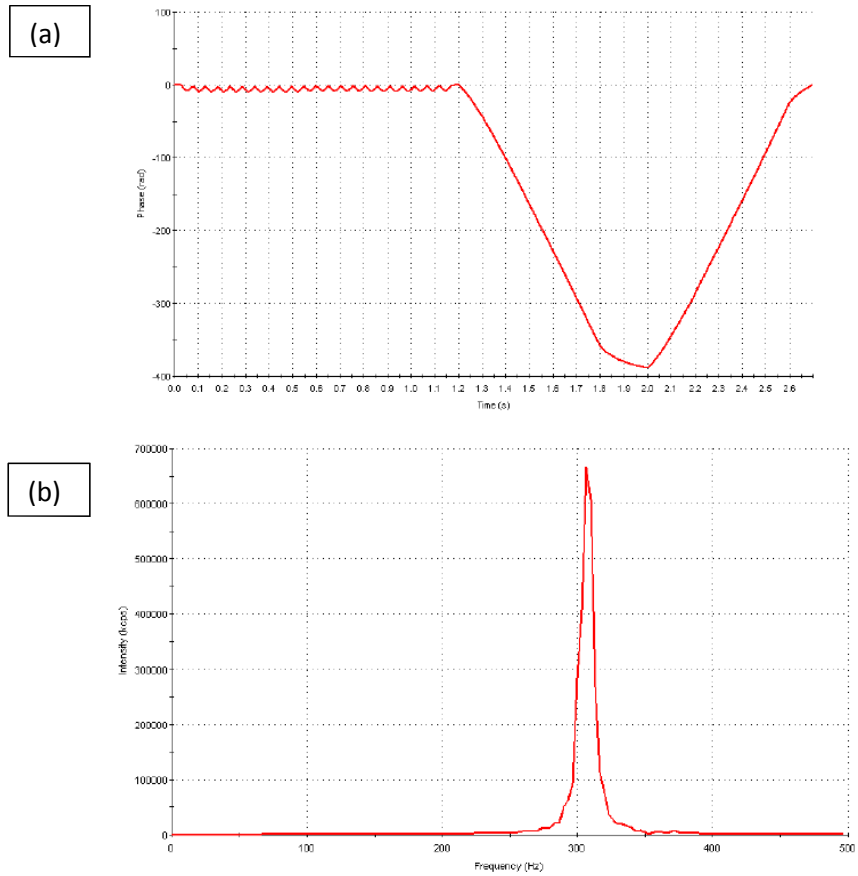


Figure 3.23: (a) Phase plot, indicating fast field reversal with time and (b) distribution plots, which determine the distribution of result values and both should be as close to these ideals of good data as to be obtained. ⁵⁵

Two important checks must be performed during measurement. These are to view the phase plot and frequency distributions, as shown in Figure 3.23, and make any necessary adjustments to ensure a good reading, as shown in Figure 3.24 for the size distribution where the fit of the three measurements is as uniform as possible.

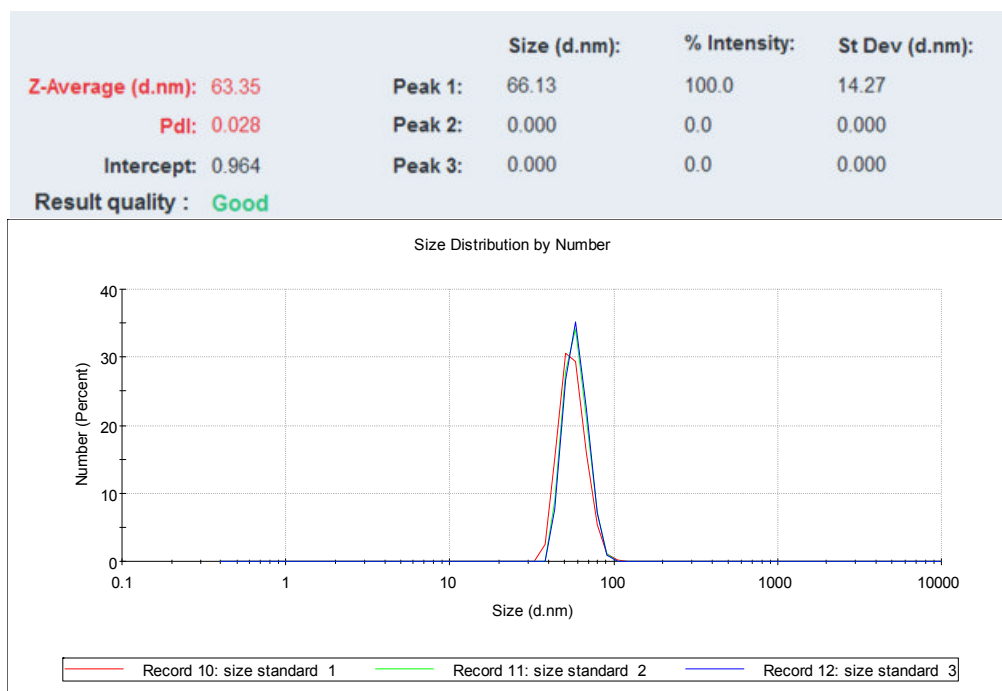


Figure 3.24: Example of good quality size measurement of SUVs using a Zetasizer nano.

When measuring the surface zeta potential the whole process does take about 1 h per measurement, so a series of pH experiments can take a day and some deterioration of the sample is possible during this time.

3.8. Other analysis tools

The principle analysis tools used to gather data for this thesis, of contact angle, FRAP and DLS were described in detail above. AFM, along with TIRF and dark field are methods that were used less frequently and only in collaboration with other researchers who were experts in their operation, so they are also described briefly here.

3.8.1. UV/vis spectrometry

The UV vis spectrophotometer was used to collect data on the adsorption spectrum of proteorhodopsin and Cytb03 before and after incorporation of the proteins into lipid vesicles. To calculate the absorbance after incorporation the vesicle need to be re-solubilised with detergent to release the protein. From that data an estimate of the amount of protein which has been incorporated can be made. During UV vis spectroscopy two samples are measured simultaneously, one is the sample to be tested in buffer and the other is buffer only.

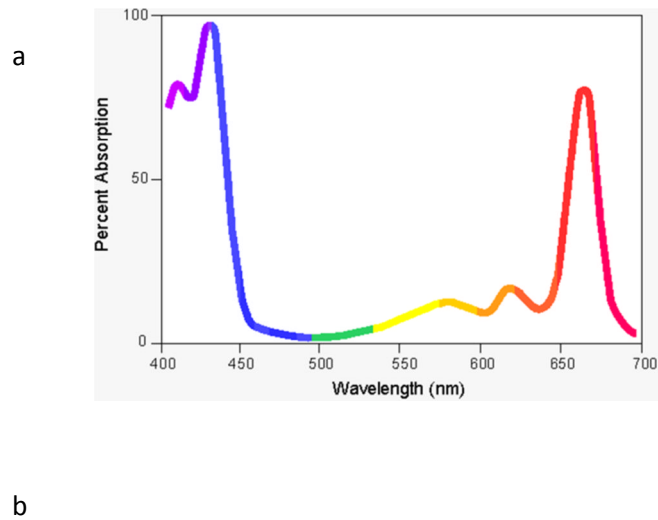


Figure 3.25: (a) Example of UV vis spectrum, indicating peaks of absorbance and the colour of the light at that wavelength. (b) Example of a UV vis absorbance v wavelength plot.

Light from a monochromatic source is split into two beams so that one passes through each of the two samples. The light through the buffer becomes the reference beam (I_0) and should have almost 100% transmittance. The light from the sample (I) is compared to it and as the concentration of the sample is increased, by a known amount, the transmittance will fall. A plot is made of the concentration (x axis) against transmittance (y axis), which is an exponential plot.

The Beer Lambert law is used to convert this exponential percentage transmittance into a more useful linear plot whereby the negative log of the transmittance yields an absorbance value for a given compound or protein.

3.8.2. Atomic Force Microscopy (AFM)

In this project AFM microscopy was used to confirm the results of lipid bilayer formation after performing FRAP and analysing the diffusion coefficients on a limited number of samples. The results required from the imaging were: (1) to assess the root mean square (rms) roughness of the bilayer or lipid vesicle surface, (2) to make a breakthrough force curve measurement and (3) to completely remove an area (or use a pre-formed scratch) of sample of the bilayer on the polymer in order to assess the combined height of both. The scanned images of the polymer supported bilayers were made using standard AFM methodology. The measurements were made using a cantilever with a silicon nitride tip, which was 100 nm or less at its point. (see Figure 3.25) The deflection of a laser beam, following the movement of the tip was detected by a piezo detector. This signal was converted into a height or phase image as shown in Figure 3.27.

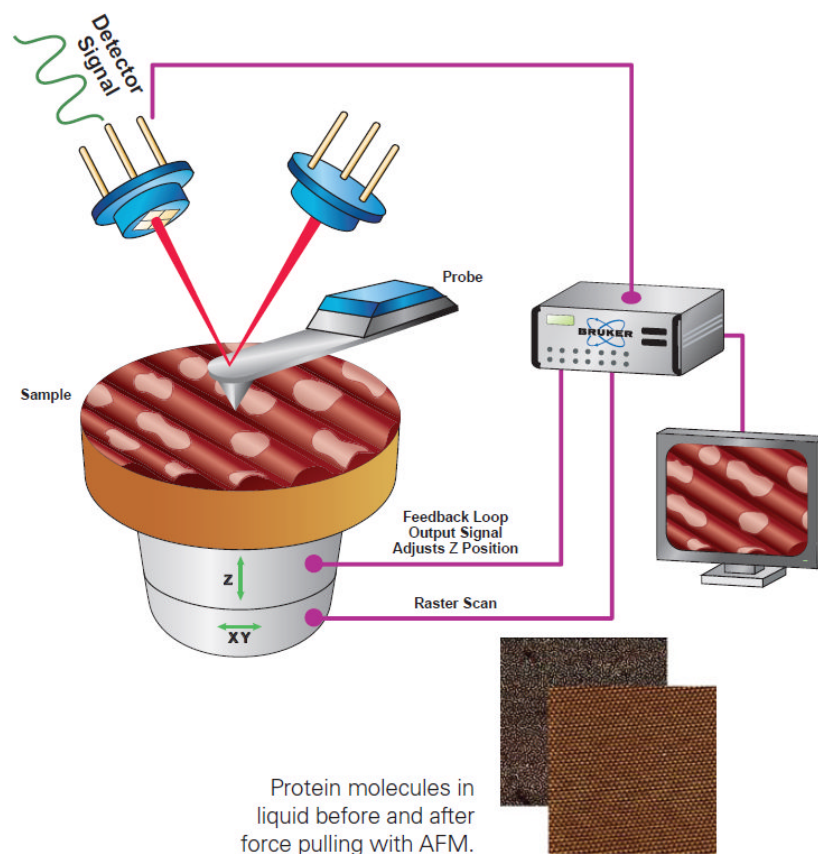


Figure 3.26: Cartoon showing the incident and reflected laser light from the AFM tip and how an image is produced. Taken from reference 56

The height image showed the surface topography, in a nm greyscale, where a whiter area represented the higher points on the scanned surface. The phase image indicated the

mechanical properties or stiffness of the sample. The images were made in contact mode, whereby the tip was drawn across the surface or in tapping mode. Tapping mode was preferred for soft samples because there was no direct contact between the tip and the sample. In addition, the tapping mode scanning process involved oscillating the tip as high resonant frequency and using a feedback loop to adjust the tip/surface interaction force to obtain the best results as scanning took place. These imaging scans indicated the rms roughness of the surface. The images were of sufficiently high resolution to distinguish between adsorbed vesicles and a lipid bilayer. The breakthrough force curve, which was made during the scanning process, proved whether or not a bilayer was formed on the polymer. The breakthrough force curve was made by applying additional force ($\sim 0.32 \text{ N m}^{-1}$) and detecting the force changes as the tip first broke through the bilayer and then passed to the other side.⁵⁷

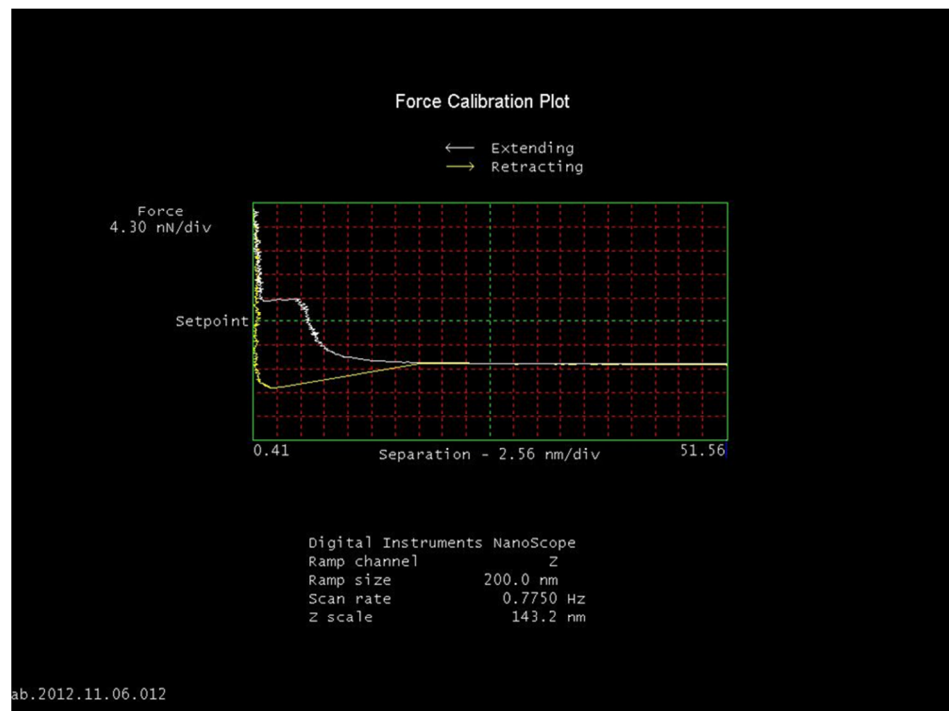


Figure 3.27: AFM force curve to measure a bilayer thickness for POPC on glass.

The force curve plotted in Figure 3.27 shows the distance scale on the Z axis where each measurement block is 2.56 nm wide. The force exerted is shown on the Y axis. The white plot (right to left) shows the force effect on the tip as it approaches and is forced through the bilayer. The force is initially constant but then increases exponentially until it breaks into and through the bilayer. At this point there is a constant force value measured along the Z axis which represents the thickness of the bilayer. On the above graph this is $\sim 5 \text{ nm}$,

which is indicative of a single bilayer. After breaking through the bilayer the force increases again as it approaches the glass surface. The yellow plot represents the reverse process as the tip is removed from its break-through point and withdrawn back through the bilayer.

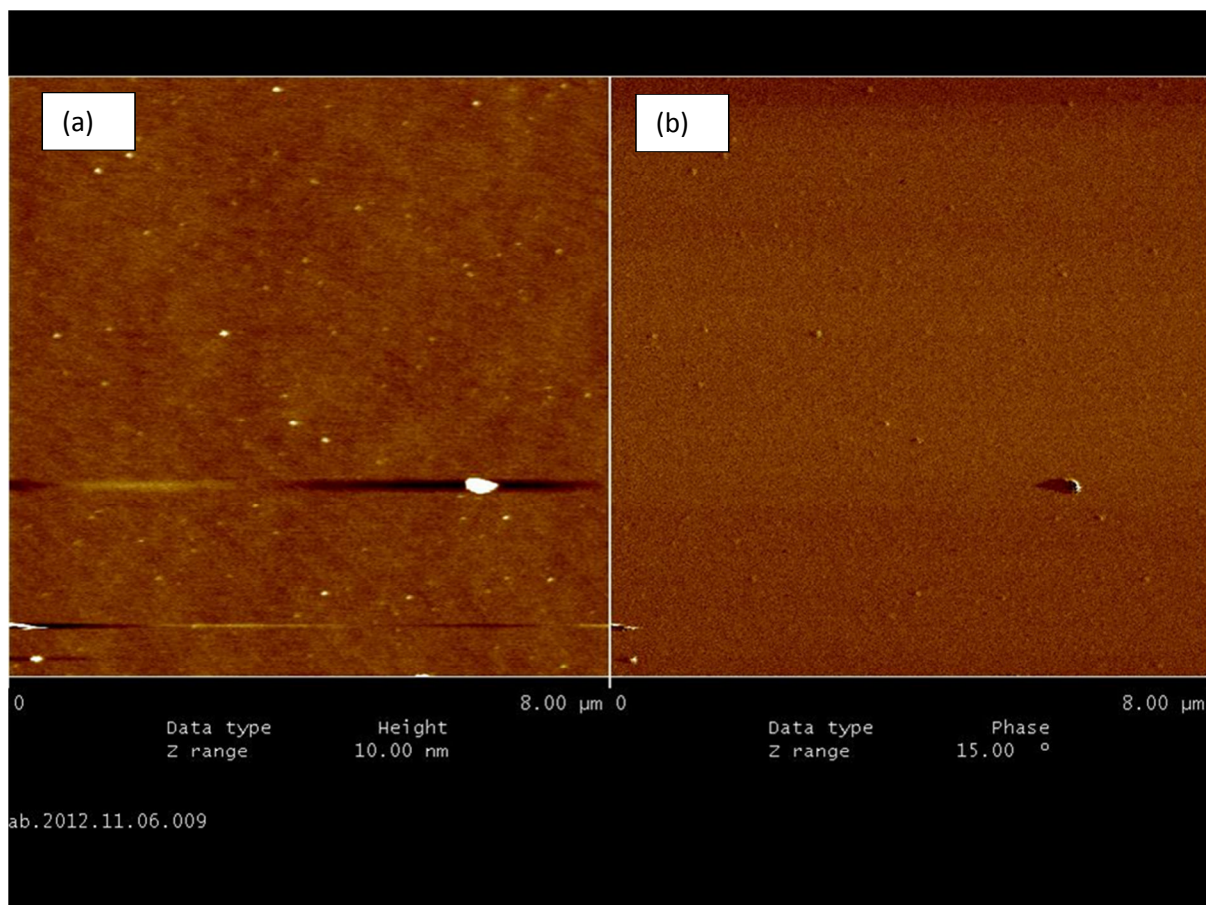


Figure 3.28: AFM surface scans of POPC bilayer (a) height scan and (b) phase image in tapping mode.

The left image in Figure 3.28 (a), shows a tapping mode height image of the lipid surface. It indicates a fairly homogeneous bilayer with some vesicles on the surface. (Lighter objects are higher and the scale bar is 10 nm). The right image, Figure 3.28 (b), is the phase image, showing the difference in phase between that applied to the tip and that experienced by the tip at the surface. This is determined by the tip's interaction with the bilayer suggestive of its (soft) mechanical properties.

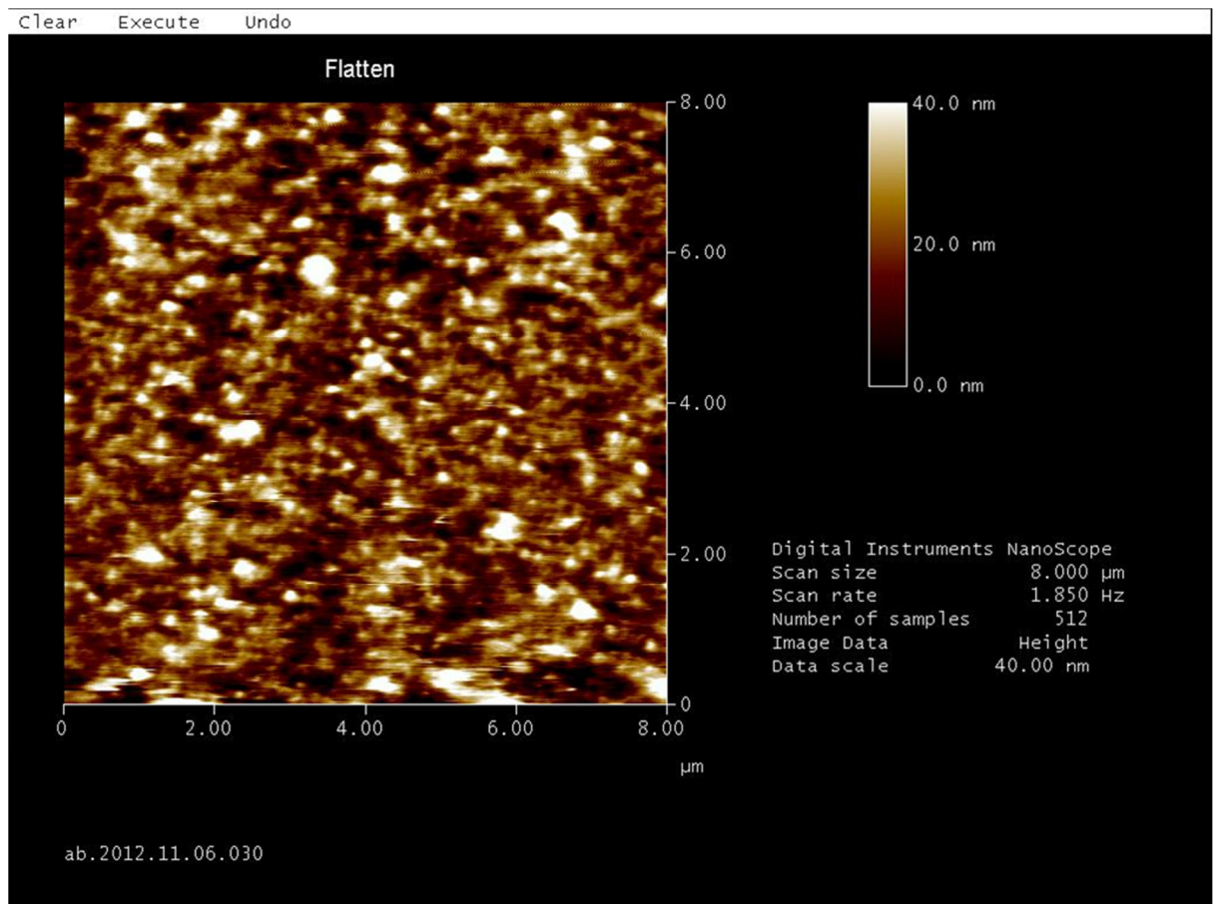


Figure 3.29: Contact mode image of surface which appears to be covered in vesicles.

The image in Figure 3.29 shows a contact mode image of a vesicular layer of lipids on a surface, of 40 nm in height, clearly showing a different picture to that in Figure 3.28 of a smooth bilayer with few elevated features. Both scans were made of an area $8 \mu\text{m}^2$.

This methodology is thus an excellent way of distinguishing between a vesicular layer and a smooth bilayer.

3.8.3. Total internal reflection microscopy (TIRF)

The information was collected from the instrument supplier, Nikon's operating manual.

Fluorescence microscopy is used extensively to study the activity of fluorophores in biological samples, but a method such as FRAP views a large area (microns in size) and does not distinguish between the fluorophores in the sample and those unwanted signals from the surrounding medium. To improve the signal to noise ratio TIRF microscopy utilises the evanescent wave generated on a small area of sample (mounted on glass in a liquid medium) when a collimated light beam is incident and then totally internally reflected at the air-water interface, according to Snell's law.^{58 59}

$$n(1)x \sin \theta(1) = n(2)x \sin \theta(2) \quad (3.34)$$

Snell's law relates the incident and refracted angles of light travelling between media with different refractive indices where $n(1)$ is the higher refractive index and $n(2)$ the lower.

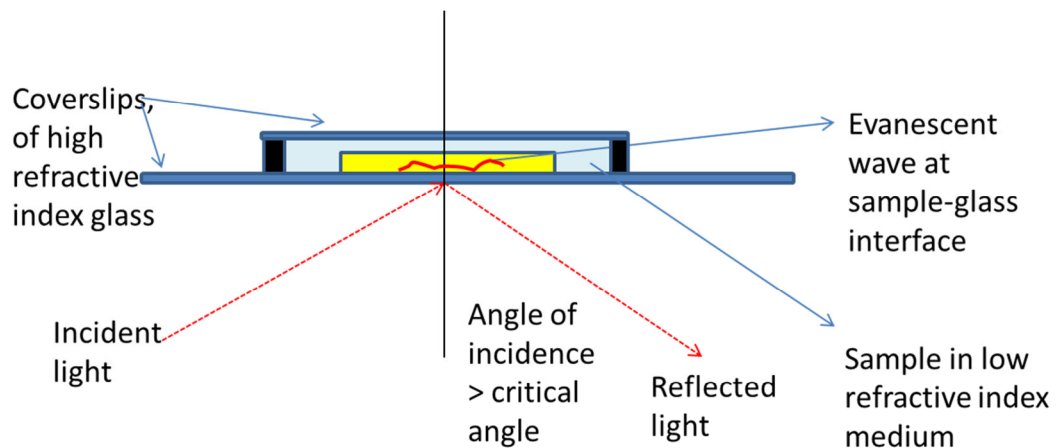


Figure 3.30: Diagram of the TIRF cell, showing the angles of incidence and reflection of the light beam to be greater than the critical angle, producing an evanescent wave at the sample surface.

When using a glass microscope slide and a sample in buffer the respective refractive indices will be approximately 1.52 and 1.35, respectively. The angle to the normal, $\sin\theta(1)$ is the angle of the incident light beam and $\sin\theta(2)$ is that of the refracted beam. The light has to be transmitted into a medium with a lower refractive index and when the light strikes the interface at an angle higher than the “critical” angle the refracted beam is reflected back into the first medium. This generates a localised electromagnetic field close to the interface in the lower index medium. This localised field excites fluorophores only in that location. This evanescent field has the same frequency as the incident light and decays exponentially, giving TIRF the ability to focus on an area of the sample 100 nm deep (by a few hundred nm), thereby restricting the observation area.⁶⁰ This makes it possible to detect single-molecule fluorescence and to observe processes taking place at the cell surface.

3.8.4. Dark field microscopy

Again, this information is mostly retrieved from the instrument maker (Nikon's) instruction manual. Dark field microscopy is used to view very thin samples which cannot be stained or used with fluorescent probes. The light which normally illuminates the sample is partially

blocked in the centre, creating a hollow cone of light, which is refocused onto the sample. Oblique light rays strike the sample and the image is created by collecting light which has scattered off the sample. Care must be exercised to keep the sample slides dust free as dust particles will cause scattering also.⁶⁰ In this thesis the system was used to observe the light scattered off 5 nm gold nanodots attached to proteins.

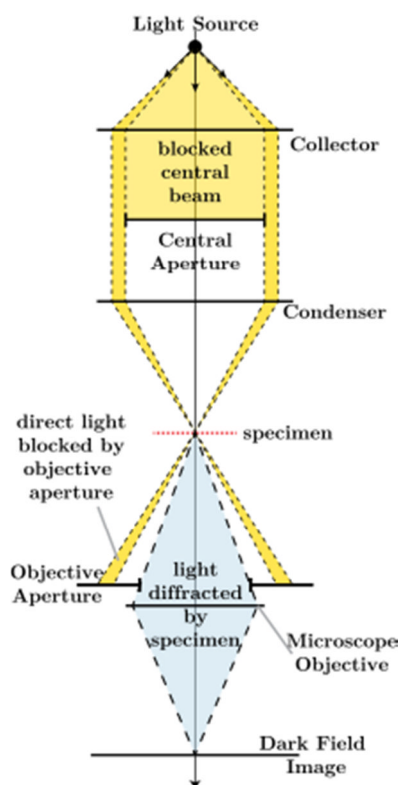


Figure 3.31: Path of light through dark field microscope, showing how the main beam is diverted away from the sample. Light diffracted by the sample itself is collected to create the image.

3.8.5. Other methods for measuring bilayer formation

In addition to the methods presented of FRAP and AFM it is also possible to characterise a well formed bilayer using ellipsometry, surface plasmon resonance (SPR) and electrical impedance (EIS) spectroscopy.

Ellipsometry measures the change in thickness of a sample, for example as a polymer layer is grown on mica to nm level accuracy by quantifying the change in the polarisation of the incident laser radiation. The polarisation change is measured by the amplitude ratio Ψ and the phase differences, Δ , without making contact with the surface.⁶¹

SPR⁶² is used to measure the formation of bilayers on a gold surface. The surface plasmon polariton is an electromagnetic surface wave that propagates in a manner parallel to the dielectric material boundary. As the wave exists at the boundary it is sensitive to changes at this boundary, such as those made by depositing a lipid bilayer on the surface.

When using EIS⁶³ an AC potential is applied across a pre-formed bilayer on a conducting surface. The sinusoidal values of the current produced are measured. The result is measured as changes in phase and analysed as a Fourier series of sinusoidal functions. The change in impedance inferred from the graphical output indicates the resistance of the bilayer to the applied voltage. If the impedance is high this indicates that a sealing bilayer has been formed with minimal defects. A low resistance would suggest defects and holes in the bilayer through which the applied field could pass without resistance.

There are advantages and disadvantages to using these in the systems presented here. Ellipsometry is used to measure the thickness of thin films on mica and is successfully employed in the dry state. It can be used to measure a system under liquid, but is more complex process. SPR is a commonly used method to follow the formation of a bilayer, but requires the samples to be formed on gold. Similarly when using the EIS method to test the integrity of the bilayer, the system must be prepared on gold. The preparation of the polymer brush PCysMA on gold was attempted but the chemistry was not perfected and the system was unstable, the polymer being removed when not maintained in organic solvent.

3.9. References

-
- ¹ Rhe, J.; Ballauff, M.; Biesalski, M.; Dziezok, P.; Grhn, F.; Johannsmann, D.; Houbenov, N.; Hugenberg, N.; Konradi, R.; Minko, S., Polyelectrolyte brushes. In *Polyelectrolytes with Defined Molecular Architecture I*, Springer: 2004; pp 79-150.
- ² Halperin A, Tirrell M, Lodge TP. *Adv Polym Sci* 1992;100:31.
- ³ Advincula, R.C.; Brittain, W.J.; Caster, K.C.; Rhe, J.; Polymer Brushes, John Wiley & Sons, 6 Mar 2006
- ⁴ Alexander, S., Adsorption of chain molecules with a polar head a scaling description. *Journal de Physique* **1977**, *38* (8), 983-987.
- ⁵ de Gennes, P. G., Conformations of Polymers Attached to an Interface. *Macromolecules* **1980**, *13* (5), 1069-1075.
- ⁶ Lee, H.-i.; Pietrasik, J.; Sheiko, S. S.; Matyjaszewski, K., Stimuli-responsive molecular brushes. *Progress in Polymer Science* **2010**, *35* (1), 24-44.
- ⁷ Barbey, R.; Lavanant, L.; Paripovic, D.; Schwer, N.; Sugnaux, C.; Tugulu, S.; Klok, H.-A., Polymer Brushes via Surface-Initiated Controlled Radical Polymerization: Synthesis, Characterization, Properties, and Applications. *Chemical Reviews* **2009**, *109* (11), 5437-5527.
- ⁸ Matyjaszewski, K. & Xia, J. H. (2001). Atom transfer radical polymerization. *Chemical Reviews* **101**, 2921-2990.
- ⁹ <http://www.cmu.edu/maty/chem/fundamentals-atrp/index.html>
- ¹⁰ Rhe, J., Ballauff, M., Biesalski, M., Dziezok, P., Grhn, F., Johannsmann, D., Houbenov, N., Hugenberg, N., Konradi, R., Minko, S., Motornov, M., Netz, R. R., Schmidt, M., Seidel, C., Stamm, M., Stephan, T., Usov, D. & Zhang, H. (2003). Polyelectrolyte Brushes *Advances in Polymer Science*, **165**, 189-198
- ¹¹ Ballauff, M.; Borisov, O., Polyelectrolyte brushes. *Current Opinion in Colloid & Interface Science* **2006**, *11* (6), 316-323.
- ¹² Liu, Q.; Singh, A.; Liu, L., Amino Acid-Based Zwitterionic Poly(serine methacrylate) as an Antifouling Material. *Biomacromolecules* **2012**, *14*, 226-231.
- ¹³ Alswieleh, A. M.; Cheng, N.; Canton, I.; Ustbas, B.; Xue, X.; Ladmiral, V.; Xia, S.; Ducker, R. E.; El Zubir, O.; Cartron, M. L., Zwitterionic Poly (amino acid methacrylate) Brushes. *Journal of the American Chemical Society* **2014**.
- ¹⁴ Naji, A.; Seidel, C.; Netz, R. R., Theoretical approaches to neutral and charged polymer brushes. In *Surface-Initiated Polymerization II*, Springer: 2006; pp 149-183.
- ¹⁵ <http://www.avantilipids.com> accessed 12 March 2012

-
- ¹⁶ Drew, D.; Fröderberg, L.; Baars, L.; de Gier, J.-W. L., Assembly and overexpression of membrane proteins in *Escherichia coli*. *Biochimica et Biophysica Acta (BBA)-Biomembranes* **2003**, *1610* (1), 3-10.
- ¹⁷ Singer, S. J., Some early history of membrane molecular biology. *Annu. Rev. Physiol.* **2004**, *66*, 1-27.
- ¹⁸ Roman, E. A.; González Flecha, F. L., Kinetics and Thermodynamics of Membrane Protein Folding. *Biomolecules* **2014**, *4* (1), 354-373.
- ¹⁹ Seddon, A. M.; Curnow, P.; Booth, P. J., Membrane proteins, lipids and detergents: not just a soap opera. *Biochimica et Biophysica Acta (BBA)-Biomembranes* **2004**, *1666* (1), 105-117.
- ²⁰ de Groot, G. W.; Demarche, S.; Santonicola, M. G.; Tiefenauer, L.; Vancso, G. J., Smart polymer brush nanostructures guide the self-assembly of pore-spanning lipid bilayers with integrated membrane proteins. *Nanoscale* **2014**, *6* (4), 2228-2237.
- ²¹ Heerklotz, H.; Tsamaloukas, A. D.; Keller, S., Monitoring detergent-mediated solubilization and reconstitution of lipid membranes by isothermal titration calorimetry. *Nature protocols* **2009**, *4* (5), 686-697.
- ²² Nagarajan, R., Molecular packing parameter and surfactant self-assembly: the neglected role of the surfactant tail. *Langmuir* **2002**, *18* (1), 31-38.
- ²³ Israelachvili, J. N., *Intermolecular and Surface Forces*. Elsevier Science: **2010**.
- ²⁴ VanAken, T.; Foxall-VanAken, S.; Castleman, S.; Ferguson-Miller, S., Alkyl glycoside detergents: synthesis and applications to the study of membrane proteins. *Methods in enzymology* **1986**, (125), 27-35.
- ²⁵ Rigaud, J.-L.; Pitard, B.; Levy, D., Reconstitution of membrane proteins into liposomes: application to energy-transducing membrane proteins. *Biochimica et Biophysica Acta (BBA)-Bioenergetics* **1995**, *1231* (3), 223-246.
- ²⁶ Linke, D., Detergents: an overview. *Methods in enzymology* **2009**, *463*, 603-617.
- ²⁷ Lipfert, J.; Columbus, L.; Chu, V. B.; Lesley, S. A.; Doniach, S., Size and shape of detergent micelles determined by small-angle X-ray scattering. *The Journal of Physical Chemistry B* **2007**, *111* (43), 12427-12438.
- ²⁸ Vacklin, H. P.; Tiberg, F.; Thomas, R., Formation of supported phospholipid bilayers via co-adsorption with β -D-dodecyl maltoside. *Biochimica et Biophysica Acta (BBA)-Biomembranes* **2005**, *1668* (1), 17-24.

-
- ²⁹ Tiberg, F.; Harwigsson, I.; Malmsten, M., Formation of model lipid bilayers at the silica-water interface by co-adsorption with non-ionic dodecyl maltoside surfactant. *European Biophysics Journal* **2000**, *29* (3), 196-203.
- ³⁰ Lee, C.; Wacklin, H.; Bain, C. D., Changes in molecular composition and packing during lipid membrane reconstitution from phospholipid–surfactant micelles. *Soft Matter* **2009**, *5* (3), 568-575.
- ³¹ Kataoka-Hamai, C.; Higuchi, M.; Iwai, H.; Miyahara, Y., Detergent-mediated formation of polymer-supported phospholipid bilayers. *Langmuir* **2010**, *26* (18), 14600-14605.
- ³² Visco, I.; Chiantia, S.; Schwille, P., Asymmetric supported lipid bilayer formation via methyl- β -cyclodextrin mediated lipid exchange: influence of asymmetry on lipid dynamics and phase behavior. *Langmuir* **2014**, *30* (25), 7475-7484.
- ³³ Ramehart Instruments contact angle manual 2012
- ³⁴ First Ten Angstroms contact angle manual 2012
- ³⁵ Fick, A., On liquid diffusion. *Journal of Membrane Science* **1995**, *100* (1), 33-38.
- ³⁶ Charge coupled device, CCD, converts photons into electrical charges and then into a digital image
- ³⁷ Lichtman, J. W. & Conchello, J.-A. **2005** Fluorescence microscopy. *Nat Meth* **2**, 910-919
- ³⁸ Structures of FITC and Texas Red www.wikipedia.com accessed 27 May 2012
- ³⁹ Lorén, N.; Hagman, J.; Jonasson, J. K.; Deschout, H.; Bernin, D.; Cella-Zanacchi, F.; Diaspro, A.; McNally, J. G.; Ameloot, M.; Smisdom, N., Fluorescence recovery after photobleaching in material and life sciences: putting theory into practice. *Quarterly reviews of biophysics* **2015**, *48* (03), 323-387.
- ⁴⁰ <http://www.colby.edu/chemistry/PChem/lab/Fluoresquench.pdf>
- ⁴¹ Lakowicz, J. R. *Principles of Fluorescence Spectroscopy*, 3rd ed. (Springer, New York, **2006**)
- ⁴² http://en.wikipedia.org/wiki/Full_width_at_half_maximum accessed 13 Apr. 12
- ⁴³ http://en.wikipedia.org/wiki/Fluorescence_recovery_after_photobleaching accessed 13 Apr. 12
- ⁴⁴ Axelrod, D., Koppel, D. E., Schlessinger, J., Elson, E. & Webb, W. W. (1976). Mobility measurement by analysis of fluorescence photobleaching recovery kinetics. *Biophysical journal* **16**, 1055-1069.
- ⁴⁵ Ohki, S.; Ohshima, H., Interaction and aggregation of lipid vesicles (DLVO theory versus modified DLVO theory). *Colloids and Surfaces B: Biointerfaces* **1999**, *14* (1), 27-45.

-
- ⁴⁶ Hermansson, M., The DLVO theory in microbial adhesion. *Colloids and Surfaces B: Biointerfaces* **1999**, *14* (1), 105-119.
- ⁴⁷ Park, Y.; Huang, R.; Corti, D. S.; Franses, E. I., Colloidal dispersion stability of unilamellar DPPC vesicles in aqueous electrolyte solutions and comparisons to predictions of the DLVO theory. *Journal of colloid and interface science* **2010**, *342* (2), 300-310.
- ⁴⁸ http://www.colloid.ch/grouppage/pdfs/Overview_DLVO_Theory1.pdf (graph)
- ⁴⁹ http://www1.lsbu.ac.uk/water/physical_anomalies.html
- ⁵⁰ Wilson, W. W.; Wade, M. M.; Holman, S. C.; Champlin, F. R., Status of methods for assessing bacterial cell surface charge properties based on zeta potential measurements. *Journal of microbiological methods* **2001**, *43* (3), 153-164.
- ⁵¹ Website for Malvern Instruments www.malvern.com, where technical and application notes can be found.
- ⁵² <http://www.malvern.com/en/pdf/secure/AN120917SurfaceZetaPotentialCell.pdf>
- ⁵³ Hoggard, J. D.; Sides, P. J.; Prieve, D. C., Measurement of the streaming potential and streaming current near a rotating disk to determine its zeta potential. *Langmuir* **2005**, *21* (16), 7433-7438.
- ⁵⁴ Evenhuis, C. J.; Guijt, R. M.; Macka, M.; Marriott, P. J.; Haddad, P. R., Variation of zeta-potential with temperature in fused-silica capillaries used for capillary electrophoresis. *Electrophoresis* **2006**, *27* (3), 672-676.
- ⁵⁵ Zetasizer Nano technical note MRK751-01 Malvern Instruments, Malvern, UK
- ⁵⁶ https://www.bruker.com/fileadmin/user_upload/1-Products/SurfaceAnalysis/AFM/Drawing-of-how-AFM-works.png Online Instruction manual for Bruker AFM
- ⁵⁷ Orozco-Alcaraz, R.; Kuhl, T. L., Interaction forces between DPPC bilayers on glass. *Langmuir* **2012**, *29* (1), 337-343.
- ⁵⁸ Ambrose, EJ (24 Nov 1956). A surface contact microscope for the study of cell movements. *Nature* **178** (4543): 1194.
- ⁵⁹ Axelrod, D., Cell-substrate contacts illuminated by total internal reflection fluorescence. *The Journal of cell biology* **1981**, *89* (1), 141-145.
- ⁶⁰ Information taken from Nikon Corporation, microscopy instrument manuals.
- ⁶¹ <http://www.horiba.com/scientific/products/ellipsometers/ellipsometry-academy/ellipsometry-tutorial/>
- ⁶² <http://www.horiba.com/scientific/products/surface-plasmon-resonance-imaging-spri/>
- ⁶³ Gamry Instruments, manual.2014.

4. Experimental methods

4.1. Bilayer formation and characterisation

4.1.1. Lipids

The lipids used for this study were POPC (1-palmitoyl-2-oleoyl-*sn*-glycero-3-phosphocholine), DOTAP (1,2-dioleoyl-3-trimethylammonium-propane) DOPG 1,2-dioleoyl-*sn*-glycero-3-phospho-(1'-*rac*-glycerol) (sodium salt) (all obtained with 99% purity from Avanti Polar Lipids, Alabaster, AL). These lipids are fluid at room temperature and have transition temperatures of just below 0 °C. Texas Red DHPE (1,2-dihexadecanoyl-*sn*-glycero-3-phosphoethanolamine triethylammonium salt; Invitrogen) was used as a fluorescent probe. The dried lipids were used as received and dissolved in a 50:50 mixture of HPLC-grade chloroform and methanol prior to transfer into glass vials in the following molar ratios:

99.5:0.5 POPC:Texas Red (subsequently denoted as "POPC"),

9.75:89.75:0.5 DOTAP:POPC:Texas Red (denoted as "10% DOTAP"),

24.75:74.75:0.5 DOTAP:POPC:Texas Red (denoted as "25% DOTAP") and

49.75:49.75:0.5 DOTAP:POPC:Texas Red (denoted as "50% DOTAP").

Similar ratios were used substituting DOPG for DOTAP, with the addition of

74.75:24.75:0.5 DOPG:POPC:Texas Red "75% DOPG"

89.75:9.75:0.5 DOPG:POPC:Texas Red "90% DOPG"

The solvent was removed by drying the lipid under a flow of nitrogen gas for 1 h. Once fully dry, the lipids were hydrated using a phosphate buffer, which is a 10 mM mixture of sodium dihydrogen phosphate and disodium hydrogen phosphate in MilliQ water (18.2 MΩ cm⁻², MilliPore Ltd, Watford, UK) adjusted to pH 7.1 with NaOH or HCl. The same buffer was used for ionic strength experiments, but with the addition of NaCl to achieve the required molarity (up to 140 mM). HCl was obtained from Fisher Scientific and all other chemicals were purchased from Sigma Aldrich.

4.1.2. Vesicle preparation

The dried lipids were rehydrated into MilliQ water or "phosphate" buffer (10mM sodium dihydrogen phosphate and disodium hydrogen phosphate in MilliQ) adjusted to pH 7 with sodium hydroxide or hydrochloric acid. (All solid chemicals are purchased from Sigma Aldrich and liquids from Fisher Scientific). The hydrated lipids at a concentration of 1 mg/mL were vortexed for 1 minute at full speed (Vortex Genie2, Jencons Ltd., Leighton

Buzzard, UK) to create multilamellar vesicles as a cloudy suspension. Small unilamellar vesicles were prepared by tip sonication (Branson Sonifier 750, Branson Ultrasonics Corp., Danbury, CT) of the suspension at 4°C for 20 minutes, during which time the suspension became clear. The suspension was centrifuged (Heraeus Fresco 17, Thermo Fisher Scientific, Loughborough, UK) for 1 minute at 14,500 G after which the supernatant was removed, leaving unwanted titanium particles. The suspension was diluted to 0.5 mg/mL for use and stored for no longer than 5 days at 4°C in the dark.

4.1.3. Bicelle preparation using long and short-chain lipids

The lipids used for this study were POPC (1-palmitoyl-2-oleoyl-sn-glycero-3-phosphocholine), DOTAP (1,2-dioleoyl-3-trimethylammonium-propane) and 1,2-hexanoyl-sn-glycero-3-phosphocholine (DHPC-C6). These were dried together and prepared as presented in 4.1.2. in the mol ratios:

12.3:37.3:49.9:0.5 DOTAP:POPC:DHPC-C6:Texas Red (denoted as “25% DOTAP- C6”) and
24.8:24.8:49.9:0.5 DOTAP:POPC:DHPC-C6:Texas Red (denoted as “50% DOTAP-C6”).

The reconstitution and tip sonication followed the protocol in 4.1.2.

4.1.4. Surface preparation

The 18 mm diameter round glass coverslips (VWR International Ltd., UK) used for studying bilayer diffusion were cleaned by sonication in a 2% Decon-90 solution (Decon Laboratories Ltd., Hove, UK). These slides were then rinsed with MilliQ water, sonicated with water and sonicated again with propan-2-ol (ultrasonic bath for 10 min). Finally, they were rinsed extensively with MilliQ water and cleaned using a piranha solution (a mixture of 30% hydrogen peroxide and 70% sulfuric acid) for 5 minutes. Polymer brushes were grown from these coverslips and immediately before bilayer formation experiments the polymer brushes were rinsed with propan-2-ol and MilliQ water with a further brief period of sonication. All samples were dried under a flow of nitrogen gas.

4.1.5. Supported Lipid Bilayer Formation by lipid vesicle incubation

Bilayer formation on bare glass (controls) and the polymer brush-coated glass took place in a custom-built flow cell (as shown in Chapter 3). For bare glass substrates, the vesicles were injected and incubated for 1.0 h at 22°C. The samples were subsequently rinsed for 20 min with degassed MilliQ water at a flow rate of 2.6 mL min⁻¹. For the brush-coated surfaces the samples were first soaked with buffer solution for 15 min followed by injection with

vesicles at 22°C, before a subsequent incubation for 1 h at 50° C, in the dark. The samples were subsequently rinsed for 20 min with degassed MilliQ water at a flow rate of 2.6 mL min⁻¹. FRAP studies were then conducted. Samples where an immobile bilayer was observed were incubated for a further 48 h at 22° C, rinsed and imaged again. Samples where an incompletely formed bilayer was seen were incubated with a second aliquot of lipid for a further 48 h at 22° C. The samples with completely formed bilayers were checked for stability after 5 days storage at 22° C.

4.1.6. Supported lipid bilayer formation using spin-coating of lipids

The polymer sample, on an 18 mm round glass coverslip, was placed in a spin-coater (WS-650 Lite spin processor, Laurell Technologies Corporation, North Wales, PA, USA). The sample was sealed under N₂ and the chamber evacuated using a vacuum pump. A “25 % DOTAP” lipid mixture of DOTAP:POPC lipids (as described above), was dissolved in isopropanol (a good solvent for PCysMA), to a concentration of 1.5 mg/mL. Aliquots of 100 µL of this mixture were injected into the evaporator onto the N₂ dried sample, which had previously been rinsed with MilliQ water and isopropanol. The sample was immediately set to spin at 500 rpm for 1s and then at 2000 rpm for 30 s. The sample was removed from the spin-coater and transferred to an oven to dry/anneal at 50°C for one hour. The hydration process took place very slowly in a damp atmosphere for 24 h, without direct contact with the water or buffer.

4.1.7. Fluorescence recovery after photobleaching (FRAP)

The incorporation of fluorescent probes into the lipid vesicles used for forming the bilayers enables the use of fluorescence spectroscopy to study bilayer behaviour. To view the samples and to perform FRAP an epifluorescence microscope was used (E300 Nikon, USA). The sample was illuminated and bleached by a high pressure mercury arc lamp. The bleached area radius, as close to the centre of the field of view as possible, is 14 µm when using a 40x objective. A combination of filter blocks and dichroic mirrors were used to excite the fluorophore at the correct wavelength. The emitted light was collected by an Orca-ER CCD camera (Hamamatsu Photonics Ltd. Welwyn Garden City, UK) and recorded on NIS elements software. A time series of images was collected to track the fluorescence recovery as the bleached fluorophores diffused out of the centre spot. A diffusion rate and mobile fraction for the bilayers were calculated by processing the images in ImageJ and using the Axelrod¹ method in OriginPro (Originlab), as described in Chapter 3.

4.1.8. Size and Zeta Potential Characterization of Lipid Vesicles (DLS)

These parameters were determined using a Zetasizer Nano ZS instrument (Malvern Instruments, Malvern, UK) at 25 °C or 50 °C equipped with a folded capillary cell (DTS 1060 or 1070). The detection angle was 12° and the particle mobility was converted into zeta potential using the Smoluchowski approximation.² Three measurements were made on each of the samples, and data were averaged (with the elimination of any poor quality readings as determined by the software (see Chapter 3)). The intensity-average hydrodynamic diameter was also determined in all cases to assess the colloidal stability of the lipid vesicles. The effect of elevated temperature (used for incubation of lipids on the brushes) was examined by maintaining the lipid vesicles in the zeta cell at 50 °C for 1 h and then repeating the zeta potential and particle size measurements. The vesicle size measurements utilized dynamic light scattering at a detection angle of 173° (with three measurements being recorded per sample of which each of these was a statistical average of up to 100 readings created by the instrument's software). The least squares algorithm was used within the instrument software to analyze the data and the "number" count used to determine the size.

4.1.9. Surface zeta potentials

These were measured for the bare glass and polymer brush-coated glass substrates and were determined using a Zetasizer Nano dip cell, (ZEN 1020), which is used in conjunction with the Zetasizer Nano ZS instrument. The dip cell holds a small flat sample (4 mm by 7 mm) of the planar surface of interest. Measurements were recorded at 25 °C and 50 °C with the sample suspended in a 0.01% aqueous dispersion of non-adsorbing sterically-stabilized polystyrene latex in 1 mM KCl as the tracer particles. Zeta potential measurements were recorded at various positions (125 μm, 250 μm, 375 μm, 500 μm and 1000 μm) from the planar substrate. The electrophoretic motion was constant across this distance range, whereas the electro-osmotic effect is reduced with distance from the surface, to a point (at 1000 μm) where only electrophoretic behavior was observed. The machine software provided the final measurement of the surface zeta potential.

4.1.10. Atomic Force Microscopy (AFM)

AFM images and measurements of the breakthrough force, as described in chapter 6, were made at 22 °C using a Bioscope AFM instrument equipped with a NanoScope III controller

(Bruker Daltonics, Billerica, MA) and an inverted wide-field Axiovert 200 fluorescence microscope (Carl Zeiss, Inc., Thornwood, NY). Oxide-sharpened silicon nitride tips were used in tapping or contact mode with a spring constant of 0.32 N m^{-1} and all images were recorded on polymer brush-coated glass substrates before and after bilayer formation. The final AFM images, described in chapter 7, where protein was incorporated into the bilayer, were acquired on a MFP-3D-SA (Asylum Research) operating in intermittent contact mode using SNL cantilevers (Bruker) with nominal spring constants of 0.24 N/m and imaging forces of ca. 175 pN .

4.12.12. ^1H NMR spectroscopy

A 2.0 % w/w aqueous solution of poly(cysteine methacrylate) PCysMA₃₀ homopolymer (mean degree of polymerization = 30) was heated to $50 \text{ }^\circ\text{C}$, at pH 7 in D₂O. Spectra were recorded over a 2 h period to examine whether hydrolytic degradation occurred under these conditions.

4.1.13. Method 1 for protein reconstitution ³

The lipids used in this study were 16:0-18:1 1-palmitoyl-2-oleoyl-sn-glycero-3-phosphocholine (POPC), 18:1 (D9-Cis) 1,2-dioleoyl-sn-glycero-3-phosphoglycerol (DOPG), 18:1 1,2-dioleoyl-3 trimethylammoniumpropane (DOTAP) lipid (Avanti Polar Lipids, Alabaster, AL).

Dye encapsulated lipid vesicles were prepared by first preparing a solution of 5,6 carboxyfluorescein (CF) at 0.05 mM in 10 mM HEPES buffer at pH6. This was added to lipids which had been dried in the ratio of 20:80 DOTAP, for cationic vesicles and DOPG for anionic vesicles. The second constituent was POPC and the final concentration of lipids was 3 mg/mL .

The CF/lipid mixture was vortexed for 1 min until cloudy. It was stored in the dark on ice until extruded. Vesicles were extruded 20 times using a 200 nm polycarbonate membrane (Avanti Polar Lipids). To remove the excess carboxyfluorescein a desalting column (Zeba spin) was used, taking lipid aliquots of $130 \text{ } \mu\text{L}$, followed by spinning for 2 min and rinsing with $5 \times 130 \text{ } \mu\text{L}$ buffer for each lipid/CF aliquot.

The mixture was maintained in the dark and $95 \text{ } \mu\text{L}$ of 0.05 mM β DDM detergent (in 10 mM HEPES at pH6.2 added to $480 \text{ } \mu\text{L}$ of CF encapsulated lipid vesicles. This was left to solubilise for 45 mins, on in the dark, on ice.

To incorporate the protein at a molar ratio of 1:500 by weight, 8 μ l of the purified proteorhodopsin at 12mg/ml in a 10 mM HEPES buffer with 0.05% β DDM was added to the liposome mixture. The final mixture contained 0.0088% β DDM, just above the CMC and was incubated for an hour on ice.

Following protein incorporation into the liposomes, Biobeads were used for detergent removal. They were prepared by twice rinsing with methanol and then three times with MilliQ. Finally they were rinsed with the HEPES buffer and left to soak overnight. Six samples were weighed out for use (160mg/per ml of lipid /protein/ β DDM mixture). The proteoliposome mixture was added onto the first aliquot of Biobeads and left for 1 h with gentle stirring. This process was repeated for each of the remaining five measures of Biobeads. After removing the final Biobeads the supernatant was diluted to 0.6 mg/mL using 10mM HEPES at pH 6.2. The sample was illuminated at 490 nm & 460 nm and the ratio of the emissions at 530 nm was measured for these two wavelengths, using a ultraviolet/visible (UV vis) (Fluorolog© HORIBA Jobin Yvon IBH Ltd., Glasgow, UK) spectrometer. A CF calibration graph against the change in pH was plotted.

4.1.14. Method 2 for protein reconstitution

A total of 5mg was dried in a ratio of 1:3 of DOTAP:POPC. This was rehydrated with 175 μ L MilliQ water and 312.5 μ L 40mM MOPS/60mM K_2SO_4) was added. It was vortexed for 0.5 min at maximum speed, followed by a very brief bath sonication to ensure all lipids were in suspension. To these multilamellar vesicles 137.5 μ L of 0.25 M Octyl β -D-glucopyranoside (OG) detergent \geq 98% (GC), Sigma Aldrich 3050 Spruce Street, Saint Louis, MO 63103, USA), was added to solubilise the vesicles. This was mixed gently by hand and centrifuged very briefly to separate detergent bubbles. A UV/vis spectrum was recorded (Perkin Elmer Lambda 35 UV/vis system, London UK) as the background measure to compare to the absorbance peak of the protein at 408 nm.

The purified Cytochrome bo3 was added to a 1% w/w protein/lipid in a quantity of 13.9 μ L at 3.6mg/mL, which is classed as purified protein and incubated on ice for 15 min. The UV/vis was repeated and compared to the background reading.

Biobeads (Bio-Rad Laboratories, Hertfordshire, UK) were used to remove the detergent in 5 stages, the first three using 0.05g Biobeads and incubating for 1 h, then using 0.1 g and incubating for 2 hours. The supernatant was collected and transferred to a centrifuge tube filled with buffer at K_2SO_4 30mM/ MOPS-KOH at 20mM. The effect of this rapid dilution should remove the last traces of detergent. It was centrifuged for 1 hour at 35000 rpm

using a at 4°C in vacuum (Optima 'S' class UL 90, Beckman Coulter, High Wycombe, UK), with a Ti50 rotor. The unincorporated protein will be removed by this step, leaving a pellet of proteoliposomes in the tube.

Quick rinsing with 488 μ L of buffer was used to rehydrate the protein. This was then centrifuged at 17,000 G for 3 minutes and the supernatant removed for use. In the first instance it is necessary to confirm that the protein is incorporated as there is no positive assay for this method. It is assumed that all unincorporated protein has been removed in the centrifuge process, so the proteoliposomes must be broken down again by adding more detergent and the UV vis spectrum repeated. Results for the published method using cytb3 and *E. Coli* lipids indicate a 35% incorporation rate.

4.1.15. Detergent depletion for bilayer formation

β DDM (Sigma Aldrich) was dissolved in 10 mM sodium phosphate buffer at 6mg/mL. Multilamellar vesicles of 25:75 DOTAP:POPC, at a concentration of 1 mg/mL in the same phosphate buffer were vortexed until cloudy. A 3:1 β DDM:lipid mixture was made and the solution diluted so that the lipids were diluted to a final concentration of 0.25 mg/mL. The mixture was left for 15 min to allow solubilisation to complete and then 25 μ L of the protein vesicles were added: "*03/11/201 C10H 5 nm Gold (20mM Mops pH7 200mM NaCl ~45% Sucrose Band II) wild type vesicles with bc1 complex as 10histidine tag on the Ct of the C subunit where the gold is bounded Ni/NTA*" (as supplied by MLC, Sheffield). After detergent incorporation the mixture was incubated on a piranha cleaned 18 mm round glass coverslip for 1 h in flow cell, at 22°C. The sample was then rinsed at 0.1ml/min for 10 min, then at 0.25ml/min for 10 min, at 1.0ml/min for 10 min then at 2.6ml/min for 20 min. The sample was then ready for FRAP.

The same protocol was used for the PCysMA, which was grafted from a similar 18 mm round glass coverslip.

4.1.16. Total Internal Reflection microscopy (TIRF), dark field

For TIRF/dark field experiments the 18 mm round glass coverslips were sealed in a home-made flow cell as described in Chapter 3. The TIRF measurements taken in collaboration with Johannes Roth, using a Nikon, TE300 inverted microscope with an Andor Luca-R EMCCD, low intensity, monochrome camera and an Olympus 60x oil immersion TIRF objective. The lasers, with an illumination radius of 30 μ m, were 594 nm and 491 nm with a

filter and dichroic mirror to collect only FITC and Texas Red emission. The bleached spot used for FRAP was of a 2 μm radius.

The dark field images were recorded through a 100x oil immersion objective and a Nikon dark field condenser. All the light was captured on a Canon EOS 550D colour camera. The setting included no binning, the electronic gain multiplier set to 50, with 80 ms acquisition times. The laser intensity was 1-5 mW. The image size was 136 μm^2 .

4.2. Polymer brushes

The polymer brushes were all prepared by chemists in the Armes and Leggett Polymer Groups at the University of Sheffield. A summary of the methods, from their original sources, is provided for completeness with signposting to where these methods were reported in the literature. This level of detail is not essential, but elements of the preparation methods are mentioned in the results chapters when they may have influenced the bilayer formation and testing.

All the zwitterionic and anionic brushes discussed in chapter 5 and the amine-based polymer brush variants (chapter 6) examined in this work were grown using surface initiated ATRP and the structures for these are shown in chapter 5 and 6.

Briefly, a 3-aminopropyltriethoxysilane (APTES) silane layer was adsorbed from ethanol onto a piranha cleaned 18 mm round glass coverslips for bilayer testing. This created a suitably reactive amine self-assembled monolayer surface which was then reacted with 2-bromoisobutryl bromide (BIBB) and triethylamine in dichloromethane (DCM). The ratio of these components was used to determine the grafting density of the brushes. These initiator-functionalized surfaces were subsequently reacted with the relevant brush monomers in an inert atmosphere where the reaction time correlated to the length of the brush and has been characterized in detail elsewhere, and summarized below.^{4 5}

All brush layers were characterized, by the Sheffield group, using a combination of AFM, XPS, and ellipsometry. For the majority of the work described herein, dry brush thicknesses between 5-9 nm were used, however, longer brushes of up to 25 nm, were tested.

4.2.1. Silane initiator

All glassware was cleaned using piranha solution before use. Silane SAMs were prepared by immersion of silicon wafer or glass microscope slides in a solution of 3-aminopropyltriethoxysilane (APTES) 2% (v/v) in ethanol (HPLC grade). After the substrates had been immersed in this solution for 30 min, the samples were rinsed with ethanol, dried

under N₂ and then baked for 30 min at 120°C. Aminosilane SAMs were immersed in a solution of bromoisobutyryl bromide (BIBB) (0.37 mL, 3 mmol) and triethylamine (0.41 mL, of 3 mmol) in 60 ml of dichloromethane (DCM) for 30 min. Subsequently, the samples were rinsed with ethanol and DCM and dried under nitrogen.⁶

4.2.2. 2-(tert-butylamino)ethylmethacrylate (PTBAEMA)

The next stage of the ATRP process requires reacting the monomer, TBAEMA, with a catalyst of Cu(I)Br/Cu(II)Br₂/TPMA in an inert atmosphere. TBAEMA (5.0 g, 27 mmol) was dissolved in isopropanol (IPA; 5.0 mL) at 20 °C, degassed by passing a continuous stream of nitrogen through the solution for 30 min while stirring the solution. TPMA (58.8 mg, 0.203 mmol), and Cu(II)Br₂ (15.0 mg, 0.068 mmol) were added to the solution and degassed for 20 min. Cu(I)Br (19.0 mg, 0.135 mmol) was added and the mixture was degassed for a further 10 min. Initiator-functionalised wafers were sealed in Schlenk tubes and degassed via three vacuum/nitrogen cycles. The monomer/catalyst mixture (2 mL) was added by syringe into each tube under a nitrogen atmosphere and the surface polymerization of TBAEMA was allowed to proceed at 20 °C (scheme 3.3). The samples were removed after various polymerization times, followed by washing with IPA and ethanol several times.⁷ The PTBAEMA was crosslinked using the following protocol: Secondary amine groups on the PTBAEMA repeats units are cross-linkable. Toluene 2, 4-diisocyanate-terminated poly(propylene glycol) (PPG-TDI) was selected because it has two terminal isocyanate groups which can form robust urea bonds. THF is a good solvent for PTBAEMA so the brushes will be highly swollen and the PPG-TDI cross linker will react with secondary amine groups through the brush layer. On other hand if the poor solvent for PTBAEMA brushes, *n*-hexane, is selected for cross-linking, then the brush layer will be collapsed and the cross linker will only react with the upper surface.⁸

4.2.3. poly (N,N- dimethylamino ethylmethacrylate) PDMAEMA

DMAEMA (47.1 g, 30 mmol) was dissolved in DMF (50 mL), deoxygenated for 20 min, and stored under N₂ prior to use. HMTETA (0.30 mL, 0.15 mmol) was added to the solution and deoxygenated for 10 min, after which Cu(I)Br (0.14 g, 0.10 mmol) was added and the monomer/catalyst mixture was deoxygenated for a further 10 min. Initiator-coated wafers were sealed in Schlenk tubes and deoxygenated via three vacuum/nitrogen cycles. The monomer/catalyst solution (5.0 mL) was syringed into each tube under a nitrogen atmosphere, and the surface polymerization of DMAEMA was allowed to proceed at 90 °C

for the desired reaction time. Each polymerization was quenched by removing the wafer from its Schlenk tube, followed by washing with IPA and ethanol several times to remove excess monomer and catalyst.⁹

4.2.4. Quaternization of PDMAEMA Brushes, with C18 and C12 chains

1- Iodooctadecane (or C12) for solutions ranging in concentration from 0.1 to 200 μM were prepared freshly in 10 mL of *n*-hexane before use. PDMAEMA brush-coated glass coverslips were prepared as described above and immersed in various 1-iodooctadecane solutions for approximately 18 h at 20 °C. The resulting surface-quaternized PDMAEMA “C-18” brushes were then rinsed using *n*-hexane, ethanol, and acetone, with further sonication in *n*-hexane for 10 min followed by drying under a stream of N₂ gas.

The reagent was selected to provide attach a C12 or C18 chain to the polymer. The solvent is chosen such that in a good solvent the brush is extended and would quaternise throughout the chain, whereas in a poor solvent the top only is quaternised.¹⁰

4.2.5. poly(2-(Methacryloyloxy)ethyl trimethylammonium chloride) (PMETAC)

2-(Methacryloyloxy)ethyl trimethylammonium chloride (METAC) (13.85 g, 67 mmol) was dissolved in 20 mL of a 1:4 mixture of water and isopropanol. Bipy (382 mg, 2.4 mmol) and CuBr₂ (11.2 mg, 0.05 mmol) were added. The mixture was stirred and degassed for 1 h and then CuBr (144 mg, 1.0 mmol) was added to the solution. Initiator-functionalized silicon wafers were sealed in Radley tubes, and degassed via repeated vacuum/refill cycles, and enough polymerization solution was added to each tube to submerge the substrate completely. After a range of polymerization times, the samples were removed and washed with water and methanol. The samples were briefly sonicated and thoroughly rinsed with deionized water and methanol, followed by drying under a nitrogen stream.¹¹

4.2.6. Preparation of poly[2-(methacryloyloxy)ethyl phosphorylcholine] PMPC brushes

MPC (6.0 g, 20 mmol) was placed in a flask under a nitrogen atmosphere after four pump/refill cycles. Water and methanol were degassed separately by a stream of nitrogen (for at least 60 min). Water (5 mL) and methanol (5 mL) were added to the MPC by syringe at room temperature. CuBr (48.4 mg, 0.338 mmol), CuBr₂ (36.8 mg, 0.165 mmol), and 2,2'-bipyridine (157.5 mg, 1.014 mmol) were added, then the mixture was stirred under nitrogen for 10 min and then briefly immersed in an ultrasonic bath to aid catalyst dissolution. Initiator-functionalized glasses were sealed in Schlenk tubes, degassed, then

filled with nitrogen. The polymerization solution (2 mL) was added to each tube from a syringe. After various times, individual tubes were opened and washed with water and methanol. The PMPC brush-coated glasses were briefly sonicated removed and then rinsed with water and methanol, and dried under a nitrogen stream.¹²

4.2.7. Preparation of poly(3-sulfopropylmethacrylate potassium salt) (PKSPMA) brushes

3-Sulfopropylmethacrylate potassium salt monomer (5.0 g, 20 mmol) was dissolved by stirring in 6 mL of methanol and 3 mL of water at room temperature. Bipy (187 mg, 1.2 mmol) and CuBr₂ (32 mg, 0.14 mmol) were added to the solution. The mixture was stirred, degassed using nitrogen stream bubbling for 60 min then CuBr (47.5 mg, 0.386 mmol) was added. The mixture was stirred and degassed for 10 min. Initiator-functionalized wafers were sealed in a Schlenk tube and degassed (four vacuum pump/N₂ refill cycles). The reaction mixture was added to this Schlenk tube using a syringe by adding enough solution to cover the sample completely. After a range of suitable polymerization times, the samples were removed and washed with water and methanol. The samples were briefly sonicated and thoroughly rinsed with deionized water and methanol, followed by drying under a nitrogen stream.¹³

4.2.8. Preparation of poly(cysteine methacrylate) (PCysMA) brushes

Surface initiator-functionalized glass cover slips were placed in Schlenk tubes, degassed, then filled with N₂. CysMA (5.0 g, 15.0 mmol) was dissolved in deionized water (12.0 mL) at 20°C and degassed for 30 min. Cu(I)Br (71.4 mg, 0.5 mmol), bipy (234 mg, 1.5 mmol) and Cu(II)Br₂ (55.6 mg, 0.25 mmol) were added to the solution. This reaction mixture was degassed for 10 min, and then briefly sonicated. Polymerization solution (2 mL) was transferred into each Schlenk tube. After 15 min, the substrates were removed, sonicated in water and rinsed with ethanol, and then dried with N₂.¹⁴

4.2.9. Preparation of poly(methacrylic acid) (PMAA) brushes

The initiator-covered silicon substrates were placed in dry vials and purged with argon for 1 h. Sodium methacrylate (5.40 g, 50 mmol) was dissolved in the ATRP medium (10 mL). The monomer solution was degassed with argon for 30 min and then transferred, using a syringe, into the polymerization Schlenk flask which had been previously purged with argon. The mixture was stirred under argon for about 10 min until a viscous brown solution was obtained. Next, the polymerization solution was injected into each reaction vial,

adding enough solution to submerge each sample completely. After polymerization, samples were removed from the vials, washed with deionized water, gently sonicated in EDTA solution (0.1M, pH 7) for 1 min, and immersed in water overnight to remove any physisorbed polymer. Finally, the substrates were rinsed with ethanol and dried under nitrogen gas.¹⁵

4.3. References

-
- ¹ Axelrod, D.; Koppel, D. E.; Schlessinger, J.; Elson, E.; Webb, W. W., Mobility measurement by analysis of fluorescence photobleaching recovery kinetics. *Biophysical Journal* **1976**, *16*, 1055-1069.
- ² Wilemski, G., On the derivation of Smoluchowski equations with corrections in the classical theory of Brownian motion. *Journal of Statistical Physics* **1976**, *14*, 153-169.
- ³ Tunuguntla, R.; Bangar, M.; Kim, K.; Stroeve, P.; Ajo-Franklin, C. M.; Noy, A., Lipid bilayer composition can influence the orientation of proteorhodopsin in artificial membranes. *Biophysical journal* **2013**, *105* (6), 1388-1396.
- ⁴ Edmondson, S.; Nguyen, N. T.; Lewis, A. L.; Armes, S. P., Co-nonsolvency effects for surface-initiated poly (2-(methacryloyloxy) ethyl phosphorylcholine) brushes in alcohol/water mixtures. *Langmuir* **2010**, *26* (10), 7216-7226.
- ⁵ Parnell, A. J.; Martin, S. J.; Jones, R. A.; Vasilev, C.; Crook, C. J.; Ryan, A. J., Direct visualization of the real time swelling and collapse of a poly (methacrylic acid) brush using atomic force microscopy. *Soft Matter* **2009**, *5*, 296-299.
- ⁶ Ahmad, S. A.; Leggett, G. J.; Hucknall, A.; Chilkoti, A., Micro-and nanostructured poly [oligo (ethylene glycol) methacrylate] brushes grown from photopatterned halogen initiators by atom transfer radical polymerization. *Biointerphases* **2011**, *6*, 8-15.
- ⁷ Alswieleh, A. M.; Cheng, N.; Leggett, G. J.; Armes, S. P., Spatial control over cross-linking dictates the pH-responsive behavior of poly (2-(tert-butylamino) ethyl methacrylate) brushes. *Langmuir* **2014**, *30* (5), 1391-1400.
- ⁸ Walsh, A.; Thompson, K.; Armes, S.; York, D., Polyamine-functional sterically stabilized latexes for covalently cross-linkable colloidosomes. *Langmuir* **2010**, *26* (23), 18039-18048.
- ⁹ Cheng, N.; Bao, P.; Evans, S.; Leggett, G.; Armes, S., Facile Formation of Highly Mobile Supported Lipid Bilayers on Surface-Quaternized pH-Responsive Polymer Brushes. *Macromolecules* **2015**.
- ¹⁰ Cheng, N.; Bao, P.; Evans, S.; Leggett, G.; Armes, S., Facile Formation of Highly Mobile Supported Lipid Bilayers on Surface-Quaternized pH-Responsive Polymer Brushes. *Macromolecules* **2015**.
- ¹¹ Alswieleh, A.M.M., Micro- and Nano-Structure of Polymers and Molecular Materials. Ph.D. thesis, University of Sheffield, July **2014**.
- ¹² Morse, A. J.; Edmondson, S.; Dupin, D.; Armes, S. P.; Zhang, Z.; Leggett, G. J.; Thompson, R. L.; Lewis, A., Biocompatible polymer brushes grown from model quartz fibres: synthesis,

characterization and in situ determination of frictional coefficient. *Soft Matter* **2010**, *6*, 1571-1579.

¹³ Ramstedt, M.; Cheng, N.; Azzaroni, O.; Mossialos, D.; Mathieu, H. J.; Huck, W. T. S. *Langmuir* **2007**, *23*, 3314.

¹⁴ Alswieleh, A. M.; Cheng, N.; Canton, I.; Ustbas, B.; Xue, X.; Ladmiral, V.; Xia, S.; Ducker, R. E.; El Zubir, O.; Cartron, M. L., Zwitterionic Poly (amino acid methacrylate) Brushes. *Journal of the American Chemical Society* **2014** *136*, 9404-9413

¹⁵ Santonicola, M. G.; Memesa, M.; Meszynska, A.; Ma, Y.; Vancso, G. J., Surface-grafted zwitterionic polymers as platforms for functional supported phospholipid membranes. *Soft Matter* **2012**, *8* (5), 1556-1562

5. Results 1: Testing bilayer formation on zwitterionic and anionic brushes

5.1. Introduction

A number of strategies have been explored in the literature to provide a ‘cushioned’ support system for the examination of the structure and function of transmembrane proteins as presented in Chapter 2. Many of these have been based on polymer cushions with bilayers deposited on them, some of which also incorporated transmembrane proteins into the bilayer. This strategy is a practical one for a number of reasons as the main requirements for a bilayer support are complex. The support system must facilitate the formation of defect-free lipid bilayers and enable the incorporation of fully-functional transmembrane proteins (TMPs) as the only conduit for charge and ion movement across the membrane. Ideally, the TMP should not interact with the polymer brush. The method chosen to produce the brush should allow chemical attachment of the polymer to the underlying solid support and allow good control of the chain growth kinetics.^{1 2 3} The polymer can then be grown to a controlled thickness, be uniform in its surface roughness and have a sufficiently high grafting density to present in its brush form. It is also vital that hydrophilic monomers are selected to provide a hydrated reservoir on which the bilayer can be supported. The ATRP approach to growing the brushes, employed in this work allows all of these criteria to be met, provided the monomers were carefully selected.

The work in this chapter focusses on a series of zwitterionic and anionic brushes with the results of work on cationic brushes presented in Chapter 7. Two zwitterionic brushes were investigated:

- poly(cysteine methacrylate) (PCysMA) and
 - poly[2-(methacryloyloxy)ethyl phosphorylcholine] (PMPC),
- and two anionic brushes:
- poly(methylmethacrylic acid) (PMAA) and
 - poly(3-sulfopropylmethacrylate potassium salt) PKSPMA.

The chemical structures can be seen in Figure 5.1, below.

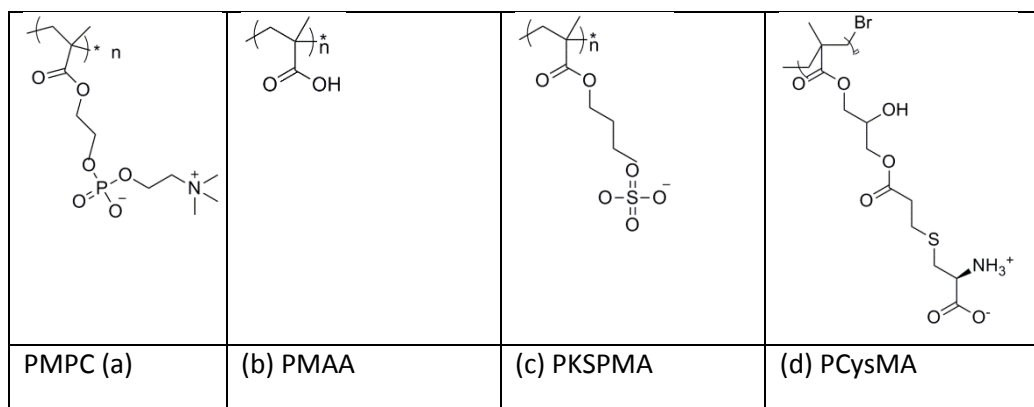


Figure 5.1: Chemical structures of the PMPC, PMAA, PKSPMA and PCysMA brushes

The PMPC brush was selected because it has been well characterised in the literature and was demonstrated to be protein resistant. Its zwitterionic nature was chosen because of its potential for weak interaction with zwitterionic, cationic or anionic lipids. The PCysMA, also zwitterionic, was chosen because there has been little work reported in the literature on this type of polymer with amine and carboxylate side chains.^{4 5} PMAA and PKSPMA were chosen because they had a negative charge when compared to the PCysMA, providing a comparison to the work on the zwitterionic brushes (and the cationic brushes in chapter 7). The preparation and characterisation of PMPC, PMAA and PKSPMA have been reported in the literature prior to this work, but only PMAA has been presented as a potential support for lipid bilayers. In this case the polymer was used to create nanopores where the proteins were chemically attached to the lipid bilayer and suspended over them, so they were not freely diffusing.⁶ PCysMA is a new polymer which had not been reported prior to this project, so it provided a novel brush for investigation.

The results will be presented as follows: the results of the zeta potential characterisation of the vesicles and glass/initiator surface, as they were common to all polymers tested, followed by the details of the individual polymer brush characterisations. This is followed by the results of incubating the vesicles on the brushes. A discussion of the results for all the polymers will be presented together in section 5.9.

5.2. Lipids and incubation methods

5.2.1. Formulation of lipids and incubation methods

Presented here are the lipid formulations, zeta potentials and a brief summary of the incubation methods. Vesicle fusion was the method used to create bilayers. A number of additional methods were tested for producing bilayers, including spin-coating^{7 8} and the use of detergent or short-chain lipids combined with long chain lipids.^{9 10} Spin-coating is

discussed here and the detergent depletion methods are discussed more fully in Chapter 6, where they were used for the protein reconstitution presented there. Finally, the results of lipid incubations on the polymer brushes will be demonstrated by showing FRAP images, diffusion graphs and AFM scans.

In terms of the lipid components, in addition to pure zwitterionic POPC, a cationic lipid, DOTAP, was added. The ratios chosen were of 10, 25 and 50 mol % with the addition of 0.5 mol % Texas Red as a fluorescent probe for FRAP experiments. The buffer used was 10 mM phosphate (with no added NaCl) in most cases, with PBS used only for specific experiments, where the effect of salt was tested (PBS contains NaCl at 140 mM).

5.2.2. Size and zeta potential of lipid vesicles

5.2.2.1. Introduction and methods

The zeta potential and size measurements of the liposomes were made in a standard Zetasizer Nano DLS system. The zwitterionic POPC vesicles and those composed of a mixture of POPC and DOTAP lipids were measured over a pH range 3 to 9, at temperatures of 25 °C and 50 °C and at a range of salt (NaCl) concentrations from zero to 140 mM. The reason for testing under these conditions was that they have been documented in the literature (as discussed in Chapter 2) ^{11 12 13 14 15 16} as having an effect on the formation of lipid bilayers and were used to inform the choice of vesicle incubation conditions on the polymer brushes.

The methods were explained fully in chapter 4.

5.2.2.2. Results and discussion – lipid vesicles

For vesicles of POPC with increasing amounts of DOTAP, in phosphate buffer at pH 7 and at 25°C no notable size variance with composition was observed. However, the average vesicle diameter of 26 ± 2 nm at 25°C did show a slight increase in size to 30 ± 1 nm after heating to 50°C (data shown in Appendix 5). It was found by Pan *et al.* ¹⁷ that the average area occupied by each lipid headgroup increased from 69.1 to 75.5 Å² as the temperature was increased from 15 to 45°C, which may explain the observed increase in diameter. This increase in volume may be significant in the fusion process and will be considered later.

The results for the changes in zeta potential of the DOTAP:POPC liposomes with pH are shown in

Figure 5.2, where it can be seen that there is an approximately linear decrease in zeta potential as the pH increases. At pH 3 the zeta potential is $+63 \pm 2$ mV, reducing to $+44 \pm 1$

mV at pH 7 and falling further at pH 9 to slightly below $+37 \pm 0.6$ mV. There are potentially two effects to consider here.

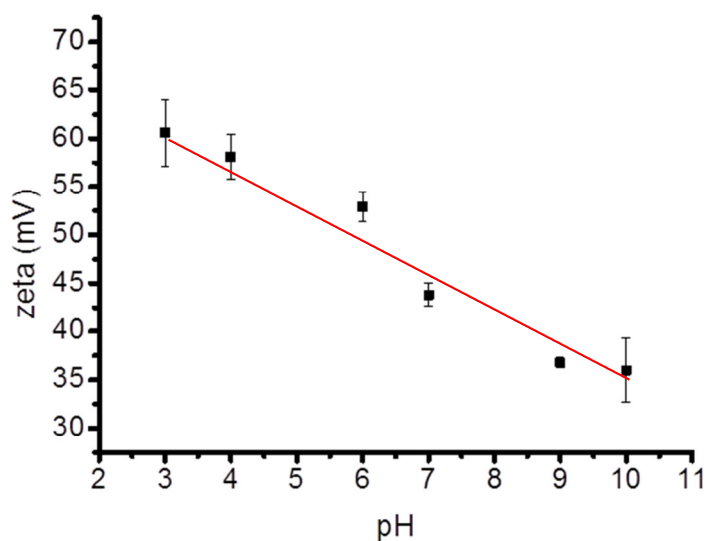


Figure 5.2 Zeta Potentials of DOTAP:POPC (25:75) lipid vesicles measured over a range of pH values.

The zeta potential of the POPC vesicles has been shown, by Cho *et al.*,¹⁸ to increase from 0 mV and -10 mV over the pH range 4 to 9. This negative charge could interact with the positive groups on the DOTAP and have the effect of reducing the net positive charge measured for the DOTAP:POPC vesicles as the pH increases. DOTAP vesicles are important in drug delivery systems, but surprisingly, there is little comprehensive data in the literature measuring the effect of changing pH on zeta potential for DOTAP containing vesicles, with which to compare these results.

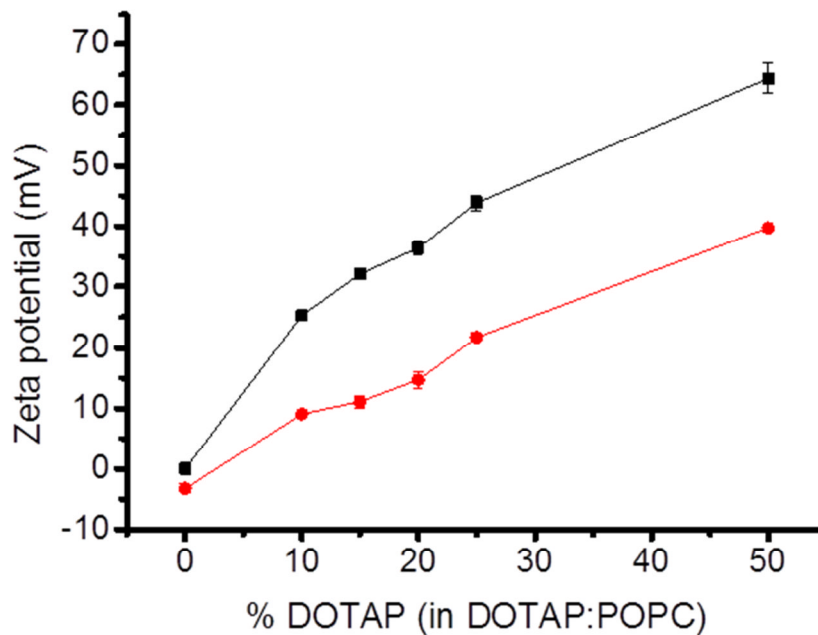


Figure 5.3: Zeta potentials of vesicles with increasing ratios of DOTAP:POPC in 10 mM phosphate buffer at pH 7 without NaCl (black squares) and with 140 mM NaCl (red circles).

In Figure 5.3 the changes in zeta potential with increasing ratios of DOTAP:POPC are presented. Results are shown for suspensions of 0.25 mg/mL lipid vesicles, measured in a 10 mM phosphate buffer (black squares with no added NaCl). At low DOTAP concentration the graphs show an almost linear increase with increasing DOTAP for both sets of conditions, as may be expected. As the proportion of cationic lipid increased from pure POPC vesicles, which showed 0 ± 5 mV zeta potential, to a mixture of 25:75 DOTAP:POPC (“25% DOTAP”), which is the charged lipid proportion used for most of the subsequent vesicle incubations on polymer brushes, the zeta potential reading increased to $+42 \pm 2$ mV. At a concentration of 50:50 DOTAP:POPC (“50% DOTAP”) the zeta increased to $+60 \pm 3$ mV.

Measuring the same vesicles in PBS buffer which contained 140 mM NaCl, (Figure 5.3, red circles) showed an apparent reduction in the zeta potential for each DOTAP:POPC ratio. At 25% DOTAP the equivalent reading with salt was $+22 \pm 2$ mV, and for 50% DOTAP it was $+38 \pm 2$ mV, approximately 20 mV lower in both cases. A note of caution is added here relating to the results with added NaCl. The software records indicated that “good” quality readings had been made (as described in Chapter 3). Despite this positive indication being given for the results where NaCl was added to the buffer, there is evidence that the cell electrodes may be degraded as they become discoloured under these conditions.

In considering work in the literature on the interactions between lipids/vesicles in a NaCl buffer, there are differing views. Work on simulations from Gurtovenko's group¹⁹ on POPC only, suggested that Na^+ bound more strongly than Cl^- to POPC, at the carbonyl carbon. Pandit *et al.*,²⁰ found similar results and suggested that this could make the measured potential of the POPC lipid more positive. The effect of NaCl on POPC lipids was also studied by Knecht and Klasczyk.²¹ Their experiments contrasted with the findings above that Na^+ binds to the POPC headgroup, whilst Cl^- remains in solution. They compared simulation with experimental data and found that Na^+ and Cl^- bind in equal measure to POPC lipids. Na^+ was bound at a location between the POPC headgroup and acyl chain, (at the carbonyl or at the phosphate group) whilst Cl^- bound between the headgroup and water (presumably at the choline site). Both Pokorna *et al.*²² and Makino *et al.*²³ considered that the orientation of lipid headgroups in POPC normal to the bilayer may be affected by the solution conditions. They proposed that headgroup bending (seen as an increase in the $\phi_{\text{P-N}}$ angle in Figure 5.4) may be caused by the negative phosphate interacting with the Na^+ ions. This work focused on the effect on POPC lipids, so a consideration of the effect on DOTAP lipids is considered below.

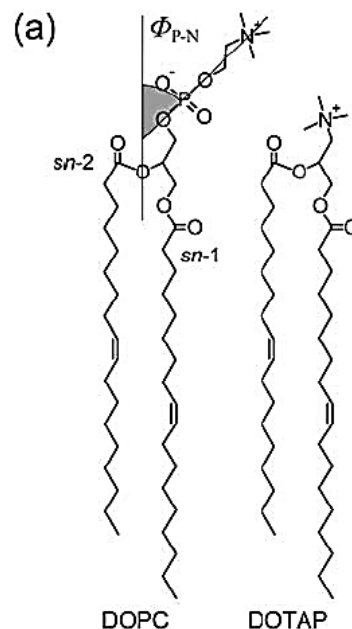


Figure 5.4: A comparison of the headgroups of DOPC and DOTAP. The angle of orientation of the PC headgroup was suggested to change as a result of changing the ionic strength of the surrounding solution.²³

For the positive zeta potential to be reduced it requires that that the amine of the DOTAP headgroup will be neutralised to some degree, by the addition of NaCl. The DOTAP used

already has Cl^- associated with it in solution, as it is manufactured as the chloride salt. Following the addition of salt to the buffer the zeta potential is lowered significantly. Possibly the POPC NMe_3^+ group or the NMe_3^+ of the DOTAP is shielded by the increased Cl^- in solution when the NaCl is added. In addition to the effect of adding salt to the buffer, Pokorna found that there were complex interactions between the headgroups of DOTAP and POPC, which they found straightened the $\phi_{\text{P-N}}$ angle in Figure 5.4, making the bilayer more compressed. Repulsion between the cationic headgroups of the DOTAP also took place and the effect appeared to depend on the ratios of the two lipids i.e. the effects were different for ratios up to 30% DOTAP:POPC, to those beyond that value, at 50% DOTAP:POPC. In experimental and simulation work they found that for both concentrations there was an interaction between the two headgroups, which influenced the orientation of the dipole in POPC. They further suggested that at higher concentration of 50% DOTAP there was an additional stabilising effect by the Cl^- ions which hindered the lipids mobility.

To summarise, the zeta potential measurements and the explanations offered from the literature are very interesting and complex. They do not satisfactorily explain all the results seen here. There is an increase in liposome size with increasing temperature, which is in agreement with theoretical work from the literature. The reduction in zeta potential of the liposomes with increasing pH is logical, assuming the POPC amine groups are deprotonated during the process. However, there is disagreement in the literature as to how the addition of NaCl affects the zeta potential of the lipids.

It is well established in the literature (as presented in Chapter 2) that an electrostatic attraction between charged vesicles (such as 25% DOTAP:POPC) and an oppositely charged surface will lead to a layer of adsorbed intact vesicles or a fluid bilayer. It is important that the surface zeta potentials of the both the liposomes and polymer brushes are known and controlled in order to maximize the adsorption of liposomes and promote vesicle fusion on both glass or polymer brush surfaces. For this reason a NaCl free buffer was used for rehydrating the lipids used in the vesicle incubation experiments. The buffer thus contained only a minimum (10 mM) of sodium phosphate, dissolved in MilliQ water, in order to control the pH.

The data presented above provides an insight into how to control the charges on the liposomes in solution. This could in theory, be used to balance the interactions of vesicles

with the polymer brush surfaces such that a fluid bilayer is formed, rather than a layer of vesicles. When the vesicles are adsorbed onto the surfaces (glass or polymer brush) it was proposed that the charged lipids within them would be attracted to the surface and the neutral lipids would rearrange around the rest of the vesicle (Figure 5.5 and Chapter 2).²⁴

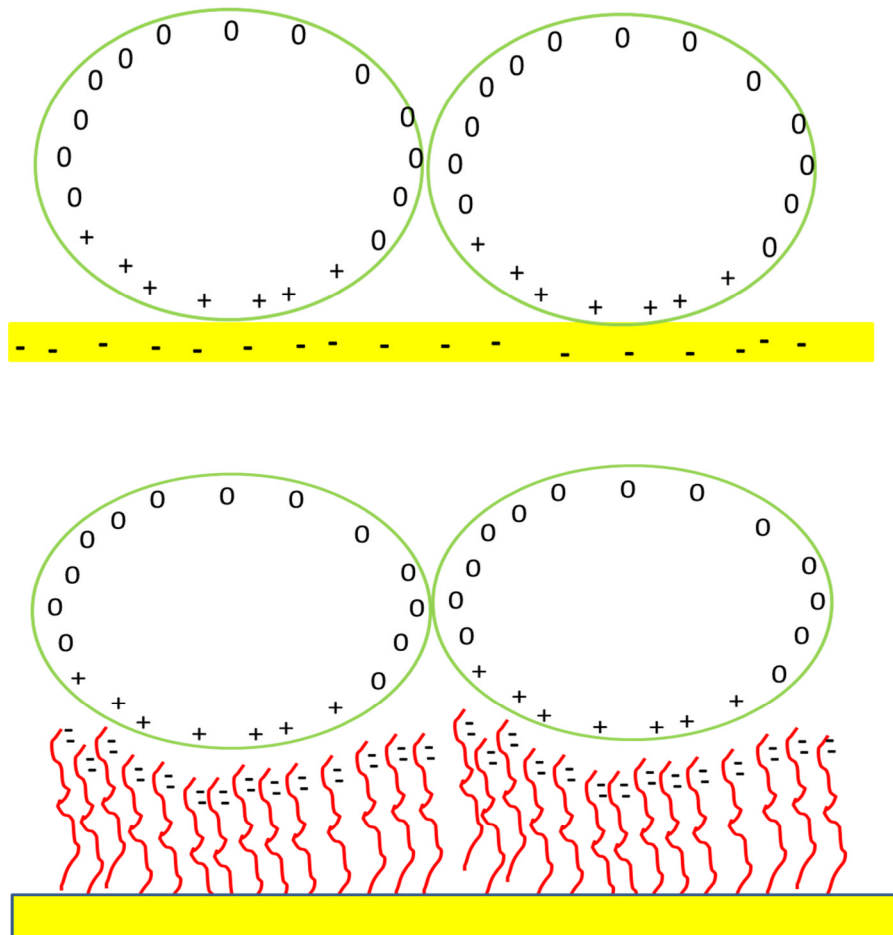


Figure 5.5: Adjacent vesicles of 25% DOTAP:POPC on an oppositely charged surface, such as glass (top) and polymer brush (below) will lead either to a layer of adsorbed intact vesicles or a fluid bilayer. Rearrangement of the charged lipids within the vesicle may reduce vesicle-vesicle repulsion and support fusion.

The charge repulsion between the vesicles would be minimized and vesicle fusion could take place. The change of shape caused by the interaction with the surface could also be a factor in promoting vesicle fusion.²⁵

To summarize, taking the temperature, pH, DOTAP:POPC ratio and the NaCl data into account these immediately suggest options for tuning the vesicle-surface interactions by changing the buffer composition and temperature. The effect of changing these conditions

on the zeta potential of the brush surface, combined with the surface zeta potential measured for the glass, must also be considered. This will be discussed later in the sections when the results of testing bilayer formation on individual polymers brushes are presented.

5.2.3. Bilayer incubation methods

5.2.3.1. Vesicle deposition

In each experiment the polymer was soaked in buffer for 15 minutes before adding the lipids. A number of lipid compositions were incubated onto the polymer samples, using vesicle deposition (one mixture per polymer sample) in a flow cell. Alternative methods for bilayer formation, including spin-coating, the use of detergent or the use of short chain lipids were also tested. The tip sonicated lipid vesicles, at 0.5 mg/mL, were prepared in a pH controlled buffers of 10 mM phosphate (with no added NaCl) and PBS buffer (containing 140 mM NaCl), as fully described in Chapter 4).

The vesicle incubation method used in early experiments was to incubate for 1 hour at room temperature, followed by rinsing and FRAP, to assess initial incubation result. For the majority of cases, where no bilayer was seen or in samples where some evidence of lipid deposition was evident without a bilayer forming, more lipids were added. The samples were then incubated at 50 °C for 1 h, followed by rinsing and FRAP. The samples were then left for 48 h at room temperature, rinsed and observed under the FRAP microscope again. They were then left for a further minimum period of 48 h before repeating the FRAP.

It became evident that this elevated temperature was critical to the successful formation of bilayers on the PCysMA in particular and in subsequent experiments the lipid was injected into the flow cell at room temperature followed by immediate oven heating to 50 °C for 1 h. The samples were then rinsed and observed using FRAP. They were left for two further 48 h periods to observe changes in the surface coverage in the hope that better quality bilayers would be achieved than were initially seen i.e. defects would be sealed.

5.2.3.2. Spin coating

Full details are shown in Chapter 4, but briefly, DOTAP and POPC lipids in chloroform:methanol were mixed in a ratio of 25:75 ("25% DOTAP") and dried under N₂. They were then re-dissolved in isopropanol (a good solvent for PCysMA) to a concentration of 1.5 mg/mL. An aliquot of 100 µL of the lipids was injected onto a dried sample of the PCysMA brush into a spin-coater. After coating, the sample was oven dried and allowed to

hydrate very slowly in a humid atmosphere. The sample was then placed in a flow cell and observed under FRAP.

5.3. Surface initiation

5.3.1. Method - glass substrate

The round 18 mm glass substrates were first piranha cleaned, rinsed in MilliQ and dried under nitrogen flow. The surface zeta potential of the glass surface was measured before the initiation step below, using an adapter for the dip-cell of the Zetasizer Nano DLS system (Chapter 4). The 4 x 7 mm square sample was placed in the dip cell immersed in a 0.01% aqueous dispersion of non-adsorbing (negatively charged) polystyrene latex beads in 1 mM KCl as the tracer particles. The surface zeta potential of glass was measured over the pH range 3 to 9. These measurements were necessary because the residual surface charge, measured before the polymer brushes were grown, may influence the final measurement of the surface zeta potential of the brushes, particularly for the shorter ones, of dry length ~ 7 nm.

5.3.2. Results – glass substrate

The clean glass surface zeta potential (before growing the brush) was characterized under the same conditions as those used to test the polymer brushes.

The results showed (Figure 5.6) that the surface zeta potentials of glass ranged from -13 ± 1 mV at pH 3, to -47 ± 4 mV at pH 7 and to -62 ± 4 mV at pH 8. Similar results for the surface zeta of glass have been published in the literature using the dip cell arrangement used for these measurements and other methods, such as streaming potential.²⁶ As pH 7 is preferred for liposome incubation on polymer brushes it can be concluded that a value of -47 ± 4 mV represents the surface zeta of the glass at this point.

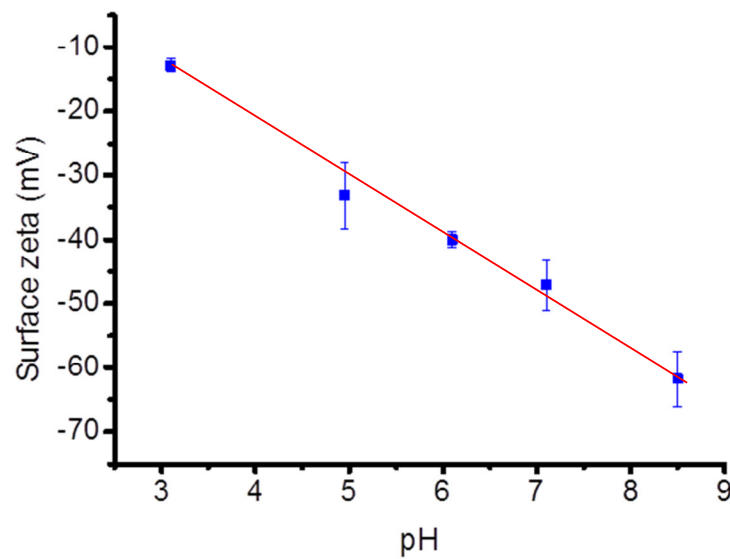


Figure 5.6: Surface zeta potentials of a clean glass surface measured over a range of pH.

The surface zeta potentials measured for the brushes may be influenced by a residual charge from the substrate²⁷ because the APTES SAM does not completely react with all the available –OH groups on the glass surface and also because there may be incomplete reactions during the initiator steps.

5.3.3. Method – surface initiation of glass

The first step in the preparation of the brushes was to functionalise the piranha cleaned glass surface with an APTES (3-aminopropyltriethoxysilane) self-assembled monolayer (SAM). The surface amine groups were subsequently converted into active amide initiator sites by reacting with excess 2-bromoisobutyryl bromide (BIBB) as shown in Figure 5.7.

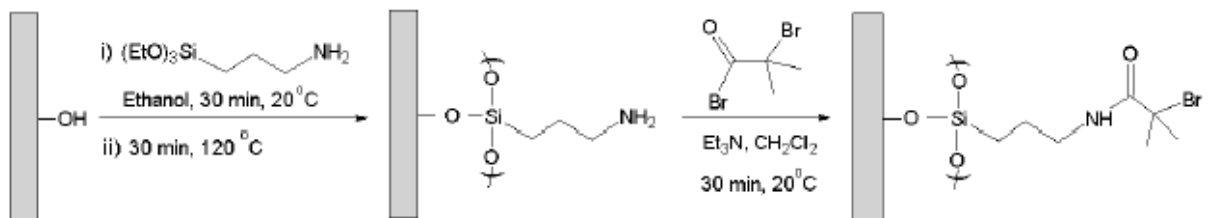


Figure 5.7: Schematic represents the formation of initiators including the formation of 3-aminopropyltriethoxysilane (APTES), and subsequent reaction with bromoisobutyryl bromide (BIBB).⁴⁵

It is important to consider the surface zeta potential response of the initiated surfaces to changing pH along with those responses for the polymer brushes. These measures were

taken using the surface zeta adapter (cell) for the Zetasizer nano. The surfaces were tested in the cell using charged polystyrene beads, suspended in a 1 mM KCl solution at a range of pH values. The electrophoretic mobility was measured and converted into a surface zeta potential, as described in chapter 3.

5.3.4. Results - surface initiation of glass

The changes in surface zeta potential with pH response for the APTES and the BIBB-APTES initiator are shown in Figure 5.8 and these measurements apply to all of the polymers presented, as they were all prepared using the same initiation step.

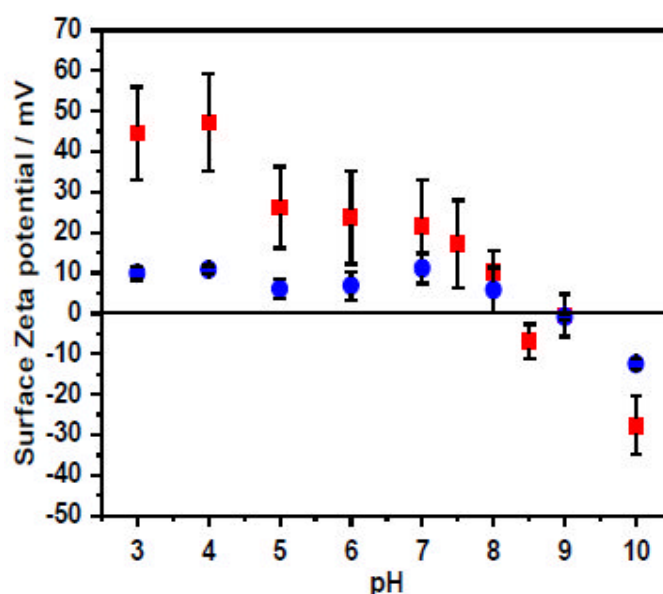


Figure 5.8: The surface zeta potential of the APTES and BIBB-APTES functionalized glass substrates immersed in aqueous solution as a function of solution pH. (■) APTES film. (●) BIBB-APTES film.⁴⁵

The APTES contains primary amine groups which generate a positive surface zeta potential, characteristic of this functional group. The effect of this can be seen in the red plot in Figure 5.8. At pH 5 to pH 7 the surface zeta is $\sim +30$ mV for the SAM. After the second reaction, with initiator, it can be seen that the surface zeta reduces to $\sim +10$ mV indicating that the amine groups have reacted with the BIBB (blue plot in Figure 5.8). The recording of a residual positive charge, measured at $\text{pH} < 8$, suggests that not all the amine groups of the SAM have reacted with the initiator. This measurement is further complicated by considering that there may be an incomplete initial reaction between the APTES and the silica $-\text{OH}$ ($-\text{O}^-$) surface groups, leaving a negative residual charge before this BIBB reaction takes place. It is important that these data are taken into account when comparing the

surface zeta potentials and pH responses of the various brushes. It is also necessary to recognise that the pH responses of different brushes are only comparable when grown from identical initiators.

5.4. PCysMA brushes - Preparation

The polymer brushes used in these experiments were formed (by the University of Sheffield polymer group) from a cysteine monomer terminating in the characteristic carboxylate (-COOH) and a primary amine (-NH₂) groups found in all amino acids.

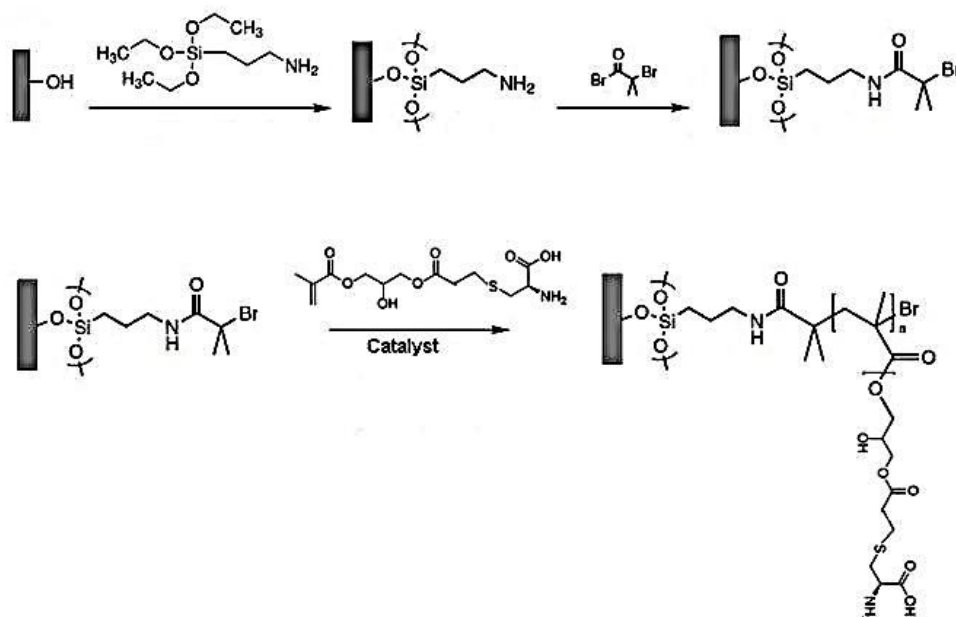


Figure 5.9: Schematic showing the production of PCysMA polymer brushes using ATRP on a silicon (glass) surface. Full details are given in Chapter 4 and reference 28.²⁸

The BIBB-APTES initiator-functionalized surfaces (described above) were subsequently reacted with the brush monomers as shown in Figure 5.9. The reactions time, as described in Chapter 4, depended on the required brush length. As an example, when using [CysMA]: [CuBr]: [CuBr₂]: [Bipy] in molar ratios of 30: 1.0 : 0.5 : 3, the reaction time required was 200 min to grow a 7 nm brush.⁴⁵ After the reaction the samples were rinsed in ethanol and dried under a flow of nitrogen.

5.4.1. Characterisation of PCysMA brush

5.4.1.1. Introduction

Before attempting to form bilayers on the PCysMA brushes they were characterised by measuring the response to changing solution conditions. The response of the brush to pH,

ionic strength and temperature, using AFM, ellipsometry, surface zeta potential, NMR, and contact angle were recorded. The AFM and ellipsometry were performed by Abdullah Alswieleh in Sheffield. The surface zeta potentials and NMR were done in collaboration with him and the contact angle done independently. Some of the data has been published elsewhere.²⁸

5.4.1.2. AFM and ellipsometry

AFM images of the dry and hydrated polymer brushes (of dry thickness 7 ± 2 nm) were taken across a range of pH. The dry brush showed few surface features and its rms roughness was measured at 0.39 ± 0.16 nm while the hydrated brush immersed in PBS buffer, at the pH 7, had an rms roughness of 0.11 ± 0.02 nm (Figure 5.10).²⁸

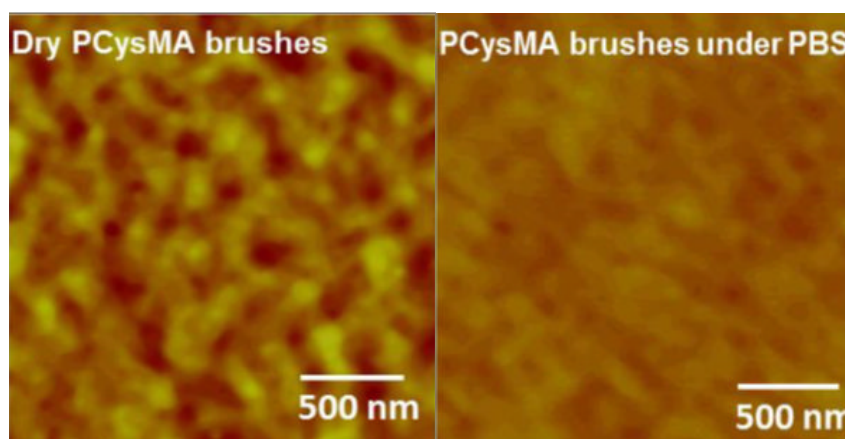


Figure 5.10: Height images using AFM of PCysMA brush grown by ATRP on silicon. Images are $2 \mu\text{m}^2$ and the lighter areas in the dry image show a higher height profile (higher rms roughness) when compared to the hydrated brush image on the right.⁴⁵

Shown in Figure 5.11, is a plot of the height response of the PCysMA brush across a range of pH measure by ellipsometry. When soaked in buffer at pH below 3 (Figure 5.11 (a)) the brush length (7 nm dry) extended to 18 ± 4 nm. In this range it acquired cationic character when the primary amine groups of the amino acid side chain were protonated and the carboxylic acid group was in its non-ionized (neutral) state (Figure 5.11 (b) left). This caused electrostatic repulsion between adjacent chains, leading to brush expansion up to three times its dry thickness. At a mid-range of pH from 3 to 9 the brush increased in length to 12 ± 3 nm, when responding to the addition of buffer. Across this pH range the PCysMA brush was in its zwitterionic form, as both the amine and carboxylic acid groups were charged (Figure 5.11 (b) centre). Under these conditions, the brush extended to a about twice its dry length.

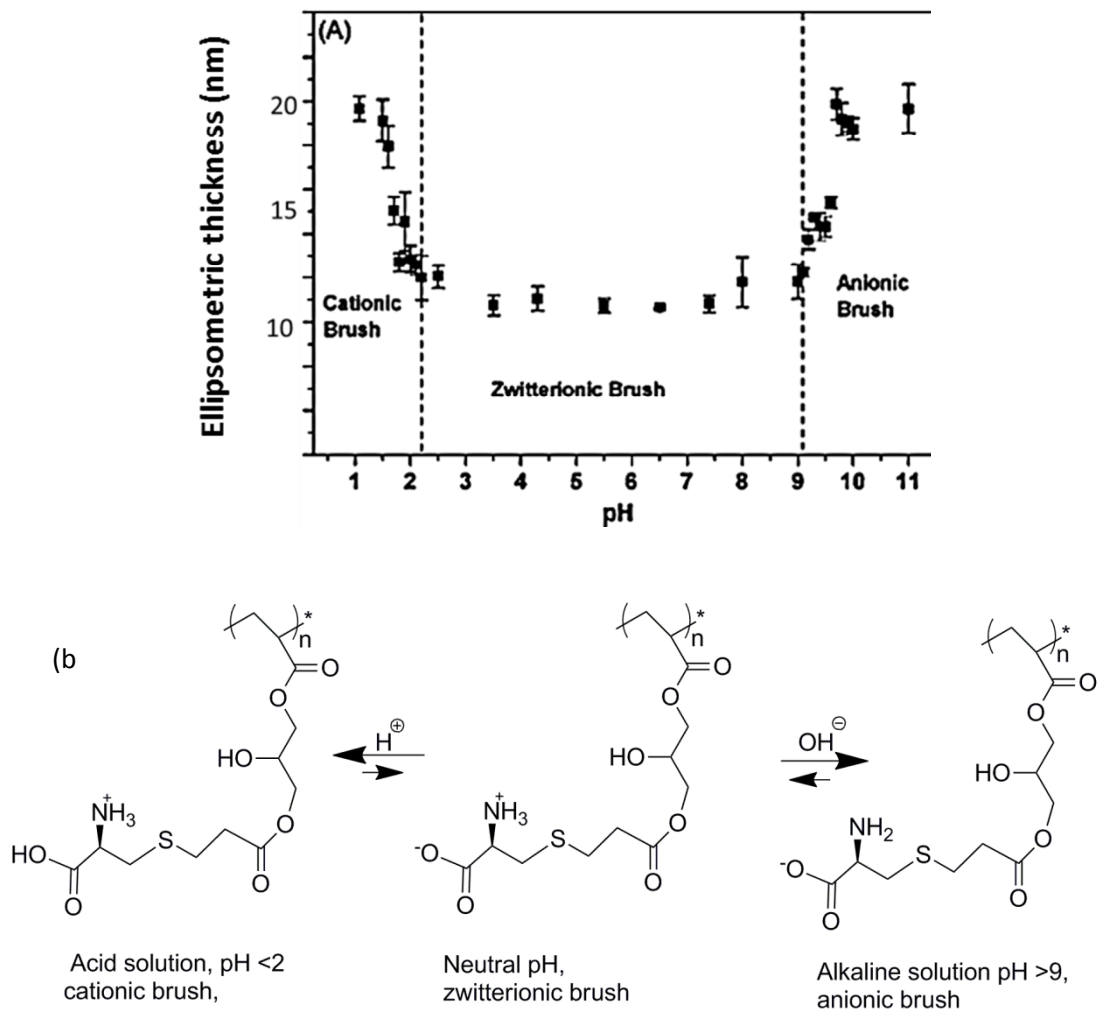


Figure 5.11: (a) Ellipsometric measurement of pH response of PCysMA in buffer showing wet thickness.²⁸ (b) Shows how the chemical structure changes with pH.

Above pH 9, the brush thickness extended to 16 ± 3 nm. The carboxylic acid was maximally ionized whilst the primary amine group became deprotonated (neutral), which resulted in an anionic brush (Figure 5.11 (b) right). Again, this caused strong electrostatic repulsion within the chains, extending the brush to three times its dry length.

5.4.1.3. Surface zeta potential

The polymer brush samples, grown on a glass substrate via the surface initiation step using BIBB-APTES, were cut to size and installed in the surface zeta adapter. They were immersed in the same (a 0.01% aqueous dispersion of non-adsorbing (negatively charged) polystyrene latex beads in 1 mM KCl) tracer as used above and described in Chapters 3 and 4). The electrophoretic and electroosmotic motion in an applied AC electric field were measured. From these measurements the surface zeta potential was calculated using the

Zetasizer Nano software. The results of measuring the surface zeta of the PCysMA brush over a range of pH are presented in Figure 5.12.

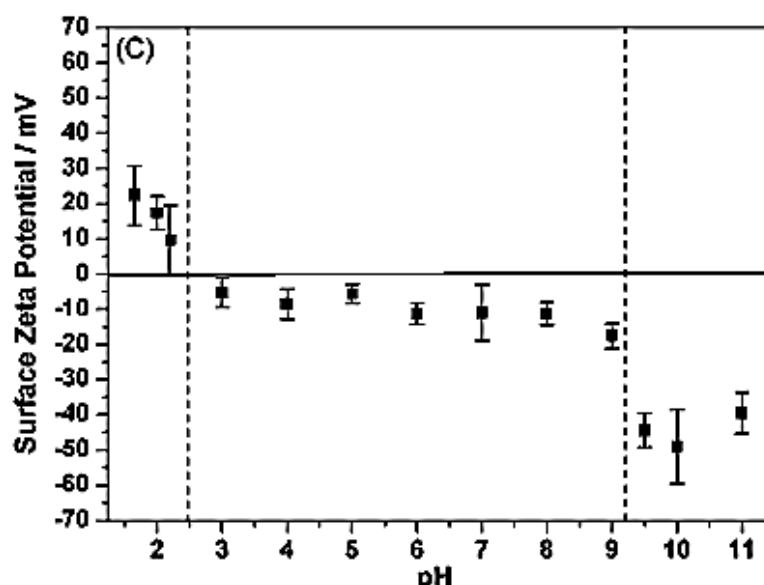


Figure 5.12: Surface zeta potential plot of PCysMA (dry length 7 nm) over the pH range from 2 to 11 it can be seen that at low pH below 3 the surface zeta is positive, from pH 3 to 8 it is ~ -10 mV and above this it become increasingly negative.²⁸

The short brush (dry length 7 nm) actually displayed a weakly negative surface zeta potential of -10 ± 5 mV over the range where it was expected to be zero (zwitterionic), suggesting some influence from the underlying anionic glass substrate and initiator (as described above and seen in Figure 5.8). Liu *et al.* also observed a similar negative potential when studying a short poly(serine methacrylate) brush, in the range where zwitterionic character was expected.²⁹ Below pH 2, the measured zeta potential of the PCysMA was $+22 \pm 7$ mV as it became cationic, while at a higher pH of 11 the surface zeta was -40 ± 5 mV, as the brush became highly anionic. (The chemical structures which correspond to this can be seen in Figure 5.11 (b)).

5.4.1.4. NMR characterisation

In order to establish that the polymer was chemically stable at 50 °C, the temperature selected for vesicle incubation, a series of tests were performed using NMR. These were performed by the staff at the NMR Centre in Sheffield. An NMR spectrum was produced 20° C and again after heating to 50 °C in D₂O for 2 h.

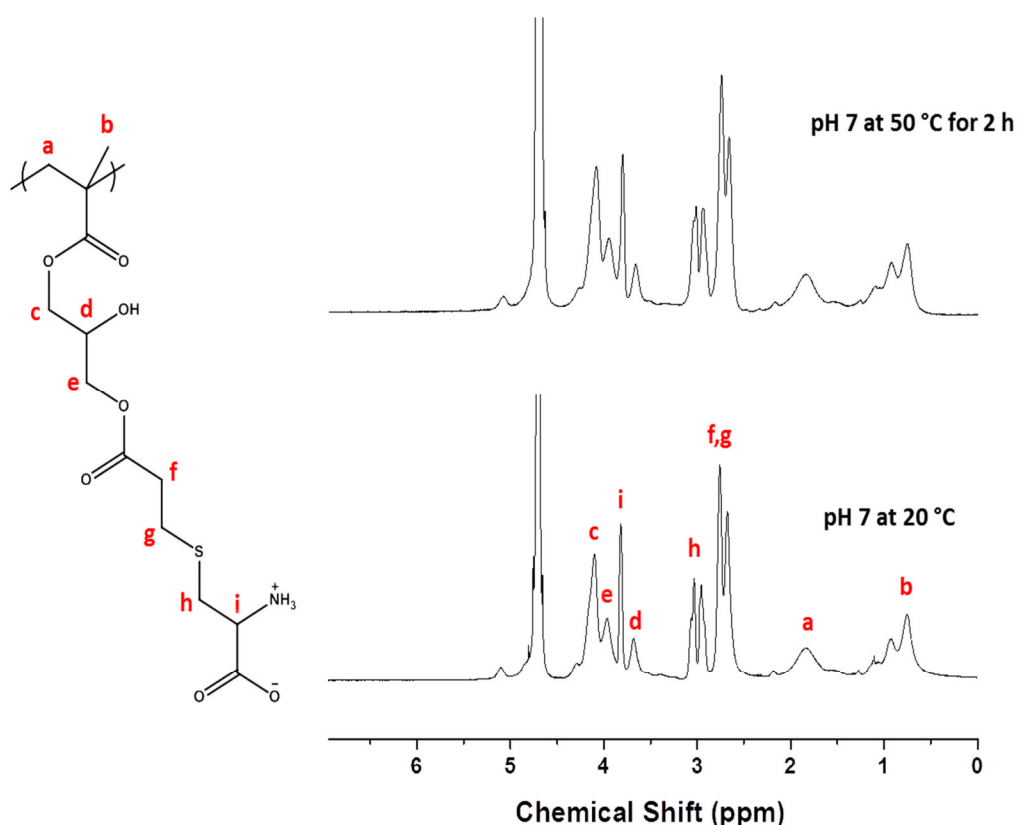


Figure 5.13: ^1H NMR spectra recorded in D_2O for PCysMA at pH 7 (lower) at room temperature and (upper) held at $50\text{ }^\circ\text{C}$ for 2 hours. Note no signs of degradation in the heated sample. Inset is the structure of PCysMA showing the positions of the protons of interest.

The results are shown in Figure 5.13, which confirmed that there were no changes in the chemical shift of any of the protons (marked in red) after heating. There had been no hydrolysis of the pendant ester groups in the brush side chains during heating in solution and no changes in chemical composition of the polymers. However, these measurements were made on free polymer strands in solution and not on the brush grown from the initiated glass surface. Contact angle measurements were subsequently performed to investigate whether the polymer was affected by the heating step when grown as a brush.

5.4.1.5. Contact angle characterisation

The water contact angle was measured on samples of the PCysMA coated glass, at room temperature and on heating up to $50\text{ }^\circ\text{C}$. The samples were rinsed and dried and inserted into a flow cell which had a Peltier heating element in the base. The advancing contact angle changes, as a result of heating the sample, were measured at each stage as the temperature was cycled between $23\text{ }^\circ\text{C}$ and $50\text{ }^\circ\text{C}$. Measurements were taken at $23\text{ }^\circ\text{C}$, after

heating to 50 °C then after cooling to 23 °C again, with two intermediate measures taken. The heating process was repeated on three representative samples.

The graph Figure 5.14 (a) plots the changes in contact angle as the sample is heated and cooled. The contact angle at room temperature was $\sim 45^\circ$, which fell to $\sim 24^\circ$ at 50 °C, increasing again back to 42 ° when cooled. A 6% increase in the surface tension of water over this range contributed only minimally as an error in the reading.

Similar work was done by Azzaroni³⁰ on a sulfobetaine polymer brush with both sulfonate and amine groups on the chain which render it zwitterionic Figure 5.14 (b)). They also found that the brush contact angle reduced significantly as the sample was heated from 22 °C to 52 °C. Their explanation was that the chains are self-associated when at room temperature with the positive and negatively charged groups attracted to each other.

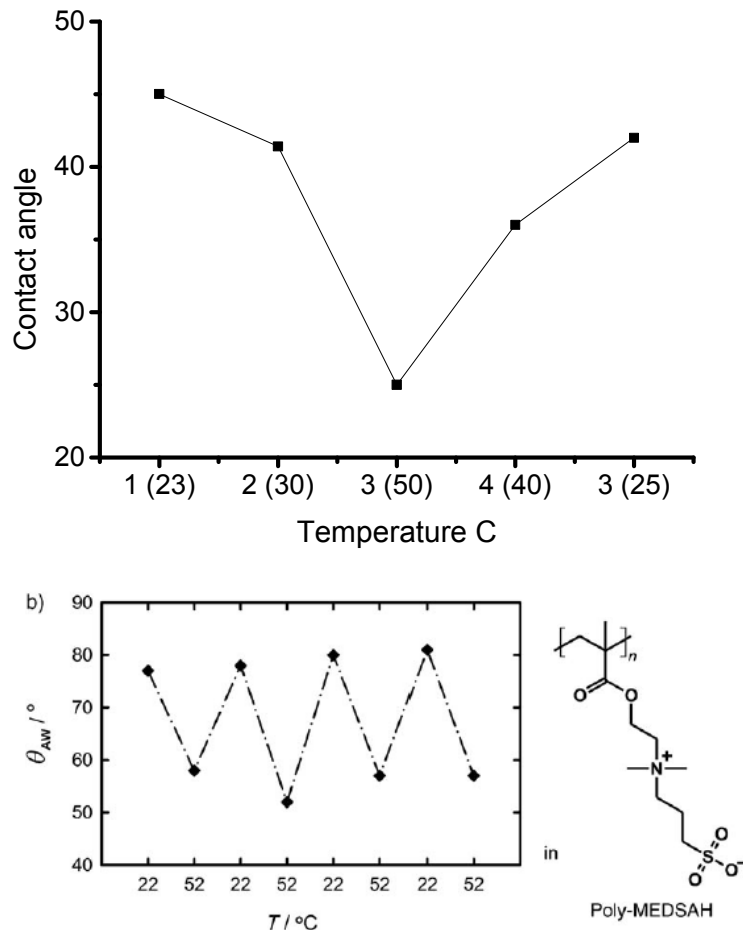


Figure 5.14: (a) Effect of heating PCysMA sample on the advancing contact angle. Sample was heated from room temperature and cooled again. (b) PMEDSAH results by Azzaroni *et al.* after heating and cooling.³⁰

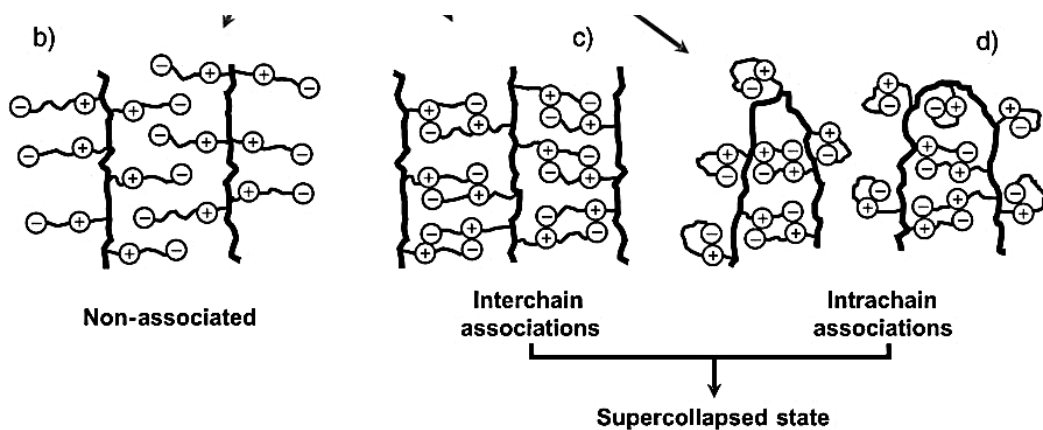


Figure 5.15: Configurations of zwitterionic chains under different solution conditions.³⁰

This is reasonable when considering high dipole moment charged chains adjacent to one another and would lead to close association between the chains. Azzaroni *et al.*³⁰ considered that in solution the chain interactions create a self-associated state, which are a function of the surrounding solution and the chain molecular weight. They suggested three conformations of these interactions: non-associated, inter-chain associated and intra-chain associated (a collapsed state) as seen in Figure 5.15. If in this instance the PCysMA chains are partially associated at room temperature, as is also suggested by the fact that the brush length is not at its maximum, but at 2/3 of its fully extended length between pH 3 and pH 8 (Figure 5.11), it is possible that upon heating to 50 °C the dipolar attractions are broken allowing the chains to become fully hydrated, charged and extended, reducing the contact angle. These suggestions are also in agreement with earlier work by Georgiev *et al.*, who studied the temperature induced swelling of another polymer, PDMAAPS.³¹

5.4.2. Lipid bilayer formation on PCysMA using vesicle fusion - FRAP results

Using the methods described above in 5.2.1., a range of lipid formulations were incubated on the polymer brush surfaces. Attempts to form bilayers by incubating vesicles of pure POPC lipid on PCysMA for 3 days, failed and no evidence of bilayer formation was seen. Whilst some isolated vesicles were adsorbed, as shown by the bright spots in Figure 5.16, these were at low density with insufficient coverage to form a bilayer.

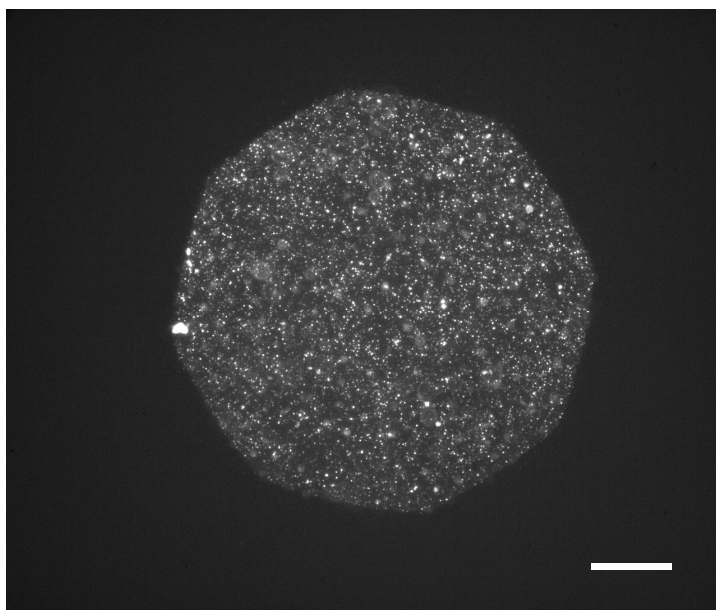


Figure 5.16: FRAP image following the incubation of POPC lipid vesicles on PCysMA brush after incubation for 3 days.

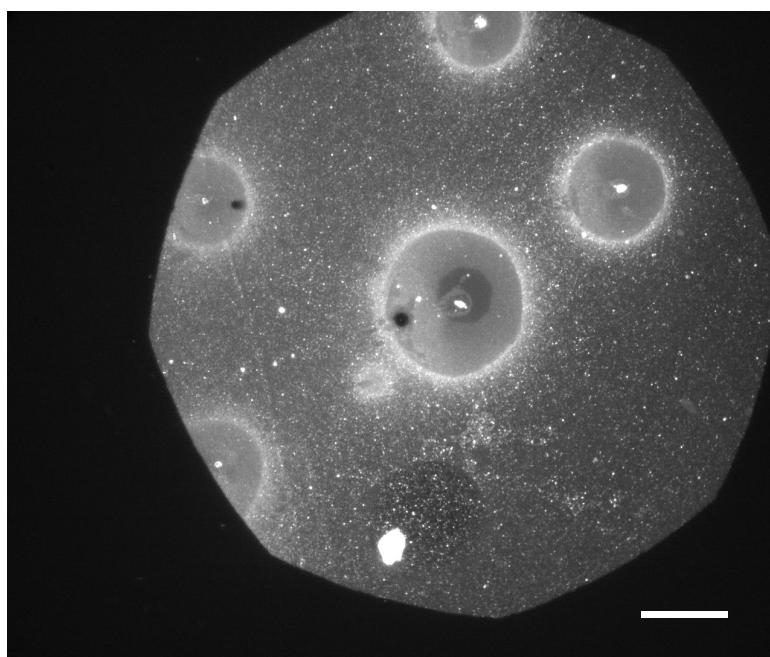


Figure 5.17: FRAP image following the incubation of 10% DOTAP:POPC lipid vesicles on PCysMA brush after incubation for 4 days. Scale bars 60 μm .

Since the surface exhibited a slightly negative surface zeta potential, positively charged lipids were incorporated into the lipid vesicles and used for incubation on the brush. Vesicles comprising 10, 25 and 50 mol % cationic lipid (DOTAP) and POPC were then tested. It was found when using 10% DOTAP (Figure 5.17) with PCysMA brushes that there was some evidence of lipid absorption and some areas which could be bilayer patches, but the quantities were still insufficient to form a bilayer.

After increasing the DOTAP concentration to 25 mol %, and incubating the vesicles on PCysMA overnight, bilayer formation was not observed immediately at room temperature. More of the vesicles were injected and the temperature immediately increased to 50 °C for 1 h. The sample was rinsed and incubated for a further 48 h period at room temperature. The result had the appearance of a homogenous lipid layer, as evidenced by the FRAP images in Figure 5.18 for which the diffusion coefficient was measured to be $1.07 \mu\text{m}^2/\text{s}$ and the mobile fraction 94%. It was assumed that the electrostatic attraction between the weakly charged surface and the highly charged vesicles resulted in a dense layer of vesicles being adsorbed. These adsorbed vesicles subsequently fused to form a good, diffusing bilayer.

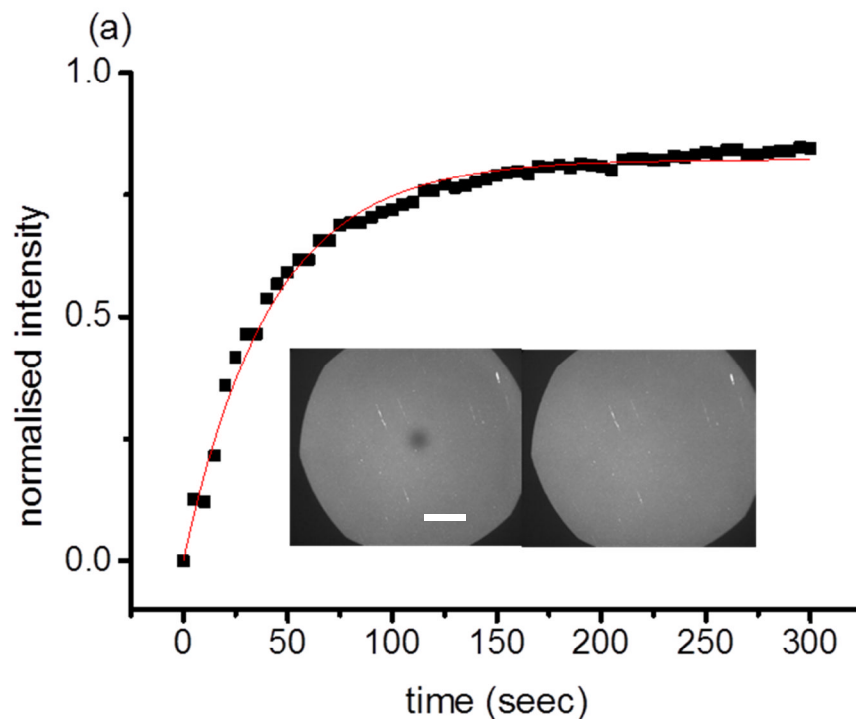
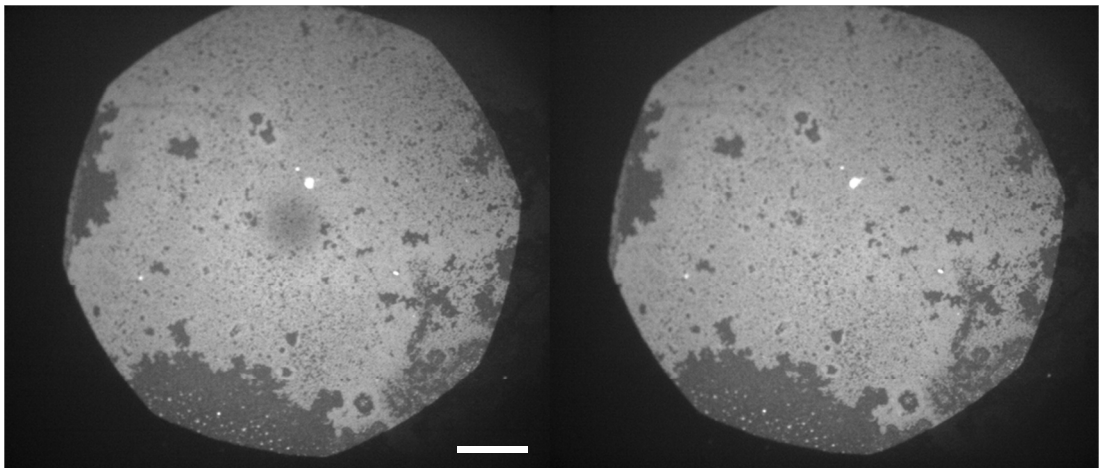
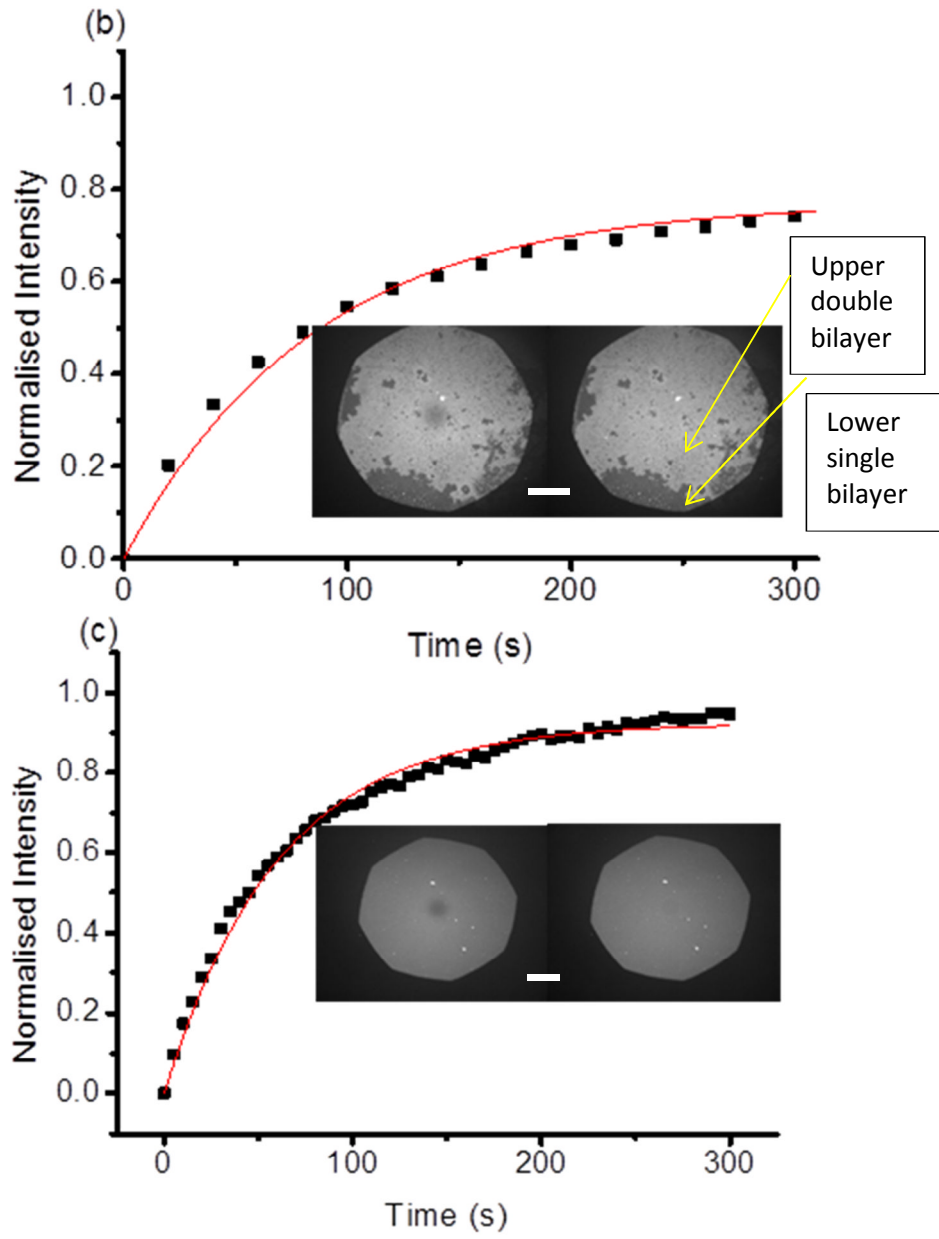


Figure 5.18: Graph showing the diffusion characteristics of a bilayer with images immediately after bleaching and after 5 minutes of FRAP recovery. The bilayer was formed on a PCysMA brush using vesicles composed of 25 % DOTAP:POPC and 0.5 mol % Texas Red in 10 mM phosphate buffer at pH 7. Two aliquots of lipid were injected, with heating to 50°C after the second. An extended incubation of 48 h then took place. The brushes had a dry thickness of ~7 nm. (Scale bar 60 μm).

Interestingly, the bilayer formation was observed to follow a two-stage process on one sample. Firstly, during the 50 °C incubation period vesicle fusion and rupture occurred leading to the formation of what is probably a double bilayer. The incomplete uppermost bilayer displayed a diffusion coefficient of $0.7 \pm 0.2 \mu\text{m}^2 \text{s}^{-1}$ and an associated mobile

fraction of 73% in Figure 5.19 (top images), which is lower than expected for a fully fluid bilayer. It is possible that some of the lipids were immobile or that the gaps in the upper bilayer created defects, slowing the diffusion rate. In the second stage, during the extended 48 h incubation period, the uppermost bilayer disappeared leaving a more complete underlying bilayer which exhibited a diffusion coefficient of $1.0 \pm 0.2 \mu\text{m}^2 \text{s}^{-1}$ and a mobile fraction of 92 % Figure 5.19 (lower images). This process was been observed to completion on only one occasion when it was captured as a video sequence.³² A patchy and loosely bound second bilayer, forming areas of double bilayer, had been observed by Parker *et al.*³³ when using the cationic surfactant HEMDAB in the presence of pentanol. In this case the presence of a hydroxyl group on the HEMDAB allowed it to form hydrogen bonds between the two layers.



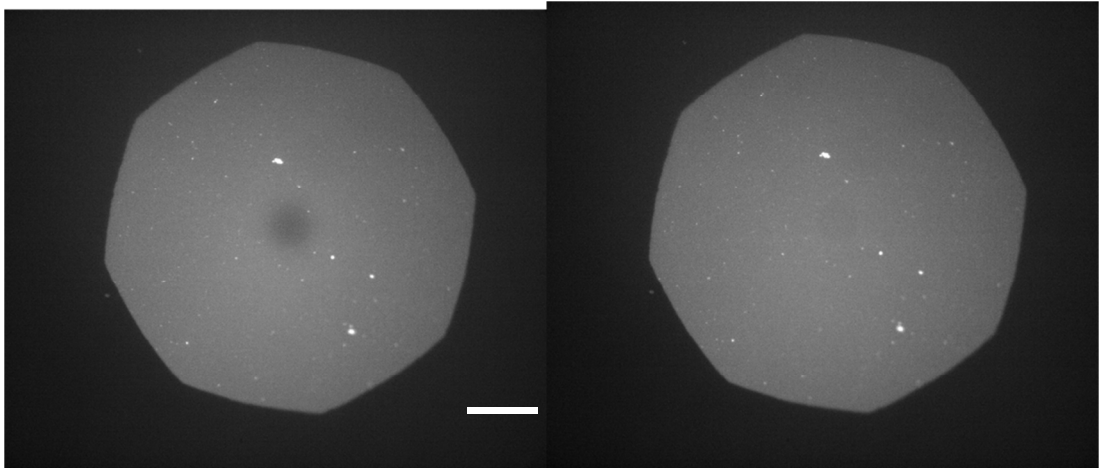


Figure 5.19: Fluorescence recovery after photobleaching graphs and images at bleaching and after 5 min. A double bilayer adsorbed on a PCysMA brush (top graph) following incubation at room temperature and then at 50°C for 1 hour, with a second aliquot of lipid. A single bilayer (graph below) formed following a further 48 h room temperature incubation of the same sample. In all cases the vesicles contained 25 % DOTAP:POPC and 0.5 mol % Texas Red in 10 mM phosphate buffer at pH 7. The brushes had a dry thickness of ~7 nm. Images were taken immediately at bleaching (left) and after 5 min recovery time (right). (Both sets of images are enlarged below the graphs.) Scale bars 60 μm .

the elevated temperature played a positive role in the fusion of the vesicles on PCysMA to form a bilayer. The next obvious step was to inject the lipids into the sample in a flow cell and immediately incubate the sample at 50 °C for 1 h, followed by MilliQ rinsing, rather than using the two step process described above. Following this protocol, the bilayer formed successfully and appeared to be fairly homogeneous, becoming more so after further incubation for 48 h at room temperature. Using FRAP, a diffusion coefficient of $1.4 \pm 0.5 \mu\text{m}^2 \text{s}^{-1}$ and a mobile fraction of 92% were measured. Provided they were maintained in a hydrated state, the bilayers remained stable for ~5 days. This result was observed on numerous samples, with good diffusion rates. The brush samples were all hydrated in buffer before injecting the vesicles and it was confirmed that no lipids were adsorbed when injected onto the dry brushes.

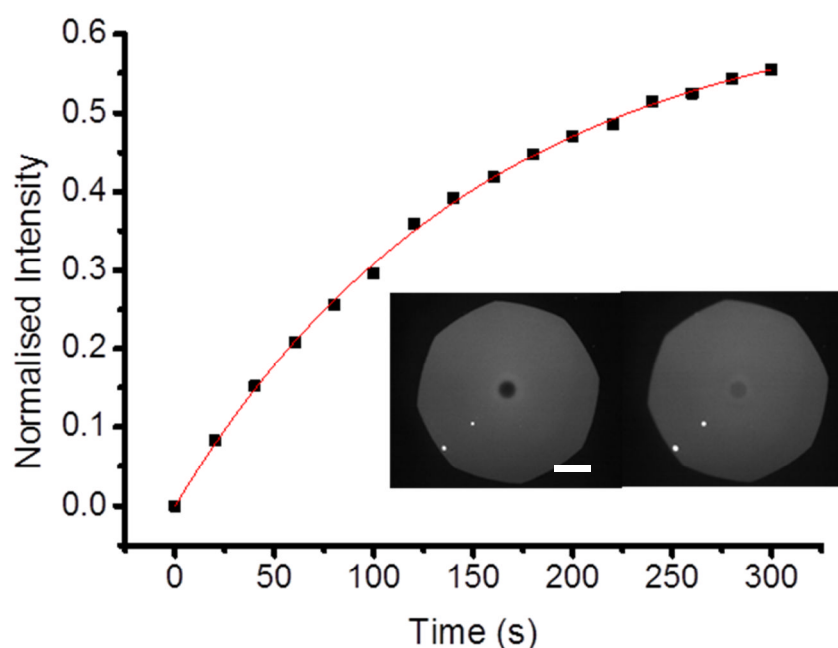


Figure 5.20: FRAP graph of a bilayer on a PCysMA brush formed after incubation at 50 °C for 1 h and a further 48 h. Vesicles contained 50 % DOTAP:POPC and 0.5 mol % Texas Red in 10 mM phosphate buffer at pH 7 were used. The brushes had a dry thickness of 7 nm and images were taken immediately at bleaching (left) and after 5 min recovery time (right). Scale bar 60 μm .

When the DOTAP:POPC ratio was increased to 50 mol%, a lipid bilayer with a diffusion coefficient of $0.3 \pm 0.06 \mu\text{m}^2 \text{s}^{-1}$ and a mobile fraction of only 69% was formed Figure 5.20. These measures are similar to those observed above for the upper layer of the double bilayer, however, despite an extensive incubation period (over 4 days) these did not evolve further (as was observed for the sample in Figure 5.19) into a single bilayer. This diffusion rate was slower than the best bilayer formed with 25% DOTAP on PCysMA. This may be the result of the presence of a second lipid bilayer or a slowly diffusing bilayer where some of the lipids are pinned by the greater electrostatic attraction between the vesicles and the brush.

Finally, vesicle deposition on longer polymer brushes was tested and the result for a 15 nm and 25 nm (dry length) brush was that lipids adsorbed to create a homogeneous layer, but they were immobile.

5.4.3. Lipid bilayer formation using vesicle fusion on PCysMA - AFM results

AFM images of the dry and hydrated PCysMA polymer brushes and the bilayer were performed with the help of George Heath. The scans before bilayer deposition showed few

surface features. The dry brushes had an rms roughness of 0.5 ± 0.2 nm while the hydrated brush immersed in buffer had an rms roughness of 0.3 ± 0.1 nm. This was in agreement with published work.²⁸

Figure 5.21 (a) and (b) show, respectively, a height image and surface profile obtained following bilayer formation on the PCysMA brush. Notably, there are few intact vesicles visible on the surface which would appear as ~ 20 nm high features. The breakthrough force curve shown in Figure 5.21 (c) was obtained by applying sufficient force to the tip until it broke through the lipid layer. The bilayer depth indicated by this breakthrough force is 5 nm, which is consistent with the expected mean bilayer thickness. By scanning a reduced area using a relatively high applied force (3 nN), a $2 \mu\text{m}^2$ area of lipid bilayer and the underlying PCysMA brush was scratched away, see Figure 5.21 (d). The height profile across the edge of this area is 18 nm (Figure 5.21 (f)), which is close to the sum of the swollen brush thickness (12 nm) plus the bilayer thickness (5 nm). Figure 5.21 (e) and (g) depict the surface profile within this scratched area. The surface roughness within this scratched area is very close to that of bare glass.³⁴

It can be concluded here that a smooth bilayer has been formed with a height profile consistent with the expected height for the hydrated brush and a single lipid bilayer.

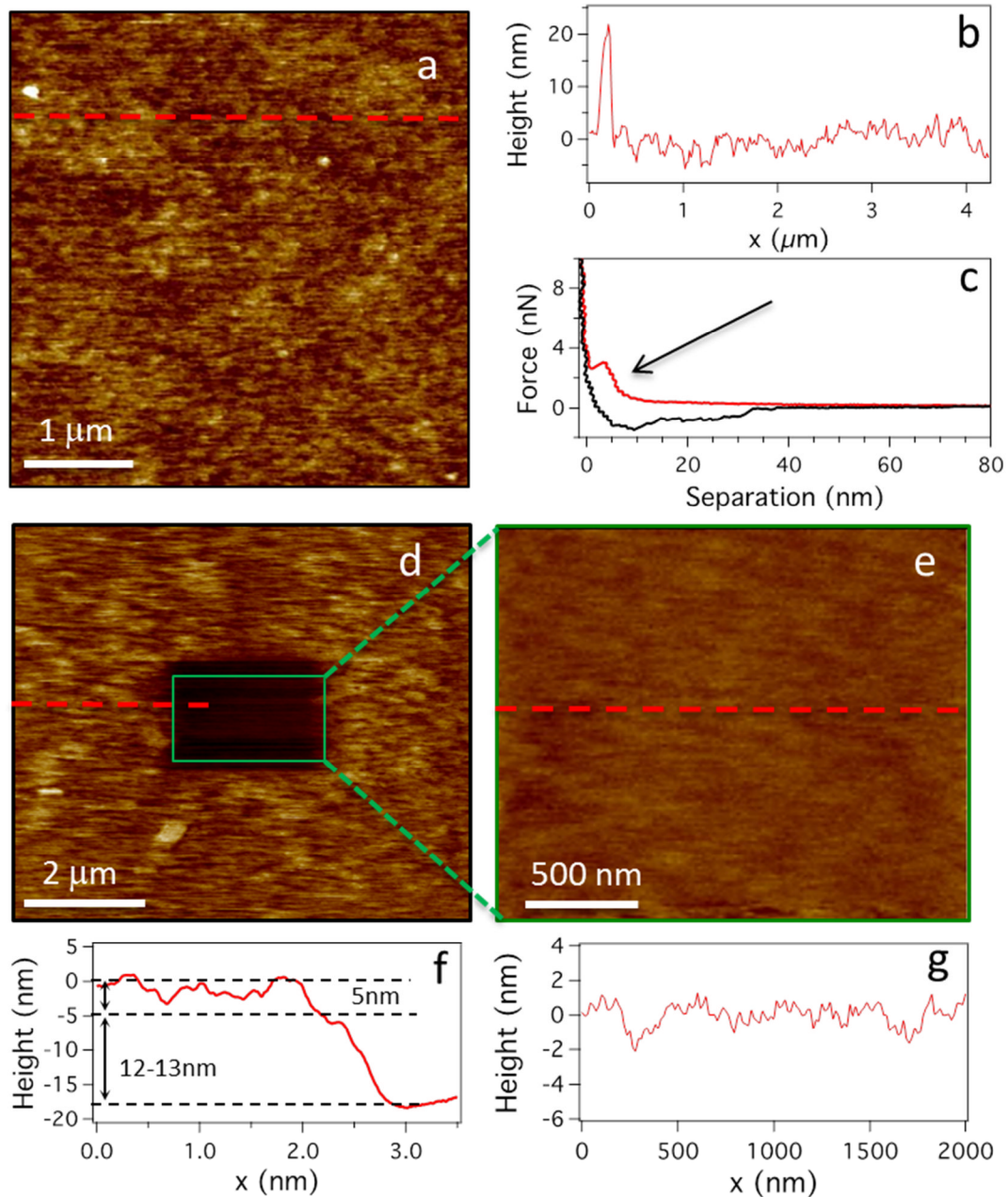


Figure 5.21: AFM images following bilayer formation on a PCysMA brush (a) height image, (b) height profile also showing single adsorbed vesicle, (c) breakthrough force curve indicating a 5 nm bilayer thickness, (d) $2 \mu\text{m}^2$ “scratched” region surrounded by lipid bilayer on PCysMA brush, (e) image at base of the $2 \mu\text{m}^2$ scratched area, (f) height profile across the bilayer /polymer scratch edge (position indicated by red dashed lines), (g) height profile of the surface at base of the scratched area.

5.4.5. Lipid bilayer formation using spin coating onto PCysMA - FRAP results

The spin-coating of 25 % DOTAP in isopropanol onto the dry PCysMA brush showed that some lipid had been adsorbed, as can be seen in Figure 5.22 (a) below. On close observation of the FRAP images it can be seen that diffusing lipids were adsorbed onto the surface, as shown by the recovery after bleaching, but were not homogeneous. The effect

seen on the surface is similar to that seen for the phase separation of lipids in bilayers. In this case it may be a result of variations in hydration or incomplete removal of the isopropanol before re-hydration with water, leaving behind hydrated patches and patches where organic solvent was present.

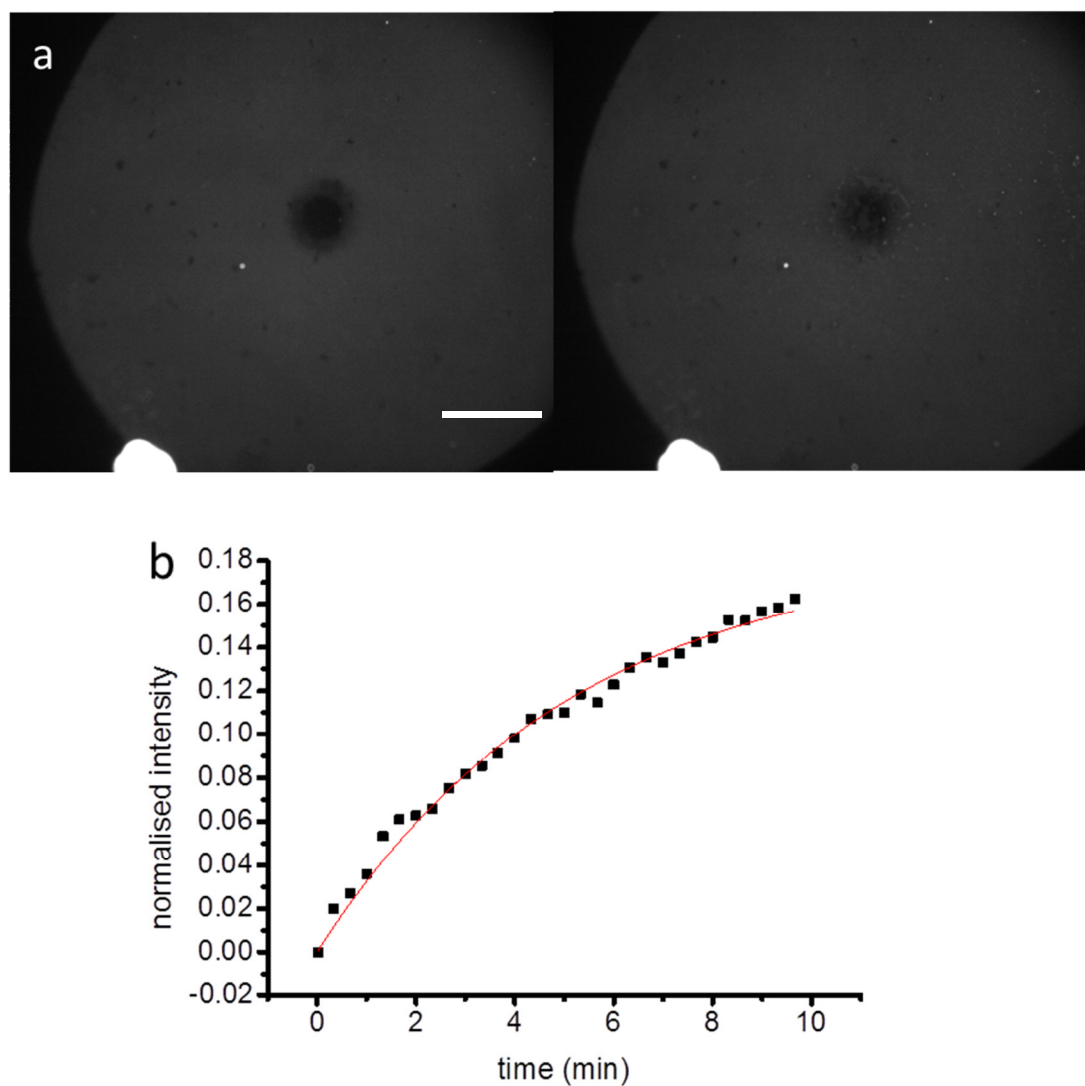


Figure 5.22: Spin-coating of 25% DOTAP lipids from isopropanol onto dried PCysMA, length 7 nm. (a) Images at bleaching point (left) and after 10 min (right) (b) Diffusion graph. Scale bar 60 μm .

The calculated diffusion coefficient was $0.26 \pm 0.1 \mu\text{m}^2/\text{s}$, but with a very low mobile fraction of 17% as shown in Figure 5.22 (b). It appeared that a large portion of the lipids were bound to the brush surface and had not been fully hydrated. On an earlier sample more intense hydration was used by directly soaking the sample in buffer after spin-coating. In this case the lipids were completely removed from the surface. Despite several

attempts to improve the process, it continued to give inferior results to the vesicle incubation method.

5.5. PMPC polymer brushes

5.5.1. Preparation and characterization

The preparation and most of the characterisation were done by the Sheffield Polymer Group. The method for preparing the PMPC brush, which also applies to the PMAA and PKSPMA below, is summarised here and presented fully in chapter 4. The monomer MPC with the catalysts CuBr / CuBr₂ / 2,2'-bipyridine, in solvent were sealed in Schlenk tubes under argon with initiator-functionalized glass coverslips. After the appropriate time, depending on the required brush length, the tubes were opened and rinsed to yield the brush-coated glass samples. In this Si-ATRP process the density of the initiator and hence brush density, is controlled by changing the ratio of catalyst components (CuBr / CuBr₂ / 2,2'-bipyridine) whilst the brush length was determined by the reaction time.³⁵

The samples were characterised by ellipsometry and AFM to determine the brush length when dry and hydrated. The AFM height measurements in buffer solution show that the rms roughness of the surface was between 0.2 and 0.4 nm, similar to measures presented for other brushes.³⁶

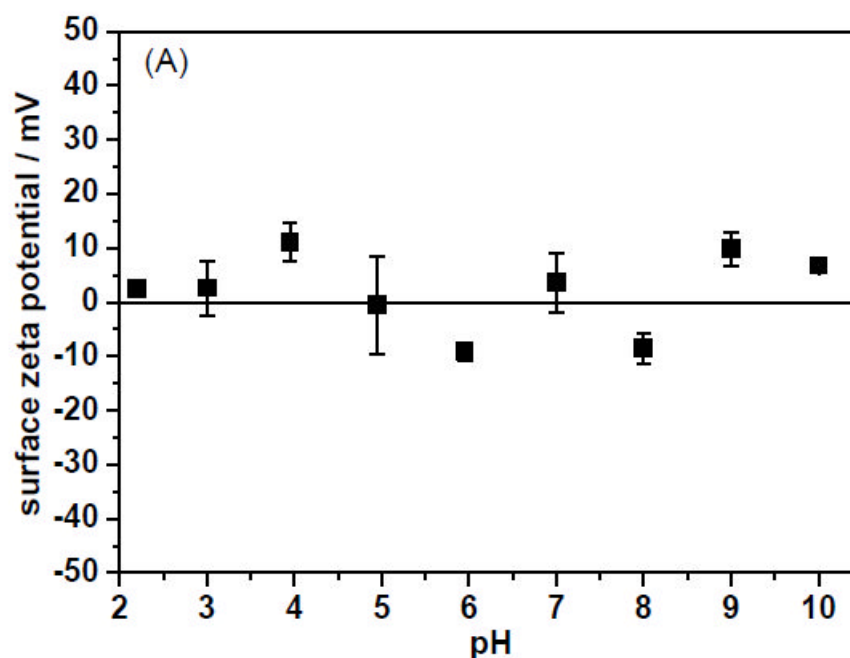


Figure 5.23: Variation of surface zeta potential of PMPC with pH, measured in 1 mM KCl.

When measuring the surface zeta potential it was found that the PMPC brushes exhibited a very low surface potential of 0 ± 10 mV over the range of pH from 2 to 10 (Figure 5.23), indicating that it maintains zwitterionic character throughout the range. It was found by Edmondson *et al.*³⁷ that PMPC swells to three times its thickness when hydrated, compared to its dry thickness and that the swelling characteristics of the brush were not affected by the addition of NaCl.

5.5.2. Results of lipid vesicle incubation

All compositions of negative and positively charged vesicles (containing DOTAP:POPC or DOPG:POPC or pure POPC) at a range of pH and buffers were tested. Even with charged vesicles, elevated temperature or osmotic shock with salt there was no clear bilayer formation and the best result showed few lipid vesicles attached (Figure 5.24).

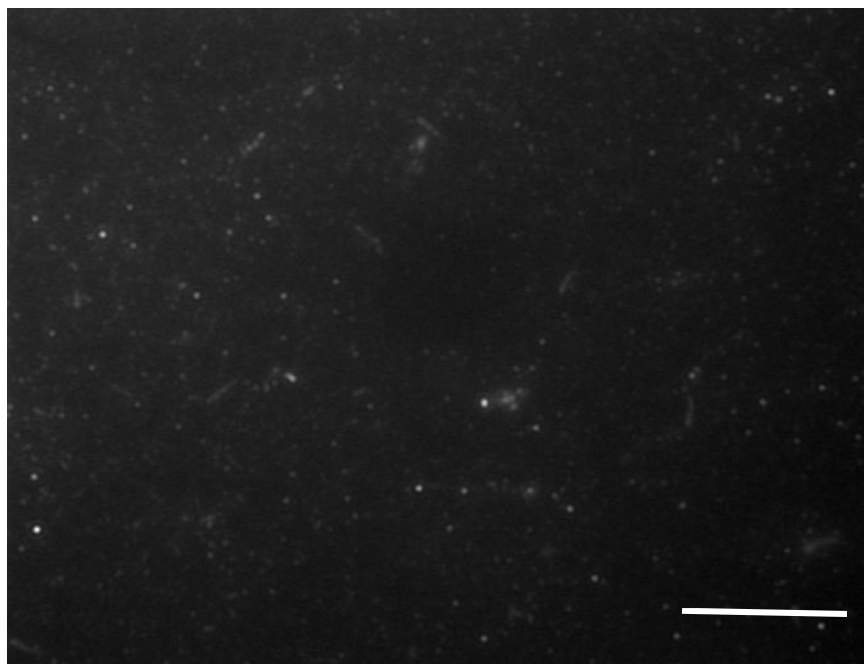


Figure 5.24: Example of the results when testing a PMPC brush, after incubating with a range of cationic, anionic and zwitterionic lipid compositions. Images show evidence of a very small amount of lipid adsorption. Scale bar 60 μ m.

PMPC is known to be protein resistant³⁸ and these results have confirmed that it is also resistant to the adsorption of lipids. This brush is obviously not suitable for supporting a fluid lipid bilayer.

5.6. PMAA polymer brushes

5.6.1. Preparation and characterization

In the next two sections are presented two anionic brushes which have highly charged surfaces. It was assumed that when using oppositely charged lipid vesicles or possibly zwitterionic ones, there would be sufficient driving force to attract lipids to the surface and possibly support bilayer formation. The reason for choosing the PMAA was because it has been well characterized in the literature and it has a terminal carboxylic acid group on the chain in common with the PCysMA, however, the PMAA has no amine group. The results of testing the PMAA may suggest whether the interaction between the positively charged lipid amine group and the negatively charged carboxylate of the polymer was critical for bilayer formation or whether a balance of charge on the polymer, seen with PCysMA, was more favourable.

The preparation method used was Si-ATRP in common with the other samples and has been reported elsewhere and summarized in chapter 4.³⁹

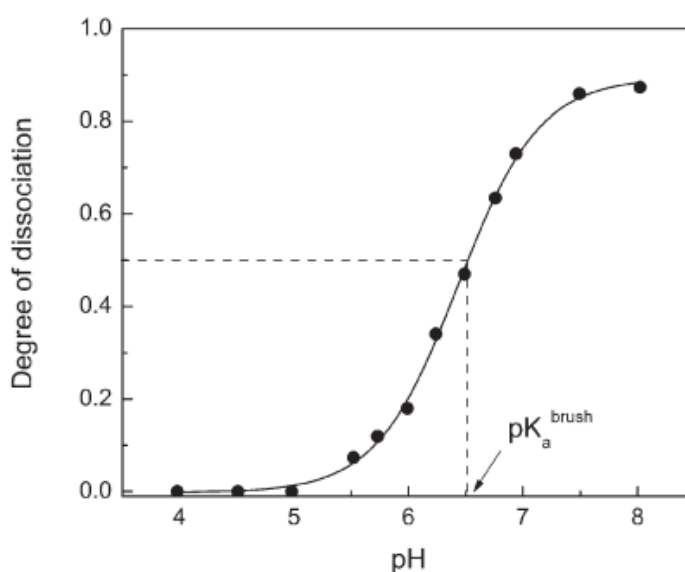


Figure 5.25: Example from the literature of the pH response of PMAA brush, showing the pKa to be 6.5 and that it is fully dissociated and extended at pH 7.5.³⁹

PMAA is a stimulus responsive polyacid brush as measured by ellipsometry and AFM and it responded by stretching and collapsing as the pH changed. The response of the polymer brush (as shown in Figure 5.25) was measured over a range of pH and it showed that the chemical changes within the chains took place over a very short timescale (seconds) and resulted in a three-fold increase in brush thickness from the collapsed state.^{40 41} The swelling began at pH 6 and increased to pH 8 by which point the carboxylate groups were

maximally (negatively) charged. The surface zeta potential was measured to be -43.2 ± 1.5 mV at pH 7.

5.6.2. Results

These PMAA brushes were incubated with lipid vesicles for bilayer formation under the same conditions as the successful zwitterionic PCysMA brush, specifically, at 50 °C for 1 h and further incubation of 48 hours to ensure the bilayer formation was complete. When incubating pure POPC vesicles no lipid adsorption was observed on the PMAA brushes, but when 10% DOTAP vesicles were used a homogenous lipid layer was observed on the surface, however, the lipids were completely immobile (Figure 5.26). When the charged lipid component was increased to 25% DOTAP as can be seen in below, (and also to 50 %,) the lipid layer did become slightly more mobile (Figure 5.26).

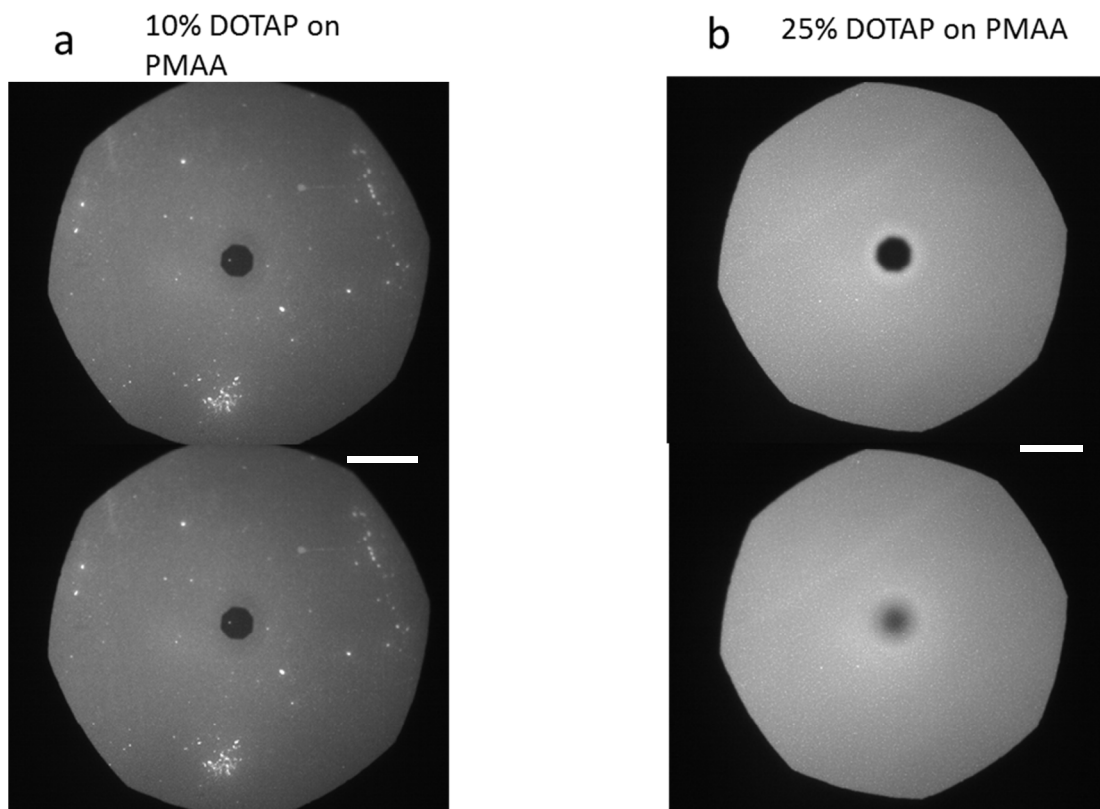


Figure 5.26: FRAP images at bleaching (top) and after 5 min (below). (a) Images of 10% DOTAP incubated on PMAA. (b) After incubating with 25% DOTAP. Both (a) and (b) used a concentration of 0.5 mg/mL in 10 mM phosphate buffer at pH 7. Scale bar 60 μ m.

A graph was produced to measure the diffusion coefficient of 25% DOTAP vesicle layer/bilayer on the PMAA brush, however, the diffusion rate for the PMAA sample (Figure 5.27, blue plot) could not be calculated using the same 'box Lucas' fit used for the other samples as the PMAA diffusion profile was 'non-standard' (see the explanation in section

5.8. below). Shown below, in Figure 5.27, is a comparison of the results and FRAP recovery times of 25% DOTAP vesicles on glass, PCysMA and PMAA. The diffusion rate on glass was $1.5 \mu\text{m}^2 \text{s}^{-1}$ (red plot) and for the PCysMA sample it was $1.4 \mu\text{m}^2 \text{s}^{-1}$ (black plot).

In order to estimate the diffusion rate of PMAA a second graph was plotted in Figure 5.28, below, detailing the first 25 s of the FRAP curves. The slopes of these graphs were: glass 0.013, PCysMA 0.018 and PMAA 0.0015. The diffusion rate for PMAA is thus a factor of 10 slower than the other two and can be estimated to be $\sim 0.1 \mu\text{m}^2 \text{s}^{-1}$.

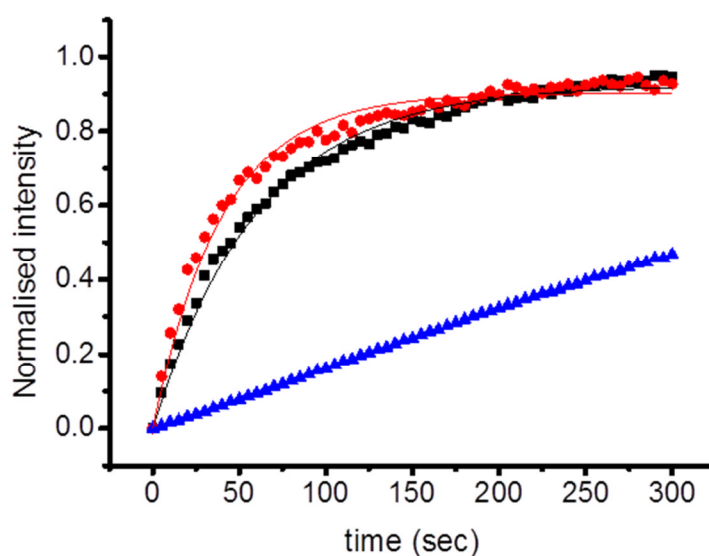


Figure 5.27: Graphs comparing the FRAP recovery rates of glass (red plot) (25% DOTAP vesicles) with PCysMA black plot (25% DOTAP vesicles) with PMAA (25 % DOTAP vesicles) blue plot.

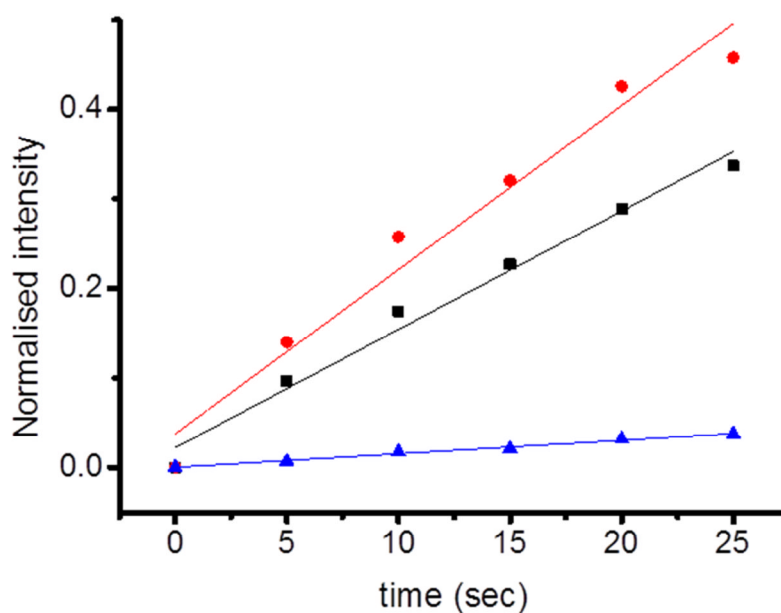


Figure 5.28: Graphs comparing the detail of the first 25 sec of the FRAP recovery graphs shown in Figure 5. 26., of glass (red plot) (25% DOTAP vesicles) with PCysMA black plot (25% DOTAP vesicles) with PMAA (25 % DOTAP vesicles) blue plot.

The result for PMAA where the diffusion coefficient was very slow and likely to be $\sim 0.1 \mu\text{m}^2\text{s}^{-1}$ was not sufficiently mobile to be considered a fluid bilayer. This suggests that the additional positive charge of the DOTAP strongly attracted the vesicles to the surface but they did not fuse to form a bilayer. This result is discussed more fully below in 5.9.

5.7. PKSPMA polymer brushes

5.7.1. Preparation and characterization

PKSPMA is an anionic polyelectrolyte which terminates in a sulphonate group. It was chosen specifically to elucidate whether the type of anionic group on the polymer (carboxylic acid or sulphonate) affected bilayer formation. To do this comparison the results of incubating lipids on both the PMAA and PKSPMA were compared to each other and to the PCysMA.

To prepare the PKSPMA a 3-sulfopropylmethacrylate monomer with the catalysts $\text{CuCl}/\text{CuCl}_2$ and bipyridine were reacted together in solvent in an inert atmosphere in the presence of an initiator coated glass coverslip. In common with other Si-ATRP synthesis the ratio of $\text{CuCl}:\text{CuCl}_2$ was varied to control the brush grafting density, with the reaction time varied to control polymer chain growth and hence, thickness.⁴²

The thickness of the completed brushes was measured by ellipsometry and, using AFM the brush thickness dry and in buffer were determined. The rms roughness of the hydrated brush surface was determined to be low, at 0.2 to 0.5 nm and the dry brush height was 8 ± 2 nm which exhibited a two fold increase in height upon hydration. The surface zeta potential of the brush was measured as -33.8 ± 2.2 mV at pH 7.2.

5.7.2. Results

The results for the FRAP studies following vesicle incubation on the PKSPMA were very similar to those seen for the PMAA brush. When incubating POPC vesicles, no lipid was adsorbed and with the incubation of 10% DOTAP vesicles an immobile, but homogeneous layer was observed as seen in Figure 5.29, left images).

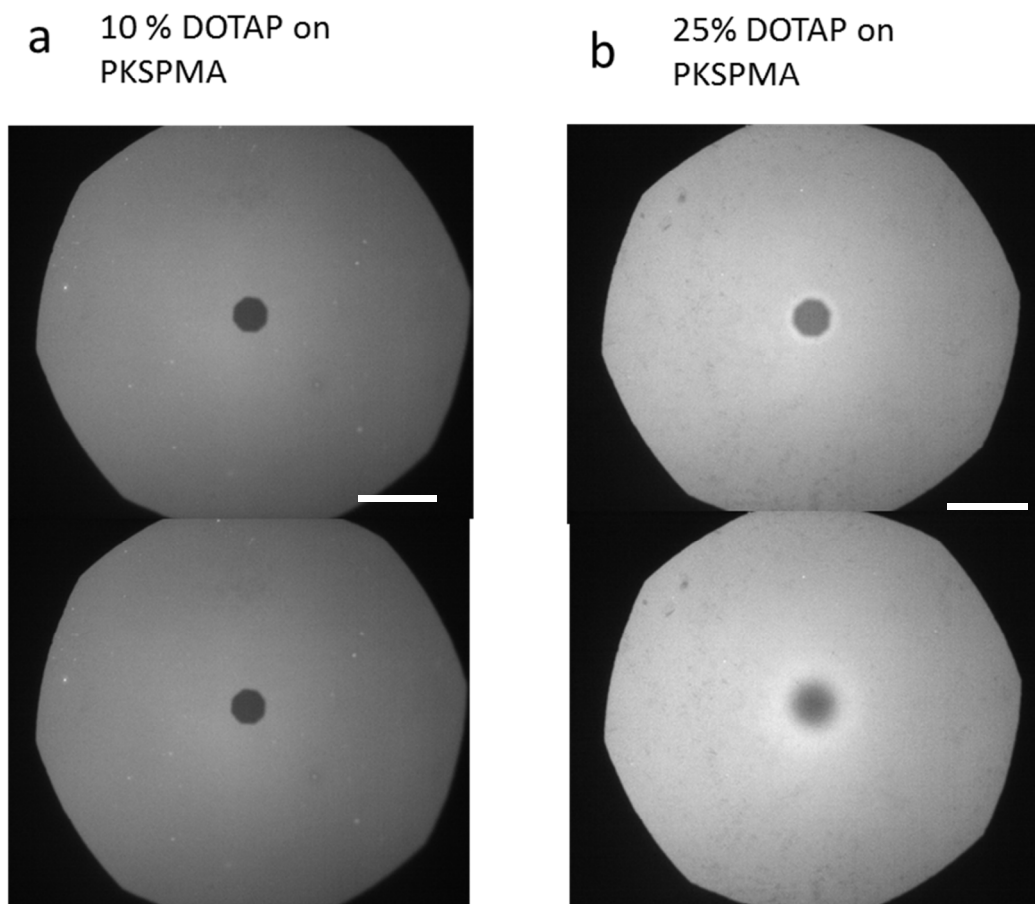


Figure 5.29: FRAP images at bleaching (top) and after 5 min recovery (below). (a) Images of 10% DOTAP incubated on PKSPMA. (b) PKSPMA incubated with 25% DOTAP. Both (a) and (b) used a concentration of 0.5 mg/mL in 10 mM phosphate buffer at pH 7. Scale bar 60 μ m.

When increasing the proportion of DOTAP in the vesicles to 25% this produced a lipid layer on the brush. The lipid layer was fairly homogenous but was very limited in its mobility Figure 5.29 (right images). The images at bleaching and after 5 minutes recovery time for PMAA and PKSPMA were very similar and as the diffusion rate for PKSPMA could not be calculated (because of a bleached spot anomaly, see section 5.8.) it can be assumed to be of the order of $0.1 \mu\text{m}^2 \text{s}^{-1}$ as estimated for PMAA. As the lipids or vesicles adsorbed were not fully mobile on PKSPMA, they were not considered to be suitable candidates for attempting the incorporation of TMPs.

5.8. The use of charged probes and charged lipids with charged polymers for FRAP

5.8.1. Introduction

During the testing of the above anionic polymer brush systems and the cationic samples presented in chapter 7, it was observed that an unusual FRAP bleached spot profile was present. These experiments combined the use of charged probes (negatively charged Texas Red), and lipids with opposite charges to the polymer brush surfaces. This effect is significant as it affects the recovery profile and consequently the diffusion coefficient and mobile fractions of the bilayers deposited on the polymer brushes. A number of experiments and analyses are presented below in an attempt to separate the fluorophore effect from that of the charged polymer and to elucidate the nature of the unusual bleaching profiles.

The analysis included measuring the effect on the bilayer of increasing the amount of Texas Red incorporated with the lipid. The results of this work contributed to a paper published in *Analytical Chemistry* looking at the concentration of lipids by using electric fields.

5.8.2. Method

Bilayers were prepared on glass using POPC containing a range of Texas Red (TR) fluorophore concentrations of 0.5, 1.0, 2.0, 3.0, 4.5, and 6.0 mol %. At each concentration the variation in image intensity was measured (before FRAP bleaching) in count units, using ImageJ. FRAP experiments followed and the diffusion coefficient and mobile fractions of the Texas Red in the bilayers were recorded, at each concentration.

The intensity profiles across the bleached spots were also measured by taking a plot profile in ImageJ after selecting a rectangular line area across the image of the bleached spot. (Using a rectangular area, rather than a line gives a less 'noisy' profile). The results for Texas Red images were compared to the bleached spot profiles of samples of PKSPMA, (an

anionic polymer) and PMETAC (a cationic polymer) which had been used to form bilayers with oppositely charged lipids using a low concentration (0.5 mol %) of TR.

5.8.3. Results and discussion

The FRAP images shown in Figure 5.30 are taken at time zero (left), following photobleaching and after 5 minutes FRAP recovery time (right). The concentrations of TR in the POPC are shown in white on the images. The images show the effect on the bilayer quality and bleaching spot profile when increasing the mol % of charged fluorophore in the POPC lipid. At 0.5 mol% TR the bilayer is of good quality with a diffusion rate of $1.8 \mu\text{m}^2 \text{s}^{-1}$ and a mobile fraction of 90%. At 1 mol% TR the diffusion coefficient is $1.5 \mu\text{m}^2 \text{s}^{-1}$ and 86% mobile fraction. For 2 mol% TR the diffusion coefficient is slowing significantly to $1.1 \mu\text{m}^2 \text{s}^{-1}$ and there is a significantly reduced mobile fraction of 64 %. At 3 mol % and above there is evidence of a significant immobile fraction and phase separation of the lipids, as seen in the lower images, where the bilayer no longer looks homogenous. When 6% of TR was incorporated a bright halo effect was seen around the bleached spot. The relative intensities of the images taken before FRAP were then measured and plotted graphically in Figure 5.31. The red circles on the graph Figure 5.31, (b), represent the relative intensities of the images measured before bleaching and can be compared to the theoretical results. Using the Stern-Volmer equation:

$$\Phi^0 / \Phi = 1 + \frac{k_q}{k_f + k_{nr}} \quad (5.1)$$

The relative fluorescence intensity, I^0 / I can be measured and can be substituted directly for Φ^0 / Φ . Plotting I^0 / I against quencher concentration yields a straight line with a

$$\text{slope} \frac{k_q}{k_f + k_{nr}} \quad (5.2)$$

From the graph, in Figure 5.33., of the plot of intensity against concentration of Texas Red, the expected profile is shown which follows a linear plot as the amount of fluorophore increases. However the actual plot is seen in 5.3. (b), and shows a fall off of intensity with increasing TR concentration. This was assumed to be a result of self-quenching and the expected concentration, which can be measured by the intensity and can be calculated using the equation:⁴³

$$I_q = I_0 \cdot (1 - 1 / (1 + B^3 / C_0^3)) \quad (5.3)$$

Here I_q is the apparent concentration, measured experimentally and caused by self-quenching. I_0 is the actual concentration of T Red in the bilayer. B is a fitting parameter, specific to the Texas Red, which describes the proximity effect of the dipole-dipole interactions which cause the self-quenching.

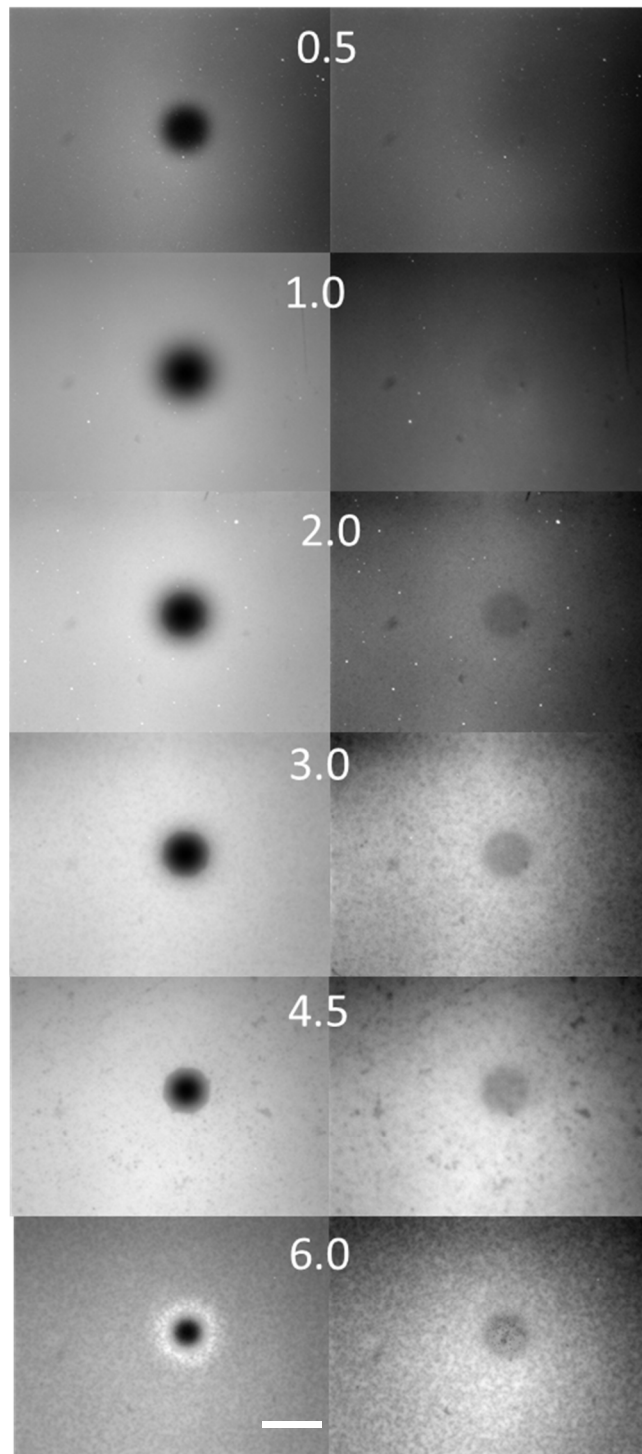


Figure 5.30: Images at bleaching (left) and after 5 min (right) for the Texas Red concentrations, in mol %, shown in white on the images. The images show the deterioration in the quality of the bilayer as the Texas Red concentration is increased. It also shows an increasing immobile fraction as the Texas Red concentration increases, as evidenced by the incomplete recovery of the bleached spot. Scale bar 60 μm applies to all images.

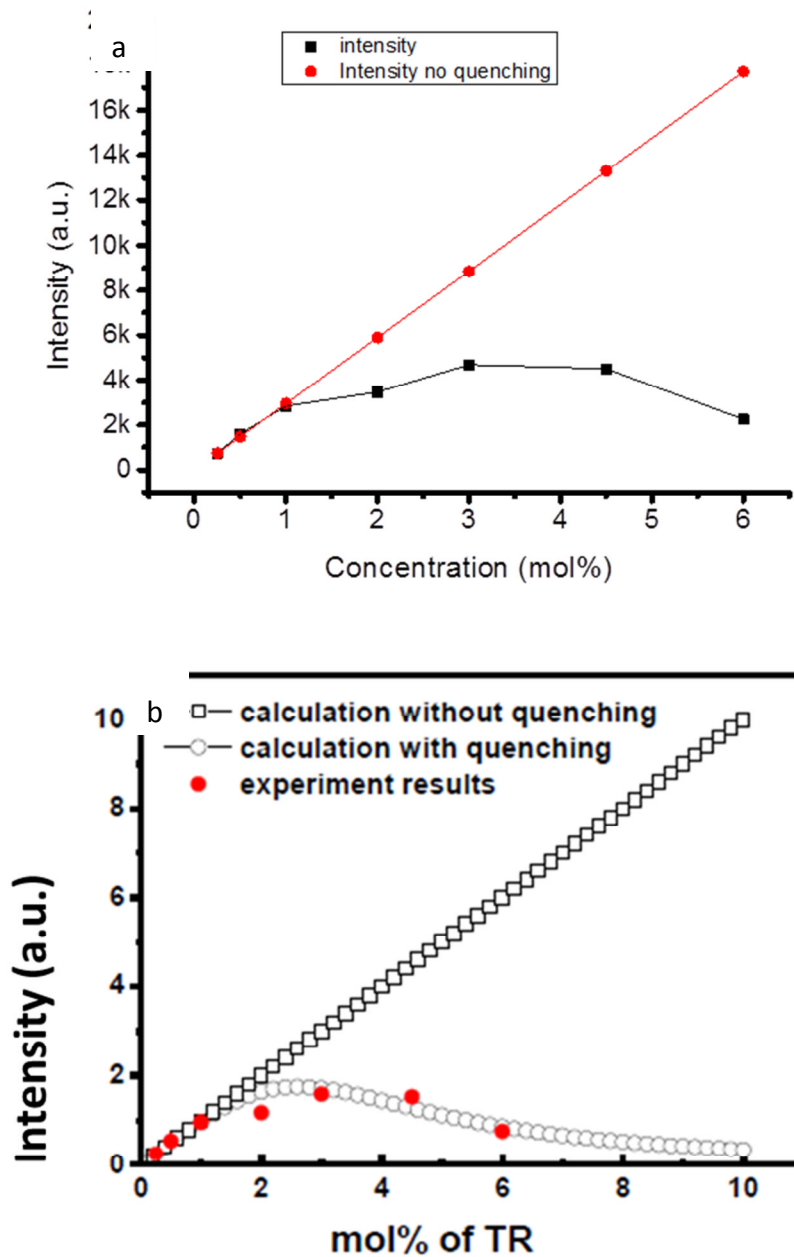


Figure 5.31: Graphical presentation of the relative intensity of fluorescence measured from the images in Figure 5.30 (before FRAP bleaching) using concentrations of 0.5, 1.0, 2.0, 3.0, 4.5, 6.0 mol % Texas Red in a POPC bilayer on glass. (a) Plot of the expected intensity level, which should increase linearly (red circles) with concentration of Texas Red. The actual result (black squares) shows that the intensity reduces with increased Texas Red concentration. (b) Theoretical result with no self-quenching (black squares) and theoretical result with self-quenching of Texas Red (black circles) with actual results superimposed (red circles), taken from ⁴⁴.

The FRAP images immediately after bleaching from Figure 5.30 were used to analyse the intensity profile across the bleached spot in more detail.

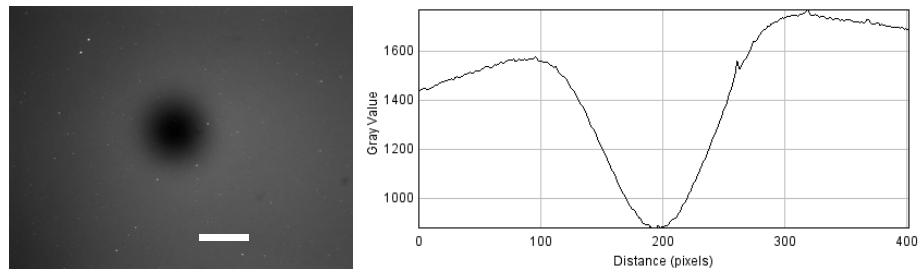


Figure 5.32: Recovery profile of a lipid bilayer formed from a zwitterionic POPC lipid and a charged Texas Red probe at 0.5 mol % (also anionic) using a glass substrate (highly anionic), (left) image of bleached spot immediately after bleaching and (right) intensity profile across the bleached spot. Scale bar 60 μm .

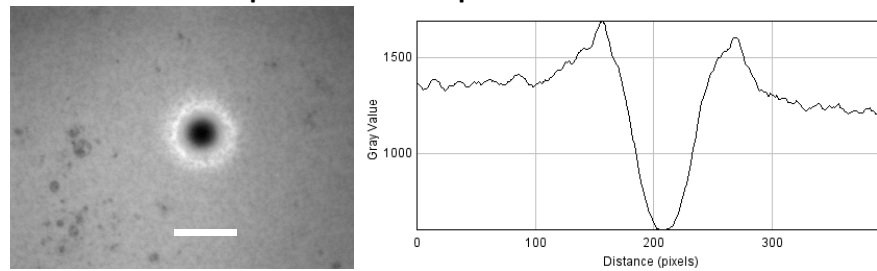


Figure 5.33: Bleached spot (left) and intensity profile (right) of lipid layer formed from POPC (zwitterionic lipid) and 6% Texas Red (anionic probe) on (highly anionic) glass, showing a lighter halo around the bleached spot and peaks on the intensity profile. Scale bar 60 μm .

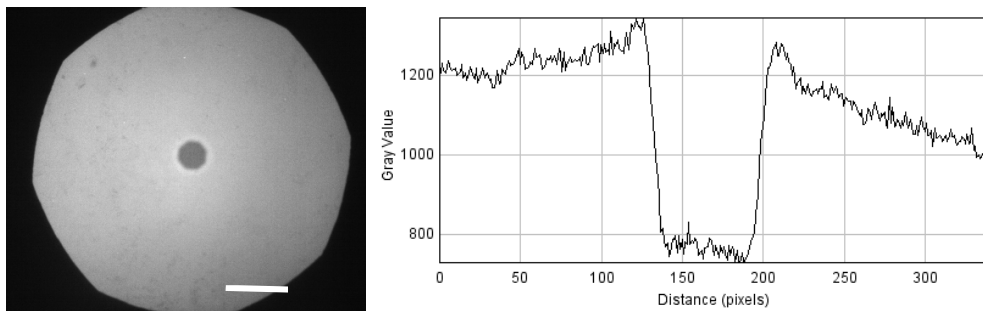


Figure 5.34: Bleached spot and intensity profile of lipid layer formed from 25% DOTAP:POPC (cationic lipid) and 0.5 % Texas Red (probe) on PKSPMA (highly anionic brush), showing a bright area around the bleached spot. Scale bar 60 μm .

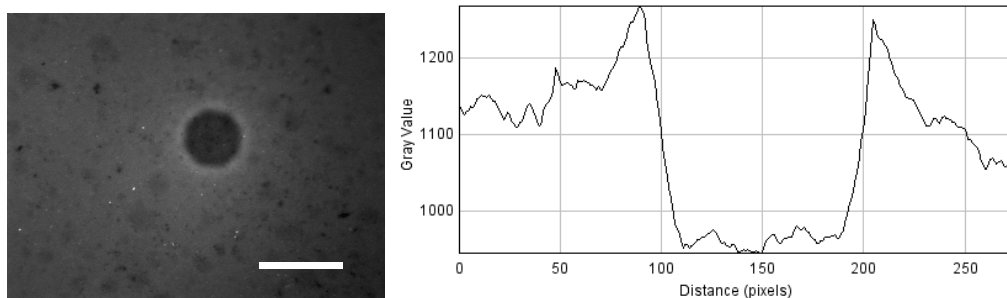


Figure 5.35: Bleached spot and intensity profile of lipid layer formed from 25% DOPG:POPC (anionic lipid) and 0.5 mol% Texas Red probe, on quaternary amine PMETAC, (highly cationic brush), again showing a bright halo around the bleached spot. Scale bar 60 μm .

The image in Figure 5.32, shows the recovery profile when using 0.5 mol % Texas Red to form a bilayer with POPC on glass. This shows an image of a homogenous bilayer, with a Gaussian profile, indicating low/zero intensity at the centre, rising uniformly to the edge of the profile area. With time the fluorescence recovery is expected to follow a profile where by the bleached spot becomes less defined and after 5 min the image will gradually become uniform in intensity and no darker area will be visible. A Gaussian profile is maintained throughout this recovery process, as the unbleached lipids diffuse into the bleached spot. Figure 5.33, at a Texas Red concentration of 6 mol %, shows an apparent increased intensity at the perimeter of the bleached spot. This subsequently produces a diffusing light 'halo' as time elapses, which spreads outwards from the bleached spot. As can be seen in Figure 5.34, PKSPMA, which is strongly anionic, and Figure 5.35, PMETAC, which is strongly cationic, there is a similar bright halo around the bleached spot. The recovery profiles for these two samples were similar to that seen for the 6 mol % TR, where the halo appears to spread outwards, but does not have a Gaussian profile.

This effect, seen with TR when using increased probe concentrations, has been attributed to self-quenching of the fluorophore.⁴⁴ A similar result has been observed by a number of researchers with other systems and may be related to this effect.^{45 46 47} This fluorescence quenching would be spread uniformly across the sample surface before bleaching and is confirmed by the results shown in Figure 5.31, where the intensity of the sample decreases after reaching a maximum for the Texas Red concentration of 1 mol %. However, this does not explain how the bright halo is generated around the bleached spot.

For the results seen with the PKSPMA and PMETAC brushes a different explanation may account for this effect. It may be associated with the copper ions remaining within the brush after the ATRP polymerisation, because of incomplete rinsing of the Cu catalyst. In the Cu(I) state these ions would quench fluorescence, but if they were oxidised to Cu(II) by the photobleaching this could lead to enhanced fluorescence, as the excited state ions relaxed back to the ground state (the Jablonski diagram in Chapter 3 explains this process). It is possible that, at the periphery of the bleached spot, the incident bleaching light is of a slightly lower intensity which is appropriate for generating this enhanced fluorescence from the Cu (II) ions. At the centre of the bleached spot the intensity of the incident light is at its maximum, so the fluorophore is completely bleached and the fluorescence from the Cu (II) is not visible or is not activated.

An interesting alternative hypothesis was proposed by Vo *et al.*⁴⁸, who published work on an anionic polymer layer (of PKSPMA) on the surface of cationic (Ludox CL) particles, using

ATRP. They proposed that the Cu(I)Br/2bpy catalyst could act as a cationic counterion within the polymer chains and not be completely removed after the ATRP process. Though this presents an interesting explanation, the same effect was also seen with cationic polymers, as shown for PMETAC in Figure 5.35, which would not be expected to attract Cu⁺ ions into the chain. If the effect was due to residual copper ions it is possible that a more rigorous process is required to remove the copper catalyst. Matyjaszewski¹ presents clear advice on the removal of copper from the reaction and Ydens et al.⁴⁹ specifically report on the importance of the catalyst removal step.

However, this does not explain the similar effect seen with concentrated TR on glass. The common thread here is that the surfaces (glass and the polymers) are all highly charged and the anionic probe (TR) is used in all cases. What is intriguing is that the same effect is seen regardless of whether the substrate for the bilayer is anionic or cationic and whether it contains a copper catalyst or not.

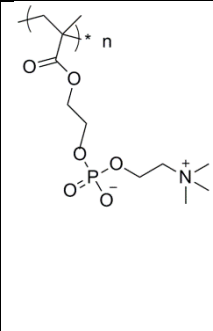
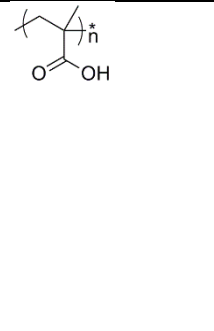
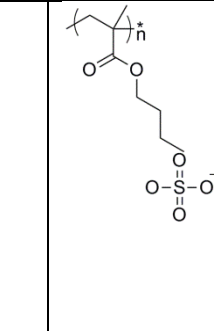
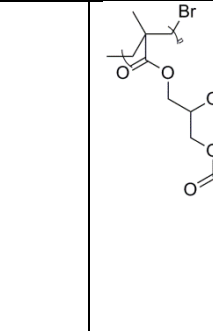
To summarise, Texas Red appeared to exhibit a non-standard recovery profile when used in high concentrations (>1.0 mol%) and when used (at lower concentrations) with charged lipids and charged polymer substrates. There was no reporting of this bright 'halo' effect in the literature, other than reports of the enhanced fluorescence of the TR fluorophore in the presence of metal ions.⁵⁰ As it is accepted that there may be metal ions present when testing the incubation of lipids on the polymer brushes, it is less obvious that they are present when incubating lipids on glass with TR fluorophore. It would be interesting to study this further to establish the nature of the brighter spot.

5.9. Discussion and conclusions for zwitterionic and anionic brushes

Vesicles interact with solid substrates via a combination of van der Waals, electrostatic, hydration and steric (bending and undulation) effects, with the first two playing a significant role in vesicle adsorption.⁵¹ Once adsorbed, the interplay between the adhesive and bending stresses can induce rupture as shown in Chapter 2, (Figure 2.12).⁵² To create a bilayer there are two elemental pathways, one which follows a speedy adsorption and almost instantaneous rupture process and the second which is slower and requires the vesicles to be adsorbed at a denser coverage before rupture is induced (Figure 2.9).⁵³ The second process may also require external stimuli, such as temperature or an osmotic pressure difference between the inside and outside of the vesicle, to aid the process.^{54 55} These pathways, which are well documented for solid silicon surfaces, will be a starting

point for discussing the mechanisms of bilayer formation on polymer brushes. There will clearly be differences, as the brush support is composed of ‘soft-matter’ polymer strands which provide less resistance for the deposited vesicles to be deformed and then fuse into bilayers. The mechanism exploited in these studies to attract vesicles to the brush is an electrostatic one, enhanced by attractive van der Waals forces. The soft polymer brush will allow movement of the vesicles and bending or undulation of the bilayer. These forces may also play a role in whether the final result is a bilayer or an intact vesicular layer.

A summary of the results is shown in Figure 5.36, below, which compares the chemical structures of the brushes, the surface zeta potentials and the FRAP recovery results. Despite intensive testing, the zwitterionic PMPC did not adsorb lipids of any composition. The FRAP images for the highly anionic PMAA and PKSPMA show lipid layers or vesicle layers which were homogenous but observed to be slowly moving (diffusion coefficients of $<0.1 \mu\text{m}^2 \text{s}^{-1}$) when highly charged (25% or 50% DOPG:POPC) vesicles were incubated on them. The results for testing the slightly negatively charged PCysMA, (with positively charged, 25% DOTAP lipids) showed the most successful bilayer formation on any of the brushes tested. The diffusion rate compared well with glass for which the diffusion rate, when using the same lipid composition, was $1.4 \mu\text{m}^2 \text{s}^{-1}$ (mobile fraction 92%). The most successful brush was a short, 7 nm (dry length) PCysMA brush, which, although in its neutral (zwitterionic) range at pH 7 exhibited a surface zeta potential of -10 mV .

			
PMPC	(b) PMAA	(c) PKSPMA	(d) PCysMA
12°	32°	24°	43°
-14 mV	-43 mV	-33 mV	-10 mV

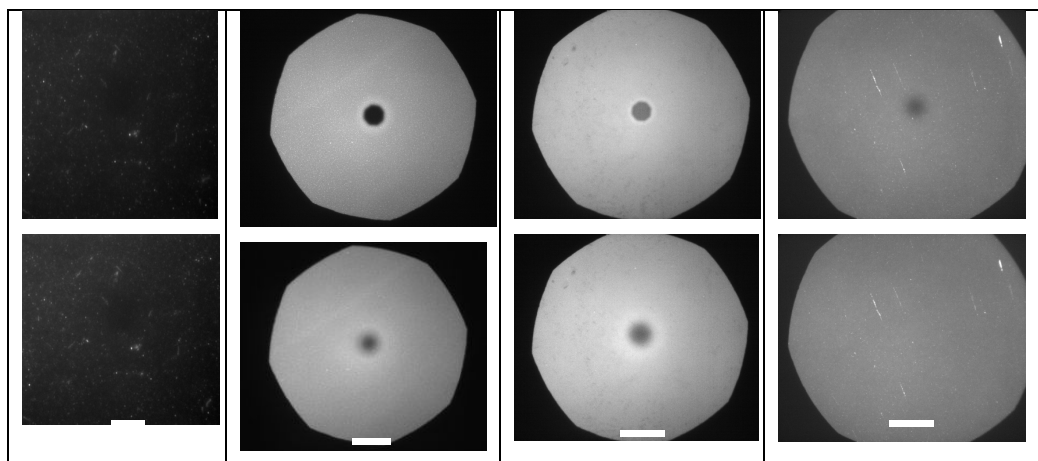


Figure 5.36: A summary of the structures, contact angles and surface zeta potentials of the four brushes, PMPC, PMAA, PKSPMA and PCysMA. Below there are two images, the top one at bleaching and below it after 5 minutes recovery. Scale bar 60 μm .

As the results had been generated by relying on an electrostatic interaction between the vesicles and the brush surfaces they could be discussed in terms of a “combined electrostatic potential”. This is the product of the zeta potentials of the lipids and the surface zetas potentials of the brushes. These charges are contributed to by the lipid headgroups: DOTAP lipid amine moieties, the POPC lipid amine and phosphate groups and those charged elements within the polymer chains which are sulphonate, carboxylate and amine functionalities. Figure 5.37 shows the zeta potentials in table form.

		Results of vesicle Incubation			
	zeta mV	POPC 1	10% DOTAP 25	25% DOTAP 43	50% DOTAP 64
PMPC	0	none	none	none	none
PCysMA	-10	none	none	bilayer $D > 1.0 \mu\text{m}^2 \text{s}^{-1}$	slow $D 0.1 < > 0.9 \mu\text{m}^2 \text{s}^{-1}$
PKSPMA	-33	none	immobile $D = 0 \mu\text{m}^2 \text{s}^{-1}$	very slow $D < 0.1 \mu\text{m}^2 \text{s}^{-1}$	very slow $D < 0.1 \mu\text{m}^2 \text{s}^{-1}$
PMAA	-43	none	immobile $D = 0 \mu\text{m}^2 \text{s}^{-1}$	very slow $D < 0.1 \mu\text{m}^2 \text{s}^{-1}$	
		Combined 'interaction potential'			
PMPC	0	0	0	0	0
PCysMA	-10	-15	-250	-430	-640
PKSPMA	-33	-33	-825	-1419	-2112
PMAA	-43	-43	-1075	-1849	-2752

Figure 5.37: Surface zeta of the brushes and zeta potentials of the lipids showing the result of the incubations for each combination of these (top). Below are the combined zeta potentials of the surface and vesicles.

Zwitterionic PMPC has a zero surface potential (0 ± 10 mV), which generates a limited electrostatic interaction potential of close to zero, with no lipids being adsorbed. PCysMA has a combined potential of -430 mV^2 , when using 25% DOTAP vesicles and this value creates a driving force for adsorption, creating a sufficiently high interaction force between the vesicles and the surface, without generating too high an inter-vesicle repulsion. Having adsorbed onto the brush surface the vesicles can fuse into a bilayer (Brisson pathway B) or remaining intact (pathway C, Figure 2.9).⁵³ For fusion to occur, the vesicles would need to interact with each other and create a deformation induced stress before rupture. The lipids in the vesicles, when initially attracted to the surface, contained an even distribution of positively charged DOTAP and zwitterionic POPC lipids arranged throughout the bilayer. It has been found in simulations that after approaching the surface, the positively charged lipids rearranged themselves to be closest to the negative charges of the polymer brush/substrate and the zwitterionic lipids would rearrange around the rest of the vesicle.¹³

With the inter-vesicle repulsion now minimised, fusion would be easier and may continue on one of the 'Brisson' pathways above. Movement of the vesicles and the forming of bilayer patches across the surface would facilitate this and bring intact vesicles in contact with the high energy edges of the newly formed bilayer patches, spreading the bilayer further across the surface.⁵⁶ This method has been demonstrated experimentally and with simulations, on solid surfaces, but it has not been proven that polymer brushes will also support this vesicle motion. According to Richter⁵⁶ the formation and interaction of bilayer patches, which are mobile across the surface are key to the formation of a good sealed bilayer. In this instance it is difficult to imagine how these patches may form in the same way on a soft polymer surface. This suggests that either the forming bilayer 'sensed' a more rigid surface (as the brushes are short at ~7 nm long) or there is a different mechanism in play whereby the vesicles rupture and fuse directly into a full bilayer. The third possibility was that the bilayer, although appearing to be homogenous under the microscope, was not sealing, had many defects and may have been composed of many unfused bilayer patches. The fact that a good diffusion coefficient and mobile fraction were measured would, however, suggest that the bilayer was of good quality. The testing of the impedance, had it been successful, would have confirmed this.

However, the process was not completed on PCysMA without a high temperature to induce bilayer formation. This was initially attributed to the slight swelling behaviour of the vesicles when heated. In addition to this mechanism, a conformational change in the brush on heating could be taking place as suggested by the results of the contact angle measurements (Figure 5.14) and the work published by Huck *et al.*³⁰ Their brush, PMEDSAH, is a sulfobetaine and is zwitterionic. As the PCysMA brush is also zwitterionic it is logical to assume that the positive and negative charges between chains will interact, effectively neutralizing these charges. Huck found that when heating the brush the contact angle reduced (from 79° at 22 °C to 58° at 52 °C), indicating that it had become more hydrophilic. The reason they proposed for this was that the heating had enabled the interactions between the charged elements on the chains to be broken. The PCysMA brushes exhibited a similar change in contact angle when heated (from 43° at 25 °C to 28° at 50 °C). This could allow vesicles to be attracted sufficiently well to the brush surface, but not to be immobilized as is the case with the high negative charges presented by the PMAA and PKSPMA chains. Additionally, the change in configuration of the PCysMA chain could physically disrupt and stress the vesicles when combined with their slight swelling at 50°C, allowing fusion and bilayer formation to take place.

AFM images and breakthrough force measurements confirmed the formation of a bilayer on PCysMA. The AFM height images (Figure 5.21 (b)) and the breakthrough force curve (Figure 5.21 (c)) both confirmed that the brush remained in its swollen, or more strictly a 2/3 swollen, state and that the bilayer was located on top of the brush.

Referring once again to the table of interaction potentials (Figure 5.37) it can be seen that as the brush-vesicle interaction potentials are increased further to $>800 \text{ mV}^2$, by introducing the acidic brushes PMAA and PKSPMA, less favourable results were observed. Immobile lipid layers were seen with 10% DOTAP, (>800 and $<1200 \text{ mV}^2$). A different result, a homogenous layer with some very slow mobility (FRAP diffusion rates of $<0.1 \mu\text{m}^2 \text{ s}^{-1}$) was observed when using 25% DOTAP ($>1400 \text{ mV}^2$). These two results are particularly interesting to explain. It is possible that re-arrangement of positively charged lipids in the vesicles close to the (negative) polymer surface could be taking place at 10% DOTAP, but with fewer charged lipids in the vesicles, this process causes insufficient deformation of the vesicles to drive fusion. At the higher charge ($>1400 \text{ mV}^2$) however, there are a number of possibilities. Firstly, there could be a layer of vesicles bound to the surface, which are slowly mobile, though, because of the high charge, it is unclear why they would be mobile. Alternatively, there could be a layer of vesicles, where the charged lipid species are attracted to the surface leaving the (slightly negative) dipoles of the POPC lipids available to attract a second layer of vesicles where the top layer is slowly mobile. Or, thirdly, a bilayer forms which is tethered by the positive charges to the negative surface and a second bilayer forms on top, similar to that seen for PCysMA in Figure 5.19 (b). One of these variants could also apply to the case for the interaction potential of -640 mV^2 specifically for 50% DOTAP vesicles on PCysMA. A homogenous layer was observed with mobility of between >0.1 and $<1.0 \mu\text{m}^2 \text{ s}^{-1}$ in this case, which could be to be the result of a double-bilayer.

To add further insight into these intriguing results the literature was reviewed for research where, rather than producing bilayers on polymer brushes, the interactions between vesicles and bilayer membranes were specifically studied, in the field of polymeric drug delivery vectors. Karam *et al.*,⁵⁷ followed the changes in emission spectra during the interaction of conjugated polyelectrolytes with a carboxylate group on the chain (anionic polymers) with cationic (DOTAP:POPC) lipids. They found that the anionic polymers were attracted electrostatically to the DOTAP lipids and to the DOPC to some degree, but they also inserted into the hydrophobic core, aiding the fusion of the vesicles. Xie *et al.*⁵⁸ studied

the interactions between weakly anionic PELs and DMPC, which they considered to be weakly cationic by virtue of the fact that the terminating tertiary amine of the headgroup was located a few angstroms above the negative phosphate. (This disagrees with Knecht's²¹ view of the headgroup, above). Xie recognised that strong interactions between polymers and membranes had been exploited in the field of drug research, but considered that a balance of weaker charges could create a different scenario where the polymer-lipid changes the local bending rigidity and spontaneous curvature of the membranes.

To summarise: two zwitterionic polymer brushes, PMPC, and PCysMA which incorporates a cysteine moiety, have been tested for their ability to support a fluid bilayer. The PMPC does not interact with lipids, but the PCysMA supports a homogeneous fluid bilayer when incubated with cationic vesicles composed of 25% DOTAP:POPC. Though technically zwitterionic, the PCysMA displays a slightly negative surface zeta potential, which may be the result of the charge influence of the surface (SAM) initiated glass substrate. When this is combined with positively charged vesicles there is a balanced interaction which supports vesicle deposition and fusion. A bilayer results, with a good diffusion coefficient and mobile fraction, comparable to that on glass. When depositing similar vesicles onto a more highly charged anionic brushes, PMAA and PKSPMA, vesicular layers are formed, with no fusion. This suggests that a narrow range of interaction potentials between the brush and the lipids is important in generating a good polymer supported bilayer for this system.

This work contributes to the knowledge of the interactions between lipids/bilayers and polymers and satisfies the project requirements for the collaboration by creating a "polymer supported lipid bilayer". It has generated many interesting questions, particularly in relation to the systems where greater interaction potentials are present which formed slower moving lipid layers or vesicular layers on the highly charged polymers. Further work to investigate the intriguing nature of the samples with what appear to be double bilayers would further increase the knowledge of the interactions between lipids and polymers, which has many applications. The successful PCysMA system has now been published in *Langmuir* and was taken forward, as discussed in the next chapter, to attempt to incorporate transmembrane proteins.

5.10. References

1. Matyjaszewski, K., Xia, J. H., Atom transfer radical polymerization. *Chemical Reviews* **2001**, *101*, 2921-2990.
2. Cheng, N., Brown, A. A., Azzaroni, O., Huck, W. T. S., Thickness-dependent properties of polyzwitterionic brushes. *Macromolecules* **2008**, *41*, 6317-6321.
3. Rehfeldt, F., Steitz, R., Armes, S. P., von Klitzing, R., Gast, A. P., Tanaka, M., Reversible activation of diblock copolymer monolayers at the interface by pH modulation, 2: membrane interactions at the solid/liquid interface. *The Journal of Physical Chemistry B* **2006**, *110*, 9177-9182.
- ⁴ Liu, Q.; Singh, A.; Liu, L., Amino Acid-Based Zwitterionic Poly (serine methacrylate) as an Antifouling Material. *Biomacromolecules* **2012**, *14* (1), 226-231.
- ⁵ Yameen, B.; Ali, M.; Neumann, R.; Ensinger, W.; Knoll, W.; Azzaroni, O., Single conical nanopores displaying pH-tunable rectifying characteristics. Manipulating ionic transport with zwitterionic polymer brushes. *Journal of the American Chemical Society* **2009**, *131* (6), 2070-2071.
- ⁶ de Groot, G. W.; Demarche, S.; Santonicola, M. G.; Tiefenauer, L.; Vancso, G. J., Smart polymer brush nanostructures guide the self-assembly of pore-spanning lipid bilayers with integrated membrane proteins. *Nanoscale* **2014**, *6* (4), 2228-2237.
- ⁷ Mennicke, U.; Salditt, T., Preparation of solid-supported lipid bilayers by spin-coating. *Langmuir* **2002**, *18* (21), 8172-8177.
- ⁸ Li, X.; Wang, R.; Tang, C.; Vararattanavech, A.; Zhao, Y.; Torres, J.; Fane, T., Preparation of supported lipid membranes for aquaporin Z incorporation. *Colloids and Surfaces B: Biointerfaces* **2012**, *94*, 333-340.
- ⁹ Morigaki, K.; Kimura, S.; Okada, K.; Kawasaki, T.; Kawasaki, K., Formation of substrate-supported membranes from mixtures of long-and short-chain phospholipids. *Langmuir* **2012**, *28* (25), 9649-9655.
- ¹⁰ Chiantia, S.; Kahya, N.; Schwille, P., Raft domain reorganization driven by short-and long-chain ceramide: a combined AFM and FCS study. *Langmuir* **2007**, *23* (14), 7659-7665.
- ¹¹ Cremer, P. S.; Boxer, S. G., Formation and Spreading of Lipid Bilayers on Planar Glass Supports. *The Journal of Physical Chemistry B* **1999**, *103* (13), 2554-2559.
- ¹² Cha, T.; Guo, A.; Zhu, X.-Y., Formation of supported phospholipid bilayers on molecular surfaces: role of surface charge density and electrostatic interaction. *Biophysical journal* **2006**, *90* (4), 1270-1274.

-
- ¹³ Dimitrievski, K.; Kasemo, B., Simulations of lipid vesicle adsorption for different lipid mixtures. *Langmuir* **2008**, *24* (8), 4077-4091.
- ¹⁴ Seantier, B.; Kasemo, B. Influence of mono- and divalent ions on the formation of supported phospholipid bilayers via vesicle adsorption. *Langmuir* **2009**, *25* (10), 5767–5772.
- ¹⁵ Zhu, T.; Jiang, Z.; Nurlybaeva, E. M. R.; Sheng, J.; Ma, Y., Effect of osmotic stress on membrane fusion on solid substrate. *Langmuir* **2013**, *29* (21), 6377-6385.
- ¹⁶ Dimitrievski, K.; Reimhult, E.; Kasemo, B.; Zhdanov, V. P. Simulations of temperature dependence of the formation of a supported lipid bilayer via vesicle adsorption. *Colloids Surf., B* **2004**, *39* (1), 77–86.
- ¹⁷ Pan, J.; Tristram-Nagle, S.; Kučerka, N.; Nagle, J. F., Temperature dependence of structure, bending rigidity, and bilayer interactions of dioleoylphosphatidylcholine bilayers. *Biophysical journal* **2008**, *94* (1), 117-124.
- ¹⁸ Cho, N.-J.; Frank, C. W., Fabrication of a planar zwitterionic lipid bilayer on titanium oxide. *Langmuir* **2010**, *26* (20), 15706-15710.
- ¹⁹ Gurtovenko, A. A.; Vattulainen, I., Effect of NaCl and KCl on phosphatidylcholine and phosphatidylethanolamine lipid membranes: insight from atomic-scale simulations for understanding salt-induced effects in the plasma membrane. *The Journal of Physical Chemistry B* **2008**, *112* (7), 1953-1962.
- ²⁰ Pandit, S. A.; Bostick, D.; Berkowitz, M. L., Molecular dynamics simulation of a dipalmitoylphosphatidylcholine bilayer with NaCl. *Biophysical journal* **2003**, *84* (6), 3743-3750.
- ²¹ Knecht, V.; Klasczyk, B., Specific binding of chloride ions to lipid vesicles and implications at molecular scale. *Biophysical journal* **2013**, *104* (4), 818-824.
- ²² Pokorna, S.; Jurkiewicz, P.; Cwiklik, L.; Vazdar, M.; Hof, M., Interactions of monovalent salts with cationic lipid bilayers. *Faraday discussions* **2013**, *160*, 341-358.
- ²³ Makino, K.; Yamada, T.; Kimura, M.; Oka, T.; Ohshima, H.; Kondo, T., Temperature-and ionic strength-induced conformational changes in the lipid head group region of liposomes as suggested by zeta potential data. *Biophysical chemistry* **1991**, *41* (2), 175-183.
- ²⁴ Dimitrievski, K.; Kasemo, B., Simulations of lipid vesicle adsorption for different lipid mixtures. *Langmuir* **2008**, *24* (8), 4077-4091.
- ²⁵ Seifert, U.; Berndl, K.; Lipowsky, R., Shape transformations of vesicles: Phase diagram for spontaneous-curvature and bilayer-coupling models. *Physical Review A* **1991**, *44*, 1182.

-
- ²⁶ Reboiras, M. D.; Kaszuba, M.; Connah, M. T., & Jones, M. N. Measurement of Wall Zeta Potentials and Their Time-Dependent Changes Due to Adsorption Processes: Liposome Adsorption on Glass. *Langmuir*, **2001**, *17*(17), 5314-5318
- ²⁷ Discussion with Prof. S P Armes, University of Sheffield Polymer group.
- ²⁸ Alswieleh, A. M.; Cheng, N.; Canton, I.; Ustbas, B.; Xue, X.; Ladmiraal, V.; Xia, S.; Ducker, R. E.; El Zubir, O.; Cartron, M. L., Zwitterionic Poly (amino acid methacrylate) Brushes. *Journal of the American Chemical Society* **2014**.
- ²⁹ Liu, Q.; Singh, A.; Liu, L., Amino Acid-Based Zwitterionic Poly(serine methacrylate) as an Antifouling Material. *Biomacromolecules* **2012**, *14*, 226-231.
- ³⁰ Azzaroni, O.; Brown, A. A.; Huck, W. T., UCST Wetting Transitions of Polyzwitterionic Brushes Driven by Self-Association. *Angewandte Chemie* **2006**, *118*
- ³¹ Poly (N,N'-dimethyl-(acrylamido propyl) ammonium propane sulfonate) (PDMAAPS)
- ³² Blakeston, A. C.; Alswieleh, A. M.; Heath, G. R.; Roth, J. S.; Bao, P.; Cheng, N.; Armes, S. P.; Leggett, G. J.; Bushby, R. J.; Evans, S. D., New Poly (amino acid methacrylate) Brush Supports the Formation of Well-Defined Lipid Membranes. *Langmuir* **2015**, *31* (12), 3668-3677. The video sequence is available in the supplementary information to this paper.
- ³³ Parker, J. L.; Christenson, H. K.; Ninham, B. W., Forces between bilayers of a cationic surfactant with hydroxylated headgroups: effects of interbilayer adhesion on the interactions. *The Journal of Physical Chemistry* **1988**, *92* (14), 4155-4159.
- ³⁴ Takeda, S.; Yamamoto, K.; Hayasaka, Y.; Matsumoto, K., Surface OH group governing wettability of commercial glasses. *Journal of Non-crystalline Solids* **1999**, *249*, 41-46.
- ³⁵ Morse, A. J.; Edmondson, S.; Dupin, D.; Armes, S. P.; Zhang, Z.; Leggett, G. J.; Thompson, R. L.; Lewis, A. L., Biocompatible polymer brushes grown from model quartz fibres: synthesis, characterisation and in situ determination of frictional coefficient. *Soft Matter* **2010**, *6* (7), 1571-1579.
- ³⁶ Chen, M.; Briscoe, W. H.; Armes, S. P.; Cohen, H.; Klein, J., Robust, biomimetic polymer brush layers grown directly from a planar mica surface. *ChemPhysChem* **2007**, *8* (9), 1303-1306.
- ³⁷ Edmondson, S.; Nguyen, N. T.; Lewis, A. L.; Armes, S. P., Co-nonsolvency effects for surface-initiated poly (2-(methacryloyloxy) ethyl phosphorylcholine) brushes in alcohol/water mixtures. *Langmuir* **2010**, *26* (10), 7216-7226.
- ³⁸ Nakai, K.; Morigaki, K.; Iwasaki, Y., Molecular recognition on fluidic lipid bilayer microarray corralled by well-defined polymer brushes. *Soft Matter* **2010**, *6* (23), 5937-5943.

-
- ³⁹ Santonicola, M. G.; de Groot, G. W.; Memesa, M.; Meszynska, A.; Vancso, G. J., Reversible pH-controlled switching of poly (methacrylic acid) grafts for functional biointerfaces. *Langmuir* **2010**, *26* (22), 17513-17519.
- ⁴⁰ Parnell, A. J.; Martin, S. J.; Jones, R. A.; Vasilev, C.; Crook, C. J.; Ryan, A. J., Direct visualization of the real time swelling and collapse of a poly (methacrylic acid) brush using atomic force microscopy. *Soft Matter* **2009**, *5* (2), 296-299.
- ⁴¹ Parnell, A. J.; Martin, S. J.; Dang, C. C.; Geoghegan, M.; Jones, R. A.; Crook, C. J.; Howse, J. R.; Ryan, A. J., Synthesis, characterization and swelling behaviour of poly (methacrylic acid) brushes synthesized using atom transfer radical polymerization. *Polymer* **2009**, *50* (4), 1005-1014.
- ⁴² Ramstedt, M.; Cheng, N.; Azzaroni, O.; Mossialos, D.; Mathieu, H. J.; Huck, W. T., Synthesis and characterization of poly (3-sulfopropylmethacrylate) brushes for potential an Basak, S.; Chattopadhyay, K., Studies of protein folding and dynamics using single molecule fluorescence spectroscopy. *Physical Chemistry Chemical Physics* **2014**, *16* (23), 11139-11149. tibacterial applications. *Langmuir* **2007**, *23* (6), 3314-3321.
- ⁴³ Lakowicz, J. R. *Principles of Fluorescence Spectroscopy*, 3rd ed. (Springer, New York, **2006**)
- ⁴⁴ Bao, P.; Cheetham, M. R.; Roth, J. S.; Blakeston, A. C.; Bushby, R. J.; Evans, S. D., On-Chip Alternating Current Electrophoresis in Supported Lipid Bilayer Membranes. *Analytical chemistry* **2012**, *84* (24), 10702-10707.
- ⁴⁵ Alswieleh, A.M.M., Micro- and Nano-Structure of Polymers and Molecular Materials. Ph.D. thesis, University of Sheffield, July **2014**.
- ⁴⁶ Stephan, M.; Mey, I.; Steinem, C.; Janshoff, A., Combining reflectometry and fluorescence microscopy: An assay for the investigation of leakage processes across lipid membranes. *Analytical chemistry* **2014**, *86* (3), 1366-1371.
- ⁴⁷ Schönherr, H.; Johnson, J. M.; Lenz, P.; Frank, C. W.; Boxer, S. G., Vesicle adsorption and lipid bilayer formation on glass studied by atomic force microscopy. *Langmuir* **2004**, *20* (26), 11600-11606
- ⁴⁸ Vo, C.-D.; Schmid, A.; Armes, S. P.; Sakai, K.; Biggs, S., Surface ATRP of hydrophilic monomers from ultrafine aqueous silica sols using anionic polyelectrolytic macroinitiators. *Langmuir* **2007**, *23* (2), 408-413.
- ⁴⁹ Ydens, I.; Moins, S.; Botteman, F.; Degée, P.; Dubois, P., Removal of copper-based catalyst in atom transfer radical polymerization using different extraction techniques. *e-Polymers* **2004**, *4* (1), 414-420.

-
- ⁵⁰ Aslan, K.; Gryczynski, I.; Malicka, J.; Matveeva, E.; Lakowicz, J. R.; Geddes, C. D., Metal-enhanced fluorescence: an emerging tool in biotechnology. *Current Opinion in Biotechnology* **2005**, *16* (1), 55-62.
- ⁵¹ Israelachvili, J. N., *Intermolecular and Surface Forces*. Elsevier Science: 2010. (Chapter 21)
- ⁵² Wu, H. L.; Chen, P. Y.; Chi, C. L.; Tsao, H. K.; Sheng, Y. J. Vesicle deposition on hydrophilic solid surfaces. *Soft Matter* **2013**, *9*, 1908–1919.
- ⁵³ Richter, R. P.; Bérat, R.; Brisson, A. R., Formation of solid-supported lipid bilayers: an integrated view. *Langmuir* **2006**, *22* (8), 3497-3505.
- ⁵⁴ Lind, T. K.; Cárdenas, M.; Wacklin, H. P., Formation of supported lipid bilayers by vesicle fusion: Effect of deposition temperature. *Langmuir* **2014**, *30* (25), 7259-7263.
- ⁵⁵ Jackman, J. A.; Choi, J.-H.; Zhdanov, V. P.; Cho, N.-J., Influence of osmotic pressure on adhesion of lipid vesicles to solid supports. *Langmuir* **2013**, *29* (36), 11375-11384.
- ⁵⁶ Richter, R.; Mukhopadhyay, A.; Brisson, A., Pathways of lipid vesicle deposition on solid surfaces: a combined QCM-D and AFM study. *Biophysical Journal* **2003**, *85*, 3035-3047.
- ⁵⁷ Karam, P.; Hariri, A. A.; Calver, C. F.; Zhao, X.; Schanze, K. S.; Cosa, G., Interaction of anionic phenylene ethynylene polymers with lipids: from membrane embedding to liposome fusion. *Langmuir* **2014**, *30* (35), 10704-10711.
- ⁵⁸ Granick, S., Phospholipid membranes as substrates for polymer adsorption. *Nature Materials* **2002**, *1* (2), 129-133.

6. Results 2. Transmembrane protein incorporation into a polymer supported lipid bilayer

6.1. Introduction

The aims of the collaboration project included exploring ways of incorporating proteins into structures at “*low-dimensions*”. These nanoscale structures would allow the functionality of light harvesting proteins of the *Rhodobacter Sphaeroides* to be studied both individually and as groups of proteins. The methods included creating corrals of patterned polymers that would isolate or group the proteins together, with the possibility to use electric fields to concentrate the proteins into confined locations. Other methods being explored were the tethering of proteins onto nanodots or onto polymer chains. Finally, the contribution of this project is to explore the incorporation of freely diffusing transmembrane proteins, specifically the cytochrome bc1 complex, into a bilayer on a polymer support. Cytochrome bc1 is associated with the light harvesting complexes I and II and the reaction centre. Its exact location in the membrane is not known, but its function is to oxidise QH₂ to quinone to generate a proton motive force.¹⁸

Having successfully prepared a suitable polymer support, with a bilayer consisting of 25% positively charged lipids, methods for incorporating proteins were explored. Three main challenges needed to be met. Firstly, few protein reconstitutions in the literature employed positively charged lipids, preferring instead to use negatively charged ones in common with the composition of naturally occurring cell membranes. Secondly, there was limited information in the literature specifically on the reconstitution of the *Rh. Sphaeroides* cytochrome bc1 complex. Thirdly, the proteins had to be orientated in a specific way in the polymer supported bilayer in order to maximise its functionality.

Initially, a published method was followed for incorporating proteorhodopsin (PRh) into lipid vesicles, as it reported the use of positively charged lipid vesicles with specific orientation of the protein.¹ A second published method was then followed which was used for incorporating cytochrome bo3, into a natural membrane.^{2 3} Cytbo3 is a similar protein to the target, Cytbc1. Despite their being elements of both methods which would lead to the successful incorporation of correctly oriented proteins in the required cationic vesicles they both required a detergent removal and protein reconstitution step. This process is notoriously difficult to achieve as there are no rules on which detergent and reconstitution method apply to a specific protein. With this in mind a third option was also explored wherein a *detergent depletion* method would be adapted to incorporate the protein

directly into solubilised multilamellar vesicles (MLVs) or a preformed lipid bilayer, without the need to reconstitute it into unilamellar lipid vesicles.

6.2. Attempted reconstitution of proteorhodopsin into cationic lipid vesicles

6.2.1. Introduction and method

When studying the incorporation of proteorhodopsin (PRh) into lipid vesicles Tunuguntla and co-workers¹ proposed to utilise the fact that the PRh 'N terminal' contained negatively charged residues and the 'C terminal', positively charged ones. They reported that PRh inserted into a positively charged vesicle with its positive C terminal on the outside. When reconstituting into a negatively charged vesicle the N terminal faced to the outside as shown in Figure 6.1. This potentially provided an easy method of reconstituting PRh into a 25% DOTAP vesicle with the correct orientation. The best available structure of PRh from the Protein Data Bank is shown in Figure 6.1, but there is no detail here that indicates where the N and C termini are located. However, Tunuguntla used protein lysis to demonstrate the location and orientation of these groups.

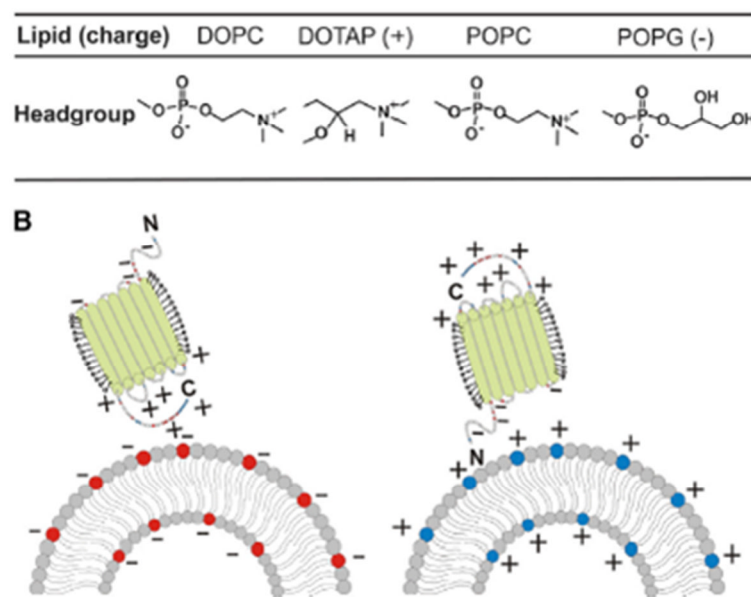


Figure 6.1: Schematic of the cationic (DOTAP) and anionic (DOPG) vesicles showing the direction of insertion of PRh (left). Inset (right) is the Protein Data Bank schematic of the PRh protein structure.¹

The dried lipids, composed of 20% DOTAP:POPC or 20% DOPG:POPC, were rehydrated with 10 mM HEPES buffer at pH 6.2 into which 5(6) Carboxyfluorescein (CF) had been dissolved.

The resulting multilamellar vesicles were extruded to form unilamellar vesicles using a 200 nm polycarbonate membrane.

Using a UV-vis fluorimeter the sample of the vesicles was then illuminated with 490 nm and 460 nm light and the emission intensity, captured at 530 nm, was measured and calculated as a ratio. (The ratio: emission at 530 nm after illuminating at 490 nm divided by the emission at 530 nm after illuminating at 460 nm). The results were plotted graphically over a pH range of 4 to 8 as shown in Figure 6.2 and confirmed to be similar to those reported in the literature by other groups^{4 5} (Tunuguntla did not report the calibration curve in their paper).

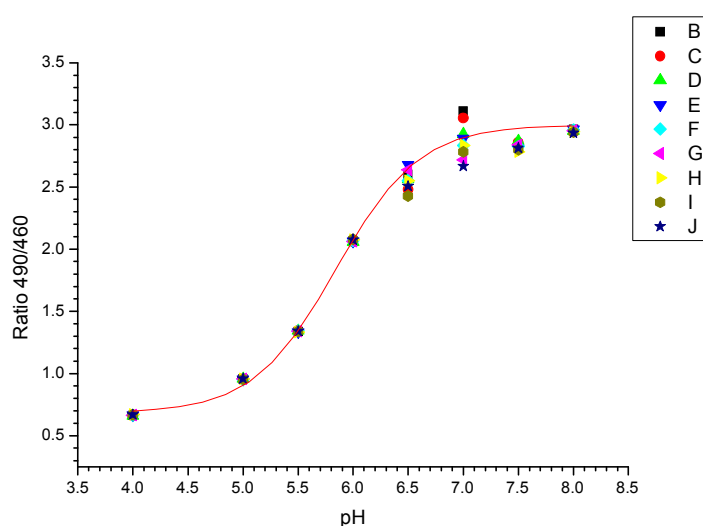


Figure 6.2: Calibration graph for 5(6) Carboxyfluorescein (CF), plotting pH against the emission ratio at 530 nm after irradiating with light at 490 and 460 nm. (The inset grid indicates the run number).

The remaining vesicles were incubated with β DDM to solubilise them, after which the protein (PRh) was added, which was expected to insert into the bilayer of the vesicles. The detergent was removed using Biobeads, followed by dilution into HEPES at pH 6.8. After this protein incorporation process, the proteoliposomes were irradiated to facilitate proton pumping. A change in emission wavelength, if successfully detected, would correlate with a change in pH, read from the calibration graph. This in turn would indicate that the PRh was functioning and protons were pumping either from inside to outside the vesicle, or vice versa.

6.2.2. Results and discussion

The protocol, which takes 3 to 4 days to complete, was repeated three times. Figure 6.3 shows a typical result. The DOPG vesicles appear, by eye, to contain PR, as indicated by the characteristic pink colour of the protein; however, the DOTAP vesicles do not show such a positive result.

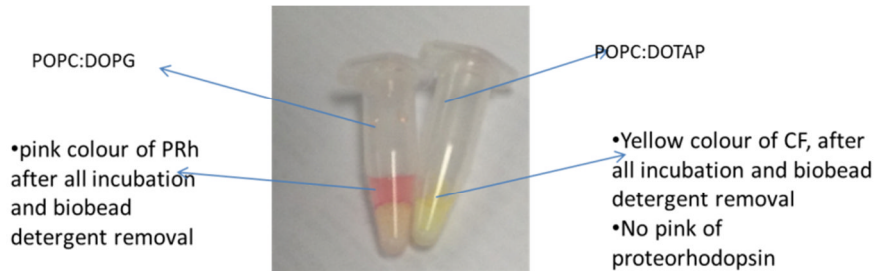


Figure 6.3: Photograph of the vials of liposomes after encapsulating CF, inserting PRh and removing the detergent with Biobeads. The yellow colour indicates that CF is present and the pink indicates that PRh is present. The results indicate that the protein is present in the POPC:POPG sample, but not in the DOPC:DOTAP sample.

For both samples the initial emission ratio/pH readings were taken before any irradiation, column 2 in Figure 6.4. The samples were irradiated for a period of 10 min and the emission/pH ratios reported again. No changes, from the initial readings of pH 6.2, were observed for the measurements of pH taken after irradiating the PRh in the DOTAP vesicles. This result which is not surprising as there did not appear to be any indication of the presence of the characteristic pink colour of PRh in the sample.

Reading at Time (min)	I_{490}/I_{460} No illumination ratio (pH)	I_{490}/I_{460} 10 min illumination (pH)
POPC:DOPG		
0	2.43 (6.2)	2.8 (7.0)
5		2.9 (7.0)
10	2.44 (6.2)	2.5 (6.3)
15		2.43 (6.2)

Figure 6.4: Emission ratio readings for DOPG vesicles after incorporating PRh, before and after illuminating for 10 min.

The result where the PRh had been attempted to be incorporated into DOPG:POPC vesicles did look more positive and changes were seen in the measurements to record the change in pH after irradiation of the PRh, as shown in column three of the grid above. There

appeared to be a change in the pH to 7 from the initial value of 6.2, after irradiating for 10 min which decayed back to the original value after 15 minutes. No change was seen when irradiating for a period of less than 10 min. This 'decay' of the reading after 10 minutes would suggest the vesicles may not be sealed and that the CF was leaking out of imperfections in the vesicle bilayer. Unfortunately this change in pH result was obtained on only one occasion and could not be repeated.

After discussing these results with the biochemists of the group, it was concluded that the DOTAP vesicles did not incorporate the PRh protein. Indeed it was discovered that the method reported in the paper did not show that calcium was actually used to facilitate this process. It was also considered that, despite observing a change in pH when the protein was incorporated into DOPG vesicles, the one observation could not be relied upon as evidence of the method being successful.

Furthermore, it was very likely that the solubilisation process would create points of leakage for the CF from the vesicles at the same time as allowing the protein to insert. Additionally the proteorhodopsin, if it did insert, may have done so in a random configuration, pumping protons both into and out of the vesicle.

Finally, it was suggested by Liphardt,⁶ that PRh becomes light responsive (proton pumping) during oxygen depletion. If this is the case, and that it only functions in an oxygen depleted environment, then our protocol should have included anaerobic conditions.

It was thus concluded that much more work and careful analysis would be required at each stage before this method could be used.

6.3. Attempted reconstitution of Cytb03 into cationic vesicles

6.3.1. Introduction and method

A successful protocol for incorporating Cytb03 into lipid vesicles was developed in Leeds and this was used for the next study. The protein was originally reconstituted into *E.coli* vesicles for electrochemical studies and this adapted method, originally from Verkhovskaya *et al.*,² was followed as a first step. It was then changed so that the *E.coli* vesicles were substituted for 25% DOTAP vesicles.

Briefly, the method (explained in full in chapter 4) used, firstly, natural *E.Coli* dried lipids, then lipids of 25% DOTAP:POPC. These were rehydrated with MOPS buffer to create a cloudy suspension of multilamellar vesicles. To this was added a small amount of octylglucoside (OG) detergent. A UV-vis spectrum was taken as the background reading. Cytb03 was added, in a 1% w/w ratio with lipid at 3.6mg/mL, and incubated for 15 min. The UV spectrum was taken again. Biobeads were used to remove the detergent and the result

was centrifuged at high speed for 1 hour. The resulting pellet was redissolved in buffer and centrifuged again at slower speed. On one sample the presence of the protein in the liposomes was confirmed by adding OG detergent to release the protein and taking a further UV-vis spectrum. After confirming the presence of the protein in the vesicles (using the UV vis method) a sample of the proteoliposomes was incubated onto glass. The diffusion coefficients of the bilayers were tested, using FRAP and the result was examined using AFM. The preparation process was then repeated with the aim of incubating the proteoliposomes onto PCysMA brushes.

6.3.3. Results and discussion

The incorporation of cytb03 into *E.coli* vesicles worked well and approximately 37% of the protein, as measured by the change measured levels of UV-vis absorption at 408 nm, was calculated to be incorporated. This was in line with expectations.⁷ When 25% DOTAP:POPC vesicles were substituted for *E.coli* vesicles the ratio was lower, at 17%, but still showed a positive result. The results are shown graphically in Figure 6.5.

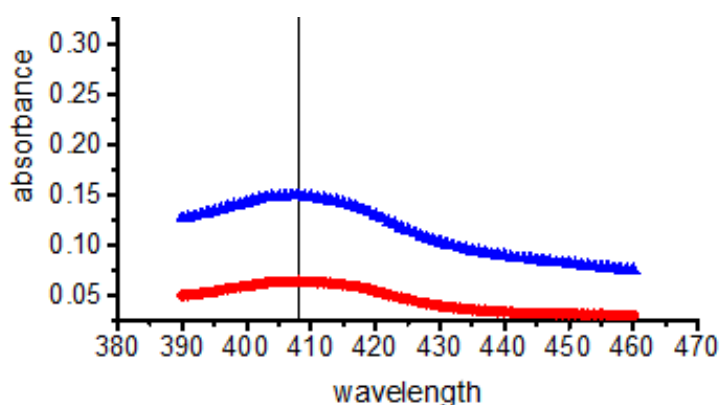


Figure 6.5: Plot of absorbance against wavelength showing back ground (black), absorbance of cytb03 in *E.coli* (blue) and cytb03 in 25% DOTAP:POPC vesicles. In *E.coli* ~37% of the protein was incorporated; in 25% DOTAP this measure was lower at 17%. The line shows the 408 absorbance line, characteristic of cytb03.

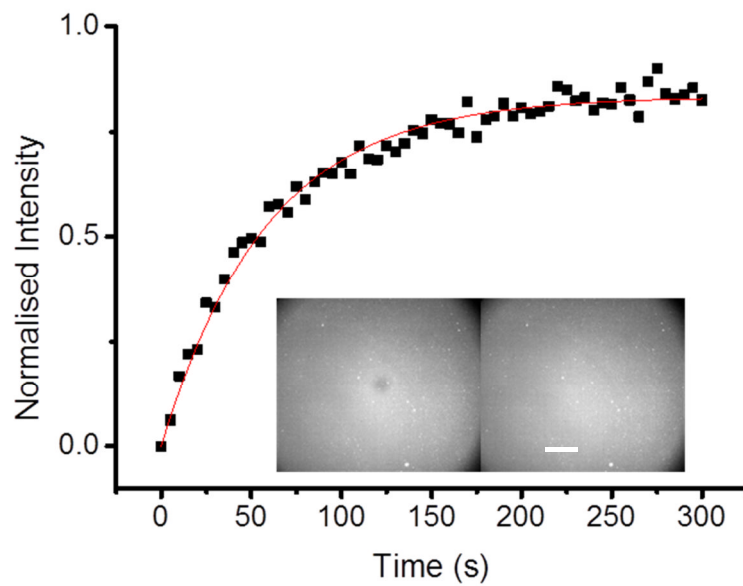


Figure 6.6: Fluorescence recovery plot of a 25% DOTAP:POPC lipid bilayer incorporating cytb3 incubated on glass coverslip. Images are inset which were taken at bleaching and after 5 min of fluorescence recovery. Scale bar is 60 μm .

The proteoliposomes were then incubated onto piranha cleaned glass coverslips and the results examined using FRAP. The images in Figure 6.6 show good fluorescence and the second image clearly shows the recovery of the bleached spot. From the diffusion plot a diffusion coefficient of $1.1 \mu\text{m}^2 \text{s}^{-1}$ and a mobile fraction of 86% were calculated. The surface of the bilayer was not as homogenous as would be expected with lipids on glass, but this may be a result of the diffusion being hindered by the presence of the protein. The sample was then scanned using AFM in an attempt to confirm the presence of a bilayer and protein.

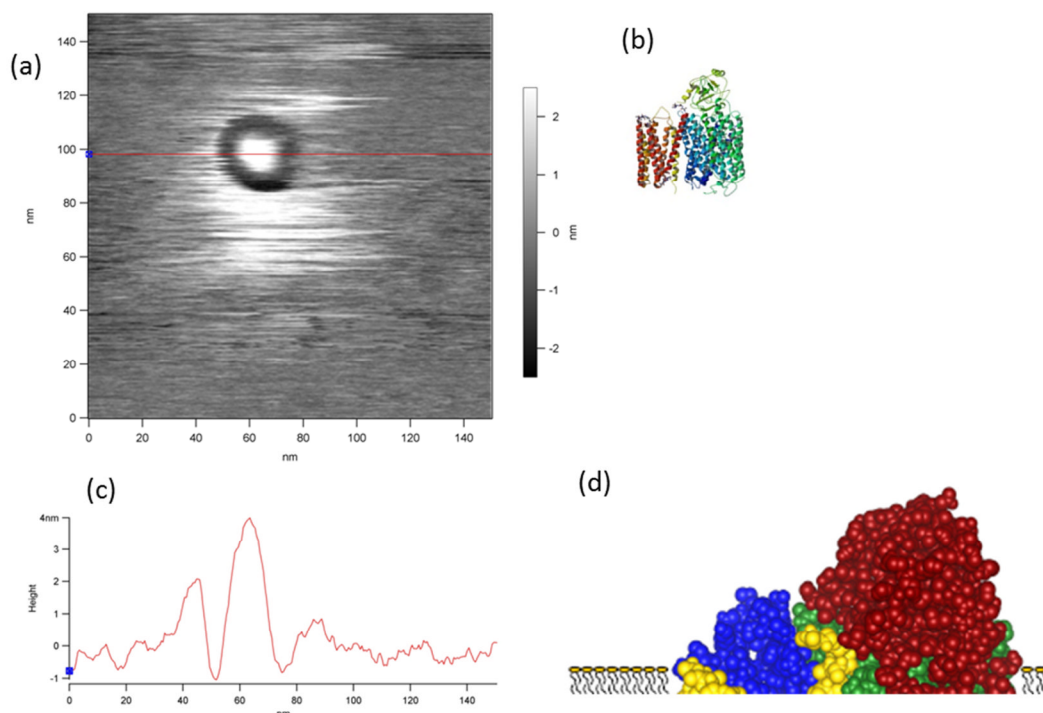


Figure 6.7: Top left (a) is the AFM height scan of the cytb₀₃, with (b) the PDB structure of it. Below in (c) is the surface scan height measurement and (d) a schematic of the top of the protein in a bilayer.

The AFM scan, in Figure 6.7 (a) (performed by Khizar Sheikh) showed a good, smooth bilayer with deformations within it consistent with the presence of the Cyt bo₃. The height scan, Figure 6.7 (c) shows a peak at 4 nm above the level of the bilayer, which correlates with the known height (Figure 6.7 (d) of the protruding (red area) top of the protein. On each side of the peak were annuli which are caused by deformations of the bilayer lipids by the protein.⁸ Also in Figure 6.7 (c), to the left, is another peak which corresponds to the blue area of the schematic, Figure 6.7 (d), of the protein in a bilayer. This AFM image taken with the FRAP recovery curve provided fairly convincing evidence of the presence of the protein in a bilayer suggesting this method may be useful to incubate similar proteoliposomes onto a PCysMA brush.

The next stage of the process was to incubate similar proteoliposomes onto a PCysMA polymer brush. The FRAP images of the results for this are presented in Figure 6.8. They

show a very slowly recovering bilayer.

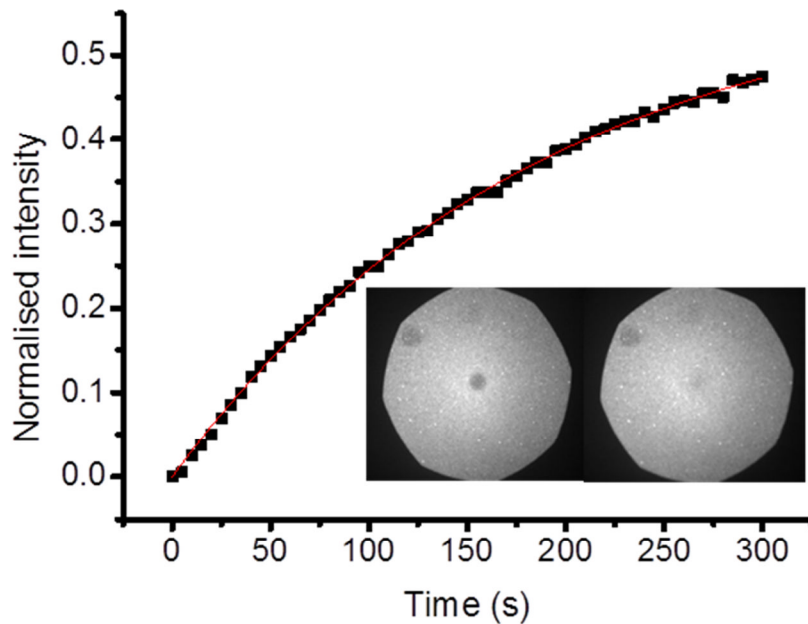


Figure 6.8: FRAP recovery curve of 25% DOTAP:POPC lipid vesicles containing Cyt b03 incubated on a short (7nm) PCysMA brush.

These images show a vesicular surface with a very slow recovery (diffusion) rate of the bleached spot ($0.33 \mu\text{m}^2 \text{s}^{-1}$) and a low mobile fraction (59%) compared to the high diffusion rates seen in Figure 6.6. It is possible that the method of incubating the vesicles, at 50°C , or the presence of the proteins themselves have slowed the diffusion rate. Aspects of this method did appear to work well and future work would include repeating this process.

6.4. The use of short chain lipids or detergent depletion for direct reconstitution of proteins into a bilayer

6.4.1. Lipid bilayer formation using short chain lipids

6.4.1.1. Introduction and methods

There have been a number of interesting publications^{9 11 12} which suggested that short chain lipids, such as 1,2-hexanoyl-sn-glycero-3-phosphocholine (DHPC-C6), in combination with long chain lipids like POPC, DOTAP or DOPG, produced bicelles, rather than vesicles. These bicelles can be formed either by tip sonication or extrusion. It has been further suggested that the DHPC-C6 acts as a mild detergent to solubilise the vesicles so that bilayers formed more easily than when the long-chain variant was used alone. The short chain lipids, being soluble in water, would be removed during the rinsing protocol which

followed lipid vesicle (or bicelle) incubation on the substrate. The presence of the short chain, detergent-like, molecules in conjunction with the long chain lipids was anticipated to facilitate the incorporation of transmembrane proteins into the bicelle or directly into the bilayer, before rinsing.^{9 10}

It had been suggested, by Hauser and others,^{11 12 13} that the bicelle structures are either layers of two bilayers with short chain lipids inserted at the long edges, as can be seen in Figure 6.9., or that they may take the form of elongated bilayer patches with a rim of detergent surrounding the bilayer core in the form of a nanodisc.

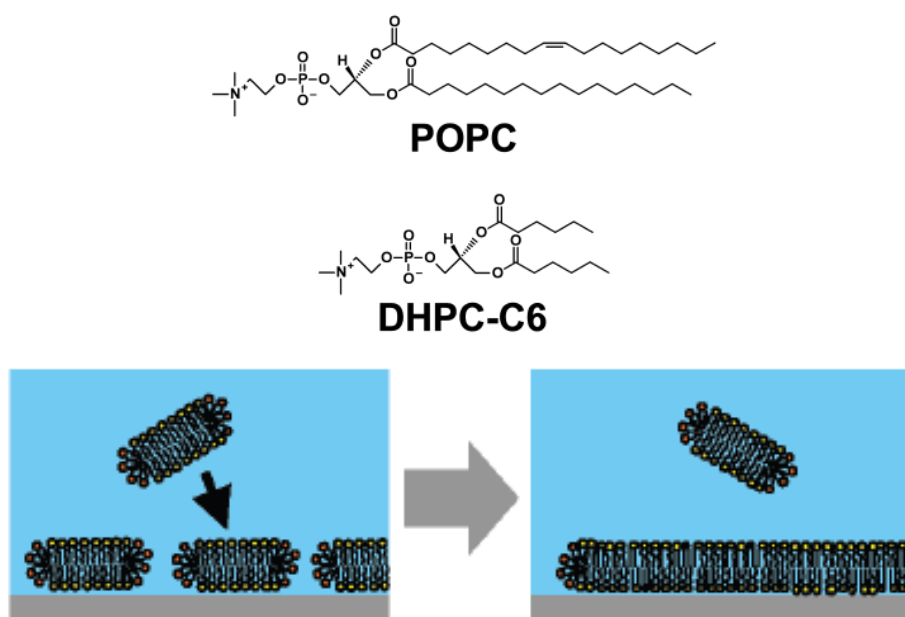


Figure 6.9: Shows the structure of the long chain lipid POPC and short chain DHPC-C6 with a schematic of the expected structure of the bicelle leading to bilayer formation on glass. Images obtained from⁹.

The bicelles chosen for testing were prepared by drying POPC or 25 mol % DOTAP:POPC or 50 mol % DOTAP:POPC, with DHPC-C6 and reconstituting in buffer before tip sonication. The ratio used of long chain to short chain lipid was approximately 50:50 and the final concentration for all lipids in buffer was 0.5 mg/mL, as detailed in Chapter 4. The bilayer formation methods were exactly the same as those used previously for forming bilayers on glass and PCysMA and took place in a flow cell at room temperature or at 50 °C.

6.4.1.2. Results and discussion

After successfully creating bilayers on glass, which showed similar characteristics to bilayers on glass without DHPC-C6, vesicles which included DHPC-C6 were incubated onto a short PCysMA brush of 7 nm (dry thickness). The homogeneity of the bilayers and the diffusion

coefficients were very similar to those reported in chapter 5 when similar lipids were used without the addition of DHPC-C6. Shown below in Figure 6.10., are the diffusion plots together with images at bleaching and after 5 min recovery time, for “25% DOTAP-C6” and “50% DOTAP-C6”. The cationic lipid component was 25% DOTAP in Figure 6.10 (a), where the graph shows a good diffusion coefficient of $1.4 \mu\text{m}^2 \text{s}^{-1}$, however the mobile fraction is low at 76% and the surface not very homogeneous. The lower graph, Figure 6.10 (b), shows the case where DOTAP constituted 50% of the long chain component. The diffusion coefficient of the bilayer in Figure 6.10 (b) was much slower at $0.3 \mu\text{m}^2 \text{s}^{-1}$ and the mobile fraction was 85%. This result was very much in line with the result for “50% DOTAP” shown in Chapter 5, where no DHPC-C6 was included, but showed no significant improvement over it. In the latter example (in Chapter 5) the slower diffusion was attributed to either a possible double bilayer or the result of unruptured vesicles on the PCysMA surface. As shown here, the use of the short chain lipids would be expected to solubilise the lipids and not be expected to support the formation of a vesicular layer on the PCysMA brush. This may suggest that the previous slow diffusion rate in Chapter 5 was the result of a second bilayer when the highly charged 50% DOTAP vesicles were incubated on the PCysMA brushes. AFM was not performed on the sample but, in hindsight, it would have been helpful in determining the nature of the adsorbed layer.

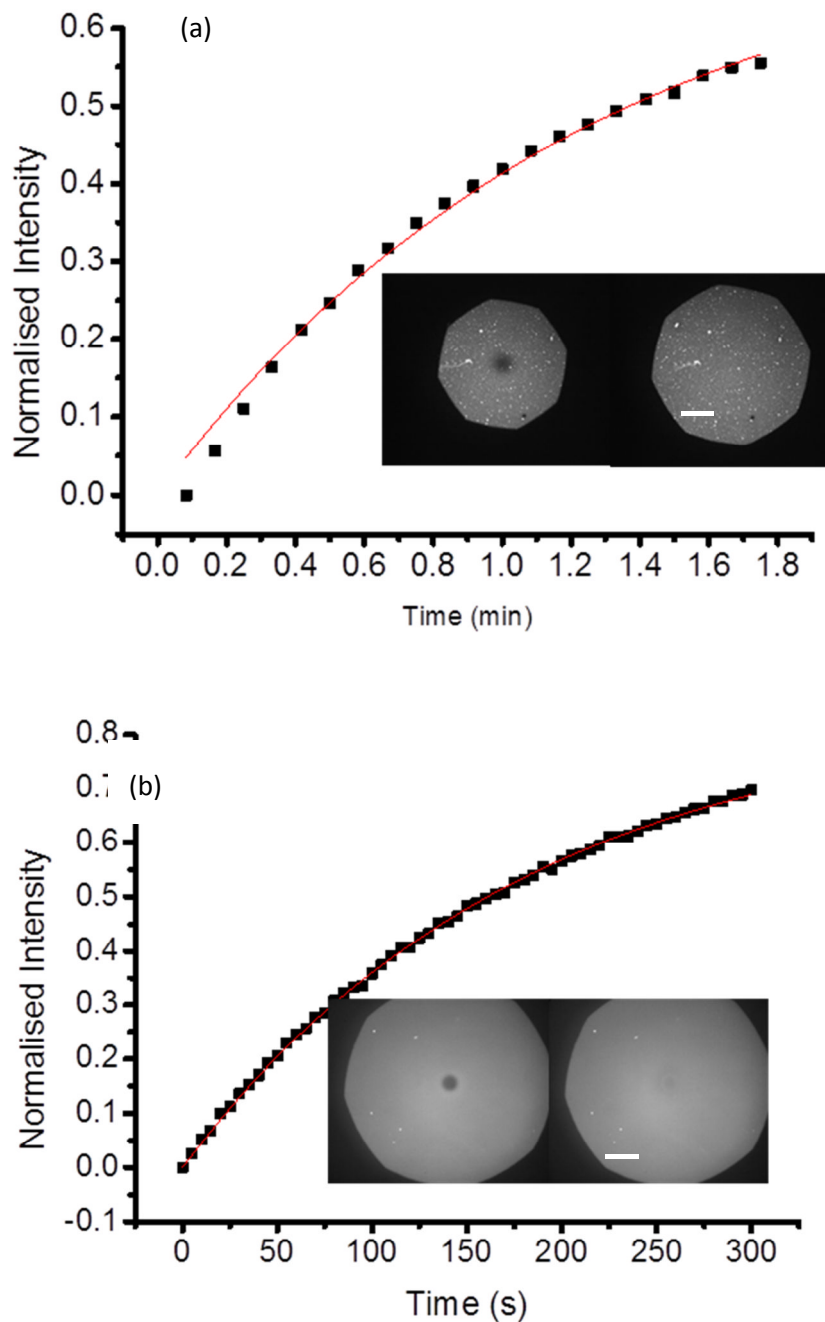


Figure 6.10: 50:50 mixture of long (DOTAP:POPC) and short chain (DHPC-C6) lipids incubated on a 7 nm PCysMA brush. Inset, are the images at bleaching and after 5 min. (a) has a 25:75 ratio of DOTAP:POPC and (b) 50:50 ratio of DOTAP:POPC. Scale bars 60 μm .

In summary, bilayers can be formed by incubating a mixture of long and short chain lipids onto glass or PCysMA. During the incubation period it was expected that the bicelles, if that was in fact the structure, were adsorbed and possibly solubilised by the DHPC-C6. The DHPC-C6 would then be rinsed away, releasing the long chain lipids to fuse into a homogeneous bilayer on the substrate (glass or polymer). The result did indicate that a

bilayer had formed with good diffusion, though the results were inferior to those obtained without the short-chain lipid. However, the method could be developed to aid the incorporation of a protein into the bilayer, by using the short-chain lipid to solubilise the membrane.

6.4.2. Lipid bilayer formation using β DDM detergent solubilised mixed micelles

6.4.2.1. Introduction and methods

As demonstrated above, the use of detergent-like molecules as part of the lipid composition showed some positive results when incubated onto glass and the PCysMA brush. However, whilst this method was being investigated it was found, during the purification of cytbc1, that β DDM was the only detergent in which the protein was not denatured.¹⁴ Whilst it was possible that this denaturing may be reversed after the protein was reconstituted into a bilayer using a different detergent, it was preferable to maintain its functionality by keeping it in β DDM. It was therefore necessary to establish a detergent depletion method which utilised this specific detergent rather than the DHPC-C6.

Briefly, the method used was adapted from Vacklin¹⁵ and Lee¹⁶ as reported in chapter 4. Multilamellar vesicles (MLVs) were prepared from dried long chain lipids (25% DOTAP:POPC) reconstituted into 10 mM phosphate buffer at high concentration (2 mg/mL) by vortexing for 1 min. The β DDM detergent was then added to dilute the suspension to 0.5 mg/mL and solubilise the MLVs ready for incubation on the substrates. The solubilised MLVs were incubated onto glass and then onto PCysMA brushes.

To characterise the mixed-micelles and ascertain the minimum concentration of detergent required to solubilise the vesicles, an analysis was performed, using the Zetasizer Nano, to determine the change in size of the MLVs when detergent was added. Multilamellar vesicles were formed in buffer solution and the size measured before and after adding a range of concentrations of detergent.

6.4.2.2. Results and discussion

The MLVs when first prepared, were found to have a diameter of 309 ± 55 nm. By adding a small amount (1% β DDM) an initial fall in size to 113 ± 13 nm was seen. Following this, at approximately 2.5 wt %, swelling to 247 ± 12 nm took place. As more DDM was added there was a rapid fall in size to <10 nm after 5 wt % was added. It remained at this level when more DDM was added. It appeared that 5 wt % of DDM would suffice to solubilise the vesicles, however, Vacklin's method successfully used a higher weight ratio of 3:1. It

was considered prudent initially to follow this successful method and later to systematically reduce the ratio of DDM being used.

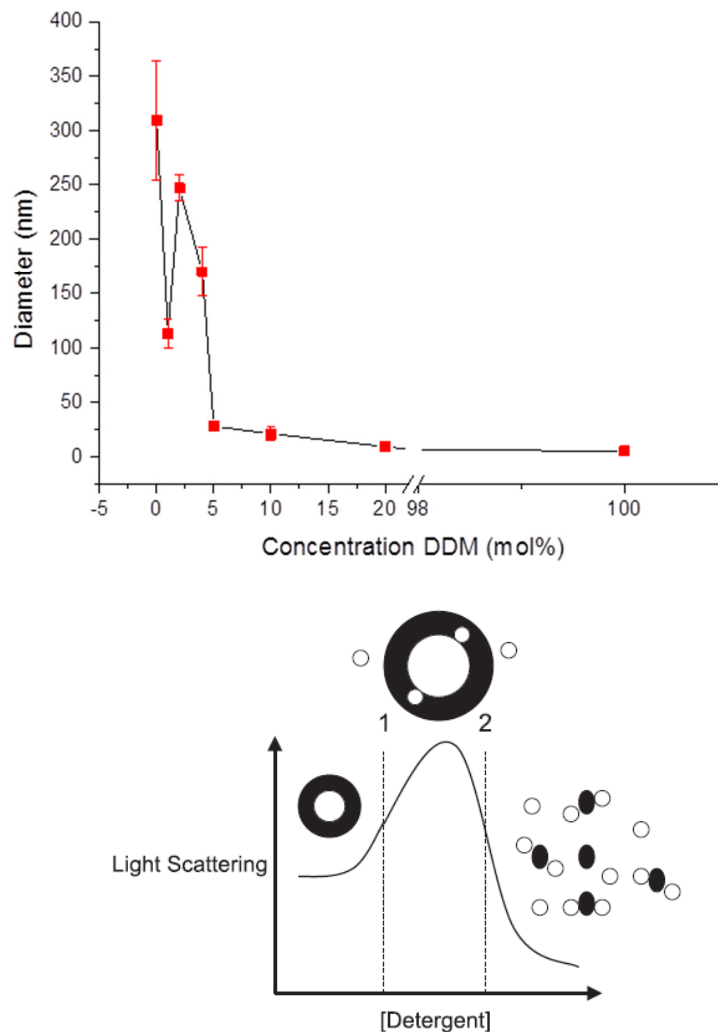


Figure 6.11: Plot of change in diameter of 25% DOTAP:POPC MLVs when solubilised with increasing amounts of β DDM (top). Below is a diagram, depicting the characteristics of the MLV as it is solubilised with detergent, published by Seddon *et al.* ref 17.

The plot of the changes in the diameter of the MLVs as detergent is added can be compared to work done by Seddon *et al.*¹⁷ as shown in Figure 6.11 (b) above. After the initial measurement of 309 nm detergent at 1 wt % was added and an immediate fall in diameter to 113 nm was seen. This initial fall in size could be attributed to the removal of an outer bilayer from the multi-layered vesicle, though this was not observed by Seddon. After this initial fall, the MLVs increased in size, swelling to 247 nm. This was a result of the partitioning of detergent into the bilayers within the vesicles causing them to swell. As more detergent was added the vesicles were destroyed and the solution consisted of detergent saturated vesicles and lipid-saturated mixed micelles. When these became

saturated they broke down into smaller mixed-micelles. As more detergent was added the proportion of phospholipid within the vesicle was diluted. The concentration of detergent at which they change character to mixed-micelles is about 5 wt % β DDM. The results are shown in Figure 6.11 (a) above.

6.4.3. Lipid bilayer formation and attempted protein incorporation using β DDM detergent

6.4.3.1. Introduction and methods

The cytochrome bc₁, complexed with RC-LH1-PufX and referred to as C10H, was received (from the biochemists in Sheffield) in a vesicle in which the cytb_{c1} were tagged with gold nano-dots. It was anticipated that they could be imaged using the dark field microscope. The vesicles may have contained other elements of the light harvesting (LH) complex, but were expected to consist mainly of the reaction centre-light harvesting 1 complex described above. The C10H composition and structure had not been fully elucidated at the time of the experiments, but initial electron microscope studies of the crystallised vesicles had been published.¹⁸

The analysis methods chosen for this work of incorporating these C10H vesicles into lipid bilayers on the PCysMA brush included the FRAP methodology employed in all previous experiments. Analysis by total internal reflection microscopy (TIRF), and dark field microscopes was also introduced. The TIRF system was used to eliminate fluorescence from outside the focal plane and improve the spatial resolution of the sample, without using a fluorescent probe, which may interfere with the readings made in future experiments when the light harvesting component functionality would be measured. Dark field was included as an imaging tool to enhance the sample contrast so that the gold nanodots would be visible without interference from the sample itself or any fluorescent probe.

Bilayers formed from MLVs solubilised with β DDM were first prepared on glass and investigated using the FRAP, TRIF and dark field microscopy. Following the successful bilayer formation using the DDM-MLV method on a piranha cleaned glass substrate, a light harvesting protein was incorporated and viewed first in a bilayer on glass, by FRAP, TIRF and dark field. The process was then repeated incubating onto a short, 7 nm, PCysMA brush, grown from a glass substrate.

6.4.3.1.1. β DDM solubilisation

The process for incorporating the LH complex C10H into a bilayer was to utilise the β DDM solubilisation method described above. Initially multilamellar vesicles were formed by vortex mixing dried 25% DOTAP:POPC lipids in 10 mM phosphate buffer. These were then solubilised by adding sufficient β DDM to produce a final 3:1 ratio by weight of β DDM :total lipid. This suspension was incubated on a glass coverslip in a home-made cell, which could be used under a combined dark field and TIRF microscope (shown in Chapter 3, Figure 3.4 (b)). The cell was made from a microscope slide and a round glass coverslip sealed with a 3D printed rubber 'O' ring in between. Taps were inserted into the 'O' ring and sealed with UV activated glue. The reason for using this design rather than a regular flow cell was because the TIRF/dark field microscope has a limited working distance of only 2 mm and the regular flow cell is 15 mm deep. The samples were rinsed very slowly at 0.1 mL min^{-1} for 10 min, then, the rate was slowly increased to 2.6 mL min^{-1} over a 20 min period. FRAP, TIRF and dark field microscopy methods were then used to examine the sample. Following the successful bilayer formation using this lipid mixture on glass, the method was modified and after the detergent solubilisation, an aliquot of the C10H vesicles was added to the solubilised vesicles. The protein-lipid mixture was then incubated onto a glass coverslip. The same method was used again, substituting the glass substrate for the PCysMA brush grown on glass.

6.4.3.2. Results and discussion

6.4.3.2.1. Bilayers on glass using DDM/lipid and C10H vesicles

The lipid/DDM mixture was first incubated onto a glass coverslip, showing that a good, homogenous diffusing bilayer was formed. Following this, a 3:1 ratio by weight of β DDM:25% DOTAP:POPC lipid and C10H vesicles was incubated onto a glass coverslip. The result was a good, fluid bilayer with few visible defects. The results, shown in Figure 6.12 (a), using FRAP, showed a diffusion coefficient of $0.87 \mu\text{m}^2 \text{ s}^{-1}$ with a mobile fraction of 80%, which compares well with the rates on glass using vesicles of only long chain lipids. The reduced diffusion rate could be the result of the protein vesicles interacting with the glass and creating a barrier to full diffusion. The mobile fraction of 80% is indicative of this.

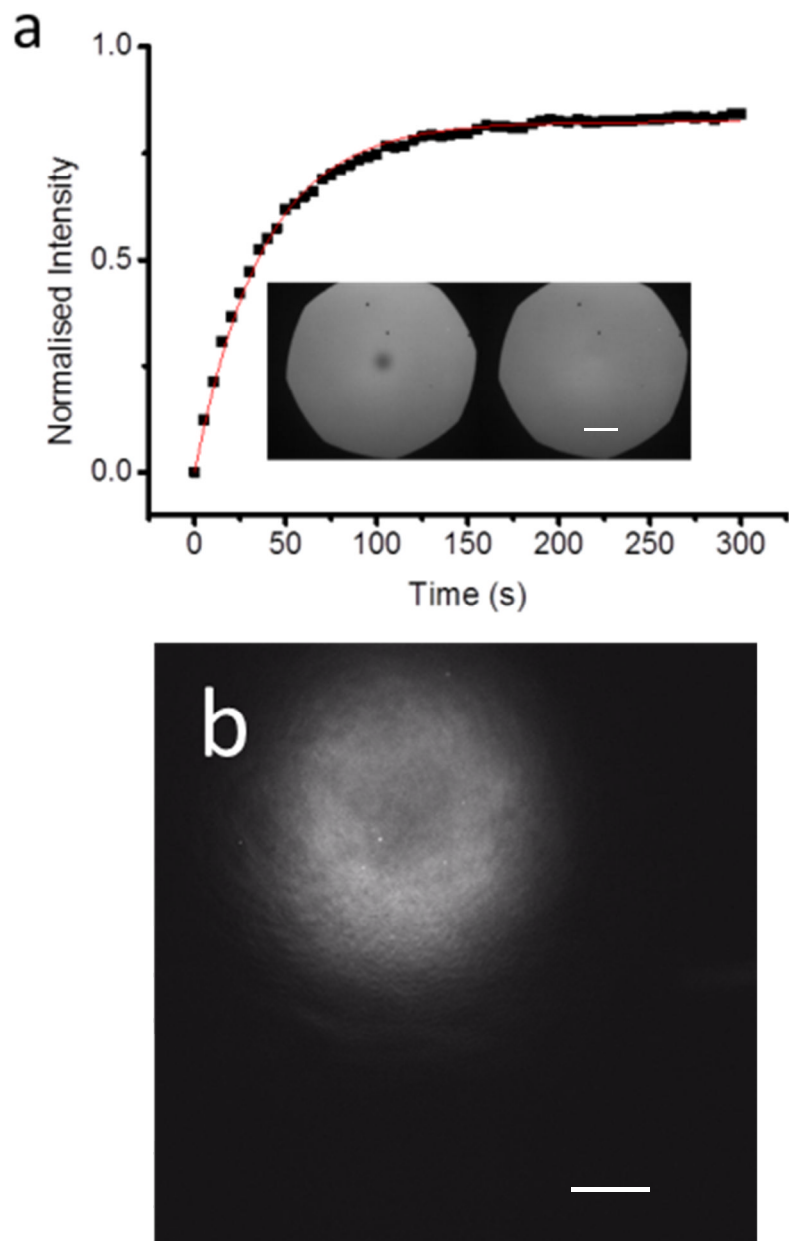


Figure 6.12: (a) Diffusion coefficient of 3:1 β DDM:lipid bilayer incubated with C10H vesicles on glass showing images at bleaching and after 5 min. Scale bar 60 μm . (b) the same sample viewed using TIRF. Scale bar 100 μm .

The diffusion and recovery were confirmed on the same sample and also viewed under TIRF, as seen in Figure 6.12 (b). The lower image shows the bilayer 7 min after bleaching. The bleached spot, which has fully recovered, was in the top left corner (it is not the darker area in the centre).

Figure 6.13 (a) below, shows images of a DDM:lipid bilayer only (with no C10H) viewed under dark field, where the sample was illuminated by reflected light.

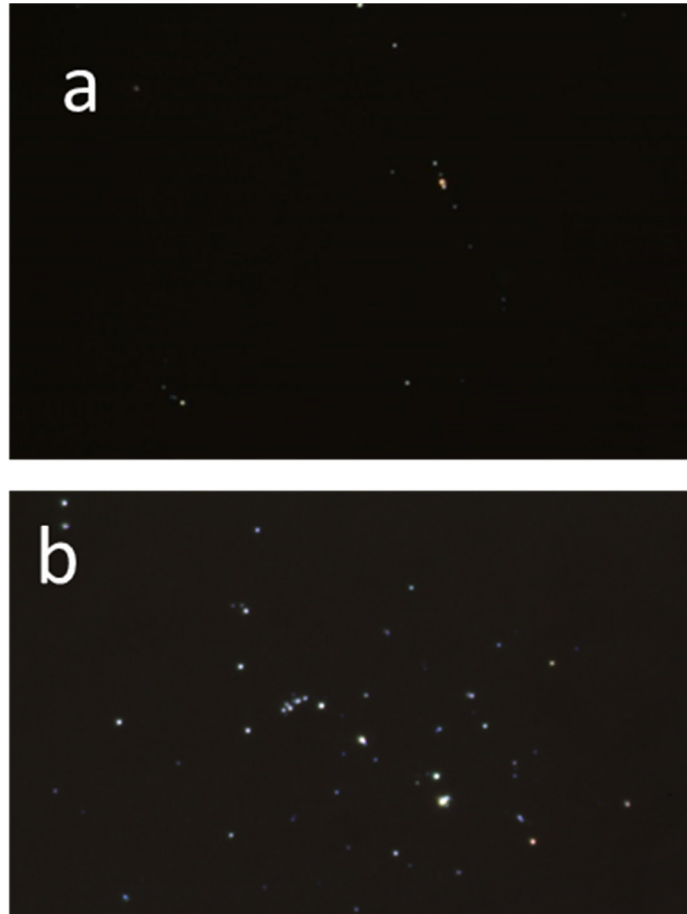


Figure 6.13: (a) Dark field image of a DDM solubilised bilayer (b) DDM solubilised bilayer containing C10H vesicles, in which the cytb1 was tagged with gold nanoparticles. Scale bar 100 μm .

This shows very little reflection from any objects on the surface. Below in (b) is the dark field image of the same bilayer after the incorporation of gold-tagged C10H vesicles. Light coloured dots can be seen, as would be expected from light reflecting (diffracted) from the gold nanoparticles. These experiments should be repeated before conclusions can be drawn about the success of the protein incorporation, as the method is very dependent on the exclusion of any dust or other foreign bodies from the system. Time constraints meant that this experiment was performed once only, but proved that the apparatus and process worked, in principle.

6.4.3.2.1. Bilayers on PCysMA using β DDM/lipid and C10H vesicles

Following the same method as above the incubation, of 25% DOTAP:POPC vesicles with β DDM and C10H vesicles on the 7 nm PCysMA brush, took 5 days to fully form into a fluid bilayer. The results can be seen in Figure 6.14. The top images show the progression of the incubation over a period of days, with the bilayer becoming more fluid and homogenous

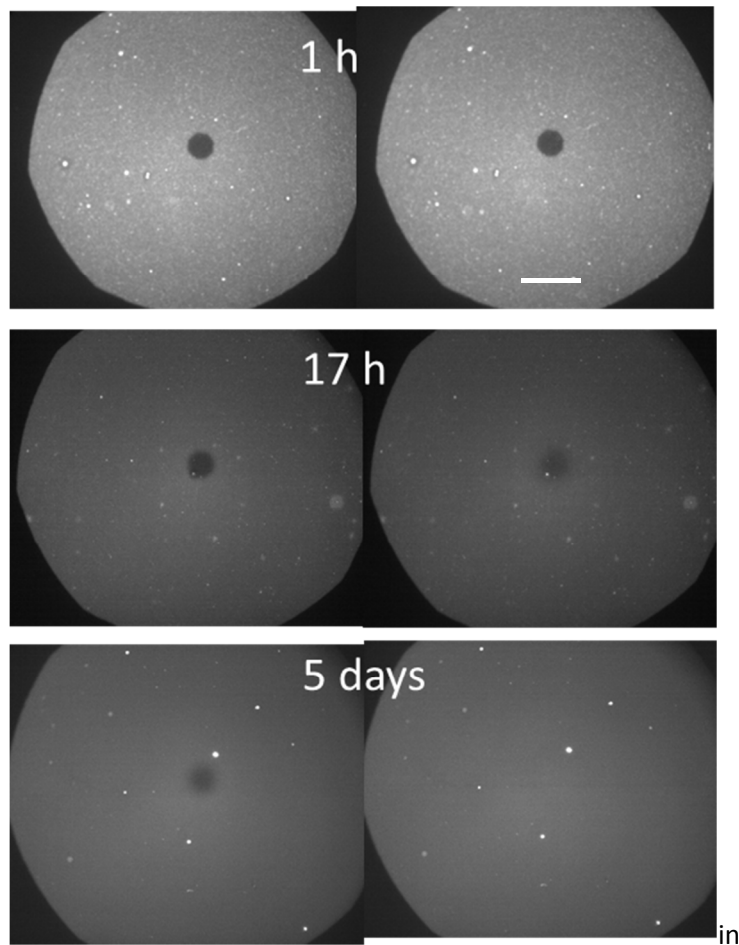


Figure 6.14: FRAP images of bilayer on PCysMA using β DDM/MLVs and C10H vesicles, (top) after 1 h, (mid) after 24 h and (lower) after 5 days. Scale bar of 60 μ m applies to all images.

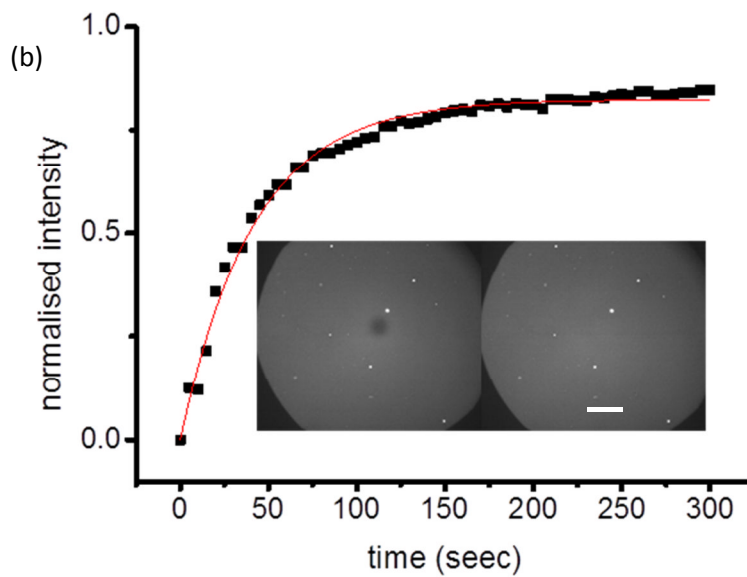


Figure 6.15: Diffusion graph and FRAP images, bilayer on PCysMA using β DDM/MLVs and C10H vesicles, after 5 days incubation. Images at bleaching, (left) and after 5 min recovery (right). Scale bar 60 μ m.

during this period. The final result showed a good diffusion coefficient of, $1.4 \mu\text{m}^2 \text{s}^{-1}$, a rate similar to the “standard” diffusion rate of lipids on glass. However, a mobile fraction of 82% was measured (Figure 6.15 (b)), which indicated that some of the lipids were immobilised. This could suggest that there was an interaction between the polymer brush and the protein, which may have immobilised the proteins. However, the same formulation of lipids and detergent on PCysMA with no proteins gave good diffusion rates and a similar mobile fraction of 80%. It can be concluded that the DDM itself may be slowing the diffusion rate in some way and this would need to be investigated. It may be interacting with the PCysMA or creating defects in the bilayer because it is not fully removed by rinsing. It should also be noted that using an elevated temperature and extended incubation time, the protein may have been denatured. However, as the objective was not, at this stage, to prove the activity of the protein, but to prove that the bilayer was present, with proteins incorporated on a polymer brush, the sample was next used for AFM imaging.

The top left AFM scan of the same sample, shown below in Figure 6.16 (a), does not indicate that a good fluid bilayer is present, which is disappointing but not surprising, as the sample had to be stored for 2 weeks whilst awaiting modifications to the AFM. It had then to be removed from the flow cell before AFM imaging. The sample showed a non-homogeneous surface, which could possibly be the polymer brush. The height profile in Figure 6.16 (b) indicated that the layer was about 7 nm high, which is the same as the dried polymer. There was no definitive bilayer breakthrough curve in Figure 6.16 (c). There were, however, elevated features which resembled the dimensions of a C10H vesicle of approximately 100 nm in diameter and between 20 to 30 nm high, in agreement with Cartron *et al.* as shown in Figure 6.17.¹⁸ It is appreciated that these could actually be mounds of aggregated dried lipids.

The bilayer deposition method onto the PCysMA brush, initially included a heating step, to 50°C, to ensure that the bilayer was formed, in line with the findings in Chapter 5. This was not an ideal condition for incorporating a protein, so the first steps to modify the method have been successful. First a bilayer on PCysMA was produced by incubating 25% DOTAP:POPC vesicles at 50 °C, followed by the addition of a β DDM/protein mixture *after* the bilayer had formed.

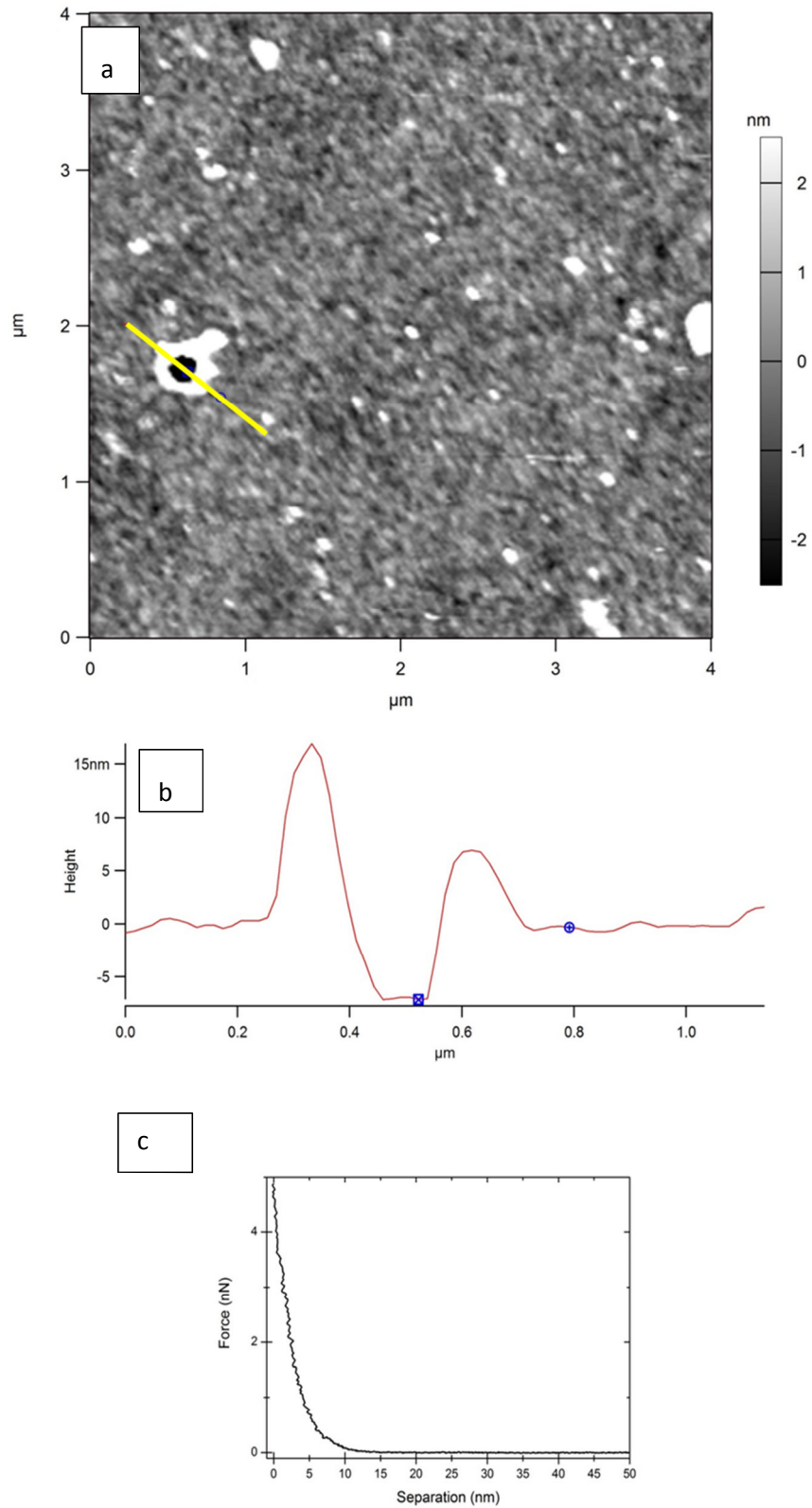


Figure 6.16: AFM scans of the bilayer on the sample seen in Figure 6.15. (a) yellow line marks the scan, which is seen in profile in (b) height profile indicates a height of 20 nm. (c) Shows a breakthrough force curve, which does not indicate a bilayer breakthrough characteristic.

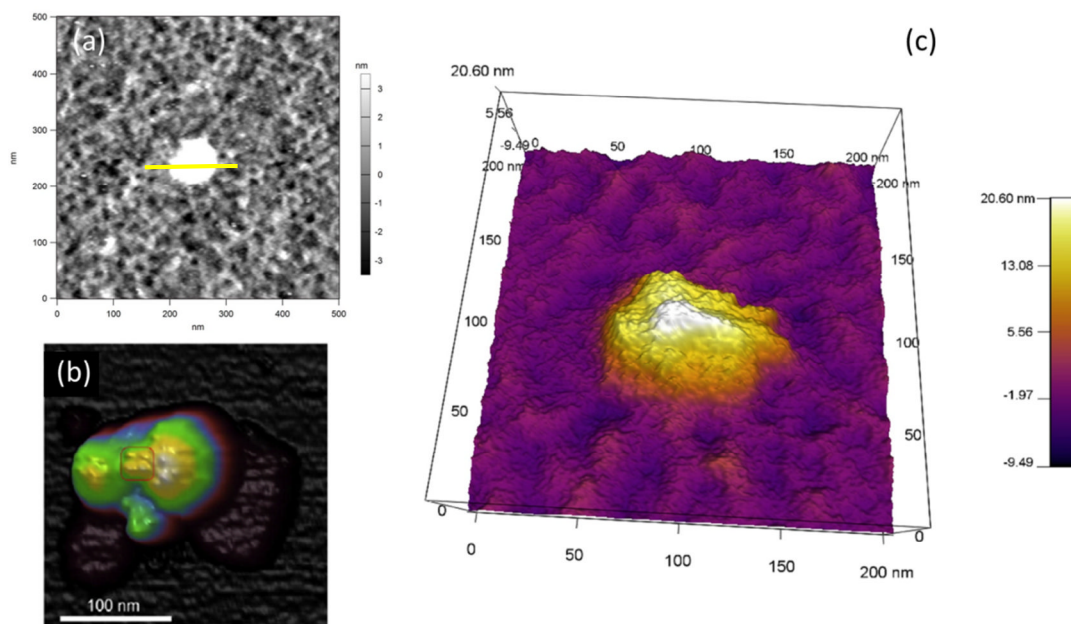


Figure 6.17: Further AFM images of the potential C10H vesicle on PCysMA. Image (a) shows an elevated feature which is shown also in false colour in (c). The image (b) is a published image of the crystallised C10H vesicle.¹⁸

6.5. Summary, conclusions and further work

The first positive steps have been demonstrated here, to introduce a method for incorporating light harvesting components into a fluid bilayer on a polymer brush support. Three methods were investigated, the first two being reconstitution methods which required the incorporation of proteins into liposomes before they were incubated onto glass or a polymer brush. These first two methods were not entirely new, but the incorporation of the proteins into cationic vesicles, required for the successful incubation onto PCysMA is not widely published. The third method required the solubilisation of a preformed bilayer with β DDM on the PCysMA brush and subsequently incubating a light harvesting C10H vesicle onto it, which is novel.

The first method for incorporating proteorhodopsin into cationic and anionic vesicles was chosen to demonstrate that cationic vesicles could be used for the reconstitution, despite the fact that natural membranes are usually anionic. The method also suggested that because of the surface charge on the vesicles all proteins would present in the same orientation, which is important when testing the direction of proton pumping. It appeared to work successfully with anionic vesicles but not with cationic ones, which were the ones needed for taking this method forward. The method showed weaknesses in the practical steps which lead to leakage of the fluorescent dye from the vesicle and in the case of the cationic vesicles, removal of the protein completely. It was a useful first step on the path to

working with protein reconstitution and for forging links between physics and biochemistry.

The second method indicated that the successful incorporation of Cybo3, into a cationic lipid vesicles (25% DOTAP), had taken place. The subsequent incubation of these proteoliposomes onto glass produced a bilayer with a good diffusion coefficient of $1.1 \mu\text{m}^2 \text{s}^{-1}$. The resultant bilayer was successfully imaged using AFM which demonstrated reasonable evidence of the presence of proteins. The same mixture was also incubated onto a PCysMA brush, again showing a diffusing bilayer. This work was delayed at this stage as no Cyt bc1 (the component of the *Rh. Sphaeroides* required for the project), had not been successfully purified ready for use at that point.

The final method involved the use of β DDM detergent to create lipid bilayers onto PCysMA and then adding an LH protein, reconstituted in β DDM. This method of producing bilayers, using detergent 'depletion' on glass and on the PCysMA brush worked very well, showing homogenous bilayers with good diffusion coefficients on both surfaces. The incorporation of a C10H vesicle (which contains gold-tagged Cytbc1 and other light harvesting components of the *Rh. Sphaeroides*) into a bilayer on glass by this method was also successful. This was confirmed by good FRAP diffusion coefficients. First attempts to also confirm this by TIRF and the use of dark field images were made. The TIRF confirmed good diffusion rates and the dark field images suggested, though didn't confirm, that these gold tagged vesicles were present on the surface. This detergent depletion method was then used to incorporate C10H vesicles into a bilayer onto a PCysMA polymer brush, which also showed a good homogenous diffusing bilayer of $1.4 \mu\text{m}^2 \text{s}^{-1}$. The mobile fractions, however, were slightly (10%) below expectation and work is required to investigate this. The successful sample was imaged using high resolution AFM. The images did strongly suggest that the C10H light harvesting components were present on the polymer brush.

Unfortunately a fluid bilayer on PCysMA was not confirmed by the AFM scans and the sample appeared to have dried out during the weeks of delay before AFM scanning (due to instrument modifications).

This work shows a potentially a good, facile and interesting method to incorporate a protein containing bilayer onto the PCysMA brush, which, given more time can be developed successfully.

6.6. References

- ¹ Tunuguntla, R.; Bangar, M.; Kim, K.; Stroeve, P.; Ajo-Franklin, C. M.; Noy, A., Lipid bilayer composition can influence the orientation of proteorhodopsin in artificial membranes. *Biophysical journal* **2013**, *105* (6), 1388-1396.
- ² Verkhovskaya, M. L.; Garcia-Horsman, A.; Puustinen, A.; Rigaud, J.-L.; Morgan, J. E.; Verkhovsky, M. I.; Wikström, M., Glutamic acid 286 in subunit I of cytochrome bo3 is involved in proton translocation. *Proceedings of the National Academy of Sciences* **1997**, *94* (19), 10128-10131.
- ³ Achalkumar, A. S.; Bushby, R. J.; Evans, S. D., Cholesterol-based anchors and tethers for phospholipid bilayers and for model biological membranes. *Soft Matter* **2010**, *6* (24), 6036.
- ⁴ Van Adelsberg, J.; Al-Awqati, Q., Regulation of cell pH by Ca²⁺-mediated exocytotic insertion of H⁺-ATPases. *The Journal of cell biology* **1986**, *102* (5), 1638-1645.
- ⁵ Mordon, S.; Devoisselle, J. M.; Maunoury, V., In vivo pH measurement and imaging of tumor tissue using a pH-sensitive fluorescent probe (5, 6-carboxyfluorescein): instrumental and experimental studies. *Photochemistry and photobiology* **1994**, *60* (3), 274-279.
- ⁶ Walter, J. M.; Greenfield, D.; Bustamante, C.; Liphardt, J., Light-powering Escherichia coli with proteorhodopsin. *Proceedings of the National Academy of Sciences* **2007**, *104* (7), 2408-2412.
- ⁷ Discussions with M.Li in the Jeuken Lab, University of Leeds.
- ⁸ Venturoli, M.; Smit, B.; Sperotto, M. M., Simulation studies of protein-induced bilayer deformations, and lipid-induced protein tilting, on a mesoscopic model for lipid bilayers with embedded proteins. *Biophysical journal* **2005**, *88* (3), 1778-1798.
- ⁹ Morigaki, K.; Kimura, S.; Okada, K.; Kawasaki, T.; Kawasaki, K., Formation of substrate-supported membranes from mixtures of long- and short-chain phospholipids. *Langmuir* **2012**, *28* (25), 9649-9655.
- ¹⁰ Suk, J.-E.; Situ, A. J.; Ulmer, T. S., Construction of covalent membrane protein complexes and high-throughput selection of membrane mimics. *Journal of the American Chemical Society* **2012**, *134* (22), 9030-9033.
- ¹¹ Hauser, H., Short-chain phospholipids as detergents. *Biochimica et Biophysica Acta (BBA)- Biomembranes* **2000**, *1508* (1), 164-181
- ¹² Sanders, C. R.; Landis, G. C., Reconstitution of membrane proteins into lipid-rich bilayered mixed micelles for NMR studies. *Biochemistry* **1995**, *34* (12), 4030-4040.

-
- ¹³ Yasuhara, K.; Miki, S.; Nakazono, H.; Ohta, A.; Kikuchi, J., Synthesis of organic-inorganic hybrid bicelles-lipid bilayer nanodiscs encompassed by siloxane surfaces. *Chemical Communications* **2011**, 47 (16), 4691-4693.
- ¹⁴ Tested by Michael Cartron, University of Sheffield
- ¹⁵ Vacklin, H. P.; Tiberg, F.; Thomas, R., Formation of supported phospholipid bilayers via co-adsorption with β -D-dodecyl maltoside. *Biochimica et Biophysica Acta (BBA)-Biomembranes* **2005**, 1668 (1), 17-24
- ¹⁶ Lee, C.; Wacklin, H.; Bain, C. D., Changes in molecular composition and packing during lipid membrane reconstitution from phospholipid-surfactant micelles. *Soft Matter* **2009**, 5 (3), 568-575.
- ¹⁷ Seddon, A. M.; Curnow, P.; Booth, P. J., Membrane proteins, lipids and detergents: not just a soap opera. *Biochimica et Biophysica Acta (BBA)-Biomembranes* **2004**, 1666 (1), 105-117.
- ¹⁸ Cartron, M. L.; Olsen, J. D.; Sener, M.; Jackson, P. J.; Brindley, A. A.; Qian, P.; Dickman, M. J.; Leggett, G. J.; Schulten, K.; Hunter, C. N., Integration of energy and electron transfer processes in the photosynthetic membrane of *Rhodobacter sphaeroides*. *Biochimica et Biophysica Acta (BBA)-Bioenergetics* **2014**, 1837 (10), 1769-1780.

7. Results 3. Testing of bilayer formation on cationic brushes

7.1. Introduction

The testing of the brushes presented in this chapter took place before the successful results shown in chapter 5. At that early stage in the experimental work, despite being informed by an extensive literature survey there were few indicators as to which formulations of brush would best support lipid bilayers. Consequently, the choice of these polymers was not a scientific one and the polymers tested were ones which the Sheffield polymer group had expertise in preparing, or had an interest in producing for other applications.

This range of cationic polymer brushes were grown by Si-ATRP and characterized by the Nan Cheng and Abdullah Alswieleh (from the Sheffield polymer groups) before being presented here for bilayer testing. The positively charged character of the brushes was the result of selecting monomers with an amine group attached to the monomer chain in a number of configurations. The brushes were a mixture of secondary, tertiary and quaternary amines and this conferred a pH response to some, but not to others.

The chemical formulae and schematics of the brush structures are shown in Table 7.2, and more detail on them is presented below in section 7.3:

- a) 2-(tert-butylamino)ethylmethacrylate (PTBAEMA) with cross-linking throughout the chain
- b) 2-(tert-butylamino)ethylmethacrylate (PTBAEMA), with cross-linking at the top of the brush only
- c) poly (N,N (dimethylamino)ethylmethacrylate) (PDMAEMA)
- d) poly(2-(methacryloyloxy)ethyltrimethylammonium chloride) PMETAC, which is the C1 quaternised version of PDMAEMA, quaternised throughout the chains
- e) poly(2-(methacryloyloxy)ethyltrimethylammonium chloride) PMETAC, as in d), but C1 quaternised at the top only
- f) poly (N,N (dimethylamino)ethylmethacrylate) (QPDMAEMA), which has been quaternised with C12 throughout the brush
- g) poly (N,N (dimethylamino)ethylmethacrylate) (QPDMAEMA), which has been quaternised with C12 at the top of the brush only
- h) poly (N,N (dimethylamino)ethylmethacrylate) (QPDMAEMA), which has been quaternised with C18 chains at the top of the brush only

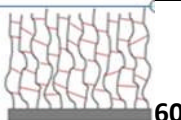
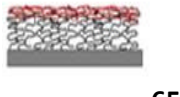
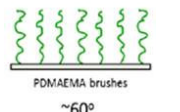
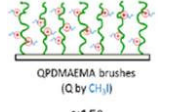
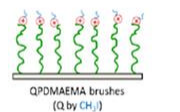
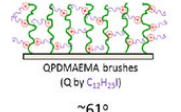
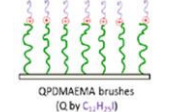
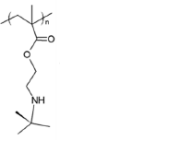
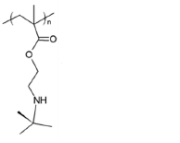
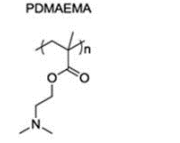
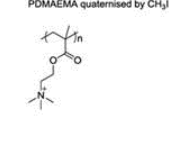
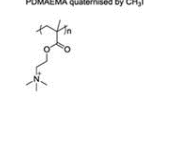
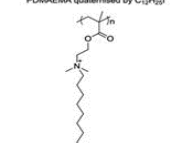
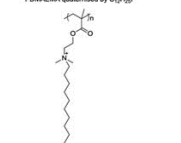
PTBAEMA (2° amine, with tertiary butyl) cross-linked in THF, a good solvent (a)	PTBAEMA (2° amine, with tertiary butyl) cross-linked in hexane, a poor solvent (b)	PDMAEMA (2° amine) (c)	PMETAC C1 Quaternary amine groups throughout the brush (d)	PMETAC C1 Quaternary amine on end of chain only (e)	QPDMAEMA C12 Quaternary amine chain throughout brush (f)	QPDMAEMA C12 Quaternary amine with C12 at chain end only (g)	QPDMAEMA C18 Quaternary amine with C18 at chain end (h)
 60°	 65°	 PDMAEMA brushes ~60°	 QPDMAEMA brushes (Q by CH ₃ I) ~15°	 QPDMAEMA brushes (Q by CH ₃ I) ~15°	 QPDMAEMA brushes (Q by C ₁₂ H ₂₅ I) ~61°	 QPDMAEMA brushes (Q by C ₁₂ H ₂₅ I) ~54°	As (g) but with longer chain
		PDMAEMA 	PDMAEMA quaternised by CH ₃ I 	PDMAEMA quaternised by CH ₃ I 	PDMAEMA quaternised by C ₁₂ H ₂₅ I 	PDMAEMA quaternised by C ₁₂ H ₂₅ I 	as (g) but longer acyl chain

Table 7.1: Brief description of cationic polymers with a cartoon of the brush structures and chemical formulae of polymer.

These represent just some of the polymer brushes tested and a further list is included in Appendix 2. It is appreciated that, ideally, a systematic testing regime should have been followed for all the brush variants. A compromise had to be reached because of the impracticality of asking for a huge range of samples to be prepared which were of consistently good quality.

Presented first is a brief summary of the preparation methods for the polymer brushes, for which full method details are given in chapter 4. All the methods require the deposition of a SAM surface initiator step and the polymerization steps follow a similar route to those in Chapter 5. A description of the characterisation of each of the brushes follows this methods summary. The preparation and characterisation were done (in Sheffield) by Nan Cheng and Abdullah Alswieleh, supplemented by information from the literature.

Details of the lipid formulations, incubation methods and buffer conditions, followed by zeta potential characterization of the vesicles are presented next. The testing of bilayer formation using lipid vesicles on each of the brushes are shown, using FRAP as the primary analysis tool. Where a lipid layer was observed, images are presented, immediately after bleaching and 10 min later, after fluorescence recovery, along with the diffusion rates and mobile fractions where they could be calculated. AFM analysis was also used. Finally, these results are discussed in conjunction with characterization data and information on the brushes and vesicles from the literature.

7.2. Lipids used for incubation

7.2.1. Formulation and incubation of lipid vesicles

The lipid vesicles used for zeta potential measurements were prepared from POPC, with the addition of an anionic lipid, DOPG. The lipids were dissolved in 50:50 chloroform : methanol and mixed into mol % aliquots of 100% POPC, 25% DOPG:POPC, 50% DOPG:POPC and 75% DOPG:POPC, 90% DOPG:POPC then dried. The vesicles used for bilayer formation on the polymer brushes included 0.5 mol % of Texas Red- DHPE (negatively charged) fluorophore. After evaporating the solvent the lipids were rehydrated using different media: (a) MilliQ water (pH ~ 5.5) (b) 10 mM phosphate (salt free) buffer at pH 7 (c) PBS buffer, containing 140 mM NaCl at pH 7. Following rehydration the multilamellar vesicles were tip sonicated to produce small unilamellar vesicles. For bilayer formation, the polymer brush samples, grown on 18 mm round glass coverslips, were sealed in a flow cell and soaked in the same buffer used to rehydrate the vesicles. After 15 minutes of soaking, the vesicle suspensions were injected into the flow cell.

Incubation of the vesicles took place at room temperature, as all the lipids were in the liquid state, having very low (~ 0 °C) transition temperatures. The incubations took place in the dark to prevent bleaching of the fluorophore. An initial incubation period of 2 h was followed by rinsing with the same media used for rehydrating the vesicles. This was followed by a further period of 48 h incubation and final rinsing. FRAP images and analyses were taken after each period of incubation.

7.2.2. Zeta potential of vesicles

7.2.2.1. Method

The size and zeta potentials of the vesicles were measured by DLS using a Zetasizer Nano. The measurements took place in a folded capillary cell so that both size and zeta measurements could be made without needing to change the sample or cell. The vesicles, at a chosen concentration of 0.25 mg/mL, were measured in the same buffer used for the incubation on the polymer brushes, where possible. Details of the method are presented in the methods chapter 4 which shows that at least three measurement runs were made for each size and zeta potential reading, where each run incorporated a number of sub-readings (from 10 to 100) specified by the software, in order to obtain a statistically reliable result.

7.2.2.2. Results

The graph in Figure 7.1 shows the size and zeta potential readings for a range of mol % of tip sonicated DOPG:POPC vesicles in MilliQ water measured at 25 °C. The vesicles diameter, measured with a mol ratio of 10% DOPG:POPC, was 24.6 ± 0.4 mV, which reduced to 17.5 ± 3 mV for a ratio of 80 % DOPG. It can also be seen from the graph that as the mol % of DOPG in the vesicles increases, the zeta potential becomes increasingly negative. The zeta potential of POPC vesicles was previously shown (in Chapter 5) to be zero mV with an error of ± 5 mV. The measured zeta potential of vesicles with 10 % DOPG:POPC was -16.4 ± 1.4 mV. Increasing the DOPG ratio to 35 mol % the zeta potential increases to -41.2 ± 1.2 mV and when increasing the DOPG content to 80 mol % the zeta potential increases to -73.1 ± 1.4 mV. DOPG has a pKa of 3 and is negatively charged between pH 5 and pH 7.²

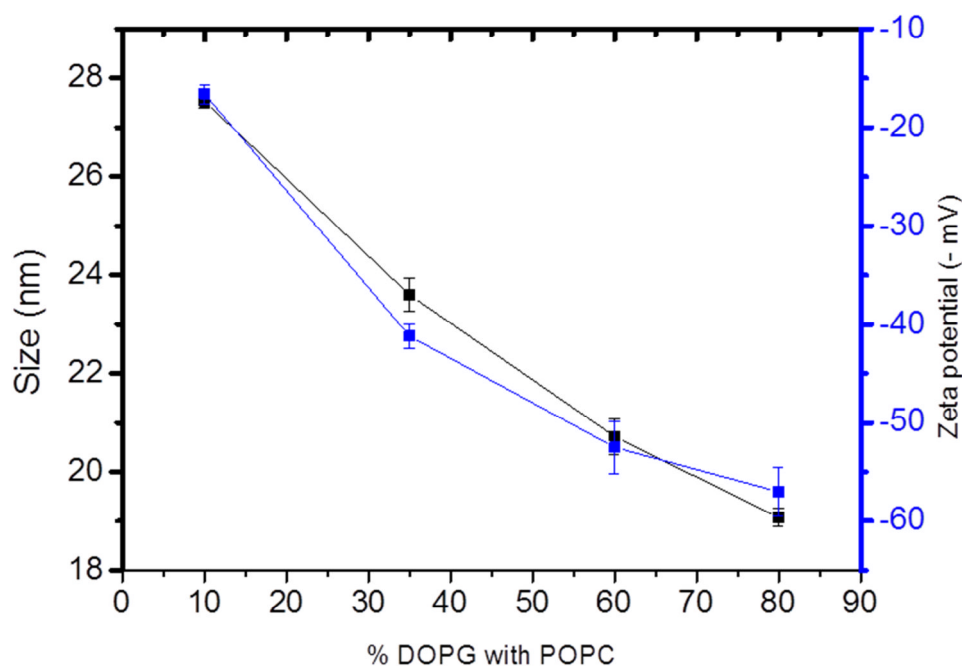


Figure 7.1: DLS study on a range of DOPG:POPC tip sonicated lipid vesicles, in MilliQ. Plots show size (black plot) and zeta potential (blue plot) changes with increasing mol % of DOPG.

7.3. Bilayer formation on cationic polymer brushes

7.3.1. Introduction

Table 7.2 shows the structures of the eight cationic (amine based) polymer brushes tested for bilayer formation and it is helpful to refer to the structures within this table for clarification of the similarities and subtle differences between them, the effects of which are discussed below. It was proposed that these subtle changes to the structure of the functional amine groups may allow tuning of the positively charged groups present as well as varying the hydrophilicity/hydrophobicity and influencing the response of the brushes to their buffer environment. For the three variants which incorporated long alkyl chains, these were expected to insert into the hydrophobic core of the bilayer membrane.

7.3.2. 2-(tert-butylamino)ethyl methacrylate PTBAEMA, “fully” and “top” cross-linked

7.3.2.1. Preparation and characterisation

This section refers to the first two brushes in Table 7.1 (a) and (b) the “fully” and “top” (or “surface”) cross-linked variants of PTBAEMA.

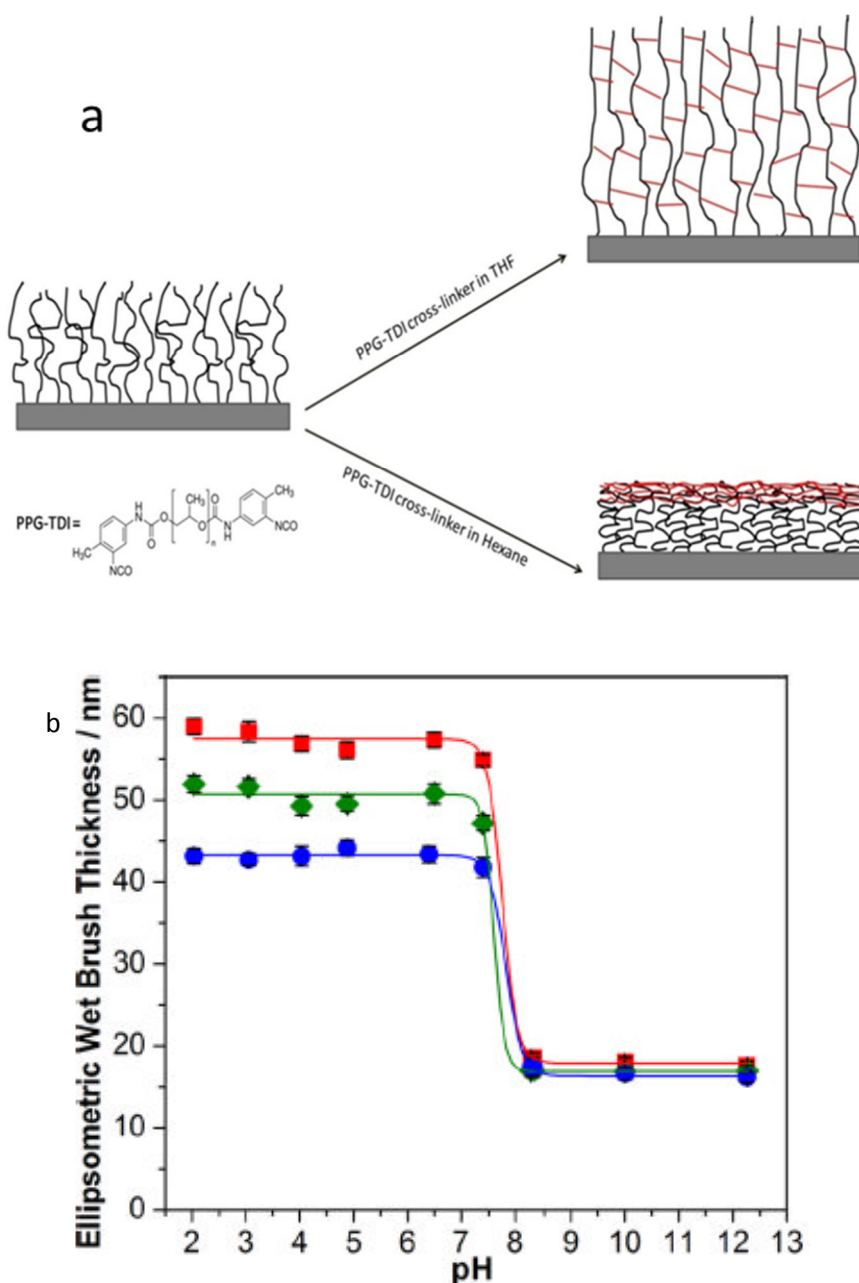


Figure 7.2: (a) PTBAEMA crosslinking in THF and hexane. (b) Ellipsometric thickness of the PTBAEMA brush. (■) = linear brush (♦) = surface x-linked, (●) = x-linked throughout. The dry length was 16 nm, measure by ellipsometry. Provided by A. Alswieleh³

Following the surface initialisation steps to prepare the glass substrate for polymerisation (as explained in Chapter 5) the next stage of the ATRP synthesis involved reacting the monomer TBAEMA with a catalyst of Cu(I)Br/Cu(II)Br₂/TPMA in an inert atmosphere. The reaction was allowed to continue for 60 min to achieve brush of 8 nm dry length, measured by ellipsometry.³

The grafting density was varied by selecting specific ratios of the catalyst components and a specific thickness of brush was achieved by selecting the polymerisation time (a time v

brush thickness study took place to establish this). The brushes were cross-linked, Figure 7.2 (a), via the secondary amine group, in two ways, using tolylene-2,4-diisocyanate-terminated poly(propylene glycol) (PPG-TGI), in either THF (a good solvent) or *n*-hexane (a poor solvent).⁴

As shown in Figure 7.2 (b), the linear form of a PTBAEMA brush (dry thickness 16 nm) is weakly basic and the secondary amine is readily protonated in acidic conditions at pH < 6 creating repulsion between the chains and stretching them from the surface.⁵ Over a narrow pH range, at around pH 7.7 (and above) the chains become deprotonated and collapse. It is important that the testing of bilayer formation is attempted at a pH value above and below that at which the brush collapses to ascertain whether this state affects bilayer formation. It is preferable, and much more valuable, if the brush is extended and not collapsed when the bilayer is formed as this is the configuration which best supports the incorporation of a transmembrane proteins. The brushes prepared in THF were cross-linked throughout and become less swollen at low pH than the hexane brushes which were cross-linked at the top only. A swelling factor of 3.3 was observed for the linear brushes, measured in solution conditions from high to low pH with the cross-linked brushes showing a lower (2.5) swelling factor. Cross-linking was expected to provide more robust surface layers with a minimal effect on the stimulus responsive behaviour.^{6 7} In these cases, the *excluded volume* contribution to the osmotic pressure on the chains was reduced i.e. the individual chains occupied a more confined area than when in linear form, giving a denser configuration to the brush.^{8 9 10}

As measured by AFM in solution, the variant with cross-linking throughout the chain had an rms roughness of 0.4 ± 0.2 nm, and the surface-cross-linked brush had a higher rms surface roughness of 0.6 ± 0.2 nm. The contact angles were similar and fairly hydrophilic at 60° , for the fully cross-linked, and 65° for the top cross-linked.⁴

As can be seen in Figure 7.3³ the surface zeta potential of the linear brush is $+35 \pm 3$ mV at pH 5 For the fully cross-linked brush this is slightly higher $+40 \pm 5$ mV when the brush was cross-linked 'throughout' and reduces to $+20 \pm 5$ mV when cross-linked at the top of the brush. This provides an opportunity to compare the lipid bilayer formation on chemically similar brushes, which have slightly different surface zeta potentials. The surface zeta potentials at pH 10 were -45 ± 5 mV (cross-linked throughout) and -18 ± 30 mV for the surface cross-linked, though this second error is too large to be reliable.

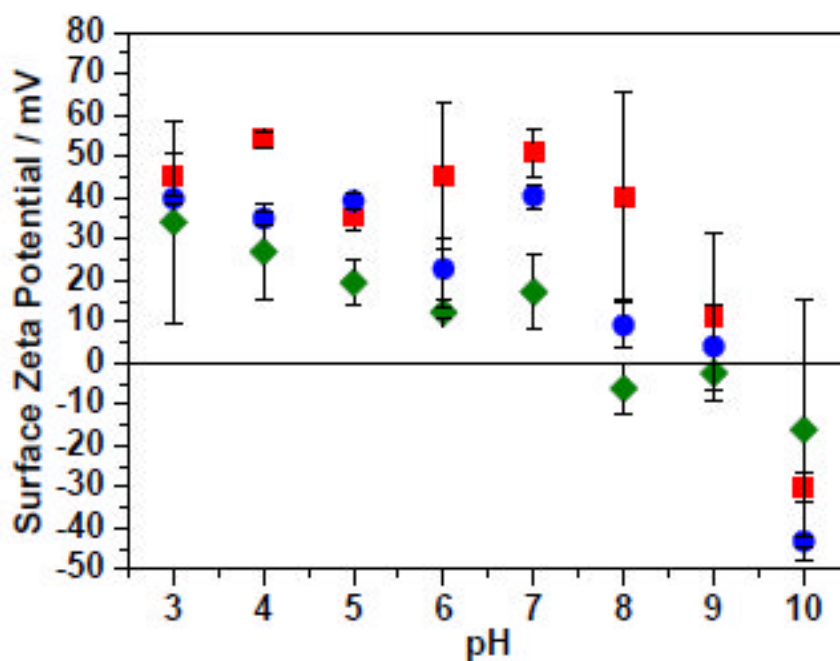


Figure 7.3: PTBAEMA (a■) linear brush, (b●) x-linked throughout and (c◆) surface x linked. Provided by A.Alswieleh.³

The results for Figure 7.3 (b) and (c) are interesting as the top cross-linked polymer may have been expected to have a stronger positive surface zeta potential than the brush which is cross-linked throughout (Figure 7.3 (b), as the former retains some positive charges lower in the chain (i.e. ones which are not cross-linked). The isoelectric point was measured at pH 9, which is higher than the point at which the brush collapses when measuring the (ellipsometric) thickness in Figure 7.2.

To summarise, PTBAEMA is formed from a secondary amine monomer. This forms a weakly basic brush which exhibits a limited pH response and is fully extended at pH 6.5 and collapses above this value, becoming fully collapsed by pH 8. There are two variants, one fully cross-linked and one top (or surface) cross-linked. The fully cross-linked variant does not swell as readily in response to low pH as the top-cross-linked and the linear brush. All have low surface roughness, when measured by AFM. The two brush variants have highly positive zeta potentials of +40 and +20 mV, respectively at pH 5. At pH 10 these had reduced to -45 and -18 mV respectively. The zeta potential of the 50% DOPG vesicles was highly negative at -50 mV (Figure 7.1).

7.3.2.2. Lipid bilayer formation results and discussion

The cross-linked PTBAEMA brushes (fully and top cross-linked) were tested first with zwitterionic POPC lipid and then with an anionic charged lipid composed of 50% DOPG. The incubations took place in MilliQ water (at pH ~5) and in PBS (containing 140 mM NaCl) at pH 7 and pH 10. The incubation with POPC indicated some adsorption of lipids, but showed a surface with many defects (Figure 7.4 (a) & (b)). The adsorbed lipid layer did bleach, but there was no fluidity of the lipids and no recovery. When a higher, 50 mol %, of charged lipid DOPG (in MilliQ, at pH 5) was used the adsorption of a lipid layer was seen (Figure 7.4 (c) & (d)). Small dark patches of defects were also observed with this sample under the fluorescence microscope with a 40x objective.

There were no significant differences between the FRAP results of the two cross-linked variants when incubated with 50% DOPG vesicles in MilliQ. A diffusion coefficient for this system was calculated to be $0.01 \mu\text{m}^2 \text{s}^{-1}$; however, the mobile fraction could not be calculated as the recovery intensity exceeded 100% as shown in Figure 7.5 and as discussed in Chapter 5.

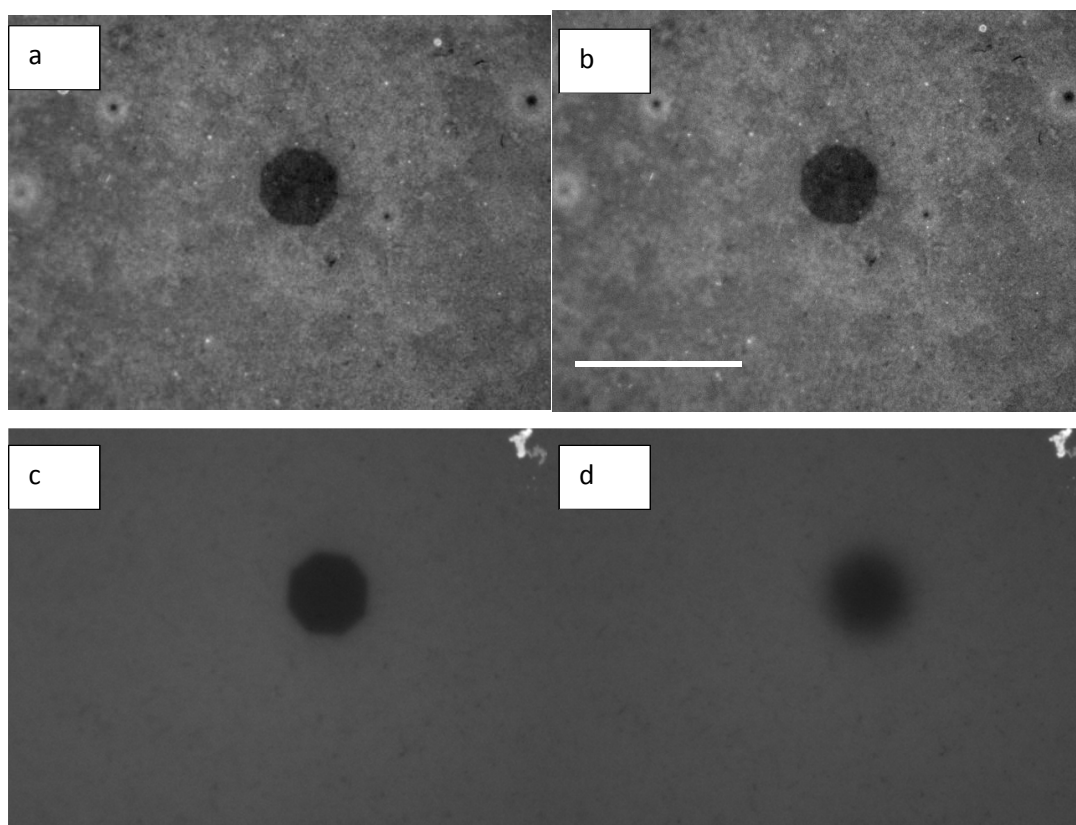


Figure 7.4: PTBAEMA, fully cross-linked incubated with (a) & (b) POPC and (c) & (d) 50% DOPG vesicles. Images at bleaching (a) & (c) showing a well-defined bleached spot and (b) & (d) after 10 minutes FRAP recovery. In the case of (d), with 50% DOPG, a very slow recovery of the bleached spot can be seen. Scale bar of $60 \mu\text{m}$ applies to all images.

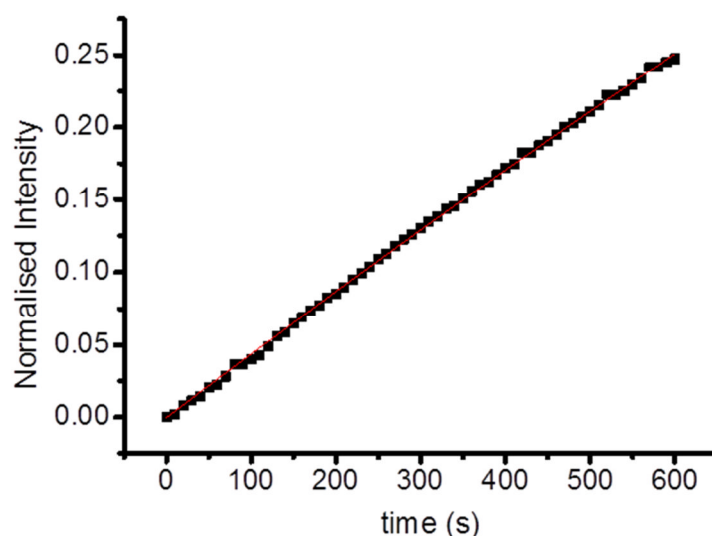


Figure 7.5: Diffusion coefficient graph for the result of incubating 50% DOPG on the PTBAEMA (fully cross-linked) brush in MilliQ.

When incubating the same 50% DOPG lipids in PBS (140 mM NaCl and pH 7) no lipids were adsorbed, though only one sample was available for testing under these conditions. It was observed that when the pH was elevated to 10 the lipids were removed from the surface, which may be the result of electrostatic repulsion between the brush surface and the negatively charged lipids. At this pH point the brush was in its collapsed state and had become negatively charged.

7.3.3. poly[2-(dimethyl amino)ethyl methacrylate] PDMAEMA

7.3.3.1. Preparation and characterisation

This polymer brush has been studied and characterised in the literature for use in medical applications,^{11 12 13 14} but not reported as supporting a lipid bilayer. PDMAEMA is a secondary amine and weak polyelectrolyte (polybase) brush (Table 7.1(c)) which when grafted to a surface by Si-ATRP will respond to pH and temperature.¹⁵ The brush was prepared by creating an APTES-BIBB initiator layer and the Si-ATRP was completed using a DMAEMA monomer and CuBr/CuBr₂/HMTETA (1,1,4,7,10,10-hexamethyltriethylenetriamine) as the catalyst.¹⁶ The grafting density of the brush was controlled by varying the molar ratio of the initiator; however, in this case the initiation efficiency is not linearly dependent and at a higher chain density the local reaction rates are affected by concentration of the reagents within the grafted chains.^{17 18} Fielding *et al.*

suggested that to be fully pH responsive the polymer should not be grown to its maximum grafting density.^{19 20 21}

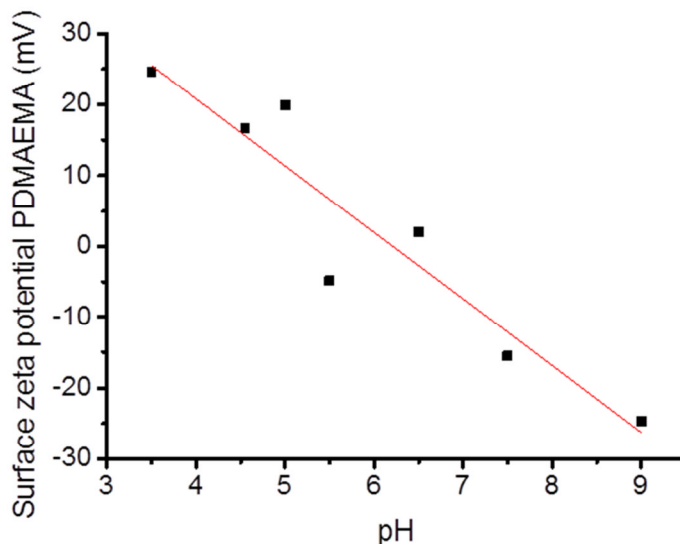


Figure 7.6: (a) Variation of surface zeta potential of PDMAEMA with pH.

The pH characteristics using ellipsometry of a 5-13 nm brush were investigated by Rauch *et al.*²² and also by Sanjuan *et al.*¹⁸ found to be only fully swollen below pH 3 when the amine is protonated and fully collapsed at pH 11, when there is no protonation. A plot of the change in surface zeta potential of the PDMAEMA with pH is shown in Figure 7.6. At pH 5 and below the surface zeta potential is +20 mV. Above pH 6 it reduces to a negative value falling to -25 mV at pH 9. This result has been confirmed independently.²³

In summary, PDMAEMA is a pH responsive secondary amine brush. The surface zeta potential of the PDMAEMA brush is positive at +15 mV at pH 5 and below and becomes negative above that pH value and is only fully extended at low pH.

7.3.3.2. Results and discussion

It was tested here as the 'linear' form of the brush (the quaternised variants are presented in the next section). The testing conditions included using POPC only, and 50 % DOPG:POPC in MilliQ without the addition of NaCl. The results for the surface zeta potential measurements are shown in

Figure 7.6, to indicate that above pH 6 the charge changes from positive to negative as was observed for the PTBAEMA brush above. This could be the result of the brush collapsing

close to the glass, where the residual negative charge may influence the measurement as discussed in Chapter 5. There may also be a residual charge remaining following the deposition of the BIBB-APTES initiator onto the glass, though at pH 7 this SAM surface was not observed to be significantly negative (Figure 5.5). The experiments performed here were made on thin (7 nm) brushes so that direct comparison may be made to the brushes presented in Chapter 5. The fall in zeta potential to a negative value could be a result of adsorbed Cl^- counterions from the tracer, KCl used to make the surface zeta potential measurements, which may have in some way been incorporated into the amine brush. The increasingly negative surface zeta potential results are clear, but the reasons for them are less so.

PDMAEMA is both pH and temperature responsive and the swelling ratio of the brush is different at pH 3 to pH 7 (and above). At pH 3 the counterions associated with the protonated (positively charged) segments dominate the contribution to the osmotic pressure and at this pH and below they are fully extended, but collapse at higher pH. PDMAEMA also exhibits a temperature induced collapse whereby as the temperature increases dehydration of the monomers is favoured and water-monomer hydrogen bonds are replaced by monomer-monomer hydrogen bonds.²⁴ At pH 10 and above 40 °C the brush undergoes partial collapse and a two phase brush develops, as presented by Edmondson *et al.*²⁴ Sanjuan's¹⁸ data further suggested that there is a linear fall in charge of the brush as the pH increased. Using the brushes in this collapsed state is not helpful for its intended purpose, so the temperature was maintained at room temperature during incubation. It is clearly advantageous to perform the vesicle incubations at room temperature and pH 5 or below, in order that the chain is charged and extended.

The result of incubating PDMAEMA with 50% DOPG at pH 5, is shown below in Figure 7.7.

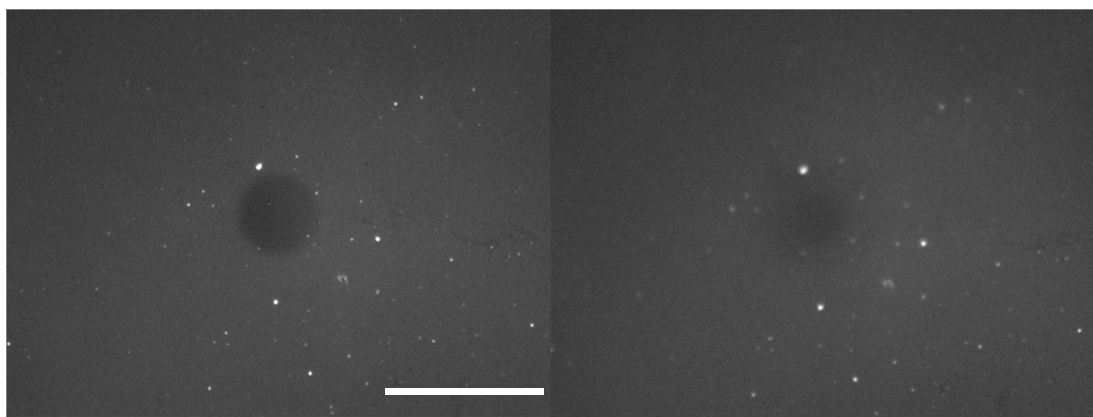


Figure 7.7: PDMAEMA incubated with 50% DOPG:POPC at pH 5. Image at bleaching (left) and after 10 min FRAP recovery (right). Scale bar 60 μm .

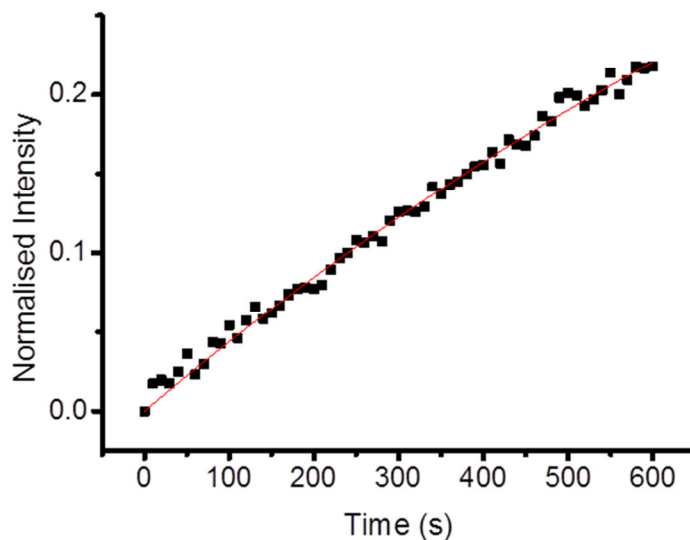


Figure 7.8: FRAP diffusion coefficient for PDMAEMA incubated with 50% DOPG:POPC.

It can be seen from the FRAP images in Figure 7.7 that a lipid layer has adsorbed, it appears fairly homogenous, but with some vesicles attached. The second image after 10 min shows that there is some diffusion but the recovery rate was very low.

Figure 7.8 shows the diffusion coefficient plot by which the rate was calculated to be $0.05 \pm 0.01 \mu\text{m}^2 \text{s}^{-1}$ with a mobile fraction of 62%. The very slow diffusion suggests that there was possibly no fusion of the vesicles to form a bilayer and the mobile fraction confirmed that there was a (40%) fraction of the adsorbed lipids or vesicles which were immobile. The failure of the vesicles to fuse could be the result of inter-vesicle repulsion.

7.3.4. PMETAC poly[2-(methacryloyloxy)ethyl trimethylammonium chloride] (C1 quaternised PDMAEMA) and C12 and C18 quaternised PDMAEMA

7.3.4.1. Preparation and characterisation of quaternised brushes

The basic tertiary amine was quaternised using a good solvent for the brush (THF) or a poor solvent (hexane).³ This generated a brush which was C1 (methyl) quaternised throughout (Table 1 (d) or quaternised at the top only (Table 1 (e)). The hydrated mean thickness was measured by ellipsometry to be 17 nm when hydrated (7 nm dry), with a contact angle of $12 \pm 3^\circ$ (Table 1 (d) and (e)). The AFM measured surface rms roughness was $< 0.3 \text{ nm}$.

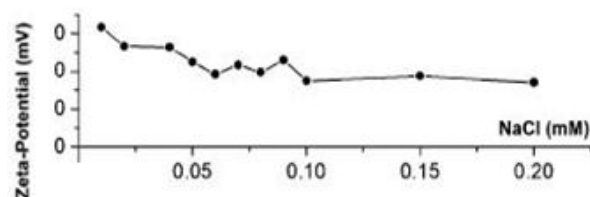
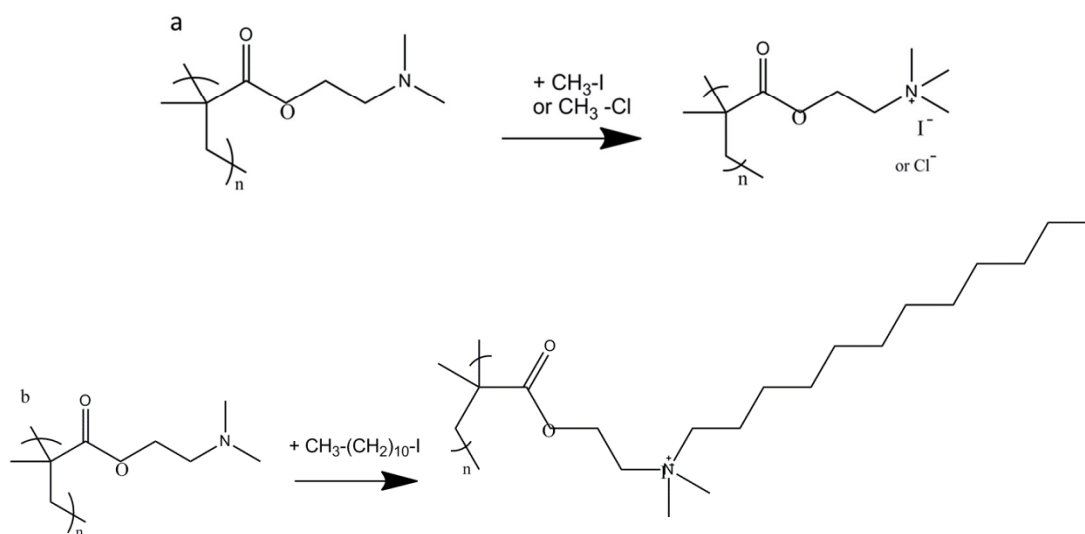


Figure 7.9: Zeta potential of PMETAC showing its surface zeta potential of +30 mV (without NaCl added to the buffer) and its response in buffer solutions with increasing concentrations of NaCl (black circles) from 10 mM to 200 mM. (The published narrative records these concentrations as 0.2 M etc., though the graph legend records 0.2 mM). From reference 25

These fully quaternised chains formed strong PELs, which have permanent positive charges, so changing the buffer pH does not affect the brush charge or height. This characteristics are clearly different from its linear equivalent, PDMAEMA, above, which did respond to changing the pH of the buffer.²⁶

Figure 7.9, taken from the work of Irigoyen *et al.*, indicates that the zeta potential of the PMETAC brush, in a buffer with no added salt (NaCl), is about +30 mV, reducing to +20 mV at 200 mM NaCl, showing only a slight reduction in zeta potential with increasing NaCl.

In addition to the above “C1” chain variant, PMETAC, the PDMAEMA polymer brush was also quaternised with longer chains, to create QDMAEMA with C12 throughout the chain (Table 1 (e), and at the brush top only (Table 1 (g)). Finally PDMAEMA was quaternised with a C18 chain at the top (Table 1 (h)). The basic reactions for this process are shown in Figure 7.10.



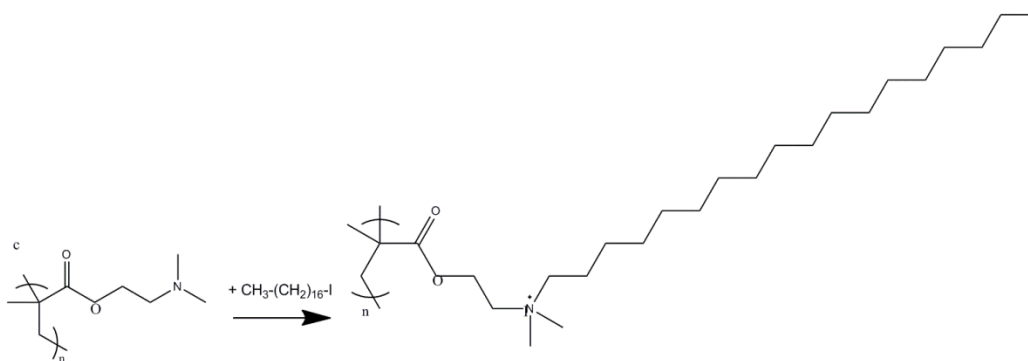


Figure 7.10: Quaternisation of PDMAEMA brushes, with (a) C1 , (b) C12 and (c) C18 chains.²⁷

In summary, this PMETAC (which is a C1 quaternised PDMAEMA) and the variants of PDMAEMA which have longer chains of C12 and C18 (QPDMAEMA) brushes do not respond to changes in pH, so will have “permanent” positive charges along the chains and will be fully extended in solution at pH 7. The PMETAC variant has a positive surface zeta potential of +30 mV in (low NaCl) buffer.

7.3.4.2. Results and discussion for PMETAC-C1 (full and top quaternised): FRAP

According to Huck *et al.*,²⁸ there is an approximately three-fold increase in brush thickness when immersed in water and the surface was effectively hydrophilic with a contact angle of 35°,²⁹ which was slightly higher than our measurements of ~15°. They stated that these brushes have permanent positive charges along the chains, which will repel each other. The conformation of the chains is influenced by changing the osmotic pressure by adding counterions in solution, as shown in Figure 7.9. Huck also suggested that the PMETAC (and the QPDMAEMA brushes shown below) contain Cl⁻ counterions which are hydrated and do not interact strongly with the quaternised amine. By immersing the brush in water the Cl⁻ counterions dissociate from the chains and allow electrostatic repulsions between the cationic charges on adjacent chains to swell the brush.

The first two of the five samples of quaternised PDMAEMA, called PMETAC-C1 (which was quaternised throughout the chain, or at the top only) were incubated with lipids to test its ability to support lipid bilayers. They were tested in MilliQ at ~pH 5 using lipid vesicles containing 0, 25%, 50%, 70% and 90% of DOPG in POPC. Figure 7.11 shows the results obtained for incubating these vesicles on the brush.

The results show that some lipid was adsorbed when incubating with POPC only (zwitterionic lipid), but the result was poor quality and there was no indication of diffusion of these lipids on the brush. When using 25% DOPG, more lipid was adsorbed, (as would be

expected when introducing a negatively charged lipid into the vesicles) but, again, the surface was not homogeneous. The bleached spot after 10 min indicated limited recovery. Slightly better results were obtained when using higher ratios of charged lipid i.e. 50%, 75% and 90%. However, the surface lipid layer was not homogeneous and the recovery rate was very slow, as indicated by the incomplete recovery of the bleached spot after 10 min.

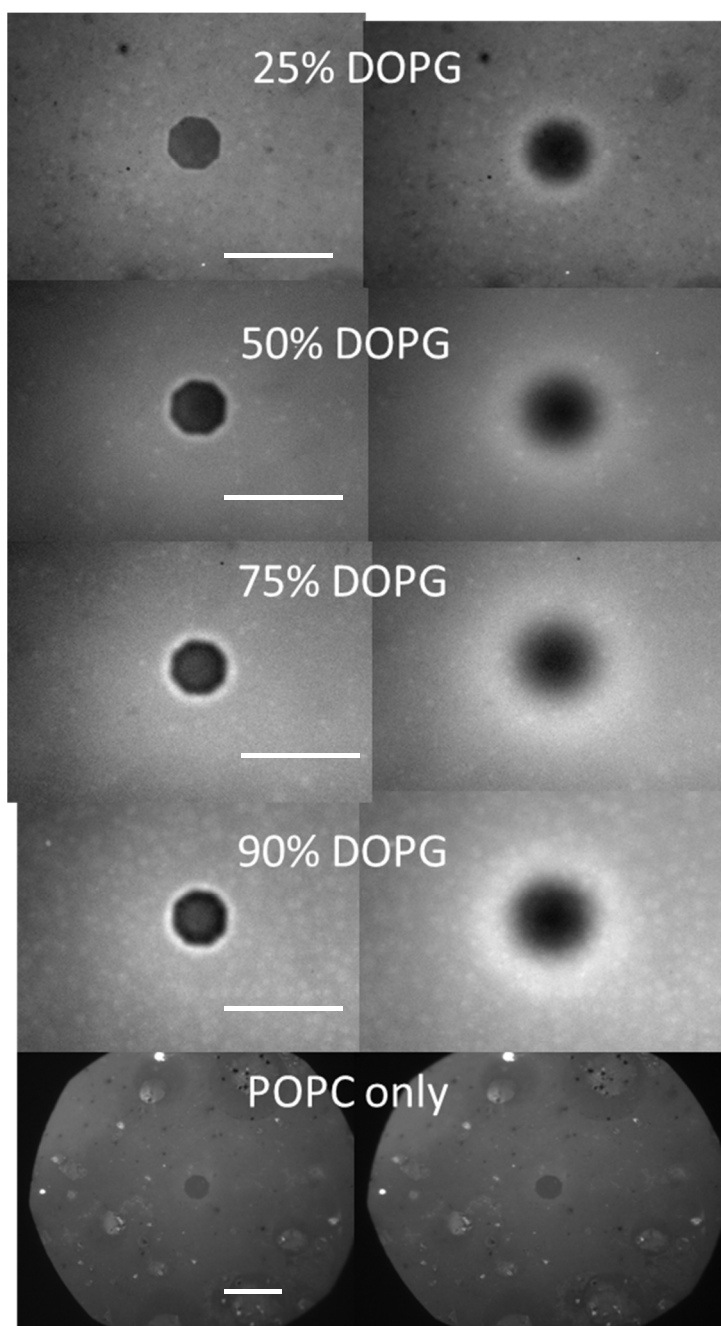


Figure 7.11: Five samples of PMETAC-C1 (fully quaternised) incubated as indicated on the image with 0, 25%, 50%, 75% and 90% DOPG:POPC vesicles. The image on the left was taken immediately after bleaching and on the right after 10 minutes recovery. Scale bars 60 μm .

In addition to the previous five examples, a further sample of PMETAC-C1 was incubated with 50% DOPG:POPC, prepared in PBS buffer (containing 140 mM NaCl at pH 7) to ascertain whether the addition of salt and a change of pH would improve the bilayer quality. The FRAP images at bleaching and after 10 minutes can be seen in Figure 7.12, which show a non-homogenous lipid layer with many defects, seen as dark dots on the image. There was very slow recovery of the bleached spot, very similar to those seen in Figure 7.11.

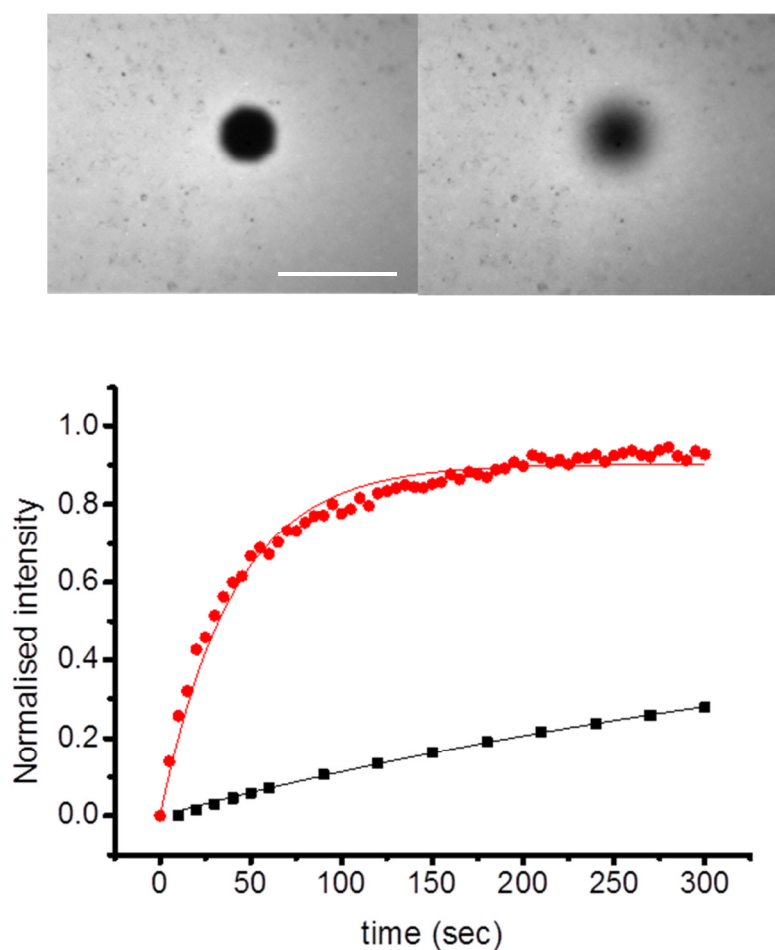


Figure 7.12: FRAP images at bleaching at after 10 min on PMETAC (C1 quaternised throughout the chain). Comparative diffusion curves for bilayers on glass ($D = 1.4 \mu\text{m}^2 \text{s}^{-1}$) with POPC (●) and for the PMETAC surface (■) using 50% DOPG lipids in PBS buffer at pH 7 ($D = 0.13 \mu\text{m}^2 \text{s}^{-1}$ and a mobile fraction of 59%). Scale bar 60 μm .

The diffusion coefficient and mobile fraction were found using FRAP and are $0.13 \mu\text{m}^2 \text{s}^{-1}$ and 59% respectively and is also shown in Figure 7.12 (black plot). A slight improvement on the previous result, but still not high enough values to be considered a homogenous recovering bilayer. In this case the surface zeta potential was +30 mV and the zeta potential

of the 50 % DOPG vesicle was -60 mV, creating a strong interaction potential. The slow diffusion rate could indicate that the lipids, whilst adsorbing on the surface as a result of the strong electrostatic attraction, could be pinned to the surface as unfused vesicles. This diffusion coefficient is more than a factor of 10 slower than the rate for a bilayer formed from the “standard” POPC vesicles on glass (Figure 7.12, red plot) and the fraction of mobile lipid is much lower than the 95% expected from this “standard”. To ascertain whether vesicles or a slowly diffusing lipid bilayer has been adsorbed AFM scans and a breakthrough force curve were performed.

7.3.4.3. Introduction and method for PMETAC-C1: AFM

Following the method described fully in chapter 4 an AFM scan was made of the surface of the supported lipid layer on the C1 quaternised PMETAC polymer (Table 1 (d)), in its hydrated form in buffer. The FRAP image showed a slowly recovering bleached spot. The AFM images and a height measurement, made across an etched area were used to determine whether a vesicular layer or a bilayer was present.

7.3.4.4. Results and discussion: PMETAC-C1: AFM

Figure 7.13 shows an AFM scan of the surface of the lipid deposited on the PMETAC-C1 brush. The surface had many elevated features of 10 nm high with a surface (rms) roughness measured at 17 nm. This surface is more characteristic of adsorbed vesicles rather than a smooth bilayer.

The AFM images, shown in Figure 7.14 show the height measurements taken across an etched area on the sample. This was made by applying a force to the tip to remove the deposited brush and lipid from the glass substrate. The height profile (Figure 7.14 (a)) was measured to be 44 nm. This represents the combined height of the surface deposition, i.e. the initiator, polymer and lipid layer together. The initiator plus polymer had a dry length of ~7 nm, which could be expected to swell up to 17 nm in liquid. A bilayer would be 4 to 5 nm thick, giving a total of ~22 nm if a bilayer was present. If vesicles were present, rather than a bilayer, they would measure up to 25 nm in height (the diameter measured by DLS), depending on their degree of flattening onto the polymer brush. This second case is closer to the 44 nm measured, strongly suggesting that a bilayer was not formed and that vesicles were present on the brush surface. It was assumed that the scratched area was exposing glass and thus gave a realistic measurement of the total height of the initiator, brush and lipid layer.

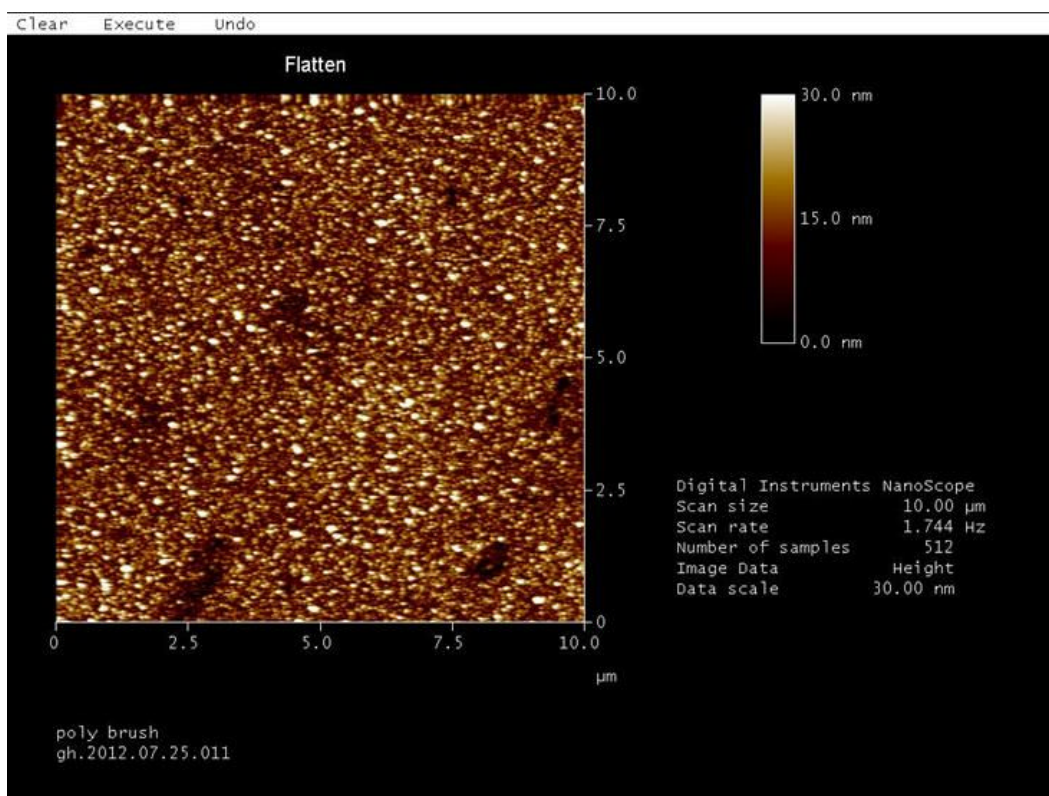
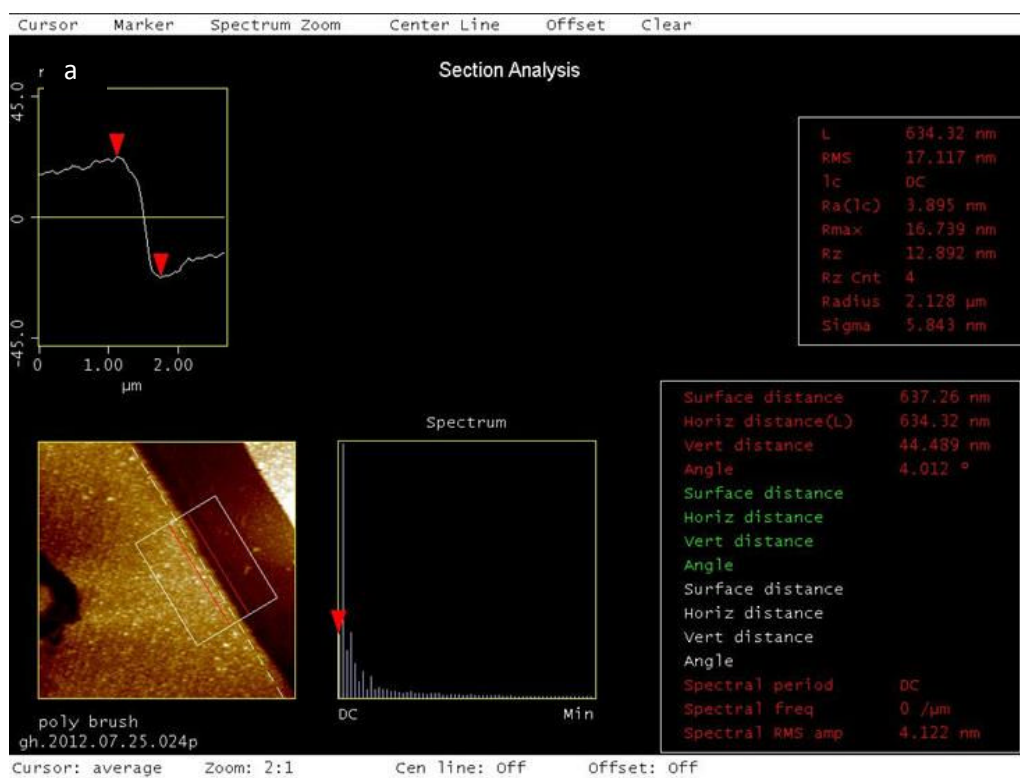


Figure 7.13: Lipid deposited on the quaternised PMETAC-C1 surface, indicating that intact vesicles are present.



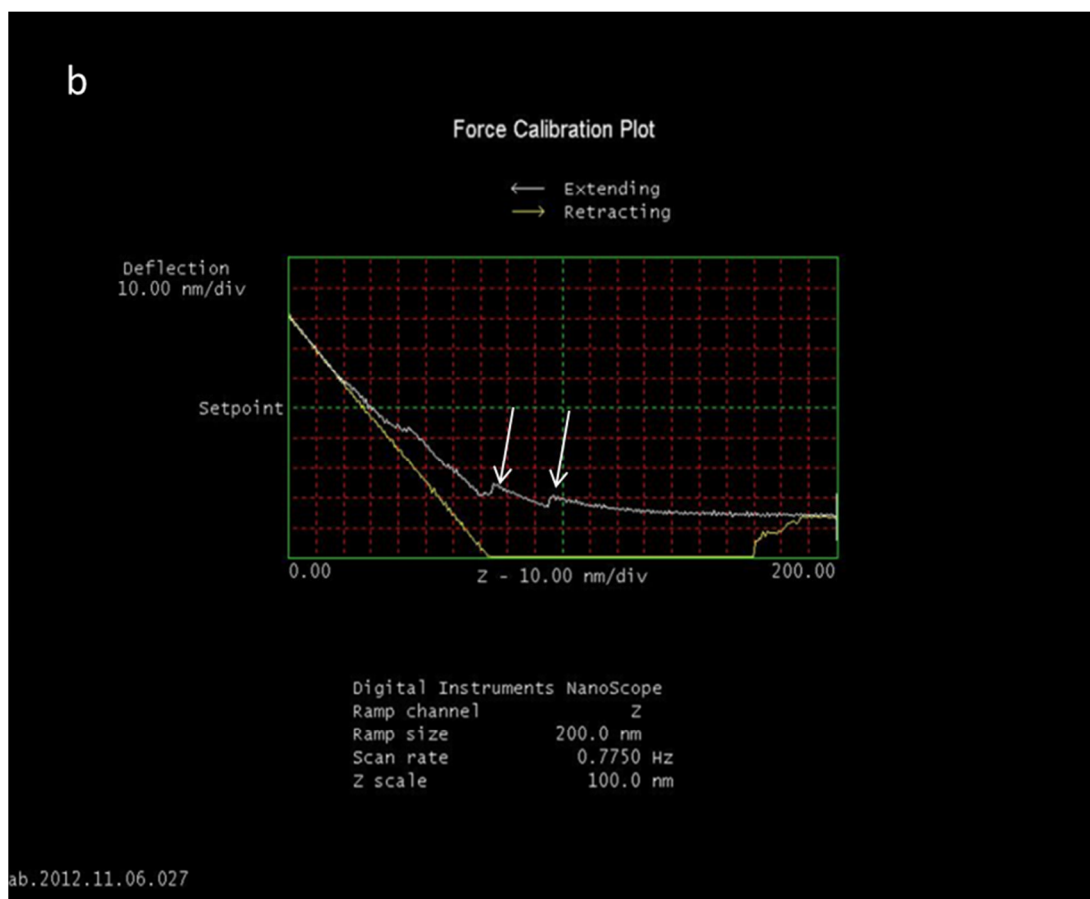


Figure 7.14: Measurements of the lipid/vesicle layer on a PMETAC (C1 quaternised) brush indicating the area size of the scan (a) and its height profile and (b) the force curve showing multiple breakthrough points (white arrows).

The third image shown in Figure 7.14 (b) shows a breakthrough force measurement taken by applying sufficient force to the tip to push it through the deposited lipid layers. When this method was applied to a bilayer on glass the force (y axis) correlated with a distance of ~ 5 nm (x axis) which confirmed the thickness of the deposited layer. However, it was more difficult to make this measurement on a soft polymer brush as this does not provide the same resistance that the glass surface does. In the above measurement (Figure 7.14) there were two breakthrough points, highlighted by the white arrows. These were indicative of the tip feeling resistance from two bilayers, as would be measured when vesicles were present (as the tip breaks through both sides of the vesicle).

In summary, the evidence presented by the very slowly recovering FRAP images and the AFM scan image and height measurements, confirms that a layer of intact vesicles is deposited on this polymer, rather than a lipid bilayer.

7.3.4.5. Results and discussion for PDMAEMA quaternised with C12 and C18

In the above example a C1 methyl group was used to quaternise throughout the brush and the samples showed contact angles of $\sim 15^\circ$ whereas when using the longer C12 acyl chains, the brushes were less hydrophilic with CAs of between 54 and 61° , as might be expected with the introduction of longer acyl chains. However, there appeared to be no relationship between the contact angle and the result of depositing lipid vesicles onto the brush sample.

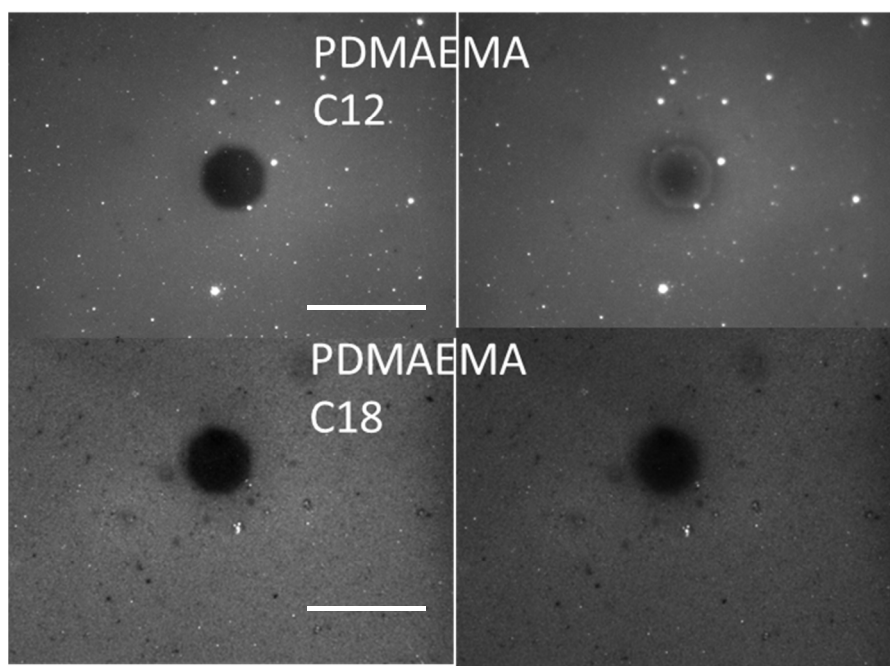


Figure 7.15: FRAP images at time 0 and after 10 min recovery time for PDMAEMA with C12 (top) and C18 (below) chains attached. Scale bar 60 μm applies to all images.

It was expected that the longer chains (C12, see Table 7.2(f) and (g) and C18, (h)) would insert into the hydrophobic core of the bilayer and aid fusion of the lipid bilayer as was demonstrated by Han *et al.*³⁰ when using cholesterol tethers. The results of incubating 50% DOPG lipids, shown in Figure 7.15, showed inhomogeneous surfaces with no vesicle fusion or bilayer formation taking place. The result for the C18 chain showed almost no diffusion of the lipid layer.

7.5. Summary and discussion of work on cationic brushes

A summary of the results is presented below, in Table 7.2. A range of amine brushes of differing configurations and pH responses were incubated with zwitterionic and anionic lipid vesicles. All the brushes shown have adsorbed the charged vesicles to a similar degree, giving full coverage of the surface with a lipid layer in most cases. None of the samples

shows a homogenous lipid layer, as would be expected for a fluid bilayer, and all show evidence of defects. The results shown in Table 7.2 are those produced from incubating with 50% DOPG in all cases, for comparison. They all exhibited slow diffusion which is indicated by the FRAP images taken after 10 minutes recovery time which showed incomplete recovery. The calculated coefficients were less than $0.1 \mu\text{m}^2 \text{s}^{-1}$ in all cases, very much lower than expected for a fluid lipid bilayer.

PTBAEMA brushes have a positive surface zeta potential in excess of +20 mV at low pH when the amine is protonated. Vesicle incubation at pH 5, when the surface was more highly charged, was required for vesicles to be attracted to the surface. At pH 7, with a reduction of the surface charge of the brushes there was less interaction with the charged lipids. The collapse of the chain took place over such a narrow (1 unit) pH range, that fine tuning of length by using changes in pH was not practical. Creating a cross-linked PTBAEMA brush, in an attempt to present a smoother surface for lipids to fuse onto, did not appear to affect the outcome when incubating vesicles. The addition of NaCl to the buffer also reduced the effective charge on the brush and vesicle surfaces, reducing the attraction between the two, but did not support the formation of a fluid bilayer.

Attempts were made to tune the PMETAC brushes interactions with the vesicles by varying the ratio of anionic lipid in the vesicles. A balance was needed that was sufficient to attract vesicles to the surface, but not too strong so as to immobilise vesicles or create high inter-vesicle repulsion, which would prevent their fusion. The results (Figure 7.11) show that, though there were slight variations between results, none produce a fluid bilayer. The FRAP results, suggested the presence of vesicles on the surface, was confirmed by AFM (Figure 7.13 and Figure 7.14).

The addition of C12 and C18 chains to create the QPDMAEMA polymer brush with the aim of promoting rupture by inserting the acyl chains into the lipid vesicle did not actually facilitate vesicle rupture in the expected manner.

The contact angle of the brush did not appear to be a factor in the end result, though it is logical that it may correlate with the surface charge. During vesicle incubation there was no indication as to whether a moderately ($CA > 40^\circ$) or highly ($CA < 40^\circ$) hydrophilic surface was more likely to form a bilayer, when incubated with the vesicles.

Referring to work from the literature on the interactions between cationic polymers and lipids, Fischlechner *et al.* presented some interesting findings. They tested a system of PEL multilayers, using a primary amine and a quaternary amine as the uppermost polymer layer.³¹ Changes in the FTIR spectra were used to assess how the spectra of the polymer

changed when reacting with lipids. These changes suggested two things: one, that there was a strong interaction between the lipid carboxyl and the primary amine group and two, that the lipid carbonyl oxygen may have been partially dehydrated. In the former case they found that the amine formed a hydrogen bond with the carboxyl, replacing the bound water. The data further suggest that there were two points of attachment between the negatively charged lipid and the amine of the polymer, namely the carboxyl and the phosphate. With POPC, binding only took place between the phosphate group and the polymer amine group. In both cases there was local dehydration of these functional groups, which was confirmed by shifts in the IR spectra. There was also the possibility of the POPC phosphate groups binding electrostatically (at long range) and through hydrogen bonding (at short range) with the primary amine groups. These binding effects would slow any diffusion of the lipids or intact vesicles on the surface.

Two further considerations may explain what is happening within these systems. One is that the very slow diffusion, rather than being the result of slowly moving vesicles on the brush surface, could be the result of vesicles diffusing, intact within the polymer strands. Wang *et al.*,³² described the interaction of cationic conjugated polyelectrolytes with negatively charged (DPPG) lipid membranes. In this case they were specifically looking for antimicrobials to perturb the membrane and they found that the cationic polymer strands, with a hydrophobic backbone, did insert into the membranes, suggesting that the polymer strands could intersperse with the lipids. Further analysis, using FCS, would be helpful to evaluate this.

In conclusion, a range of variants of cationic brushes, which were either secondary, tertiary, quaternised amines, linear or modified with carbon chains or cross-linked have been tested. There was no obvious candidate for supporting a freely diffusing lipid bilayer. The positive charges on the brushes were utilised to create an electrostatic interaction to the anionic lipid vesicles which had supported the adhesion of vesicles onto the surface. The testing showed that whilst lipids or vesicles could be deposited onto them, fluid recovering bilayers were not observed. The correct balance of charge between surface and vesicles was clearly not achieved in order that the vesicles may fuse. The objective of being able to incorporate functioning, freely diffusing transmembrane proteins into the bilayer would therefore not be possible with these systems at this stage.

This work, whilst not achieving its planned aim has added to the knowledge of electrostatic interactions between charged surfaces and vesicles. The cationic polymers (and pH responsive ones in particular) are extensively used in medical applications as gene delivery

vectors^{11 14} and their interactions with the cell membrane are also utilised in antibacterial coatings.¹² Furthermore the opportunity to adsorb intact vesicles onto the brushes could be exploited by incorporating protein into the vesicles and studying the proteins within the proteoliposomes, in a similar way to the work done by the Jeuken group.^{33 34}

The work on a variant of the PDMAEMA polymer was continued by other members of the collaboration who reduced the brush cross-linking to a, much lower, 10% than was tested above, and renamed it PDMA. When using a lower (10%) ratio of DOPG:POPC lipids and heating to 50°C for an extended period of time at pH 8, a lipid bilayer did form with good diffusion rates.

7.6. Table 1 summary of results

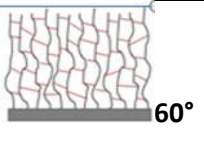
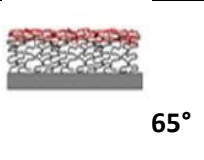
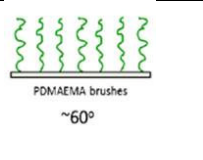
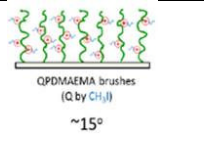
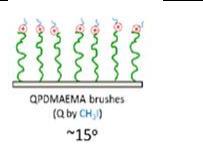
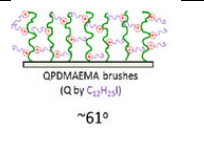
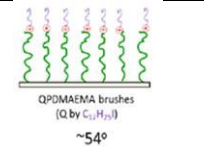
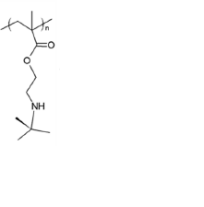
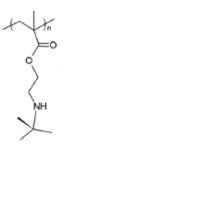
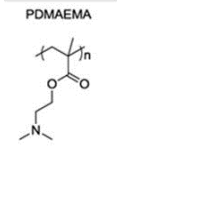
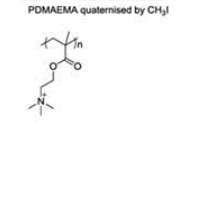
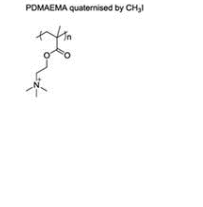
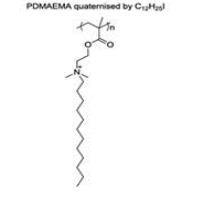
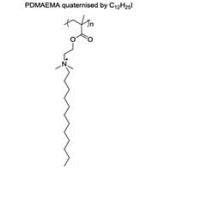
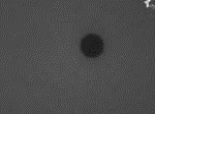
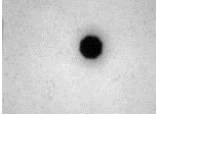
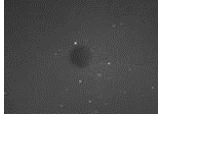
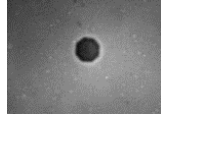
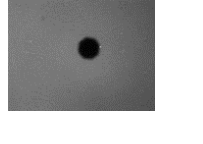
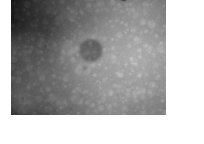
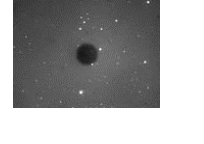
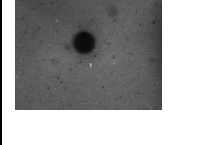
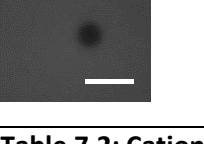
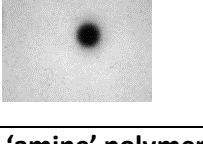

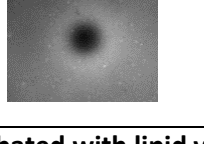
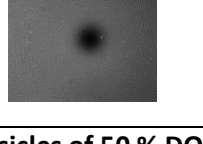
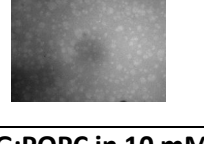
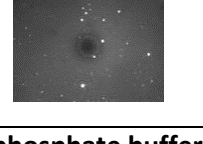
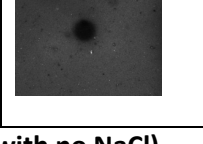
PTBAEMA (2° amine, fully cross-linked) (a)	PTBAEMA (2° amine top cross-linked) (b)	PDMAEMA (2° amine) (c)	PMETAC C1 Quaternised amine throughout (d)	PMETAC C1 Quaternised amine at chain end (e)	QPDMAEMA C12 Quaternised amine throughout (f)	QPDMAEMA C12 Quaternised amine at chain end (g)	QPDMAEMA C18 Quaternised amine at chain end (h)
							
							
							
							

Table 7.2: Cationic ‘amine’ polymer brush variants incubated with lipid vesicles of 50 % DOPG:POPC in 10 mM phosphate buffer (with no NaCl). From the top is a schematic of the brush with the contact angle, chemical structures of the monomer and attached chain. Below these are the FRAP images at time zero, immediately after bleaching and at 10 minutes after recovery. All the brushes are of 6 to 10 nm, dry length. Scale bar 60 μ m applies to all images.

7.7. References

- ¹ Li, Z.; Sahle-Demessie, E.; Hassan, A. A.; Sorial, G. A., Transport and deposition of CeO₂ nanoparticles in water-saturated porous media. *Water research* **2011**, *45* (15), 4409-4418.
- ² Sandén, T.; Salomonsson, L.; Brzezinski, P.; Widengren, J., Surface-coupled proton exchange of a membrane-bound proton acceptor. *Proceedings of the National Academy of Sciences* **2010**, *107* (9), 4129-4134.
- ³ Alswieleh, A.M.M., Micro- and Nano-Structure of Polymers and Molecular Materials. Ph.D. thesis, University of Sheffield, July **2014**.
- ⁴ Alswieleh, A. M.; Cheng, N.; Leggett, G. J.; Armes, S. P., Spatial control over cross-linking dictates the pH-responsive behavior of poly (2-(tert-butylamino) ethyl methacrylate) brushes. *Langmuir* **2014**, *30* (5), 1391-1400.
- ⁵ Morse, A. J.; Dupin, D.; Thompson, K. L.; Armes, S. P.; Ouzineb, K.; Mills, P.; Swart, R. Novel Pickering Emulsifiers based on pH-Responsive Poly(tert-butylaminoethyl methacrylate) Latexes. *Langmuir* **2012**, *28*, 11742–11753.
- ⁶ Hoffmann, M.; Lang, M.; Sommer, J.-U. Gelation threshold of cross-linked polymer brushes. *Phys. Rev. E* **2011**, *83*.
- ⁷ Huang, W. X.; Baker, G. L.; Bruening, M. L. Controlled synthesis of cross-linked ultrathin polymer films by using surface initiated atom transfer radical polymerization. *Angew. Chem., Int. Ed.* **2001**, *40*, 1510–1512.
- ⁸ Ballauff, M.; Borisov, O., Polyelectrolyte brushes. *Current Opinion in Colloid & Interface Science* **2006**, *11* (6), 316-323.
- ⁹ Moglianetti, M.; Webster, J. R.; Edmondson, S.; Armes, S. P.; Titmuss, S. Neutron Reflectivity Study of the Structure of pH Responsive Polymer Brushes Grown from a Macroinitiator at the Sapphire– Water Interface. *Langmuir* **2010**, *26*, 12684–12689.
- ¹⁰ Morse, A. J.; Dupin, D.; Thompson, K. L.; Armes, S.; Ouzineb, K.; Mills, P.; Swart, R., Novel Pickering Emulsifiers based on pH-responsive poly (tert-butylaminoethyl methacrylate) Latexes. *Langmuir* **2012**, *28* (32), 11733-11744.
- ¹¹ Majewski, A. P.; Stahlschmidt, U.; Jérôme, V. r.; Freitag, R.; Müller, A. H.; Schmalz, H., PDMAEMA-grafted core–shell–corona particles for nonviral gene delivery and magnetic cell separation. *Biomacromolecules* **2013**, *14* (9), 3081-3090.

-
- ¹² Qin, X.; Li, Y.; Zhou, F.; Ren, L.; Zhao, Y.; Yuan, X., Polydimethylsiloxane-polymethacrylate block copolymers tethering quaternary ammonium salt groups for antimicrobial coating. *Applied Surface Science* **2015**, *328*, 183-192.
- ¹³ Laymana, J. M.; Hiranib, A. A.; Pickelc, J. M.; Brittc, P. F.; Leeb, Y. W.; Longa, T. E., Influence of macromolecular architecture on nucleic acid transfection. *Polymer Preprints* **2006**, *47* (2), 70.
- ¹⁴ Liechty, W. B.; Peppas, N. A., Expert opinion: responsive polymer nanoparticles in cancer therapy. *European Journal of Pharmaceutics and Biopharmaceutics* **2012**, *80* (2), 241-246.
- ¹⁵ Jia, H.; Wildes, A.; Titmuss, S., Structure of pH-responsive polymer brushes grown at the gold–water interface: dependence on grafting density and temperature. *Macromolecules* **2011**, *45* (1), 305-312.
- ¹⁶ Chen, J.-K.; Bai, B.-J., Diagnosis of breast cancer recurrence after surgery by using poly (2-dimethylaminoethyl methacrylate) brushes as a medium on silicon surface. *Sensors and Actuators B: Chemical* **2011**, *160* (1), 1011-1019.
- ¹⁷ Edmondson, S.; Osborne, V. L.; Huck, W. T., Polymer brushes via surface-initiated polymerizations. *Chemical society reviews* **2004**, *33* (1), 14-22.
- ¹⁸ Sanjuan, S.; Perrin, P.; Pantoustier, N.; Tran, Y., Synthesis and swelling behavior of pH-responsive polybase brushes. *Langmuir* **2007**, *23* (10), 5769-5778..
- ¹⁹ Fielding, L. A.; Edmondson, S.; Armes, S. P., Synthesis of pH-responsive tertiary amine methacrylate polymer brushes and their response to acidic vapour. *Journal of Materials Chemistry* **2011**, *21* (32), 11773-11780.
- ²⁰ Moglianetti, M.; Webster, J. R.; Edmondson, S.; Armes, S. P.; Titmuss, S., Neutron reflectivity study of the structure of ph-responsive polymer brushes grown from a macroinitiator at the sapphire– water interface. *Langmuir* **2010**, *26* (15), 12684-12689.
- ²¹ Geoghegan, M.; Ruiz-Pérez, L.; Dang, C. C.; Parnell, A. J.; Martin, S. J.; Howse, J. R.; Jones, R. A.; Golestanian, R.; Topham, P. D.; Crook, C. J., The pH-induced swelling and collapse of a polybase brush synthesized by atom transfer radical polymerization. *Soft Matter* **2006**, *2* (12), 1076-1080.

-
- ²² Rauch, S.; Uhlmann, P.; Eichhorn, K.-J., In situ spectroscopic ellipsometry of pH-responsive polymer brushes on gold substrates. *Analytical and bioanalytical chemistry* **2013**, *405* (28), 9061-9069.
- ²³ Data from N Cheng, University of Sheffield, unpublished at the time of writing
- ²⁴ Edmondson, S.; Vo, C.-D.; Armes, S. P.; Unali, G.-F., Surface polymerization from planar surfaces by atom transfer radical polymerization using polyelectrolytic macroinitiators. *Macromolecules* **2007**, *40* (15), 5271-5278.
- ²⁵ Irigoyen, J.; Arekalyan, V. B.; Navoyan, Z.; Iturri, J.; Moya, S. E.; Donath, E., Spherical polyelectrolyte brushes' constant zeta potential with varying ionic strength: an electrophoretic study using a hairy layer approach. *Soft Matter* **2013**, *9* (48), 11609-11617.
- ²⁶ Azzaroni, O.; Brown, A. A.; Huck, W. T., Tunable wettability by clicking counterions into polyelectrolyte brushes. *Advanced Materials* **2007**, *19* (1), 151-154.
- ²⁷ Xu, Y.; Bolisetty, S.; Drechsler, M.; Fang, B.; Yuan, J.; Ballauff, M.; Müller, A. H., pH and salt responsive poly (N, N-dimethylaminoethyl methacrylate) cylindrical brushes and their quaternized derivatives. *Polymer* **2008**, *49* (18), 3957-3964
- ²⁸ Azzaroni, O.; Moya, S.; Farhan, T.; Brown, A. A.; Huck, W. T., Switching the properties of polyelectrolyte brushes via "hydrophobic collapse". *Macromolecules* **2005**, *38* (24), 10192-10199.
- ²⁹ Azzaroni, O.; Moya, S. E.; Brown, A. A.; Zheng, Z.; Donath, E.; Huck, W., Polyelectrolyte brushes as ink nanoreservoirs for microcontact printing of ionic species with poly (dimethyl siloxane) stamps. *Advanced Functional Materials* **2006**, *16* (8), 1037.
- ³⁰ Han, X.; Pradeep, S. N.; Critchley, K.; Sheikh, K.; Bushby, R. J.; Evans, S. D., Supported Bilayer Lipid Membrane Arrays on Photopatterned Self-Assembled Monolayers. *Chemistry-a European Journal* **2007**, *13* (28), 7957-7964.
- ³¹ Fischlechner, M.; Zaulig, M.; Meyer, S.; Estrela-Lopis, I.; Cuéllar, L.; Irigoyen, J.; Pescador, P.; Brumen, M.; Messner, P.; Moya, S., Lipid layers on polyelectrolyte multilayer supports. *Soft Matter* **2008**, *4* (11), 2245-2258.
- ³² Wang, Y.; Jones, E. M.; Tang, Y.; Ji, E.; Lopez, G. P.; Chi, E. Y.; Schanze, K. S.; Whitten, D. G., Effect of polymer chain length on membrane perturbation activity of cationic phenylene ethynylene oligomers and polymers. *Langmuir* **2011**, *27* (17), 10770-10775.

³³ McMillan, D. G.; Marritt, S. J.; Butt, J. N.; Jeuken, L. J., Menaquinone-7 is specific cofactor in tetraheme quinol dehydrogenase CymA. *Journal of Biological Chemistry* **2012**, *287* (17), 14215-14225.

³⁴ Daskalakis, N. N.; Müller, A.; Evans, S. D.; Jeuken, L. J., Driving bioenergetic processes with electrodes. *Soft Matter* **2011**, *7* (1), 49-52.

8. Summary, conclusions and future work

8.1 Summary

Many areas of science and medicine utilise the supported lipid bilayer as a useful tool for studying the structure and function of cell membranes and the proteins incorporated in them. Biomimetic lipid bilayers have been in use for over 30 years, supported by planar silicon, gold or other substrates. Microscopy, including FRAP, TIRF and dark field have proved useful tools to study the activity and mobility of these membranes in a hydrated environment. Electrical conductance studies also utilise the lipid vesicle and planar bilayer for studying the activity of proton pumps and charge movement. Developing from this, the use of polymeric supports for lipid bilayers has proven invaluable. They provide a more natural environment than planar glass for functional studies of incorporated proteins. The use of polymers in a range of chemical structures is also important to create vehicles in which to deliver drugs and genetic interventions, such as DNA fragments. The importance of this area of science, therefore, is developing rapidly.

The work presented here was part of a collaboration project and as such there were specific expectations, demands and challenges for what should be achieved. The overarching project can be summarised as “controlling molecules at low dimensions” by extracting and placing the components of the light harvesting bacterium, *Rh. Sphaeroides* in confined locations. The ultimate aim of this was to recreate the functioning photosystem “on-chip”. The confined locations were to be created by the use of polymers which would be patterned to create corrals or would be used to tether individual proteins to the polymer strands. The contribution of this project was to create a biomimetic lipid membrane environment in the form of a polymer supported bilayer. This was to be developed further by depositing a protein incorporated lipid bilayer on a polymer brush, or by surrounding tethered proteins with a lipid bilayer. It was proposed that the proteins would then be maintained in their natural state and their functionality, both individually and in concert, could be examined. The polymer chemists of the group were tasked with creating the brushes to be used as the substrates on which to test bilayer formation.

From the outset, there were many challenges to resolve with the polymer brushes, most importantly to choose suitable monomers of controllable architecture. It was important to select the monomers with care to ensure the electrostatic charge could be controlled as well as the brush length and response to pH and temperature. The brushes also had to be suitable for other, more

practical, applications (in medicine or technology) and not just of curiosity value for the project. The practical issues of creating polymer brushes with consistent sample quality as well as carefully selected properties did prove a huge challenge, particularly at the beginning of the project when the amine (cationic) surfaces were tested.

Having been presented with a series of cationic, zwitterionic and anionic brushes, the task of producing a mobile lipid bilayer on these polymer brush supports was a primary requirement. The brush surfaces tested, which were strongly cationic (amines) or strongly anionic (sulphonate or carboxylates) proved very useful for adsorbing layers of in-tact vesicles; a process driven by the electrostatic interactions between the surface and oppositely charged vesicles, indicating that the work was heading along a hopeful path. Many conditions and configuration of these brushes were examined but no successful combination was found which supported fusion of these adsorbed vesicles into a fluid bilayer. There are, however, many instances in the literature where proteins have been incorporated into vesicles, as proteoliposomes, and their functionality studied. Also, the study of interactions between anionic charged vesicles and cationic polymers is a significant area of research where polymersomes are used as drug delivery vehicles. Thus this work did add to the knowledge in this field, despite not providing an ideal result for the project.

One common feature of this work was that the zeta potentials of all surfaces and lipid vesicles used were tested under a range of solution conditions. This work provided a way of measuring the strength of the interactions between the brush surface and the vesicles being incubated on them. Work then focussed on two zwitterionic brushes and it was interesting to note that one, PMPC, did not interact with vesicles of any kind: it was determined that with an interaction potential of around zero mV^2 there was no driving force for the adsorption of vesicles. This became an important candidate brush for creating the lipid-resistant walls of the corrals described in Chapter 1. However, a second, novel amino acid brush of PCysMA did support fluid bilayers. The PCysMA supported lipid bilayer was fully characterised using FRAP and AFM and proved to be homogenous, highly diffusing ($1.4 \mu\text{m}^2 \text{s}^{-1}$) and to have high mobility (>92%). Most importantly the result was reproducible. The key to this was evaluated and there appeared to be a narrow range of interaction potentials of around 460mV^2 that supported successful bilayer formation. Below this “optimum” interaction value, with a smaller charge interaction (but above zero mV^2), a layer of intact vesicles could be adsorbed but no diffusion was observed. At higher interaction potentials, (> 800mV^2) vesicles were adsorbed. There was no fusion into a bilayer and very slow diffusion of the vesicles was observed. At these higher interaction potentials similar results were seen with all the brush surfaces which had

either high negative or high positive zeta potentials, when incubating with lipid vesicles of opposite charge.

Following this success a number of methods were tested to incorporate a functioning transmembrane protein into the bilayer. The first of these used cationic vesicles (of a 25% charge ratio DOTAP:POPC) to create proteoliposomes incorporating proteorhodopsin. Despite the literature evidence, this did prove very difficult, though the method worked better with anionic vesicles (of 25% DOPG:POPC) than with cationic ones. A second method, to incorporate a cytochrome bo3 protein into a cationic vesicle showed promise and AFM images were obtained of a brush containing the light harvesting protein. However, much more interesting and promising was a simple detergent depletion method to create a bilayer on the PCysMA brush, containing significant elements (as C10H vesicles) of the *Rh Sphaeroides* light harvesting system.

8.2 Future work

At all stages there were opportunities to develop the experimental work further.

It is my conclusion that the cationic (amine) surfaces, despite being classified as “unsuccessful” in terms of this project, are useful test systems for studying vesicle interactions with anionic lipids and, potentially, to support in-tact vesicles which could incorporate light harvesting (or other) proteins. Future work in this area would involve exploring the higher charged DOTAP containing vesicles, which were adsorbed on the cationic polymer surfaces, to confirm the nature of the interactions of the adsorbed layer. This could be done by combining the techniques of surface plasmon resonance (SPR), QCMD and AFM. SPR and QCMD can be used to follow adsorption in real time to determine whether vesicles were adsorbed in-tact and whether they fused following adsorption. AFM would be used to determine the thickness of the adsorbed layer and prove firstly that vesicles were adsorbed and secondly whether they represented one or more layers of vesicles on the surface. Some FRAP images suggested that there could be diffusion of lipids *within* the polymer brush as seen in Table 7.2.(e) and using FCS to study the diffusion of the lipids or vesicles within this lipid layer would be helpful in this case.

The successful PCysMA brush work could be developed, firstly by establishing that the bilayer is fully (charge) sealing. This can be done by growing the brush from a conductive surface such as gold and taking conductance measurements, by using EIS. Attempts to do that here were affected by the poor bonding of the polymer to the gold, so this would need to be improved.

Attempts to incorporate of light harvesting components into lipid vesicles have been presented in this work, and whilst success was indicated by the AFM images, the incorporation of proteins into vesicles is a complex method and prone to problems. However, this work could be pursued for the research on cationic polymer brushes to be developed further into a useful platform for measuring protein activity. This would mean incorporating proteins into anionic vesicles adsorbing them onto a cationic polymer, which have been grown from a conducting (gold), substrate. Measurement of the functionality of the protein using an electrical readout or via a pH change could then take place.

The most interesting part of the project was to develop a method to incorporate proteins onto polymer brushes and directly into a lipid bilayer via the detergent depletion method. The initial confirmation that the proteins were present in the bilayer, as indicated by dark field experiments presented above, need to be repeated and the results confirmed. Finally, the detergent depletion method should be taken further and repeated, with AFM scans being done as soon as possible after bilayer formation to obtain high quality images which would help to confirm the presence of the proteins on a polymer brush in a fluid bilayer. It would also be necessary to establish that all the proteins are oriented in the same manner, so that proton pumping takes place in one direction.

The next stage of the project, not explored in this thesis would be to measure the charge transfer activity of the incorporated proteins. This could be done in a simple manner by measuring a pH change caused by the movement of protons from one side of the membrane to the other. Protocols to do this are available within the University of Leeds. This would prove the utility of this polymer supported bilayer for the study of protein activity in general and not only relating to the light harvesting system of the project.

In summary, this project promised to be very interesting and significant, providing insight into the development of a new field of low-dimensional science which bridged physics, chemistry and biology. Expertise in these fields was to be combined with the aim of understanding that: interactions may work differently at low dimensions, and to use this knowledge to potentially generate energy from absorbed light, in "biomimetic photosynthesis". The reality of trying to produce one of the building blocks for this work as a polymer supported lipid bilayer was very challenging. It exposed many questions, not least to understand the complex area of the interactions between solid surfaces, polymers and lipid bilayers in a hydrated environment. My first question on reading about this project, though possibly naïve at the time, was about the interactions between the solid support and a lipid bilayer and it now seems it was the most pertinent and important one

to ask. The end result of this work, to publish a method to create a fluid, polymer supported lipid bilayer was successful and satisfying, but left an important and intriguing unanswered question which is why this particular system worked when others didn't. The development of the detergent depletion method, to incorporate a functioning transmembrane protein, also indicated early success and has the potential to be used for a range of protein reconstitutions.

Appendix 1.

Copied from the funding application, this quotation from the Low-Dimensional Chemistry project document shows the importance of the supported lipid bilayers to the project.

“Polymer brushes, proteins and supported lipid bilayers are also employed as structural elements in every work package. Embedded in this supported layer will be membrane proteins. We will develop new polymer brush supports for lipid bilayers, designed to maximise the mobility of membrane lipids and proteins. Lipid bilayers will be supported on brushes and measurements made of the diffusion coefficients of membrane components. We will incorporate binding pockets designed to accommodate membrane proteins within the brush layer. We will fabricate macroscopically extended arrays of metallic nanostructures, and functionalise these with membrane proteins. The membrane proteins will be embedded in supported lipid bilayers, resting upon polymer brush ‘cushions’ formed in the regions of surface surrounding the nanodots. We will construct a wholly synthetic membrane channel by fabricating a stimulus-responsive polymer brush nanostructure at the entrance to a nanoscopic pore in an inorganic film. The pore will be embedded in a supported lipid bilayer.

Proton-permeable polymer brush layers will be developed that will support the maintenance of proton gradients. Supported lipid bilayers will be formed on proton-permeable polymer supports. We will investigate the potential for using polyelectrolyte brush films for osmotic storage of charge. We will assemble a supported lipid bilayer structure in which ATP synthase is embedded, and then subject it to a transmembrane gradient. We will measure the motion that results from the conversion of chemical to mechanical energy in the proton gradient.”

Appendix 2.

A full list of polymers tested for bilayer formation, but not included in the results chapters. In all cases no successful bilayers were formed.

PMPC-PHPMA-PMPC (triblock)

PMPC-PHPMA (diblock)

PMPC-PDMAEMA

PMPC-PDMAEMA C18 top (+ve)

PMPC-PDMAEMA C12 top (+ve)

PMPC-PDMAEMA C1 top (+ve)

PMPC-PKSPMA (-ve)

Gold nano dots with (possibly) LH1 protein attached on dots of 15, 40 and 50 nm height
PCBMA of 10 and 22 nm dry length.

Micro-patterned PCysMA

The following abbreviations apply:

PMPC poly[2-(methacryloyloxy)ethyl phosphorylcholine]

PDMAEMA	poly (N,N- dimethylamino ethylmethacrylate)
PKSPMA	poly(3-sulfopropylmethacrylate potassium salt)
PHPMA	Poly(hydroxypropyl methacrylate)
PCBMA	Poly(carboxybetaine methacrylate)
PCysMA	Poly(cysteine methacrylate)

Appendix 3.

The two grids below show the measurements of the size of 25%DOTAP:POPC vesicles using DLS at 25°C and 50°C.

Up to 100 'background' readings are taken by the software for each complete 'top level' reading requested by the user. In this case the user requested 3 'top-level' readings, but (oddly) the software does display header data to reflect the average of these three readings shown by the graph below it (only displaying one of them). Thus the standard deviation recorded below on each reading header is the SD within the machine's measurement protocol for one 'top level' reading.

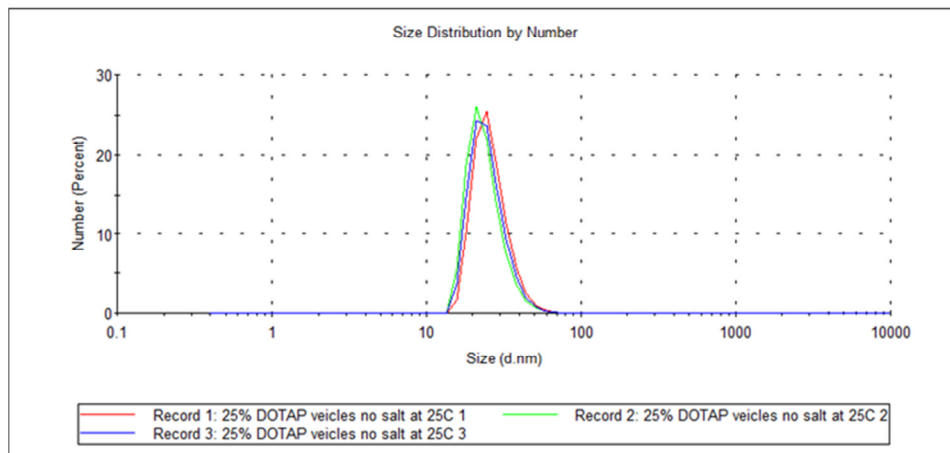
The average vesicle size and its variance have been calculated manually from 3 such 'top-level' readings, shown by the graph below, as reported in Chapter 5.

Measurements of the size of 25% DOTAP:POPC vesicles using DLS at 25°C:-

Temperature (°C): 25.0	Duration Used (s): 60
Count Rate (kcps): 249.3	Measurement Position (mm): 5.50
Cell Description: Clear disposable zeta cell	Attenuator: 9

	Size (d.nm):	% Number:	St Dev (d.nm):
Z-Average (d.nm): 54.81	Peak 1: 26.33	100.0	7.337
Pdi: 0.345	Peak 2: 0.000	0.0	0.000
Intercept: 0.932	Peak 3: 0.000	0.0	0.000

Result quality : Good



Measurements of the size of 25% DOTAP:POPC vesicles using DLS at 50°C:-

Temperature (°C): 50.0 **Duration Used (s):** 70
Count Rate (kcps): 136.9 **Measurement Position (mm):** 5.50
Cell Description: Clear disposable zeta cell **Attenuator:** 8

	Size (d.nm):	% Number:	St Dev (d.nm):
Z-Average (d.nm): 72.16	Peak 1: 33.26	100.0	9.090
Pdl: 0.346	Peak 2: 0.000	0.0	0.000
Intercept: 0.936	Peak 3: 0.000	0.0	0.000

Result quality : Good

